Efficient Kiln Drying of Quality Softwood Timber

Murray C. McCurdy

A Thesis submitted in fulfilment of the requirement for the Degree of Doctor of Philosophy in Chemical and Process Engineering to the University of Canterbury

Department of Chemical and Process Engineering

University of Canterbury

2005

Contents

Abstract

This thesis is a study of the kiln drying of radiata pine with a primary focus on the change in wood colour that occurs during this process. The energy efficiency of the drying process has also been examined using computer modelling. The aim of this work was to develop guidelines for commercial wood dryers who wish to produce high quality appearance grade timber in a competitive commercial environment.

The colour change in radiata pine wood during kiln drying is mainly caused by sap compounds accumulating at the wood surface and reacting to form coloured compounds. The initial research involved drying experiments designed to determine the relationship between this colour change and the kiln schedule and also measure the accumulation of colour forming compounds.

The kinetics of the colour change reaction were also measured using two methods, one in-vitro and the other using small samples of wood. From these experiments a colour change equation was developed that predicts the rate of colour formation based on the drying conditions and this was incorporated into a kiln stack model along with an energy efficiency model. The combined model was used to simulate the drying process to find schedules optimised for energy use and wood quality. The model was also used to simulate the energy efficiency of different humidity control configurations for wood drying kilns.

A kiln micro-sensor system was also developed for use in kiln diagnostics and control with the particular aim of identifying areas in wood drying kilns with adverse drying conditions.

The recommendation to kiln operators wishing to reduce colour change is to not exceed 70°C and to use lower relative humidity schedules with a wet bulb depression of 15-20°C. Operating at lower humidity can increase the energy used by the kiln so it is also recommended that kiln designers incorporate heat recovery into the humidity control mechanisms of the kiln.

Acknowledgements

I would like to thank my supervisor, Associate Professor Shusheng Pang and my associate supervisor, Professor Roger Keey for the guidance they have given me during this project. I know I am very fortunate to have had two people with such knowledge and enthusiasm to work with. Many thanks also to Professor Gerry Carrington, from Otago University for his input and for funding the first two years of this project through his FRST contract.

I am grateful for the practical help I received from CAPE technical staff, Frank Weerts, Bob Gordon and Trevor Berry and from Paul Fuller in the School of Forestry. Thanks also to Mike Lahood and Craig Marshall for their work on the kiln micro-sensors.

I also wish to thank John and Sean Fogarty of John Fogarty Ltd for the helpful advice and ideas they have given me and for providing access to their kiln for schedule testing.

Thank you to all my colleagues in the Department of Chemical and Process Engineering who have made my time there interesting and enjoyable. A special thanks to the CAPE Brewery team, it's great to see chemical engineering put to good use.

A big thanks to my family and friends for putting up with the perpetual student in their midst and offering a welcome break from academic life when needed.

Finally, I would like to dedicate this thesis to my father, John McCurdy, who was my first mentor.

Chapter 1

Introduction

Objectives

The title of this thesis is "Efficient Kiln Drying of Quality Softwood Timber". The following discussion will break this title down to what it really means and provide a context for the thesis.

Timber is a name given to wood that has been prepared for the purpose of building or carpentry (Robinson and Davidson, 1999). Wood is the hard tissue found beneath the bark that forms the bulk of woody trees and shrubs. In botanical terms wood is the Xylem of these plants.

Softwood is the common name of a group of trees and shrubs, having a similar ultra structure, known technically as Gymnosperms. The term softwood is in no way representative of the mechanical properties of the wood of Gymnosperms as many types of softwood are in fact quite hard and tough. An example of softwood is Pinus radiata, a tree of significant economic importance to countries such as New Zealand, Chile and Australia.

Kiln drying is an industrial unit operation used to accelerate the drying of wood. A wood drying kiln is essentially an enclosed space where air speed, temperature and humidity are controlled. Natural air-drying of wood can take weeks or even months while a wood drying kiln can complete the process in less than a day.

Efficient means producing satisfactory results with an economy of effort and a minimum of waste (Robinson and Davidson, 1999). This is quite a broad definition and in the context of kiln drying could represent the efficient use of land, labour, money, energy or the wood resource itself.

Quality can be defined as the degree or extent of excellence of the wood based on its various properties (Robinson and Davidson, 1999). Quality is not something that can be determined from first principles as it relies on the perceptions of end-users and may change with time. The concept of quality will be defined more clearly later.

The field in which this study has been done is timber drying with an emphasis on softwood timber, specifically Pinus radiata. Within this field the factors studied were the efficiency of the drying process and the quality of the product. Within this broad context there were three major objectives for this thesis.

1. Study and Quantify the Factors that affect Kiln Efficiency

There are numerous factors that can be used to quantify the efficiency of the kiln drying unit operation; some of these have already been identified above. These factors need to be identified and quantified to determine how they affect the overall efficiency of the kiln drying process. This quantification needs to be done in terms of energy units as well as in monetary units.

2. Develop and Validate Optimised Conditions for Kiln Drying of High Quality Timber

The conditions inside a wood drying kiln determine how the timber dries within it. The conditions inside the kiln are influenced by the kiln design and the schedule that it is run on. Specific colour quality parameters need to be defined and then the influence of different conditions on those quality parameters determined. From this knowledge optimised conditions can be determined and then tested.

3. Develop Micro-sensor Technique for Evaluating and Improving Kiln Design, Performance and Control

The kiln schedule determines the average overall conditions within a kiln, while the combination of the kiln schedule and the kiln design determines the conditions affecting each individual board within the kiln. The nature of this interaction is not well understood and a set of tools are required to measure the conditions within a stack of drying timber.

Introduction

Forests are a natural resource that has been used by modern humans since the dawn of their existence. They provided food and shelter as well as wood for the construction of tools and weapons for protection, hunting and war. Wood was also a convenient and abundant source of fuel for heating and cooking (Bechmann, 1990).

In modern times the forests are still a significant resource for all human civilizations, especially for the wood that they supply. With the development of new technologies the demand for wood has increased as has the diversity of uses. Wood is generally light and strong compared to other materials available, though there is considerable variation between species. The thermal properties and appearance of wood makes it a natural material that is both aesthetically pleasing and pleasant for human contact.

World Forest Resources

The total world forest cover as estimated by the FAO (2001) was 3.9 billion hectares in 2000, equivalent to 0.6 ha per capita which includes natural and plantation forests but excludes agricultural plantings. Based on the FAO data this forest area comprises approximately 95% natural forests and 5% plantation forests and has an estimated wood volume of 386 billion cubic metres. The majority of these forests are either tropical (47%) or boreal (33%) with the remainder in temperate (11%) and subtropical (9%) regions.

The main resource produced from the world's forests is wood with about 78% of the forests accessible and available for wood supply. The harvest of wood from these areas exceeds 3.4 billion m^3 annually and

trade in forestry products accounts for 13.6% of the world's consumption of imports. Approximately half of this consumption is used for fuel wood and the majority of the commercial wood is harvested from natural forests. Wood is a tradable commodity as there is a considerable regional imbalance in supply and demand. As an example New Zealand produces significantly more wood than it consumes. Historically the majority of international wood trade has been geared towards the USA, Canada, Japan and Europe, however rapidly developing countries, particularly China and India, are becoming more significant. The value of global imports of wood-based forest products, including fuel wood and charcoal was US$141.4 billion in 2002 (FAO, 2004).

There are a variety of non-wood products that come from the flora and fauna of the world's forests, including food, fodder, medicines, dyes and perfumes. The total import value of these products and processed goods made from them in 2002 was approximately US$7 billion (FAO, 2005a). This is small compared to the wood based products but these non-wood resources are particularly important to people who live in extreme poverty that depend on forest resources for subsistence production. As well as products forests provide these people with environmental services and protection such as watersheds, soil erosion control, microclimate, biodiversity and cultural services.

Forests also have a similar value in industrialised countries as well as providing recreation and tourism. Concerns over climate change and the ratification of the Kyoto protocol also add another value to forests as terrestrial carbon sinks (or stocks). Carbon credits are now a new tradable product provided by the forests.

Primary Processing

Wood in the form of trees in the forest is of little value as a tradable commodity. Commodities are produced from a forestry resource through primary processing (Walker, 1993). These commodities may be used as they are but are more often processed further into higher value products. The processes used include sawmilling, drying, preservation, energy production, pulp and paper manufacture and the production of wood panels. The commodities produced include solid wood, veneer, plywood, MDF, heat and electricity. Secondary processing produces higher value products such as furniture, mouldings and building structures from the primary resources. An overview of the primary processing of wood products is shown in Figure 1.

The increased value resulting from processing can be illustrated with the following examples. A radiata pine log has a value of $70-200 per m3 depending on quality. With a little processing the log can be made into structural sawn timber with a value of $190-300 per m3. Higher quality logs could be manufactured into clear moulding fetching $900-1100 per m3. At the high end of the structural market are glulam beams worth $3000-4000 per m3.

The value of primary processing can also be demonstrated by looking at the value added to the forest sectors contribution to GDP by different parts of the sector. Globally the forest sector provided about US$354 billion of GDP in 2000, which is 1.2% of the total GDP. Forestry, which includes the production

of standing timber and wood for fuel and industrial use, only contributed 22% to this total contribution. The remainder was provided by the wood industries and the pulp and paper industries (FAO, 2005b).

The production of higher value products through secondary processing usually requires a high quality resource and attention to detail during primary processing.

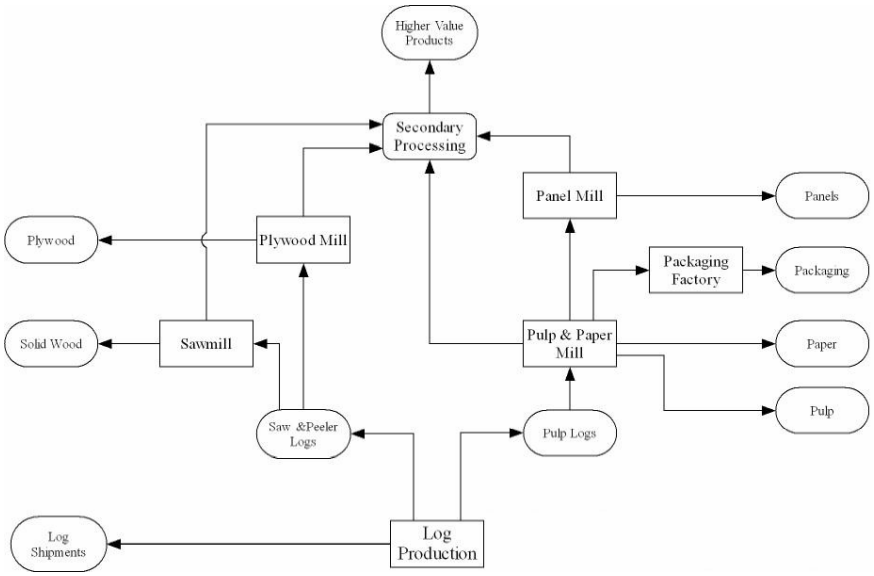

Figure 1 Overview of primary processing of wood products.

The NZ Forestry Resource

In New Zealand the earliest human settlers, from Polynesia, utilised the native timbers for the construction of buildings, boats and for fuel. The later arrival of European explorers, most notably Captain James Cook in 1769, initiated a mast and spar trade to Europe (Roche, 1990). With the subsequent colonisation by European settlers an indigenous timber market was established by 1840, which continued to grow in the nineteenth century.

The size of the native forest resource had decreased considerably by the turn of the century and in the early twentieth century the government became more involved in forestry. The state forest system developed from this involvement and brought about the planting of exotic trees, predominantly softwoods, for harvest in plantations. This has proved to be a very successful strategy as New Zealand has probably the fastest softwood growth rate in the world (Kerr, 1996). A comparison of selected softwood growth rates for different countries is shown in Figure 2 with only Australia and Chile showing comparable rates to NZ.

The forestry sector is now a very important part of the New Zealand economy. Forestry products accounted for 11.2% of exports for the year ended 31st December 2004 and approximately 4% of national GDP (MAF, 2005a). This is from a volume of trade of over 14 million m^3 roundwood equivalent and is roughly the same volume as the domestic wood trade. A similar volume of forestry products was exported in the previous three years. Products from this sector are currently the third largest export earner

for NZ after dairy products and meat (T.S.S., 2005) and incidentally under the Kyoto forests guidelines the forestry sector helps to offset the carbon emissions of the two larger export sectors. In 2002 approximately 25,000 people were directly employed in the forestry and primary processing industries, with at least twice this number employed indirectly related to the industry.

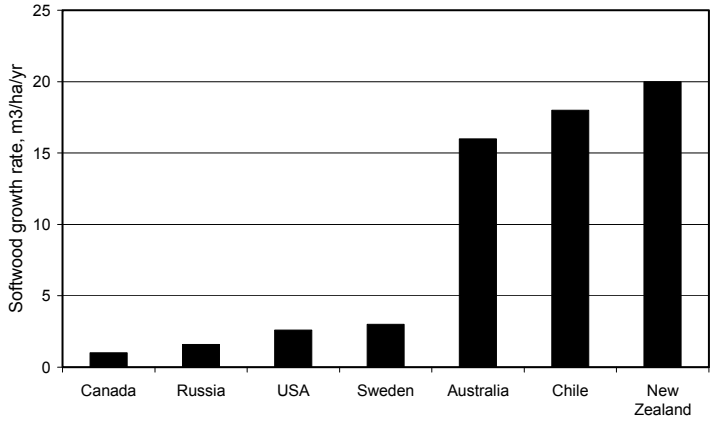

Figure 2 Comparison of softwood growth rates in different softwood growing countries.

The majority of the output of forestry products in New Zealand comes from managed plantation forests, with indigenous forestry dwindling to a fraction of a percent in recent years. The New Zealand forest estate is unusual by world standards in that more than three quarters of the forest area is in protected natural forest. The estimated removal of roundwood from NZ forests for the period from 1994 to 2004 is shown in Figure 3. In this period the removal of roundwood from indigenous forests has decreased overall, while the removal from plantation forests has increased overall. The recoverable volume of wood in NZ plantation forests is predicted to continue increasing in the foreseeable future, with the total harvest doubling by 2040 (MAF, 2000).

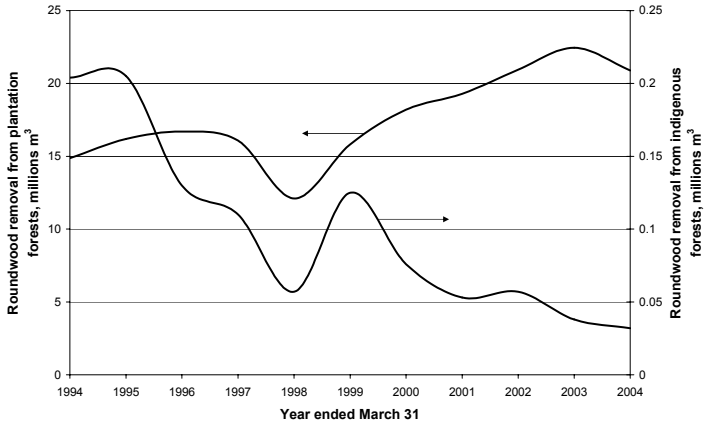

Figure 3 Estimated roundwood removals from NZ plantation and indigenous forests for the period 1994 to 2004.

The majority of the wood harvested in NZ comes from a single species, radiata pine. Radiata pine makes up 89% of the planted production forest area and Douglas fir accounts for 6%. The remainder of the forest area is planted in hardwoods (3%) and other softwoods (2%) (MAF, 2004).

The NZ forest industries reliance on radiata pine has stemmed from the species' suitability to the NZ environment. The trees grow very quickly in the temperate New Zealand climate as they do not enter a dormant phase except during winter in the far south. Cool night temperatures also aid growth by preventing the trees from wasting energy growing during darkness.

The New Zealand forestry sector has almost 100 years experience in the sustainable plantation farming of timber and develops and uses the most advanced forestry techniques in the world. This experience and technology mean that New Zealand has one of the highest quality forestry resources in the world. As an example New Zealand has twice as much pruned clearwood producing forest than any other country in the world.

Primary Wood Processing in NZ

The diagram in Figure 4 shows the harvest of timber in NZ and the general processing and export of wood products for the year ended 31st March 2003. The total roundwood equivalent removal of wood in 2003 was 15.8 million m^3 compared to 19.7 million m^3 in 2004. This diagram shows that just under a third of the roundwood removed from the forests was exported overseas as logs and chips. This proportion was similar in 2004. Logs and chip are low value products and while they are easy to produce their export represents an opportunity cost to the NZ economy of lost jobs and revenue from primary processing. There is also the environmental cost of wasted fuel and carbon emissions from shipping vast quantities of water that has no value or use.

The NZ forest sector has a varied primary processing capability. The large processing companies that own their forestry supplies have invested in new technologies and are therefore are generally technologically advanced. Some of the small and medium enterprises are slower with technology uptake due to higher risks and so lag behind technologically.

Wood Quality

Wood quality can be defined as the degree or extent of excellence of the wood based on its various properties as noted earlier. The quality of a finished wood product is also influenced by the quality of the original log and the quality of the wood processing used to transform it.

Log quality is largely based on three properties; size (diameter and length), shape (straightness, ovality and taper) and presence or absence of knots. There are other measures of log quality such as intra-ring checking index and resin pocket classes that provide a more detailed analysis of log quality (Park, 2005). The highest quality logs are the pruned peelers and the pruned sawlogs, which are large, high quality straight logs, used for the manufacture of high value wood products such as veneer, plywood and appearance grade lumber.

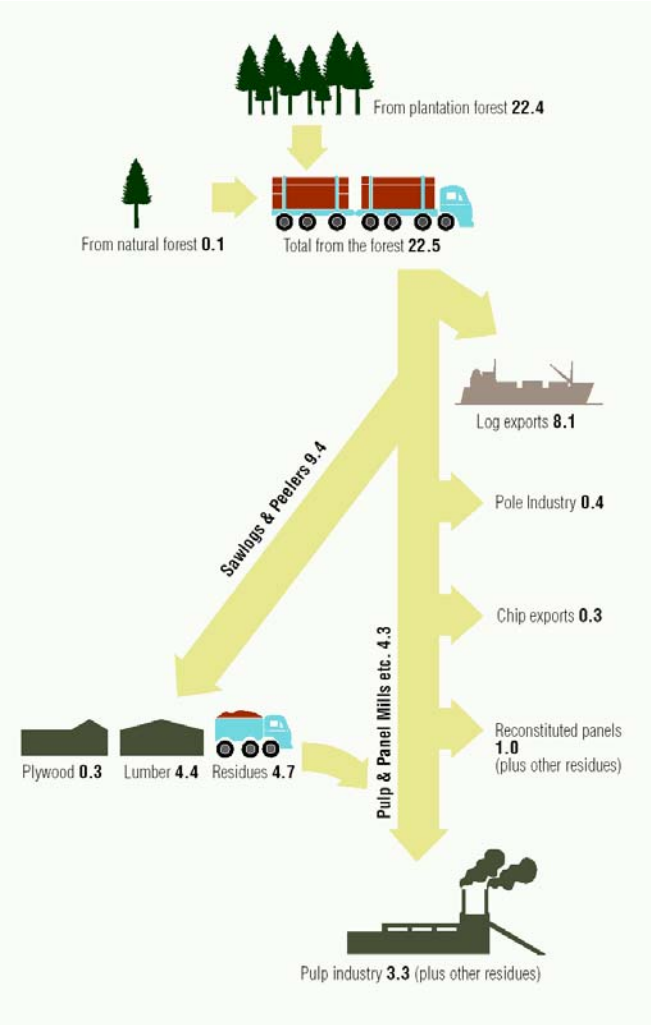

Figure 4 Log flow in the New Zealand forestry industry based on 2003 harvest and production statistics (from NZFOA, 2005). The estimated RWE removals for the year ended 31 December 2004 is 19.7 million m3 (MAF, 2005b).

Where pruned sawlogs are cut into boards in a sawmill the next step is usually to dry the boards, a process that requires careful attention to maintain the timber quality. The Australian/New Zealand standard for the assessment of drying quality in timber (AS/NZS 4787:2001) defines six criteria that can be used wholly or partly to measure dried timber quality. These criteria are as follows:

1. Moisture content gradient.
2. Residual drying stress.
3. Checking.
4. Collapse.
5. Distortion.

6. Discolouration caused by drying.

There is a seventh mandatory criterion for all grades that the wood is at the required target moisture content.

The moisture content gradient is defined as the difference in moisture content at the surface and in the core of boards. The moisture content gradient can affect the suitability of the wood for specific applications and in particular large differences in moisture content can affect the stability of wood during down stream remanufacturing such as ripping and moulding.

Residual drying stress is tension and compression that develops in a board as a result of the sectional variation of moisture content noted in the previous paragraph and the variation in shrinkage associated with this. The high temperature and reduced moisture content of the wood surface during the drying process can lead to plastic deformation of the surface layer when the wood yields under the tensile stress caused by differential shrinkage. This plastic deformation results in residual stress remaining in the board after drying which can lead to distortion during subsequent working of the wood. The residual stress can be relieved with steam conditioning.

Checking occurs when the drying stresses exceed the tensile strength of the wood and cause the fibres to separate. This separation results in a void known as a check which can occur inside the board where it is known as an internal check or at the outer parts of the board where it is known as a surface check or an end check depending on location. Checking in softwoods is seldom severe enough to reduce the structural strength of a board but can severely degrade timber for appearance purposes.

Collapse is a form of degrade that appears as abnormal shrinkage and severe sectional deformation which results in both of the faces being concave. This is usually only a major problem in hardwoods and is due to tension stress from cohesion forces during drying causing delicate fibres to collapse. Collapse is often associated with severe internal checking. In radiata pine collapse is not a severe problem and usually only manifests as small indentations on the drying surface (Deev and Keey, 2001).

Distortion is a change in shape of a wood product when it is dried. This can be a change in sectional shape such as cupping or diamonding resulting from differences in tangential and radial shrinkage. There may also be changes in longitudinal shape due to variations in grain orientation causing bow, spring or twist.

The NZ/Australia timber drying standard defines discolouration as any change in colour from the pre-dried state to the post-dried state. This discolouration can have a variety of chemical causes and is usually made worse by the heating during kiln drying. This discolouration is less acceptable when the variation in colour is inconsistent, as is the case with sticker stain and kiln brown stain.

The standard applies to both hardwoods and softwoods with the collapse criteria only applying to hardwoods. The standard also identifies three product types and which criteria are important to each of these. The first of these is non-appearance products such as framing and decking where only target moisture content and distortion are of importance. The second is appearance products such as exposed

beams and flooring, for which checking and discolouration are also important. The final type is furniture and joinery grade products, where the moisture content gradient and residual drying stresses are also important. Appearance and furniture grade wood is generally used to make higher value products

This thesis was developed from the premise that the NZ forest sector needs to develop more high value products to maintain and ultimately improve its competitiveness in international markets. A further premise is that in the short to medium term there needs to be more investment in new technology to increase efficiency and productivity. This will bring the structure of the NZ forest sector closer to that of Sweden or the USA. This is really the only option as only radical change in New Zealand's political and economic structure would allow the sector to compete long term with China and South America.

In the current (2004/2005) economic climate the risk associated with new investment in processing plant is too high for many in the industry to take. This leaves the industry in the unfortunate position of needing to invest in new technology to remain competitive but not having the capital available to take the risk. Excluding government intervention, the forest sector needs short term measures to improve the value of forest products without the risk associated with new plant investment.

The discussion in this chapter has shown that quality is one of the key factors required for the production of higher value products. New Zealand already has a large volume of pruned logs which can produce high quality wood products, so the next step in the value chain is to convert this into high quality commodity products through primary wood processing.

The following chapter reviews the literature and discusses in more detail the connection between wood drying and wood colour. Following that Chapter 3 describes the equipment and experimental methods used in this thesis to measure the relationship between wood drying and wood colour.

The results of drying studies to determine the effect of various drying schedules on colour change in wood are presented in Chapter 4. The results presented in Chapter 5 are from more detailed experiments to discern the temperature-based kinetics of the colour change in wood. The results of these experiments are then incorporated into a kiln drying model in Chapter 6 to simulate the relationship between kiln energy efficiency and wood quality for different drying schedules and kiln configurations.

Chapter 7 gives details on the development of kiln micro-sensor technology for diagnostic and control purposes. Finally, Chapter 8 brings the information from the previous chapters together and discusses it in the context of the objectives of this thesis.

Chapter 2

Wood Drying and Wood Colour

Introduction

This Chapter will firstly introduce the practical operation of kiln drying of softwood timber and various drying technologies. Then the science and fundamental understanding of the drying process will be discussed. Finally current knowledge on wood colour and colour changes will be covered and its effect on wood quality reviewed.

Reasons for Drying Wood

In order to meet with market requirements of stability and uniformity for dry timber, majority of softwood timber is dried in controlled drying kiln although a small proportion may be air-dried or be sold green. There are a number of advantages to dry the green timber to required moisture content (Kho, 1993; Walker, 1993):

1. Improved dimensional stability: Wood is hygroscopic, which means that its moisture content changes with changes in temperature and relative humidity of its surroundings. The change in moisture content results in a change in dimensions that can affect the shape of the piece of wood. Drying the wood to moisture content similar to its end-use environments reduces the risk of dimensional changes when the wood is in place.
2. Enhanced quality: Drying timber increases its strength making it more suitable as a building material and with enough care in the drying process also reduces warping, checking and splitting.
3. Improved keeping properties: Some species of micro organisms such as fungi and bacteria can thrive in green wood but do not survive well below 22% moisture content. Drying can therefore prevent degrade from stain or decay. High temperature drying of wood can also help protect against insect attack.
4. Reduced transportation costs: Green timber is much heavier than the equivalent volume of dried timber due to the extra weight of the water. The dried timber will therefore cost less to transport.
5. The temperature of drying can sterilise timber for export.

The drying of wood can also improves its properties for further processing such as chemical treatment and gluing.

Technologies in Commercial Wood Drying

Given the value added by drying wood there are a number of different technologies that have been developed for the commercial drying of timber. It is very difficult to remove moisture from wood mechanically, so the most technologies rely on removing the water as vapour and supplying the latent heat required for evaporation. The majority of these use air as a drying medium in a well controlled kiln, heating the wood and transporting the water vapour away from the boards.

Air Drying

The earliest and most basic form of timber drying is air drying, where boards are stacked out in the open to dry naturally with heat from the sun and wind for air circulation. While this is a basic process it is far from simple due to the variable nature of the environment and almost complete lack of control over the drying conditions and quality. It can also be difficult to dry the timber to a required target moisture content using air drying. The lack of control and the long drying times associated with air drying have seen it lose favour as better and faster drying technologies became available.

There have been some improvements made on air drying that allow more control and faster drying times. Forced air drying is a system where fans are used to increase the speed and uniformity of air flow through the stacks of timber. This does improve the drying rate but is still at the mercy of the climate because if the air humidity is too high then the moisture transfer between the board surface and the circulating air is largely retarded. To gain more control over humidity accelerated air drying was developed where the air was heated as well as being forced through the stacks. While this method is an improvement it does embody a trade off between wasting drying potential and variation in drying through the stack. The increase in temperature is also limited and subject to climatic conditions.

Kiln Drying

In the pursuit of better control over the drying of wood the process was enclosed to form what is known as a wood drying kiln. Kilns come in different shapes and sizes and operate in a number of different ways. In New Zealand there are two main types of kilns that are used, forced circulating air heating and venting kilns and dehumidification kilns. In countries and areas where the conditions are suitable solar kilns are also used.

Forced air Heating-Venting Kilns

In a conventional heating-venting kiln a filleted stack of wood is placed in the kiln chamber with fans above it to circulate air through the fillet spaces. The air is heated by heating coils that can be electrically heated or contain a heat transfer fluid circulating through a boiler. Humidification in the kiln is usually achieved using either a heated water bath or though direct steam injection. Moisture evaporated from the wood is removed from the kiln through the roof vents. Hot moist air is vented and cool dry air is drawn in using the pressure difference generated by the fan. In ultra high temperature drying (for example with

drying temperature above 160°C) the moisture of evaporation can be vented directly without the need to draw in cool air. The photograph in Figure 5 shows a heat-vent kiln designed and built by Fogarty Kilns of Invercargill, New Zealand.

The different schedules used in kilns are categorized based on the temperature that the kiln operates at. The categories are shown in Table 1 along with some basic data for the drying of 50mm thick lumber.

Dehumidification Kilns

A dehumidification kiln also uses a filleted stack with fans overhead to circulate the air. To control the temperature and humidity a dehumidification kiln uses a heat pump. Air is drawn in and cooled to the dew point by the heat pump evaporator to remove the condensate of the moisture. Then the cooled air is heated again by the heat pump condenser. This is a very energy efficient drying process with regard to the amount of energy used to evaporate the moisture from the wood. The process is however limited as to the dry bulb temperature that can be produced and the wet bulb temperature that can be maintained due to limits on the safe working temperature of the compressor. As the dry bulb temperature is normally lower than 70°C, the rate of drying is also slow compared to a heating-venting kiln where the drying temperature can be up to 200°C.

The energy requirements of a modern dehumidification kiln are shown in Table 2 compared to two heat-vent kilns, as determined by Carrington et al. (1998). This clearly shows that the dehumidification kiln uses significantly less energy overall, though it does have a higher electricity requirement. Carrington et al. (2003) have also shown that dehumidification kiln schedules reduce the formation of checking and kiln brown stain compared to an accelerated conventional temperature schedule.

Figure 5 A heating-venting kiln built by Fogarty Kilns of Invercargill, New Zealand.

Other Drying Technologies

There are a number of other methods of drying timber that will not be considered in this thesis as they tend to be used for specialist applications or are not used at all in New Zealand. These drying technologies include radio frequency and microwave drying using electromagnetic radiation in the microwave and radio frequencies to heat the moisture in the wood. There is also vacuum drying and superheated steam drying which are used to a limited extent in New Zealand. Other technologies include solvent and salt seasoning, boiling in oil, organic vapour drying and press drying (Pratt, 1974).

Table 1 Summary of drying schedule categories where the drying time is based on 50mm thick lumber (based on Kerr, 1996).

	Low Temperature	Conventional Temperature	Accelerated Conventional Temperature	High Temperature
Temperature (°C)	40-60	70-80	80-100	120-140
Airflow (m/s)	1.5	3.0	4.5	5.0-8.0
Drying time	15 days	5 days	2.5 days	13-20 hours
Minimum final MC (%)	10-11	6	3	2
Capital cost per m3 dried	low	High	medium	Low
Annual production per dryer (m3)	2000	3600	6000	180000
Sterilization	No	Yes	Yes	Yes

Table 2 Energy use in a dehumidification kiln compared to two heat-vent kilns based on drying of radiata pine from 140% to 12% at 70°C (Carrington et. al., 1998).

Energy Type	Dehumidifier Kiln	Coal-fired Kiln	Gas-fired Kiln
Fuel (GJ/m3)	-	2.4	2.2
Electricity (GJ/m3)	0.6	0.3	0.3
Total on-site energy (GJ/m3)	0.6	2.7	2.5

Wood Drying Mechanism

The complex and heterogeneous structure of wood means that it does not dry the same way as other porous materials. This is due to the limited pathways for moisture movement in wood during drying and the way wood permeability changes during drying.

Structure of Radiata Pine

Radiata pine (*Pinus radiata*) is a softwood (gymnosperm), and in New Zealand's temperate climate, there is a cyclic production of wood in the vascular cambium during the growth season. A cycle of fast growth in the early season (spring to mid-summer) and slow growth in the late season (late summer to autumn) produces an annual growth ring. The earlywood, or springwood, in Pinus radiata sapwood is a creamy white colour while the latewood, or summerwood, is a darker cream colour. When dried the latewood changes to a light brown colour showing the growth rings clearly.

The three dimensional structure of Pinus radiata is shown on the electron micrograph in Figure 6. The majority of the volume of the wood is made up of fibrous cells called axial tracheids with the remainder consisting of resin canals and radial tissue.

Axial tracheids, or simply tracheids, are axially oriented wood cells that make up over 90% of the total wood volume (Bamber & Burley, 1983). A cyclic pattern of seasonal growth in the vascular cambium results in the gradual increase in thickness of the cell walls. The earlywood tracheids are shorter and slightly thinner walled than the latewood tracheids, which have thicker walls and a smaller radial diameter. The tracheid length variation across a growth ring was examined by Nicholls and Dadswell (1962) and found to range from 2.6mm in the first formed earlywood to 3.2mm in the latewood. Patel (1971) measured tracheid lengths ranging from 0.73mm to 4.74mm with a mean of 2.70mm for one sample with the tracheid length increasing further from the pith. Cown (1975) showed a within ring difference between the earlywood and the latewood ranging from 0mm to 1mm with the latewood tracheids being longer. Patel (1971) also found that first-formed earlywood cell walls are 0.003mm thick while last formed earlywood cell walls are about 60% thicker at 0.005mm. The difference in radial diameter is more significant, as the earlywood tracheids at 0.045mm are 250% greater than the latewood tracheids at 0.013mm.

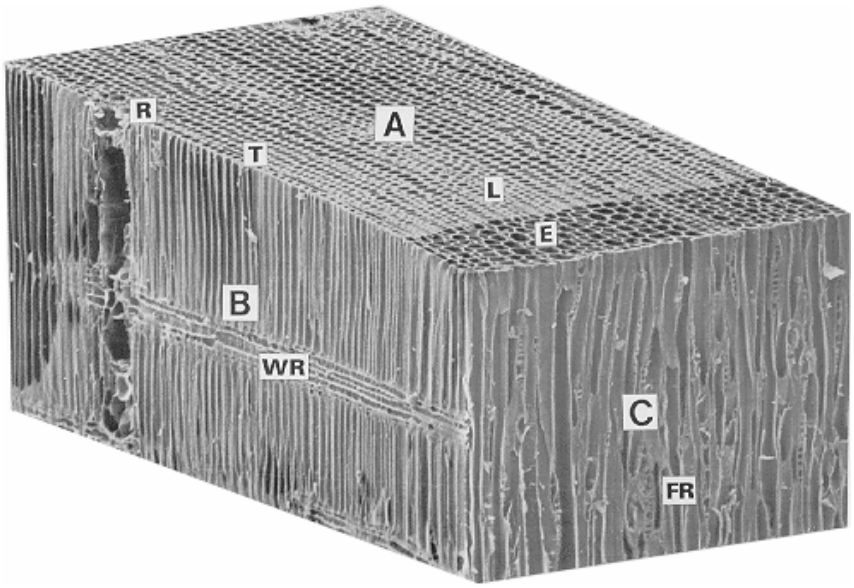

Figure 6 Electron micrograph of a section of Pinus radiata showing latewood (L) and earlywood (E). Also shown is a resin canal (R), a wood ray (WR) and a fusiform ray (FR). (Kinninmonth & Whitehouse, 1991)

The tracheid cell wall contains a number of layers. The outer layer is the primary cell wall, which originates from cambial division. Microfibrils in this layer are randomly arranged and this layer is initially unlignified. After cell differentiation, a process known as secondary thickening forms the secondary cell wall. The formation of the secondary cell wall increases the structural strength of the tracheid and reduces the permeability of the cell wall. To facilitate the flow of water and dissolved

nutrients between tracheids (longitudinally and tangentially) structures known as pits are formed during wall development. Pits are areas in the cell wall where secondary thickening has not occurred. These pits can be simple or bordered.

The micrograph in Figure 7a shows a number of bordered pits connecting earlywood tracheids. An earlywood bordered pit is shown in Figure 7b with the secondary cell wall exposed to show the torus and margo. The margo is a part of the primary cell wall which contains no secondary thickening. The torus in the centre of the margo does have secondary thickening. In a living tree the perforations in the margo allow water to pass through the pit easily. The latewood pit in Figure 7c has no apparent perforations, so water will pass through slower. This is not a problem in the tree as the latewood is mainly structural and does not provide pathways for moisture transport. The earlywood pit shown in Figure 7d has been closed by a process called pit aspiration, which will be discussed later. Simple pits are holes in the secondary cell wall exposing the primary cell wall.

Another difference between the two types of tracheids is the size and frequency of bordered pits on the cell walls. The earlywood tracheids have more pits than the latewood tracheids and these pits are larger. Latewood tracheids are more likely to be encrusted with resin and do not aspirate as readily.

Radial tissue in radiata pine makes up only a small part of the wood volume. It is however very important in a growing tree as it provides radial pathways for sap flow. There are two types of radial tissue, *uniserate* rays and *fusiform* rays. *Uniserate* rays are made up from a single stack of cells and contain both ray parenchyma and ray tracheid cells. The ray tracheids are situated at the top and bottom of the ray with normally one or two rows. In between these rows are several rows of ray parenchyma. These are thin wall cells connected by simple *pinoid* (pine-like) pits, and are the living cells of the tree. *Pinoid* pits do not have perforations in the primary cell wall. *Fusiform* rays are larger and, as the name implies, spindle-shaped and often contain a resin canal bordered by epithelial cells. The radial resin canals connect up with longitudinal resin canals to provide the resin transport system for the tree.

The ray tracheids are different from the axial tracheids in a number of ways. At about 0.2mm in length they are considerably shorter and also contain dentations (Phillips, 1968) in the secondary cell wall, which are absent in the axial tracheids. The bordered pits in the ray tracheids are much smaller than those on the axial tracheids.

Moisture Movement

The pathways for moisture movement are determined by the structure of the wood. Axial flow of moisture is facilitated by the axial tracheids. Flow from tracheid to tracheid in the tangential direction is also through the bordered pits as most of them are located on the radial faces of the tracheids. Flow of moisture in the radial direction is through the radial tissue and by a tortuous pathway through the bordered pits. This means that the pathway for moisture movement will differ depending on whether the wood is dried quarter-sawn or flat-sawn (McCurdy and Keey, 2002).

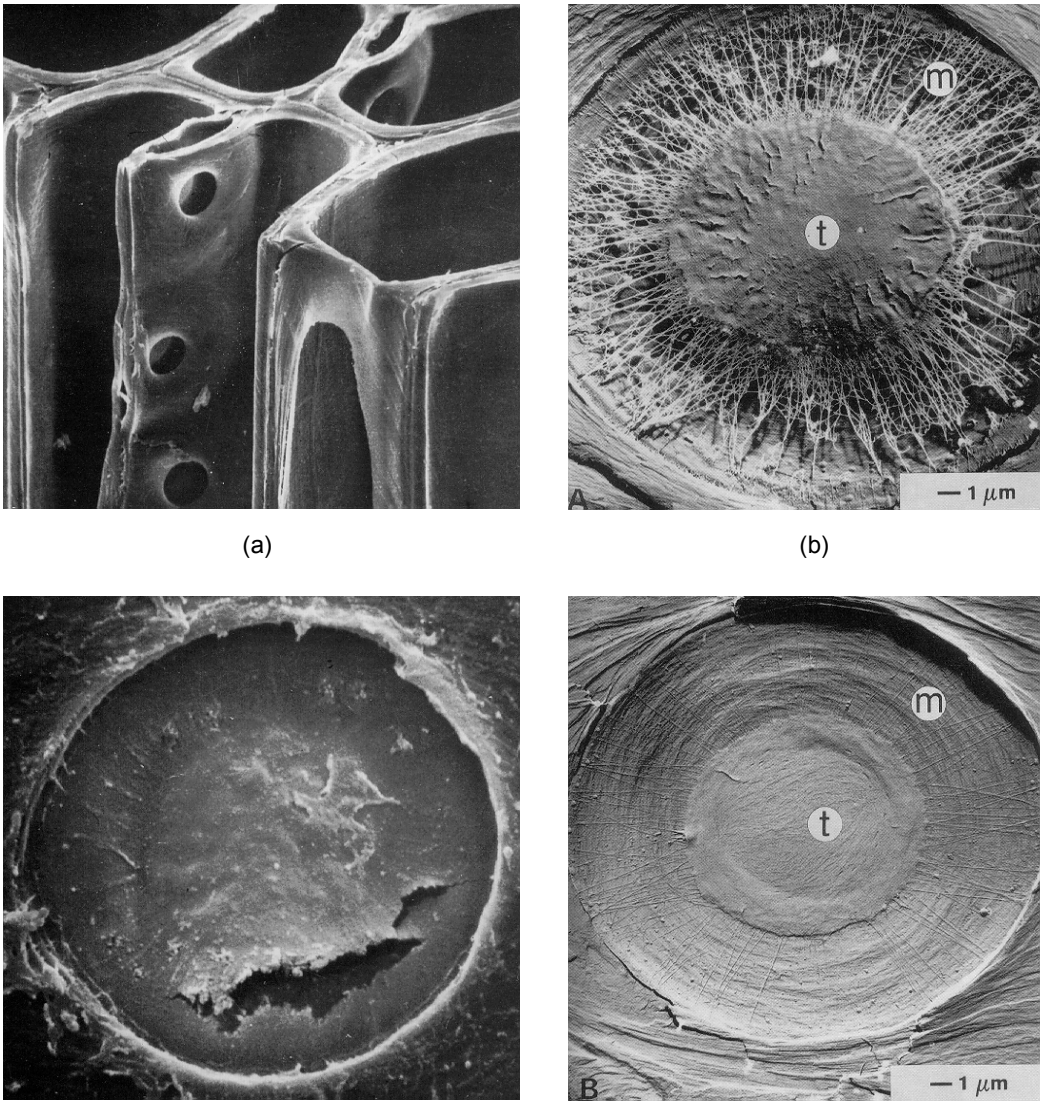

Figure 7 Bordered pits in radiata pine; a) section showing the pits in the cell wall between two tracheids; b) an un-aspirated earlywood tracheid showing margo (m) and torus (t) intact; c) latewood bordered pit; d) aspirated earlywood pit. (Butterfield and Meylan, 1972; Kininmonth and Whitehouse, 1991; Butterfield and Meylan, 1980)

When bordered pits close, by pit aspiration, the movement of water through these pits is almost totally impeded. The exact mechanism of pit aspiration is still a matter of debate. One explanation is the Hart and Thomas model (1967) of pit aspiration and the other is the dynamic pit aspiration model proposed by Booker (1996).

In the Hart and Thomas model the pits close as the air-water meniscus enters them. As the meniscus enters the pit the radius of curvature decreases with a corresponding increase in the capillary tension until it reaches the pores in the margo. At this point, the capillary tension pulls the margo and torus against the secondary cell wall. In an elaboration of the model, Nicholas (Siau, 1971) proposed that, as the water

recedes into the small openings in the torus, the capillary tension increases causing the torus to deform into a dish. There is, however, little evidence for the existence of openings in the torus (Booker, 1996) so another model has been proposed by him.

The newer dynamic pit aspiration model is based on the idea that tracheid lumens empty very quickly by cavitation. Initially, the entire water column is under tension and then one tracheid cavitates. This creates a pressure in the cavitating tracheid, resulting in a large pressure differential that forces water through the pit at high speed. When the meniscus reaches the pit border it is moving at a high speed and slams the torus against the cell wall. This seals the pit so the water column is brought to an abrupt halt and the force of this deceleration causes the torus to dish.

The radial movement of moisture is through the ray tissue. This movement is also through bordered pits that are smaller than those on the radial faces of the axial tracheids. However these two types of pits are connected to each other forming a network for moisture movement in all directions. The smaller pits do not normally aspirate due to their thick margos and resinous encrustation. There will also be some movement through the ray parenchyma.

These complex pathways mean that moisture is not lost evenly from the wood and the uneven loss results in the development of a moisture-content profile. During drying the surface of a board loses moisture rapidly forming a dry outer shell surrounding the wet inner core (Pang, 1994; Pang et al., 1994). This phenomenon can be seen quite clearly in the CT scanning experiments done by Wiberg (1996).

As the wood dries, it reaches a point when the liquid is no longer continuous thus the liquid convective flow is interrupted. Further drying will evaporate the remaining liquid and vapour flow is important. When the wood reaches the fibre saturation point (FSP), there is no longer any free moisture in the cell lumens. Under normal high temperature kiln conditions FSP is at a moisture content of 20-25%. At this point moisture movement is by vapour flow and bound water diffusion. Further moisture loss from the wood below fibre saturation point results in dimensional changes in the wood fibres causing them to shrink.

Liquid Movement Models

As with pit aspiration there is still some debate as to the exact mechanism of liquid movement in wood during drying. There are two different mechanisms that dominate the thinking in this area.

Firstly there is the Skaar/Siau theory proposed by Skaar (1972) and the second, more recent, hypothesis presented for liquid movement is Booker's transpiration cohesion theory. These models have been reviewed by Booker (1996) and can be summarised as follows.

In the Skaar/Siau model, as described by Siau (1984), the damaged cells at the surface initially contain water while some of the cells within the wood contain air bubbles. As drying progresses, the moisture is lost from these cells and the air-water meniscus recedes into the bordered pits closest to the surface reducing the radius of curvature and therefore increasing the capillary tension in the wood. This tension causes the air bubbles in the wood to enlarge beginning with the largest bubble followed by the smaller

bubbles. When the cells have emptied, the tension continues to increase until the meniscus breaks into another cell and empties it. This model is used with the Hart and Thomas model for pit aspiration. These two models together require that there be micropores in the cell walls and air bubbles pre-existing in the sap. Neither of these requirements has been shown experimentally, though Côté (1967) suggests the existence of holes left by plasmodesmata in pit membranes. The existence of air bubbles has been shown to be theoretically implausible by Booker (1996). This is because in the living tree the bubbles would dissolve into the sap stream at night when water tension drops to zero.

Work by Wiley et al. (1975), Spolek and Plumb (1981), Furuyama et al. (1994) and Hunter (1995) also supports this type of model for moisture flow based on capillary pressure. These models also predict the presence of overpressures inside wood during drying. Experiments by Perré et al. (1993) appear to show that overpressures exist though this may be due to the experimental design (McCurdy, 2000).

The alternative model proposed by Booker (1996) the evaporation of moisture from the surface draws water through the walls of water-filled cells by vacancy diffusion. This creates a tension in the water in the wood that deforms the cell walls, as moisture is evaporated. The water is in a metastable state due to the lack of air or impurities to provide nucleation points. Eventually the tension reaches a point where the metastable state becomes unstable and a vapour bubble forms in a cell by a process called cavitation. The cavitating cell empties almost instantly releasing the pressure on its cell wall and water flows into other cells. When the cell is emptied the bordered pit close by dynamic pit aspiration and the cell lumen is sealed off from the other water filled lumens. The tension remains on the other cells.

It is normally assumed that the diffusion is a Brownian movement of water molecules through the non-interacting matrix of cellulose, hemicellulose and lignin molecules that make up the cell wall. This, according to Booker, results in a diffusion rate, which is much lower than what would be required for the drying rates. In Booker's hypothesis the diffusion is assumed to occur by vacancy diffusion in which the matrix plays an active role in the water transport where the hydrophilic groups attached to the matrix molecules form sites that bind water molecule. Water molecules can jump into a vacant site and can jump out of a site to create a vacant site.

By vacancy diffusion, water molecules reshuffle among sites as water is removed from the drying surface. This means that water molecules effectively move from one side of the cell wall to the other instantaneously. The jump frequency increases as the temperature is increased and it reduces as the moisture content drops below fibre saturation point.

Moisture Movement below Fibre Saturation Point

The models above describe the movement of moisture in the wet zone, where the wood is above fibre saturation point. In the dry zone below fibre saturation point all the moisture is either in the form of vapour in the lumens or bound water in the cell walls. There is also a point known as the irreducible saturation point where the continuity in the liquid column has broken and liquid flow can no longer occur. This is above fibre saturation point as there are still isolated pockets of liquid water present in the wood. For now this will not be considered in any detail.

Moisture movement below fibre saturation point was assumed by Choong (1963) to occur by two mechanisms: 1) vapour movement through the cell and pit cavities, and 2) bound water movement through the cell walls. The relative importance of vapour movement and bound water diffusion can vary with the wood permeability and drying temperature. The bound water diffusion rate can be related to chemical potential difference which in turn can be described by temperature and pressure gradient (Stanish, 1986; Pang, 1994). The vapour movement is driven by the vapour partial pressure gradient based on the Darcy's law. The bound moisture movement is considered to be negligible by Nijdam (1998) based on chemical potential calculations by Stanish (1986).

The Surface Zone during Drying

Regardless of the mechanism by which the wood is drying, the moisture leaves the wood by evaporating from the external surfaces and it is in the surface zone where most of the interesting processes occur during drying. Before drying the surface of a green board is at essentially the same moisture content as the core of the board, assuming that there has been no air drying prior to kiln drying. On drying the moisture at the surface of the board evaporates and the surface layer dries out, while the core moisture content remains the same. It has been observed that the surface dries to below the FSP in the early stage of drying even the core moisture content is very high. This phenomenon has been expained by Pang (1994) as a consequence of pit aspiration in the surface cells during sawing. As the wet surface from which moisture is evaporating recedes below the surface of the wood it becomes an evaporative front. Normally the evaporative front recedes to a position 1-2mm below the surface where it remains until the board approached a moisture content of 50-60% depending on the drying temperature. During this period of drying, the liquid flows from the core toward the evaporative front due capillary action generated by moisture gradient (Spolek and Plumb (1981)).

Colour and Wood

This section will provide an introduction to the field of colour science and review literature relevant to the study of colour in wood. At first glance colour seems like a relatively simple, however, delving deeper into the subject reveals that the rigorous description of colour involves physics, chemistry, the psychology of sensation and perceptions and the philosophical questions of colour realism. In this review the philosophy of colour will not be covered, other than to say that a physicalist view is generally taken, which assumes colour is a physical property of an object. More detailed information on the philosophy of colour is provided by Byrne and Hilbert (1997) for those who are interested.

The section firstly introduces a scientific definition of colour and how it relates to light, along with what causes it and how it can be measured and expressed. Later in the section wood colour is discussed, in particular the variation between species and how colour is related to the physical and chemical nature of wood. Finally the problems associated with colour development during wood processing and associated degrade are discussed.

The Science of Colour

The information contained in this section is abbreviated from Nassau (2001) unless otherwise stated. This book provides detailed coverage of colour science.

Colour and Light

The term colour is used to describe three subtly different aspects of reality. The first of these is a property of an object, the second a property of light and the third a class of sensations. With regard to wood colour all of these aspects are important. The wood has a colour, or a range of colours, which is one of its properties. This property of the wood influences the colour of the light rays reflected from its surfaces. In turn the light rays cause a sensation upon entering the human eye and this is perceived as a colour.

Isaac Newton described colours as a spectrum in 1666. This was the first rigorous scientific representation of the concept of colour and signalled the beginning of colour science.

Visible light is a small but very important part of the electromagnetic spectrum. The nature of light can be described as normally acting as a transverse wave controlled by set of wave equations but under certain conditions will act as a particle controlled by the same equations. This is the basis of quantum theory developed in the early 20th century and the details are not necessary for this project.

The visible spectrum comprises electromagnetic radiation in the 400-700nm wavelength range, as shown in Figure 8. Above 700nm the spectrum moves into infrared and below 400nm it moves into ultraviolet, neither of which is detectable with normal human vision. The shorter wavelengths of light have a higher frequency and energy than the lower wavelengths light.

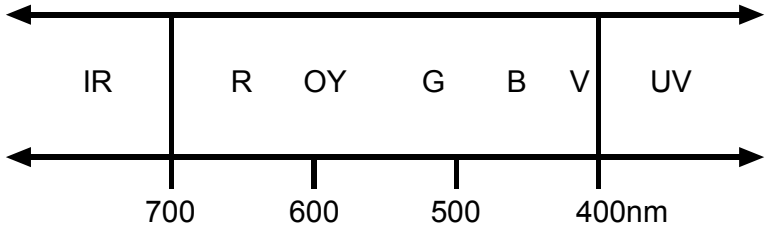

Figure 8 The visible spectrum between 400nm and 700nm, showing the approximate positions of red, orange, yellow, green, blue and violet light. To the left is infrared and to the right is ultraviolet.

Colour Mixing

The mixing of colour can be either additive or subtractive depending on the nature of the colours being mixed. Where pigments such as paints and inks are being mixed the mixing is subtractive. This means that as each pigment is added to a mixture it removes part of spectrum of wavelengths from the colour of the mixture. Effectively any colour can be made from the mixing of the three primary subtractive colours; magenta, cyan and yellow. The combination of these three colours gives black or the absence of colour where all visible wavelengths have been removed from the spectrum.

When different colours of light are mixed the mixing is additive, which means the wavelengths from each source of light are added together to produce the final colour. This means that each source of light adds a spectrum of wavelengths to the mixture. The three primary additive colours are red, green and violet (blue). When these three colours are mixed together the result is white. This does not mean that all wavelengths of light are present in the mixture as new wavelengths of light are not created in the mixing process.

Human Vision and the Standard Observer

The human eye has two types of light receptors, known as the rods and cones. The rods are receptors that are sensitive to a broad range of wavelengths and as such do not perceive actual colours. The rods are far more sensitive to light than the cones and only come into play under low light conditions and peripheral vision. There are three different sets of cones in the human which are designated S, M and L relating to their sensitivity to short, medium and long visible wavelengths respectively. They are also referred to as blue, green and red cones based on the wavelength of peak sensitivity. The peaks in sensitivity occur around 440nm (blue), 540nm (green) and 580nm (red).

Commission Internationale d'Éclairage (CIE) defined the Standard Observer in 1931 which is a set of colour matching equations that correspond to the spectral sensitivity of the human eye. There are three colour matching functions corresponding to the three sets of cones. The 1931 Standard Observer is based on a viewing angle of 2° and a Supplementary Standard Observer defined in 1964 is based on a viewing angle of 10°. The viewing angle determines the field of view at a distance and the area projected onto the retina.

The colour matching functions for the 2° Standard Observer are shown in Figure 9. These colour matching functions give what are known as the tristimulus values for an equal energy spectrum of light as a function of wavelength. These values mimic the response of the three cones in the human eye to a spectrum of light where all wavelengths are present with the same energy. Colours can be defined based on these colour matching functions by calculating the XYZ tristimulus values for each colour. These values are calculated by integrating the product of the colour matching functions, the relative spectral power distribution of the illuminant, S(λ), and the spectral reflectance of the object, R(λ), over the visible spectrum. This is done using the following set of equations:

$$X = K \int_{380}^{780} S(\lambda)\bar{x}(\lambda)R(\lambda)d\lambda \qquad 2.1$$

$$Y = K \int_{380}^{780} S(\lambda)\bar{y}(\lambda)R(\lambda)d\lambda \qquad 2.2$$

$$Z = K \int_{380}^{780} S(\lambda)\bar{z}(\lambda)R(\lambda)d\lambda \qquad 2.3$$

$$K = \frac{100}{\int_{380}^{780} S(\lambda)\bar{y}(\lambda)R(\lambda)d\lambda} \qquad 2.4$$

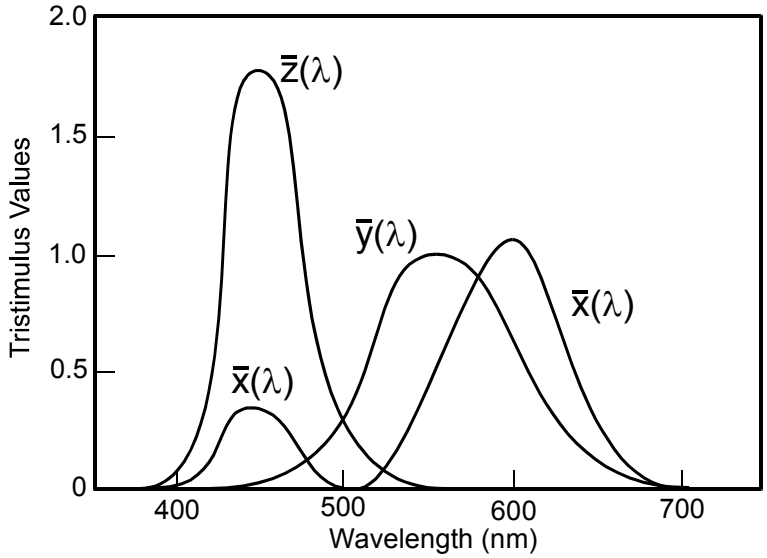

Figure 9 Colour matching functions for the 2° Standard Observer.

Colour Spaces

A common standardized way of representing colour in a way that can be easily visualised is the 1931 CIE xy chromaticity diagram developed by Commission Internationale d'Éclairage. This colour space, shown in Figure 10, graphs colour in two dimensions and is independent of lightness. The chromaticity coordinates x and y are calculated from the XYZ tristimulus values using the following formulae:

$$x = \frac{X}{X + Y + Z} \qquad 2.5$$

$$y = \frac{Y}{X + Y + Z} \qquad 2.6$$

This is also known as the Yxy colour space as the tristimulus value Y is the lightness. In this colour space the pure spectral colours that can be represented by a single wavelength of light are situated on the curved perimeter. Non-spectral hues that result from the mixing of red and violet light are positioned on the straight line between the two ends of the curve. The central point in the diagram represents white or CIE standard daylight, D65. This chromaticity diagram is supposed to represent all of the colours that can be perceived by normal human sight, though there will be variations from person to person. It is quite an old standard, with some flaws, and there are newer alternatives being developed (Fulton, 2005), but for now it remains the standard.

The CIELab colour space was developed in 1976 to deal with the problem of non-uniform minimum perceptual colour differences in the CIE xy chromaticity diagram. This three dimensional spherical colour space, shown in Figure 11, was developed by applying a non-linear mathematical transformation to the chromaticity diagram. The three rectangular coordinates used to describe the spherical space are defined by the following equations:

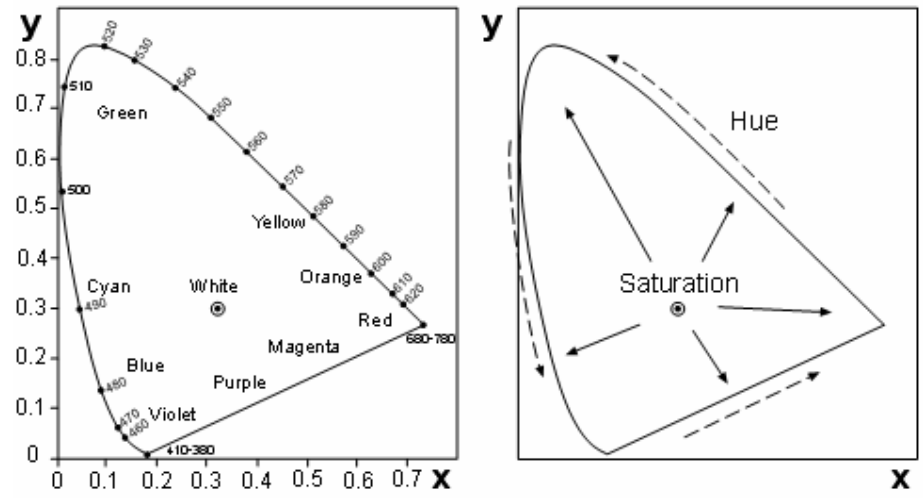

Figure 10 CIE 1931 xy chromaticity diagram

$$L^* = 116\left(\frac{Y}{Y_n}\right)^{1/3} - 16 \qquad 2.7$$

$$a^* = 500\left[\left(\frac{X}{X_n}\right)^{1/3} - \left(\frac{Y}{Y_n}\right)^{1/3}\right] \qquad 2.8$$

$$b^* = 200\left[\left(\frac{Y}{Y_n}\right)^{1/3} - \left(\frac{Z}{Z_n}\right)^{1/3}\right] \qquad 2.9$$

In these equations X,Y and Z are the tristimulus values for the object colour and X_n, Y_n and Z_n are the tristimulus values for a perfect reflecting diffuser. Where the ratios X/X_n, Y/Y_n and Z/Z_n are less than 0.008856 the cube roots are replaced by the following formula:

$$\left(\frac{X}{X_n}\right)^{1/3} = 7.787\left(\frac{X}{X_n}\right) + \frac{16}{116} \qquad 2.10$$

$$\left(\frac{Y}{Y_n}\right)^{1/3} = 7.787\left(\frac{Y}{Y_n}\right) + \frac{16}{116} \qquad 2.11$$

$$\left(\frac{Z}{Z_n}\right)^{1/3} = 7.787\left(\frac{Z}{Z_n}\right) + \frac{16}{116} \qquad 2.12$$

The coordinate L* represents the lightness of the colour and has a value from 0-100 with a lightness of 0 being pure black and a lightness of 100 being pure white. The vertical centre of the colour space along the L* axis is achromatic and is therefore a greyscale. The two horizontal axes that cross at L*=50 show the values for the chromaticity coordinates a* and b*. The a* chromaticity coordinate has a value from -60 (green) to +60 (red) with a value of a*=0 meaning the colour contains no green or red component. The b* chromaticity coordinate has a value from -60 (blue) to +60 (yellow) with a value of b*=0 meaning the colour contains no blue or yellow component.

When measuring the difference between colours it is often convenient to represent the colour change as an overall change in colour based on the distance between the two colours in the colour space. This colour difference, ΔE*ab is given by the following equation based on Pythagoras' Theorem:

$$\Delta E^*_{ab} = \sqrt{\left(\Delta L^*\right)^2 + \left(\Delta a^*\right)^2 + \left(\Delta b^*\right)^2} \qquad 2.13$$

The spherical colour space can also be described using the cylindrical coordinates of the L*C*h colour space. In this coordinate system the lightness, L*, is identical to that in the CIELab system. The Metric Chroma, C*, is a measure of how saturated a colour is and can be calculated from the chromaticity coordinates using the following equation:

$$C^* = \sqrt{\left(\Delta a^*\right)^2 + \left(\Delta b^*\right)^2} \qquad 2.14$$

The Metric Hue-Angle, h_{ab}, is an angular measure of the actual colour with units of degrees. This can be calculated from the chromaticity coordinates using the following equation:

$$h_{ab} = \tan^{-1}\left\{\frac{b^*}{a^*}\right\} \qquad 2.15$$

When the L*C*h system is used to measure colour difference between samples the Metric Hue-Angle Difference, ΔH*, is calculated from the following equation:

$$\begin{aligned}\Delta H^* &= \sqrt{\left(\Delta E^*_{ab}\right)^2 - \left(\Delta L^*\right)^2 - \left(\Delta C^*\right)^2} \\ &= \sqrt{\left(\Delta a^*\right)^2 + \left(\Delta b^*\right)^2 - \left(\Delta C^*\right)^2}\end{aligned} \qquad 2.16$$

All of the colour spaces mentioned here have been used to describe the colour of wood in the literature. Early papers such as Sullivan (1967) and Moslemi (1969) use the tristimulus values to describe colour. There is however some ambiguity as to whether the results presented are tristimulus values or chromaticity coordinates. This makes it difficult to convert the results to the newer colour spaces. Since the introduction of the uniform colour spaces in 1976 the majority of papers have described colour using either the L*a*b* or L*C*h format with the former generally being more popular. The argument for using the latter system given by Stenudd (2004) is that only a single coordinate is required to describe a particular change in colour such as hue. This is a reasonable assertion and certainly it is more convenient for analysis purposes but generally the lightness is the coordinate most often presented as an indication of wood colour and this is the same for both systems. The a* and b* chromaticity coordinates also offer a more intuitive idea of the hue as a mixture of primary colours red, blue, green and yellow. Once understood this system allows a more rapid understanding of the colour than the hue angle which requires more knowledge of what colour each value corresponds to.

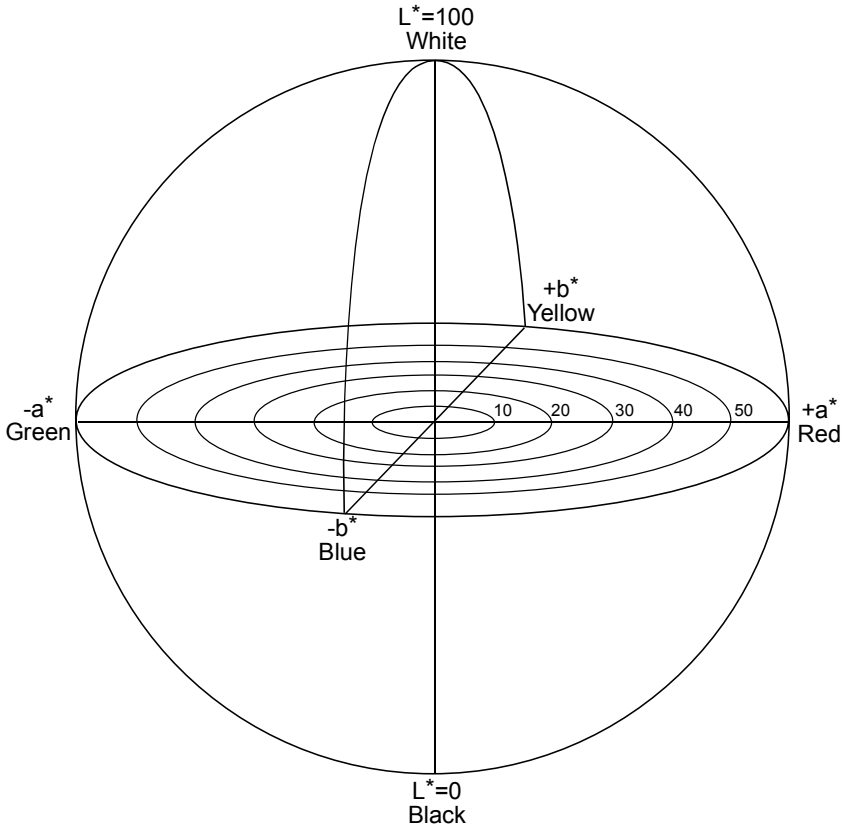

Figure 11 L*a*b* colour space.

Light and Matter

The previous sections have described what colour is in terms of wavelengths of light and how colour is perceived. Colour has been described by various colour spaces. In these cases colour has been viewed as a property of light. The following section will explore colour as a property of an object, with the ultimate

goal to discover what aspects of an object cause it to alter light to produce a colour. The first step is to look at the way light interacts with an object.

When a beam of light intersects an object of bulk matter the two can interact in a number of different ways, as shown in Figure 12. The light can be reflected from the surface by either specular or diffuse reflection or a combination of the two. Specular reflection occurs if the surface of the matter is very smooth, while a rough surface will result in more diffuse reflection. Light from a diffuse reflection from an object reveals the colour of the object more than a specular reflection as during a diffuse reflection the light penetrates deeper into the surface and therefore interacts more with the substance of the object. If the surface is very rough or coated in powder then the light will be almost completely scattered, minimising the penetration and therefore reducing the colour. This is why many coloured compounds appear white when they are in powder form.

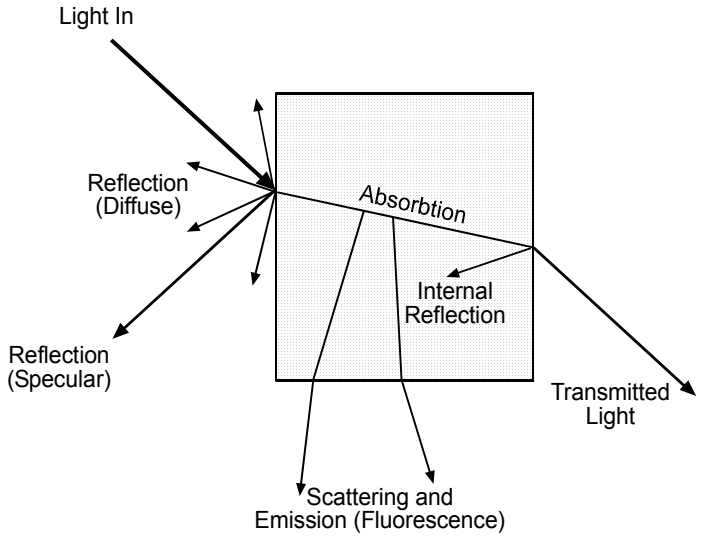

Figure 12 Interaction of a beam of light with bulk matter.

The light picks up the colour of the object, in most cases, by penetrating a short distance into the surface where some of the light is absorbed. The object may absorb differently over the spectrum of wavelengths in the light beam. In this case the light is then reflected back through the surface with a different colour to the incident beam. In a transparent or translucent object some of the light will also be transmitted through and come out the opposite side. Upon passing through the object some wavelengths of light are absorbed thus changing the colour of the transmitted light.

Causes of Colour

With an understanding of how light interacts with bulk matter the next question is what actually causes the colour change to occur. According to Nassau (2001) there are fifteen causes of colour, in five categories, shown in Table 3. The cause most relevant to colour in wood is the sixth: Transitions between molecular orbitals in organic compounds.

Molecular Orbitals

The following is a very brief overview of the causes of colour in organic compounds. This subject is quite complex, involving both subatomic physics and physical chemistry, and can only be dealt with here in the broadest sense.

Atoms of matter comprise of a number of negatively charged electrons orbiting a positively charged nucleus. The electrons can occupy discrete orbitals around the nucleus that represent different levels of energy as determined by the solution set of the Schrödinger wave equation. Each of the solutions in this set are described by four parameters: the principle quantum number, n; the angular momentum quantum number, l; the magnetic quantum number, m; and the spin quantum number, s. Combinations of allowable values for these parameters result in the following atomic orbitals, in order of increasing energy: 1s, 2s, 2p, 3s, 3p, 3d, 4s,…etc. The Pauli exclusion principle states that no two electrons can have the same quantum numbers, which means that each s-orbital can only contain two electrons and the p-orbitals can only contain 6 electrons each. Higher orbitals d, f, g, h… can contain more electrons.

Table 3 The 15 causes of colour (adapted from Nassau (2001))

	Vibrations and Simple Excitations
1.	Incandescence
2.	Gas excitations
3.	Vibrations and rotations
	Transitions Involving Ligand Field Effects
4.	Transition metal compounds
5.	Transition metal impurities
	Transitions Between Molecular Orbitals
6.	Organic compounds
7.	Charge transfer
	Transitions Involving Energy Bands
8.	Metals
9.	Pure semiconductors
10.	Doped or activated semiconductors
11.	Colour centres
	Geometrical and Physical Optics
12.	Dispersive refraction, polarization, etc…
13.	Scattering
14.	Interference
15.	Diffraction

When atoms are bonded to create molecules their atomic orbitals interact and form molecular orbitals that share electrons between the atoms. This is what creates covalent bonding between atoms in a molecule. It is the interaction between p-orbitals and the π-molecular orbitals that result from these interactions that play the greatest role in the formation of colour.

Normally the electrons in an atom or molecule will occupy the lowest energy orbitals first, but if the electrons are excited by a photon with sufficient energy (frequency) they can move to a higher energy orbital. This transition is normally from the highest occupied molecular orbital (HOMO) to the lowest unoccupied molecular orbital (LUMO). Simple molecules the energy required for the electrons to make

the jump from HOMO to LUMO is too high for transition to be triggered by the photons in visible light and therefore these compounds tend to absorb light in the ultraviolet region.

The addition of conjugated double bonds to a molecule in the form of non-cyclic polyene structures, nonbenzenoid ring structures and benzenoid rings, reduces the energy required to cause an electron to jump HOMO to LUMO. For a simple polyene structure this energy reaches the visible spectrum when there are 8 conjugated double bonds present. A similar transition occurs when 6 benzenoid rings are present in the structure.

The energy required for transition of electrons in a conjugated system can also be reduced by the addition of acceptor groups that effectively extend the conjugated system by either direct conjugation or involving non-bonding p-orbitals that interact with the π-orbital system. Typical acceptor groups include nitrate, cyanide, carboxylate and carbonate groups. Donor groups such as primary, secondary and tertiary amines and hydroxides can be added that can pump electrons into the conjugate structure.

Measuring Colour

There are a number of standard scientific instruments for measuring colour as well as a variety of specialised instruments used in specific fields. Spectrophotometers are the most sophisticated and versatile instruments used for colour measurement. Spectrophotometers provide the most detailed information and are the most accurate. They provide spectral data for reflectance and/or transmittance against wavelength over either a continuous or stepped spectrum.

Colorimeters are a less sophisticated instrument commonly used in the measurement of colour. The colorimeter uses filters to approximate the tristimulus colour matching functions of the standard observer. These instruments may still be adequate for industrial colour matching but the increased affordability of spectrophotometers means they have little value for scientific research.

Wood Colour

The aesthetic appeal of wood as a material used for decorative purposes is based on a number of properties. Wood species have different grain structures, which are perceived as the contrast in colour between different parts of the wood structure when viewed as a surface. There is a diversity of colours for wood from very light yellow colours (Holly), browns (Beech and Teak) and reds (Cedar), through to dark brown and black (Walnut and Ebony). The colours of various species expressed using the CIELab colour space are shown in Table 4 below. The data in this table shows that there are a wide range of colours and in particular there is a wide range of lightness values for different species. Radiata pine is considered to be a light coloured wood and has a lightness normally of 80-85 when dried at low temperatures for appearance grade timber.

The colour and visual texture of a wooden surface is also determined by how the surface is treated. Williamson and Dawson (2003) quoting Dawson et al. (1993) show that finishing a surface with coarse sandpaper increases the lightness when compared to a sawn surface. Further finishing with fine sandpaper actually reduces the lightness compared to both the sawn and coarse sandpapered surface. This

is similar to the results presented by Sullivan (1967) where a decrease in the grit size used to prepare a wood surface reduced the luminence (similar to lightness) and increased the purity (saturation) of the wood colour. These results can be explained by the principles mention in the section on light and mater earlier in this chapter.

Table 4 Wood colour of various different species expressed using the L*a*b* colour space.

Common Name	Botanical Name	L*	a*	b*	Reference
Ebony	*Diospyros crassiflora*	26.2	0.5	0.8	Janin et. al. (2001)
Wenge (FS)	*Milletia laurtentii*	36.6	7.0	8.4	Janin et. al. (2001)
Purple Heart	*Peltogyne venosa*	38.1	17.9	3.7	Janin et. al. (2001)
White Oak	*Quercus alba L.*	65.36	5.7	21.06	Beckwith (1979)
Northern Red Oak	*Quercus rubra L.*	67.79	6.86	20.80	Beckwith (1979)
Scarlet Oak	*Quercus coccinea Muenchh*	70.93	6.80	19.82	Beckwith (1979)
Yellow Poplar	*Liriondendron tulipifera L.*	81.30	0.17	18.76	Beckwith (1979)
Red Maple	*Acer rubrum L.*	84.10	2.70	14.61	Beckwith (1979)

The chemical composition of wood is approximately 71% carbohydrates, 27% lignin and 2% extractives. The carbohydrates in wood do not absorb light in the visible region as they do not contain sufficient conjugated double bonds and donor-acceptor groups. The lignin and the extractive compounds do however absorb visible light, particularly in the UV-blue region. It is therefore the lignin and extractive compounds that are responsible for giving wood its colour. Gao (2005) has shown that the darker colour associated with compression wood in radiata pine is due to the higher levels of lignin in this type of wood.

Using the ISO#2469 brightness (k/s) as a standard for wood colour Gao (2005) has shown that the two coefficients that make up the brightness are influenced by different properties of the wood being measured. The absorption coefficient, k, is mainly influenced by the lignin and extractives content of the wood while the scattering coefficient, s, is mainly affected by the wood density, moisture, extractives and the surface texture.

The chemical structure of lignin is not fully known as it is very complex and, in most cases its chemical properties attract more attention than its chemical structure. The structural units that have been identified in softwood lignin contain one or more benzenoid ring structures and when the units are combined to form the three dimensional network polymer there are also a number of hydroxide groups present that act as electron donors and carboxylate groups that act as electron acceptors (Kininmonth & Whitehouse, 1991). It is the combination of resonance ring structures and electron donor-acceptor groups that gives the lignin its visible light absorption properties.

The nature of the extractives present in radiata pine is better understood than the lignin as these are simpler organic compounds with more clearly defined structures. Many of the extractive compounds such as the stilbenes and polyphenols have resonance structures and donor-acceptor groups that make them appear coloured.

Colour Change in Wood

There are a number of processes that may cause a colour change in wood, these can be divided into microbial and non-microbial (Williamson & Dawson, 2003). The development of microbial stains will not be covered in this review as the problems associated with these types of stains in radiata pine wood can be controlled with chemical treatment before drying and the drying processes normally used in New Zealand inhibit this form of staining.

The non-microbial staining of wood can be divided into three categories: chemical, mineral and enzymatic with the first category being responsible for discolouration of Radiata pine during drying (Williamson and Dawson, 2003). The form of staining that is of primary concern to the New Zealand timber industry is kiln brown stain.

Kiln Brown Stain

Kiln brown stain is a brown discoloration that forms near the surface of kiln dried radiata pine boards. It is often unnoticeable while the timber is rough sawn but is revealed when the surface is removed in downstream remanufacturing. The stain is not a problem for structural grade timber but has a major impact on the use of the timber for appearance purposes. The colour of the stain is quite different from the colour of the normal wood and is not uniform in intensity or coverage.

Most of the current understanding of kiln brown stain comes from research performed at the Forest Research Institute at Rotorua, New Zealand, during the 1990s (McDonald et al., 2000, 1997; Kreber et al., 2001, 1999a, 1999b, 1998a, 1998b, 1997; Kreber and Haslett, 1998, 1997a, 1997b; Wastney et al., 1997; Laytner, 1994). The research at FRI focussed on gaining an understanding of the mechanism of kiln brown stain formation and also on methods for preventing it from occurring. More recently research has been undertaken at the University of Canterbury (Pang and Li, 2006, 2005; Dieste and Williamson, 2002; Dieste, 2002; McCurdy et al., 2001) with the aim of understanding and solving the problem. There is now also an increasing contribution from international researchers, as wood dryers overseas increase the temperatures of their kilns and encounter similar problems.

The following review of kiln brown stain research will be split into two parts. The first part will cover fundamental research into the mechanism of kiln brown stain formation and related research that aids in this understanding. The second part will focus on different attempts at solving the problem of kiln brown stain that have been published.

The Mechanism of Kiln Brown Stain Formation

The generally accepted mechanism for the formation of kiln browns stain is as follows: During drying sap is drawn to the surface of drying boards where the moisture and other volatile compounds evaporate into the passing air. The non-volatile compounds in the sap are deposited at the surface and increase in concentration as drying proceeds. The various compounds at the surface then react to form the coloured substances that appear as kiln brown stain.

Movement of Sap Compounds

The movement and accumulation of non-volatile sap compounds, also referred to as redistribution, is the first step in the formation of kiln brown stain. This phenomenon has been studied by a number of researchers. Researchers have measured the redistribution of low molecular weight sugars (Long, 1978; Terziev et al., 1993; Theander et al., 1993), soluble nitrogenous compounds (King et al., 1974; Boutelje, 1990), sugars and nitrogenous compounds (Kreber et al., 1998a; Terziev, 1995) and the redistribution of soluble carbohydrates (Macfarlane et al., 1983).

Long (1978) measured the redistribution of glucose and xylose during the air drying of 55mm Scotch pine (*Pinus sylvestris* L.) boards. These experiments showed that the concentration of glucose at the surface was approximately ten times greater than in the centre at the end of drying. In this case the thickness of the surface sample was 2mm. In a follow up study by Macfarlane et al. (1983) using a similar experimental technique the same result was found for Scots pine but Sitka spruce (*Picea sitchensis* Carr) only showed slightly more than two-fold increase in sugars at the drying surface. This difference was attributed to the lower permeability of spruce compared with pine.

Boutelje (1990) studied the movement of nitrogenous compound in two species, *Pinus sylvestris* (pine) and *Picea abies* (spruce). In this study the nitrogen content was measured by two methods and expressed as absolute values and ratios of surface and centre nitrogen levels. The measurements were taken on the end, radial, tangential and edge surfaces of the boards. The results of these experiments showed that there was a small increase (<2×centre levels) in nitrogen levels at the surface in boards without yellowing. Conversely there was a significant increase in surface nitrogen levels (2-4.5×centre levels) in boards that had yellowed. In this case the boards used were 65mm thick and the surface layer analysed was 1-2mm thick.

Terziev et al. (1993) used 50 mm boards taken from the same stand used by Boutelje (1990) and show an approximately 16-fold higher concentration of low molecular weight sugars at the surface compared to the centre at the end of drying under a fast schedule. A slow schedule with a similar dry bulb temperature (59-60°C) but smaller wet bulb depression showed lower concentration at the surface. The authors conclude that the drying schedule has a significant effect on the redistribution of sugars during drying and also suggest that there may be some movement of sugars below fibre saturation point. If confirmed, the possible explanation is that the bound water diffusion carries the sugar but this needs further investigation as below fibre saturation point vapour flow is dominant and this cannot transport sugars.

Another explanation for the results becomes apparent when they are plotted graphically as shown in Figure 13. The peak in sugar concentration at the surface is narrower for the fast schedule than it is for the slow schedule. The concentration further away from the surface is however higher for the slow schedule. The most likely explanation for these observations is that during the slower schedule the sugars have more time to diffuse back into the core of the board driven by the concentration gradient. At the same drying temperature, the temperature of the board will also be greater in the slow schedule due to the smaller wet-bulb depression which will increase the rate of diffusion. The diffusion is also against the

direction of bulk flow of liquid in the board and the slower drying rate means that the bulk flow will be slower in the slow schedule. There is also the possibility of movement of water by osmosis up the concentration gradient playing a part in the redistribution.

A further study by Terziev (1995) using the same schedules showed an approximately two-fold increase in the surface concentration of nitrogen for the fast schedule with a smaller increase for the slow schedule. The concentration of nitrogen further below the surface was slightly higher for the slow schedule. This study also showed that there was no significant increase in nitrogen concentration at the surface of air-dried boards.

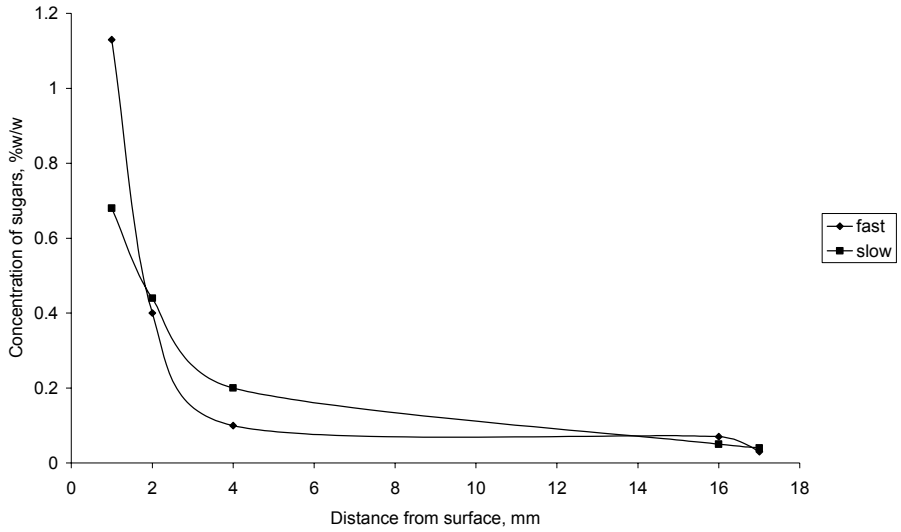

Figure 13 Concentration of low molecular weight sugars in wood after drying at two different schedules (adapted from Terziev et al., 1993).

Kreber et al. (1998a) also showed an accumulation of kiln brown stain precursors (nitrogen and sugars) occurs during drying at two different schedules with dry-bulb/wet-bulb temperatures of 90/60°C and 120/70°C. For both schedules the nitrogen levels were more than doubled at the surface over the period of drying. In this experiment 5mm thick samples were taken from the surface layer of the 40mm thick boards tested. The total extractive yield from the surface of the 120/70°C sample continued to increase when the surface was below the fibre saturation point. The authors attributed this increase to the hydro-thermal degradation of hemi-cellulose.

Studies on 50mm thick *Pinus radiata* boards dried using a high temperature schedule (120/70°C) showed an approximately six-fold increase in total sugars in the 5mm closest to the surface (Dieste, 2002). . The nitrogen concentration increased by a factor of about 1.4 in the surface layer. Given that the schedule used is fast the peak in concentration is likely to be narrow so the actual concentration is likely to be diluted by the thick surface layer removed for analysis in this study. If it is assumed that most of the sugars and nitrogen were in 2mm of the sample taken then the concentrations should be similar to those found by the studies mentioned previously.

Overall there appears to be a 10-20-fold increase in sugars at the surface of wood during drying for permeable species like Pinus radiata. In the experiments noted above the size of the boards used was similar (50-65mm in thickness) so it is difficult to draw any conclusions as to the effect which board thickness has on the concentration of sap compounds at the surface. It is however reasonable to assume that the potential surface concentration is higher in thicker boards due to the lower surface to volume ratio. The increase in nitrogen at the surface seems to be about 2-fold, which suggests that the nitrogenous compounds are less mobile compared to the sugars.

The initial concentration and location of compounds will also influence the surface concentration during drying. There is considerable variation in sap compound depending on environmental factors. Paterson (1975) showed a 3-fold variation in concentration of glucose and fructose in Pinus radiata sapwood over a year. This did not appear to be a perfectly cyclic variation with season as the second spring levels were not as high as the first spring levels. A similar seasonal variation was identified by Cranswick et al. (1987). This variability makes it difficult to determine a starting concentration for sugars and nitrogenous compounds in green Pinus radiata.

Wood Colour Changes by Maillard Reaction

The thermo chemical reaction of sugars and nitrogenous compounds is known as the Maillard reaction named for Louis-Camille Maillard who first described the reaction in 1912. Given the existence of these compounds in virtually every biological system the reaction has far reaching consequences particularly in food science and medicine (Fayle & Gerrard, 2002).

The nature of the Maillard reaction has not been fully defined and in fact little is known beyond the first few steps in the reaction. The first steps of the reaction are a series of reversible reactions the carbonyl group on a sugar molecule forms a Schiff base with the amine group on a protein or amino acid. This Schiff base undergoes further sequential rearrangement to form an aminoketose defined as the Amadori product. Beyond the Amadori product, which is colourless for a reaction involving a simple amino acid, the possible reaction mechanisms become increasingly complex. This is because the products of the different reactions are themselves reactive and form different compounds depending on what other reactants they encounter. The end result of these reactions is assumed to be the formation of large amorphous polymeric structures known as melanoidins. While these structures are not clearly defined, due to the huge number of possibilities, proposed structures have multiple ring structures (non-benzenoid) and also many donor-acceptor groups such as amines and carboxylates (Tressl et al., 1998). Clearly the presence of resonance structures and donor-acceptor groups in the melanoidins reduces the energy required to excite electrons in the molecular orbitals allowing the absorption of visible light. This is exhibited in the colour of the Maillard reaction products that range from yellow through to dark brown-black.

In 2000, McDonald et al published a paper describing extensive research into the chemical nature of kiln brown stain. This paper presents a variety of research based around the chemical analysis of sap and extracted sap samples. The experiments achieve complete elimination of kiln brown stain through

removal of the sap and hot water extraction of soluble compounds. The compounds present in largest quantities in the extracts were sugars, cyclitols, proteins, free amino acids, lignins and tannins. The first four of these substances can easily act as reactants in the Maillard reaction and the latter two can also probably react as well. This paper provides evidence that the Maillard reaction is the dominant cause of kiln brown stain formation.

Characterization of Kiln Brown Stain Formation

Some work has been done to determine the rate of the Maillard reaction that produces kiln brown stain. Dieste and Williamson (2002) developed an empirical model for colour rate from measurement of surface colour of Pinus radiata wood during high temperature drying (120°C/70°C). This model related the development of colour to the concentration of nitrogen at the surface and is shown in Equation (2.17) below.

$$\frac{dC}{dt} = k \cdot [N]^m \qquad 2.17$$

In this equation [*N*] is the concentration of nitrogen in the wood in the 5mm closest to the drying surface and t is the drying time in hours. *C* can be one of three colour variables shown in Table 5 along with the rate constant, *k*, and the reaction order, *m*.

This model was based on only four observations of drying time so there were only four data points (each with 12 repetitions) for calculating the fit of the kinetic equation. This may explain why the data fit so well to the equation. This work was useful in that it shows the importance of surface nitrogen concentration in the development of colour during drying and describes a very rigorous approach to the measurement and modelling of colour development.

One limitation of this model, however, is that it only describes the colour development for one drying schedule and this schedule is at a much higher temperature than that normally used for appearance grade timber. Secondly nitrogen concentration is not easily measured and is not likely to ever be measured in a commercial drying operation; there is currently no technology to allow the continuous monitoring of surface nitrogen levels during drying. For a model to be useful commercially it must be based on variables that are easily measured, understood and controlled in a commercial environment.

Table 5 Rate constant and order from equation 1 for different colour variables. From Dieste and Williamson (2002).

Colour variables	m	K	R2
Y	0.979	0.826	0.925
R457	0.614	0.528	0.924
b*	0.156	0.342	0.923

Sehlstedt-Persson (2003) developed colour change models for pine and spruce based on the colour change in heat treated sap. The factors in these models were temperature and time, which could roughly

correspond to drying temperature and drying time. The equation developed for pine is shown below in Equation (2.18).

$$\Delta E^*_{ab} = -1.43 + 0.066 \cdot T - 5.31 \cdot t + 0.09 \cdot T \cdot t \qquad 2.18$$

In this equation T is the temperature in °C for the range 60-95°C and t is the time in 24h periods for the range 0-5. This is a useful model as it expresses the development in terms of variables that can be measured and controlled in a commercial kiln drying environment. It is also useful because the colour is expressed in the same units as those used to measure the colour of wood. Two aspects that are missing from this study, however, are validation against real drying data and the effect of increased concentration of sap at the surface during drying. In addition this study does not account for the involvement of the cell wall material in the development of colour.

McDonald et. al. (1997) measured the reaction rates of various artificial sap solutions and radiata pine sap extracts. This study produced colour development rates, based on absorbance, for different temperatures but not a model of colour development. Some of the results from this study are shown below in Table 6. The synthetic KBS solutions were made by mixing 0.2M solutions of glutamic acid and the sugar in equal parts. This concentration corresponds to 29.4g/L of glutamic acid, 36g/L of glucose and fructose and 68 g/L of sucrose. The concentrations of each of these compounds in sap are 0.4071g/L, 0.1194g/L, 0.1273g/L and 0.5337g/L respectively (McDonald et. al., 2000) so the concentrations used are both significantly higher and in different ratios to that of real sap.

Table 6 Relative rates of absorbance increase (@ 280nm relative to glucose at 60°C) for synthetic KBS trials (sugar + glutamic acid). Data from McDonald et.al. (1997).

Temperature (°C)	Glucose [abs/h]	Sucrose [abs/h]	Fructose [abs/h]
60	1 [0.002]	3 [0.005]	10 [0.016]
80	10 [0.017]	33 [0.058]	63 [0.115]
100	33 [0.223]	120 [0.839]	800 [1.44]
120	900 [1.64]	2200 [3.91]	3200 [5.69]

The experiments did however show that the chromaphores produce by the artificial solutions at 220nm and 280nm were similar to those produced by real sap solutions heated under the same conditions. This suggests that the artificial solutions are a reasonable substitute for real sap. The results also show that fructose produces a far greater rate of colour change than glucose and sucrose, a disaccharide of fructose and glucose, has an intermediate rate.

Stenudd (2004) developed models to describe the colour response in silver birch (*Betula pendula* Roth.) during kiln drying. This model predicts the change in the lightness chroma and hue of the wood colour from the drying temperature and humidity. The technique was however applied to the core of the boards dried so was not measuring kiln brown stain and the colour responses were not indicative of a Maillard reaction mechanism.

In a similar study Sundqvist (2002) measured the colour development in Scots pine (*Pinus sylvestris* L.), Norway spruce (*Picea abies* L. H. Karst) and birch (*Betula pubescens* Ehrh.). The temperatures used for the drying of the pine and spruce varied from 48°C to 82°C during the capillary phase and 84°C to 111°C during the diffusion phase. In this study the colour measurements used as a basis for producing predictive models were taken from 3mm below the surface which means the majority of the kiln brown stain layer was probably removed. Therefore, focus is on model prediction of core colour change rather than the formation of kiln brown stain.

In the two models by Stenudd (2004) and Sundqvist (2002) the colour was only measured at the end of each drying run so the models developed give no indication of the rate of colour formation during drying.

Opportunities for Reducing Kiln Brown Stain

On the basis that the formation of kiln brown stain is due to a transport process and a chemical reaction, there are a number of opportunities within the wood drying process to reduce or eliminate the KBS. These opportunities can be split into three categories; those that are applied before the drying process, or pre-treatment processes; those that are applied during the drying process, or modified drying processes; and those that are applied after the drying process, or post-drying processes.

Pre-treatment Processes

A number of studies have been conducted that have attempted to find a solution to eliminate the kiln brown stain, the majority of them being pre-treatment processes. Biological treatment (McCurdy et al., 2002) showed some promise for removal of the kiln brown stain precursors based on the reduction of carbohydrate content in water stored logs (Powell et al., 2000). The technique used did eliminate the formation of kiln brown stain due to two effects. Firstly, a combination of leaching and bacterial metabolism reduced the levels of soluble compounds in the sap. Secondly, the bacteria destroyed the bordered pits so that they could not aspirate. This meant that the evaporative front did not stay at the surface and therefore no accumulation could occur. Unfortunately the bacteria also caused the wood to darken considerably which worsened during drying.

Compression rolling has been shown to reduce the incidence and severity of kiln brown stain for two schedules (Kreber and Haslett, 1997b). The mechanism of this treatment is considered to be due to densification and pit aspiration in the surface layer thus reducing the surface permeability and impeding transport of stain precursors to the surface. The decrease in surface permeability also increases the drying time significantly which is a negative effect. On further economic analysis (Kreber & Haslett, 1998) the decrease in kiln brown stain was deemed insufficient to justify the cost of the compression rolling process.

Sap displacement (Dieste, 2002; Kreber et al, 2001) and chemical inhibitors (Kreber et al, 1999a; Kreber et al, 1999b; Schmidt and Kreber, 1998; Kreber and McDonald, 1997) have been used as pre-treatments. In all cases these processes were successful in reducing or eliminating stain but were not considered economically viable.

Modified Drying Processes

Vacuum drying was found to partially reduce the occurrence of kiln brown stain at conventional temperatures (70°C) but not at lower temperatures (Wastney et al, 1997). It did not however eliminate the stain and the colour of the stain was altered to a grey/tan. In a study using modified drying media, in the form of inert gasses and alcohol vapours a reduction in colour was noted for small samples dried at 50°C, 70°C and 90°C (Pang and Li, 2005; 2006). The processes did not however eliminate the formation of stain completely and would be difficult to implement in standard kilns. These two studies show that oxygen probably plays a role in the formation of kiln brown stain but that the stain can still develop in an oxygen-free atmosphere.

Modified drying schedules have been tried where the temperatures and humidities at different parts of the schedule are manipulated with only limited success. In a study by Kreber et al. (1998) it was shown that the combination of high air velocities and lower temperatures reduced the formation of stain but the rate of drying was still considered to be too low to be economically viable.

It is generally accepted that increasing drying temperature increases the severity of kiln brown stain (Kapp et al., 2002; Tarvainen et al., 2001; Haslett, 1998). The use of sufficiently low temperature schedules to reduce kiln brown stain has been considered as unviable in the New Zealand forestry sector where ACT schedules are encouraged (Kreber & Haslett, 1998). In spite of this there are commercial operations in New Zealand that do dry wood using lower temperatures (70°C) to minimise stain (Fogarty, 2003). This happens where the business has a good resource for the production of appearance grade timber and an export market that pays a premium for light coloured wood (Brightwood, 2003). Within industry various schedules have been developed, though these are generally kept secret and it is difficult to gauge their success.

Post-drying Processes

Generally it seems that industry has adopted a post-drying process involving the mechanical removal of the kiln brown stain layer as recommended by Kreber and Haslett (1998), basd on the economic analysis. This method is used particularly for appearance grade timber dried for local New Zealand markets where a slightly darker product seems to be acceptable (Sutherland, 2004).

Summary and Knowledge Gaps

There is a good understanding in the literature of the overall mechanism of kiln brown stain formation though there is some uncertainty as to the relative importance of different elements of this mechanism. An example of this is that there is significant work on the accumulation of stain precursors in the surface zone of wood during drying but only a small understanding of what effect this has on the colour change.

Studies on the effect of different kiln schedules on the formation of kiln brown stain also tend to focus on schedules that are currently in commercial use. While this may be a relevant way of analysing commercial schedules it also means that the data for colour development is over a limited range of

temperatures and relative humidity. If the solution to kiln brown stain lies in a schedule that is different from the standard commercial schedules then it will be difficult to find with this approach.

Some work has been done to quantify the formation of kiln brown stain, however thus far the rate of colour change at different temperatures has not been determined. The majority of the colour change models available are for a specific species and a specific schedule and give the final colour at the end of drying rather than simulating the progressive development of colour throughout the drying process. Again these sorts of studies may be useful for analysing a commercial drying operation but they provide little information for optimising the colour of the dried wood.

There are also few practical solutions available for combating the problem of kiln brown stain. This reflects the difficulty of finding a solution, especially when commercial viability is the main issue.

Chapter 3

Equipment and Experimental Methods

Introduction

This chapter will describe the various pieces of equipment and experimental techniques used and developed during the course of this project to quantify wood colour and wood colour changes with drying. These aspects of the project are common across the various experiments to be described in the following chapters. Basic calculation and analysis techniques are also included. They have been brought together in one chapter to avoid repetition and reduce the size of subsequent chapters.

The equipment used in the project will be described first followed by the experimental methods used with the equipment and the calculations and analysis methods will be described at the end of the chapter.

Equipment

A number of different items of equipment and apparatus were used for both the treatment and the measurement of samples. These equipment items have been categorised in the following way; drying equipment, drying control and drying rate measurement, colour measurement and sampling equipment.

Drying Equipment

The drying operation was the key part in the subject being investigated so drying equipment was clearly essential to the project. There were three main items of drying apparatus used along with ancillary equipment. The largest boards were dried in a semi-scale kiln smaller boards were dried using a drying tunnel and smaller samples were dried using a drying chamber. Ancillary equipment included various ovens and a freeze-dryer.

Semi-Scale Kiln

The semi-scale kiln that was used is located in the Wood Technology Workshop in the School of Forestry at the University of Canterbury. This is a small-scale experimental box kiln built by Windsor Engineering Ltd. A composite photograph of the kiln is shown in Figure 14. The kiln can take a stack of up to 96, 50×100mm boards of 2.4m in length. It has dual, reversible, overhead fans, heating coils, an external water bath and a pneumatic steel stack restraint. A computer, connected to a PLC, both shown on the right of the photograph, controls the conditions in the kiln, with input from wet- and dry-bulb thermometers in both of the plenum chambers. The kiln is capable of operating from low to high temperature drying.

A dummy stack, comprising kiln-dried, rough sawn 50×100mm clear radiata pine boards, was built 6 boards wide by 14 boards high as illustrated in Figure 15. The photograph only shows 12 layers as the two layers containing the samples boards have been removed. Five fillets, each 20×30mm, were place in spaces between the layers of boards. The top three layers of the stack were nailed together and fixed to the pneumatic stack restraint. The bottom nine layers were stacked normally, on the kiln trolley, without any nails holding them together. In the remaining two layers were where the sample boards were placed. The outermost boards on either side of these layers were fixed to the lower fillets with screws. The upper of these layers was attached to the top of the stack with chains so that when the stack restraint was partially raised there was a gap sufficient for the sample boards to be removed from this layer. When the restraint was fully up the upper sample layer was lifted off the lower sample layer so that the lower sample boards could be removed.

Figure 14. Composite photograph of the semi-scale kiln designed and built by Windsor Engineering Ltd located in the Wood Technology Laboratory, School of Forestry, University of Canterbury. The kiln is the boxed shaped object in the centre of the picture with the PLC in the right background and the control computer in the right foreground. The dummy stack can be seen on the far left.

Drying Tunnel

The drying tunnel used in this project is located on the mezzanine floor of the Denham lab in the Chemical and Process Engineering Department. The tunnel was commissioned in 1997 and was designed for the drying of single boards at high temperature kiln conditions (McCurdy, 2000).

The drying tunnel is a closed circuit wind tunnel as shown in Figure 16. This picture shows the tunnel in its original configuration as it was used in the early drying experiments. As can be seen in the picture the drying tunnel comprises of a number of sections each with a role in the operation of the tunnel. All of the ducting in the tunnel is made from stainless steel to cope with the corrosive nature of the wood drying

atmosphere. Connections between sections are sealed with silicone rubber gaskets chosen for high temperature and corrosion resistance.

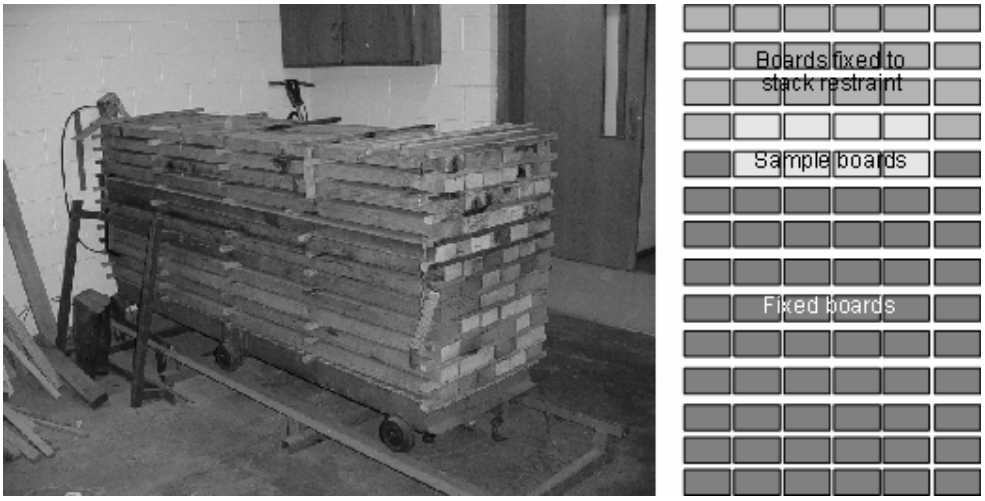

Figure 15. The timber stack made up to go into the semi-scale kiln. The diagram on the right shows the arrangement of boards within the stack.

Figure 16. Closed circuit drying tunnel used for drying single boards located in the Denham semi-scale Laboratory. Air circulation is clockwise.

The fan is a stainless steel centripetal fan that provides the air flow in the tunnel. The fan volume is 1 m^3/s^1 and has a 4kW motor. Due to the closed return of the wind tunnel the fan is able to develop high air

speeds in the tunnel, up to 25m/s, depending on the air temperature and humidity. Airspeeds below about 3m/s are not recommended as the interlock system may trip out. The fan sucks air from the lower level of the tunnel and blows it through a duct into the settling chamber. The fan sits on rubber mountings and the ducting insulated to reduce noise and vibration.

Air from the fan enters the settling chamber through a small circular duct. The large cross sectional area of the settling chamber slows the speed of the air through this section. This reduction in airspeed is necessary to limit the pressure drop across meshes located at the exit of the chamber leading into the contraction cone. The purpose of the meshes is to minimize the size of turbulent eddies in the air-stream.

The contraction cone connects the settling chamber to the test section and has two main purposes. Firstly the contraction cone reduces the cross sectional area of the tunnel down to that of the test section. This increases the airspeed. Secondly the contraction cone has curvature to give a uniform flow profile at its exit. The contraction cone has bevelled corners to prevent turbulence created by the boundary layer detachment, which can occur more readily at sharp corners. The air from the contraction cone feeds into the test section.

The test section is probably the most important part of the tunnel as this is where the samples are tested. The test section has a square cross section that is even along the entire length and the bevelled corners are continued from the contraction cone. There is a centrally located door on one side to allow access to the sample holder.

The sample holder has been designed to allow the wood sample being dried to be suspended from a balance. The sample holder, shown in Figure 17, consists of a cradle attached to a stabilising system, which is attached through a seal to a balance. The cradle, which is made from stainless steel rod, allows multiple blocks to be dried and easily removed during a run. The cradle has a small area of contact with the blocks and has a thin profile to minimise the effect on the air stream.

The stabilising system prevents the sample holder from moving around too much in the air stream thus reducing fluctuation in the balance readings. This consists of four hinges in a square formation, which prevents movement in any direction other than the vertical. These hinges are made from glass fibre fabric and stainless steel to minimise friction.

The seal mechanism has four wires attached at one end to the cradle and at the other end to the balance frame. These wires each pass through one of four ring magnets set in a Tufnel plate. There is a ferromagnetic fluid, comprising silicone oil, magnetite powder and a surfactant, suspended in the magnets that seals around the wire. This system is to minimise the effect of air pressure fluctuations in the tunnel on the balance measurements.

The sensor section houses the temperature and humidity sensors that are used to control the conditions within the tunnel. There is also an extra port in this section which allows for an air speed probe, such as a pitot tube or hot wire anemometer, to be inserted into the airstream. The pitot tube is more commonly

used when the tunnel is running at high temperature, while the hotwire anemometer is used at temperatures below 80°C.

The return bend reverses the airflow from the sensor section back towards the fan for another circuit through the tunnel. Air from the return bend flows into the heating section.

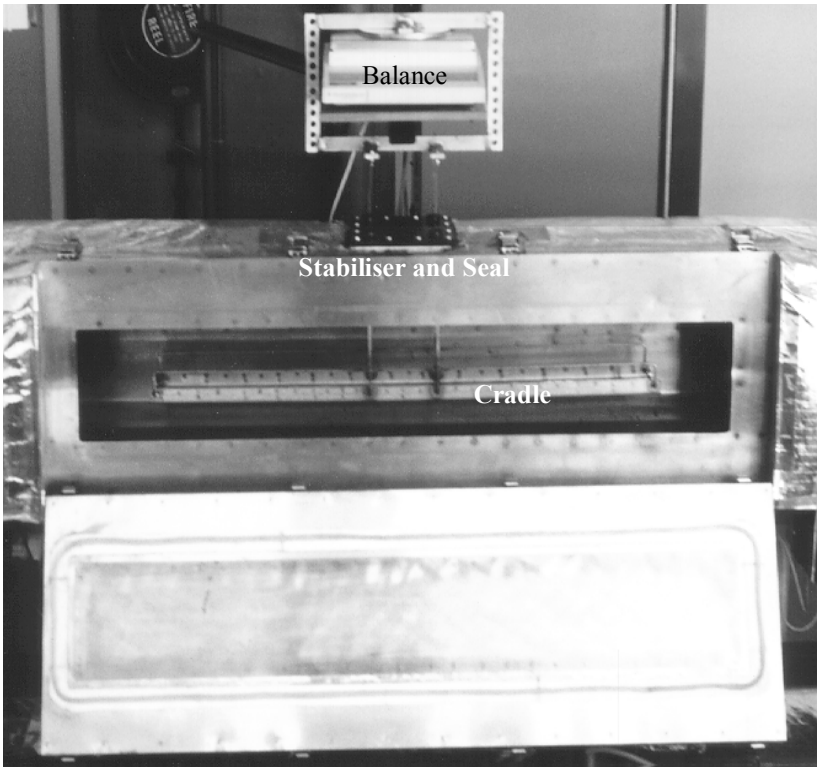

Figure 17. The test section of the drying tunnel with the door open, showing the sample holder.

The heating section contains a nichrome wire heating element, which is used to control the temperature of the air stream. This is an Avon Electric Ltd. 2.5kW drawer type electroduct element bank. The heating unit can be removed completely for servicing without having to dismantle the tunnel. A mark space ratio controller in the computer program controls the temperature of the heating element. There is an additional slot in this section for another heater or for a cooling unit that may be installed in the future.

The second part of the lower section of the tunnel had a steam inlet and an air inlet for the early experiments. The steam inlet has since been moved to the settling chamber with the addition of a new portable steam generator. The steam inlet allows steam to be added to the air stream to increase the humidity in the tunnel. The steam is fed through a pressure-reducing valve to lower the pressure to 2bar before it enters the tunnel. The air inlet is connected to a compressed air supply and is used to reduce the humidity of the air-stream. This system works well at high temperature but at lower temperatures the steam causes spiking in the humidity and the compressed air input cannot effectively control these spikes.

This can result in a slightly higher average humidity than the set point that needs to be accounted for in the set up of the control program.

A PC running Advantech® Genie™ data acquisition and control software mainly controls the operation of the tunnel. This software controls the temperature and humidity of the air-stream along with the temperature of the tunnel wall. The tunnel wall is trace-heated with Pyrotenax® bare copper element. The Genie™ software also records data from the temperature and humidity sensors along with the mass readings from the balance. A separate independent controller controls the fan. This was originally connected to the computer but produced too much interference with the humidity sensor.

The temperature sensors used for control in the tunnel are platinum resistance thermometers (PRT). One of these temperature sensors as mentioned above is positioned in the air-stream in the sensor section to measure the air temperature and is used for the control of the heating elements. Another PRT thermometer is attached to the outside of the wall of the test section to measure the wall temperature to control the trace heating. Other temperatures, not used for control, are measured using thermocouples. One of these is positioned in the fan housing while the others are attached to the wall at different points along the tunnel.

The humidity sensor used in the tunnel is a thin film capacitive element sensor made by HY-CAL Engineering. This sensor directly measures the relative humidity of the air stream with a sensitivity of approximately 1%. This humidity measurement is corrected for temperature in the computer.

The mass of the timber board being dried is monitored using a Sartorius BP8100 balance. This balance has a maximum capacity of 8100g and a reproducibility of 0.05mg.

There are a number of sensors attached to an interlock control on the tunnel to provide a safety shutdown if anything goes wrong during the tunnel operation. A low-pressure cut-out switch was supplied with the heating unit, which shuts off power to the elements if the air speed drops too low. This switch has been put into the interlock as well. Also in the interlock are fusible links that provide over temperature protection throughout the tunnel. The interlock can also be triggered if the computer goes down or by a signal from the computer. Once triggered the interlock must be reset manually on the control panel.

Drying Chamber

The drying chamber used in this project is located on level three of the S. R. Seimon Building in the Chemical and Process Engineering Department. The drying chamber was designed and commissioned as part of a final year project (Dakin, 1996). It was designed to simulate low temperature drying and vacuum for experimental drying of difficult timbers such as Hard Beech and Red Beech.

The chamber has been used for low temperature drying of Beech (Zhang, 2000) and was also modified for measuring the sorption of water into timber at low temperatures (Time, 1997). This modification saw the addition of cooling units so that the equipment could operate below ambient temperature. This project saw a further modification of the heating system as the previous designed prove unreliable, particularly at

the high temperatures and humidities required. The existing thin nichrome wire element was replaced with a heavier ceramic element. This has reduced resistance to air flow and is far more reliable.

Photographs of the drying chamber are shown in Figure 18. The three main parts of the equipment, in relation to the experiments performed in this project, are the humidification column, the air heater and the drying chamber itself.

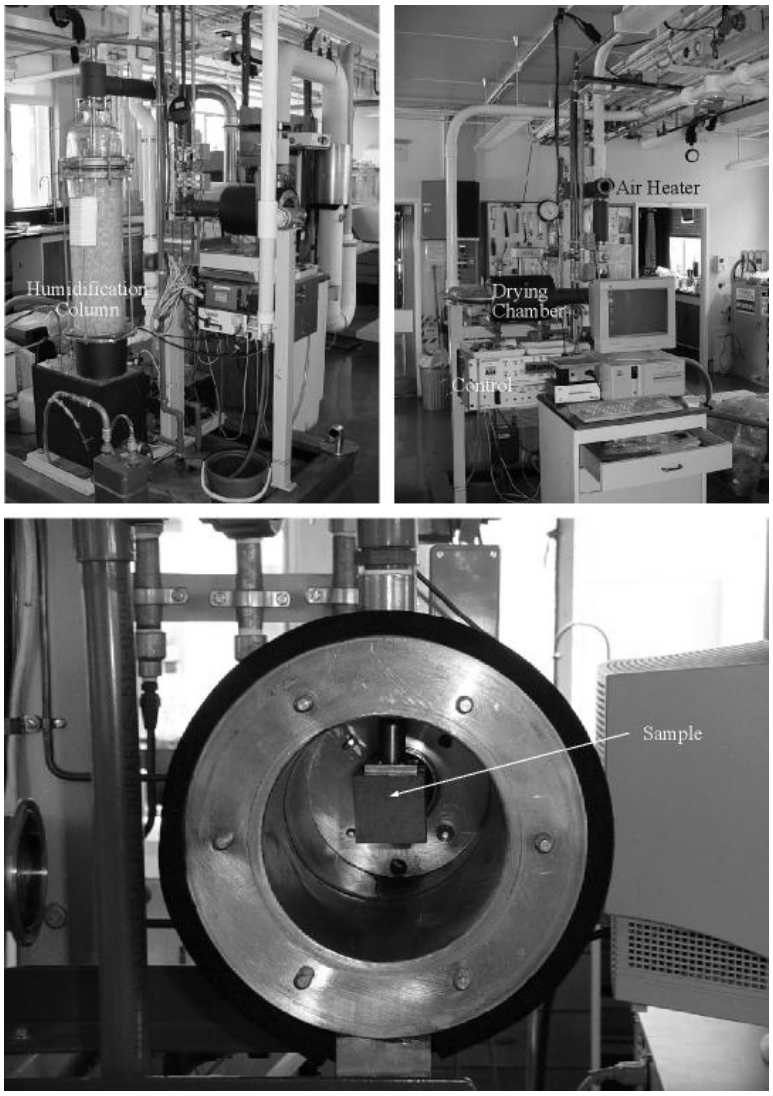

Figure 18. Images of the drying chamber with the upper left picture showing the humidification column at the back of the apparatus and the upper right showing the front of the apparatus and the position of the drying chamber and the air heater

The drying chamber is designed as an open circuit system with the airflow supplied by a Rootes blower located in the basement of the building. The air is fed into the bottom of the humidification column where it flows up through the packed column counter-current with the water flowing downwards. At the top of the column the air is saturated and the temperature is measured to determine the wet-bulb

temperature. This temperature is controlled by controlling the temperature of the water flowing down through the column.

After exiting the humidification column the air flows through the air heating section. The air heater comprises a bare nichrome wire element located inside a stainless steel tube. This element is heated to raise the air temperature to the desired dry-bulb temperature. As noted above part way through the experiments this element failed and was replaced with a heavier heating element.

The air flows from the heater into the drying chamber where it passes over the sample being dried. The sample is suspended in the centre of the drying chamber from a weighing rod. The rod is attached to a load cell that allows the weight of the sample to be measured during drying. The sample is connected to the rod by an attachment that screws onto the sample and connects to the rod with a grub screw arrangement. The chamber has a hot water jacket to prevent condensation at high humidity. During this project the load cell was found to be unreliable so it was only used as an indication of sample weight. The actual weight of samples was measured manually using a balance.

Upon leaving the drying chamber the air is vented to atmosphere. There is an orifice plate in the outlet pipe work that allows for measurement of airflow to ensure consistency between runs.

The wet- and dry-bulb and jacket temperatures in the drying tunnel are controlled by three PID controllers. These can be configured for direct set point input or for remote set point from the apparatus' computer. The computer also records the temperature and humidity during drying as well as the weight of the sample.

Freeze-drier

A Virtis 24DX24 general purpose freeze-drier was used for the drying of samples where it was necessary to avoid heating of the sample while removing moisture. This was important as the Maillard reaction is temperature sensitive. The lack of a liquid phase in freeze drying will also help to inhibit the reaction and reduce the likelihood of coloured compounds moving during the drying process. In a freeze drier samples are cooled so that all of the water is in solid phase. A vacuum is then pulled in the drying chamber which causes the water to sublime, changing from solid to gaseous phase without becoming liquid. The vapour is re-condensed into ice in another chamber that is at approximately -40°C. The freeze-drier is capable of drying at temperatures as low as -29°C but was usually operated at -5°C for this project as the samples dried faster and did not require the lower temperature to retain their shape.

Vacuum Oven

A vacuum oven was used for the drying of samples at low temperatures (below 40°C). This method was used to limit the colour development in samples and is faster and more convenient than the freeze-drier. Standard laboratory ovens, at 104°C, were used for oven-drying samples that were not going to be measured for colour.

Physical Measurement

The two most commonly measured physical properties in this project are temperature and weight. Dimensions and humidity are also measured as well thought often humidity is a derivative of temperatures.

Temperatures were measured by two different means depending on the experimental set up. On most of the large apparatus PRTs were used for temperature measurement, while in smaller experiments not involving plant, thermocouples were used.

Weight was measured using various digital balances around the department with the choice dependant on the size of sample being weighed. Most of the solid wood samples were weighed on a 0.01g resolution balance. Slices and granular samples were usually weighed on a 0.0001g resolution balance. The samples in the drying chamber were initially weighed using a load cell on the apparatus but this gave inconsistent results so the samples were removed and weighed manually on a balance.

Most dimensional measurements used in the preparation of samples did not require a great deal of accuracy so tape measures and rulers were sufficient. With the measurement of slice thicknesses, however, digital callipers with a 0.01mm resolution were used, as these measurements represented data points.

Colour Measurement

Colour measurement is a specialist operation and so requires specialist equipment. The key instrument used for the measurement of colour is the spectrophotometer and two types of these were used in this project. For solid samples a surface reflectance spectrophotometer was used and for liquid samples an absorption spectrophotometer was utilised. A digital camera was also used for relative colour measurement under the microscope and without magnification. Some initial experiments also used a visual grading system on a scale of 1 to 5 to measure the discolouration in boards. This was before the spectrophotometer was available and is considered to be unreliable. It was however performed with all of the samples present that were being compared so give an idea of the relative severity of discolouration.

Surface Reflectance Spectrophotometer

The surface reflectance spectrophotometer used in this project is a Minolta CM-2500d portable integrating sphere spectrophotometer. This instrument uses two pulsed xenon lamps as a light source, a diffraction grating for spectral separation and a silicon photodiode array as the light-receiving element. This array is a dual 40-element device that can measure at 10nm intervals over the range from 400nm to 700nm.

The portable spectrophotometer can operate independently as a unit running on batteries but in this project it was run through both laptop and desktop computers running Spectramagic colour quality control software. The instrument is connected to the computers using a serial cable and this allows the operation of the spectrophotometer to be run entirely from the computer, including settings and calibration. All of the data is also automatically recorded by the software, which means experiments are

not limited by the memory of the instrument. These data files are readily exported into a spreadsheet for further analysis.

The computer recorded the reflectance spectrum for each slice from 400nm to 700nm in 10nm increments. The spectrophotometer measured the spectrum with the specular component included (SCI) and with the specular component excluded (SCE). The SCI data has been used for the analysis; though there were only minor differences between the two sets of data as wood is predominantly a diffuse reflector. The spectrophotometer automatically converted the spectral data into the CIELab colour space coordinate L, a* and b* as well as chroma, C, and hue, h. The last two coordinates have not been analysed in detail for this thesis, though the data are available in the appendices. C and h can be calculated from a* and b* and vice versa.

Absorption Spectrophotometer

A Shimadzu Multispec-1501 absorption spectrophotometer connected to a computer running Hyper-UV software was used for measuring the absorption spectra of liquid samples. This instrument also utilises a photodiode array as the light receiving element and uses a holographic diffraction grating polychrometer for spectral separation. It has a dual light source allowing instantaneous measurement of the absorption spectrum from 190nm to 800nm. The UV light is provided by a deuterium lamp and the visible light by a tungsten halogen lamp. A quartz cuvette was used with this spectrophotometer so that the absorption in the near UV spectrum could be measured as the initial chromaphores produced by the Maillard reaction are known to absorb in the UV region.

Microscope and Camera

Where colour was measure on the microscopic scale a digital camera attached to the microscope was used to capture an image that was later analysed using computer software. The method of analysis will be described later in this chapter. The camera and microscope setup is shown in Figure 19.

The microscope used is an Olympus BX60 with a Nikon CoolPix 900 digital camera attached to it. The microscope can illuminate the specimen from above, for surface microscopy, or from below for transmission microscopy. The light source is adjustable and this adjustment is likely to have an effect on the spectrum of the light reaching the sample being observed. This combined with the fact that the ideal spectrum for the light source is not known means that the colour in the sample cannot be measured accurately using this apparatus. It does however offer a good option for measuring relative colour differences within a sample at a microscopic scale.

Digital Camera

A Sony Cyber-shot DSC-P51 digital camera was used for taking pictures where the microscope was not used. This camera has 2 mega pixels resolution and a 2× optical zoom.

Sampling Equipment

Wood Slicer

The apparatus shown Figure 19 is a wood slice that was used to cut thin slivers of wood from samples. It comprises a clamp system that holds the wood sample, which can be moved towards or away from the cutting blade by means of a threaded rod. The blade is attached to a lever system that is operated by hand to bring the blade downward, perpendicular to the movement of the clamp system.

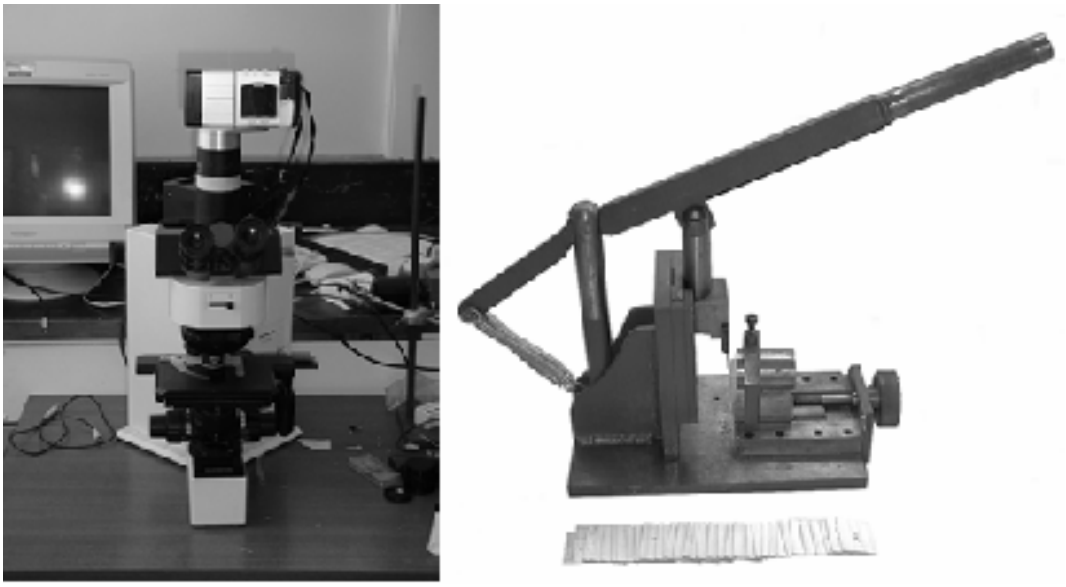

Figure 19. Microscope and camera (left). Wood slicer with examples of wood slices (right)

The cutting action of the slicer is performed in the direction of the grain of the wood sample, or the longitudinal direction. This ensures an easy cut that presents a smooth face for measurement. In the case where the wood grain is at a slight angle to the direction of the cut it is oriented such that the grain angles towards the bottom of the blade stroke. This prevents the slices from splitting along the grain, which results in a poor surface for measurement.

Hydraulic Press

A hydraulic press was used to compress green wood samples to extract the sap. The equipment comprises a large solid frame made from steel channel with two parallel vertical struts supporting a movable platform and a hydraulic ram. The bottoms of the struts are bolted to a concrete slab. The hydraulic ram is positioned above the platform and pushes downward when activated

Wiley Mill and Mortar and Pestle

A Wiley mill with a 2mm mesh was used for the reduction of wood slices into small chips. Between each sample the mill was cleaned out with a compressed air gun. The chips were then processed further in a mortar and pestle to produce a fine powder. The powder was then sealed in plastic zip lock bags for storage until used.

Experimental Methods

The first step in most of the experiments in this project involved obtaining samples of wood. This wood was then prepared to get it into a form suitable for the experimental requirements.

Sample Selection and Preparation

The wood used in this project was all obtained from local sawmills sourcing logs from the West Coast and Canterbury. In the case of large boards used in this project all of the boards were cut from the same log and carefully end-matched and edge-matched. The full size boards dried in the semi-scale kiln were obtained from a local sawmill, being selected from the grading table, based on similarities in density and moisture content. Other than this there was no further preparation for these boards. The boards were treated for sap stain at the sawmill and stored in plastic wraps at 2°C until dried.

Selection and Preparation of Large Boards

The wood used for producing the large boards used in this project originally came from a radiata pine plantation on the West Coast of the South Island of New Zealand. After felling the log was transported to the Craigpine Timber Ltd in Christchurch. It was at this point that the log was selected for producing the large boards for the experiments.

The criteria used for selecting the log were small and central pith, minimal taper and absence of knots. The log was also checked to make sure no sap stain had occurred in transit and storage. The ring structure was also studied to ensure that the log had regular growth rings and was free from compression wood identified by colour. After being selected the log was marked at both ends for sawing in the following day.

The 6m log was then cut into 40×100mm boards using the standard sawmill cutting pattern to maximise flatsawn boards, shown below in Figure 20. Each board was labelled as it was cut so that the log could be reconstructed later in the laboratory to determine which boards were edge-matched. The boards were then transported immediately, by trailer, back to the Wood Technology Laboratory at the University of Canterbury for further processing.

Upon arrival at the laboratory the boards were arranged into edge-matched groups, labelled and then cut into end-matched 1m long sample boards. Boards containing pith, large knots or those that were not flatsawn were discarded. This elimination process resulted in eighteen 1m boards (approximately), eight edge-matched pairs and one non-edge-matched pair.

The initial moisture content of each board was determined by cutting approximately 100mm off each end to produce 800mm boards. The end pieces were then weighed to determine the green weight, vacuum dried at 104°C for three days and reweighed to determine the oven-dry weight. The moisture content of each end was determined and the board moisture content was assumed to be the mean of the two ends.

The boards used of the partial drying runs were each cut into four 200mm boards. Each board was dipped in anti-sapstain chemicals before being painted on the ends and sides with waterproof two-pot epoxy

paint. They were then stored in plastic bags in a 2°C refrigerator until they were to be dried. The refrigeration and anti-sapstain chemicals kept the boards free from any microbial discolouration while in storage.

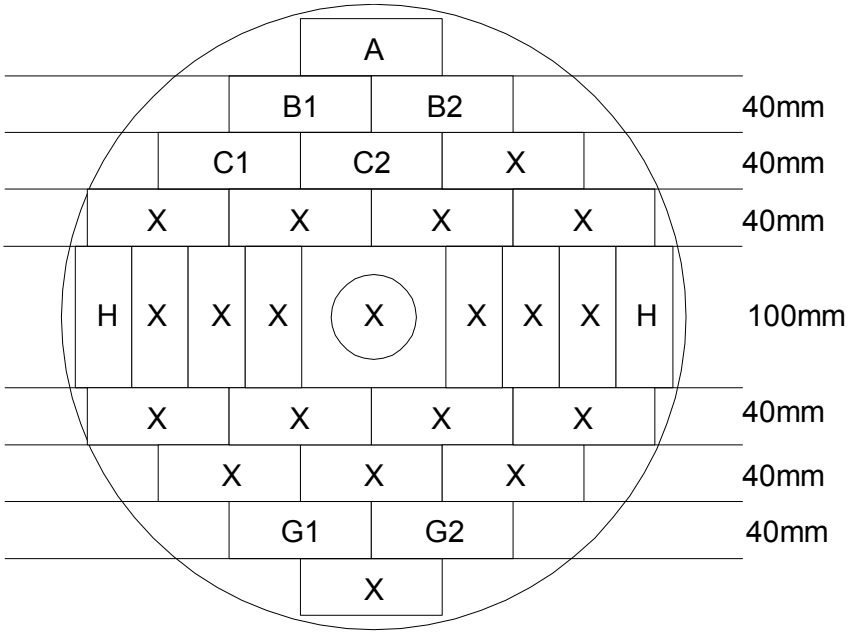

Figure 20. Sawing pattern for sample log. Lines represent initial cuts and X marks discarded boards while boards used for the experiments are marked with letters and numbers.

Selection and Preparation of Small Samples

The preparation of small samples did not require the selection of an entire log as far less wood was required. In this case only a couple of 4m boards were selected from the grading table at the McVicars Sawmill in Christchurch. These boards were selected for being from the outer wood, having high moisture content and free from compression wood. They were also clear of knots and had no microbial or non-microbial discoloration.

Upon arrival back at the lab the wood was immediately prepared. The edges were removed from the 40×100mm boards and then they were split down the middle to produce two sets of edged-matched 40×40mm boards. These were then cut into 100mm long end-matched samples. The two end samples were oven dried to determine the moisture content while the remainder was painted to seal the ends and sides. After painting the samples were wrapped in plastic and frozen for long storage, until needed.

Sample Drying

Depending on the objectives of each test, the drying of samples was performed using the corresponding drying apparatus described previously in this chapter.

Drying of Full-size Boards

The full-size boards were dried in the semi-scale kiln. At the beginning of every run the boards were removed from the refrigerator and weighed to determine the initial green weight. They were then labelled

based on their position in the stack, with a number representing the row (1 or 2) and a letter representing the column (a, b, c or d), and placed in the kiln. The weight of the boards was measured six times during the drying schedule and then at the end of drying. The boards were then removed from the kiln, stacked and allowed to cool to ambient temperature. They were then re-weighed and a sample cut from the middle of each board for the calculation of oven-dry weight.

Drying of Large Single Boards

The drying of large single boards was performed using the drying tunnel. Details of the procedure for running the drying tunnel are in the appendices. At the beginning of each drying run the tunnel was brought to the required drying conditions before the board or boards were added. All of the drying runs performed in this project using this equipment used single-step drying schedules.

In the drying of a large single board the initial mass of the board was measured immediately before drying. The board was then placed in the cradle and centred below the balance. The door of the test section was then closed, the fan speed increased to the required level and the interlock reset. At this point the data acquisition was also activated in the computer to record the drying conditions and the mass of the board.

Whenever more than one board was being dried they were loaded onto the cradle with the first board to be removed upstream and the last board to be removed at the downstream end. The boards were balanced below the cradle and as each board was removed the remaining boards were rebalanced under the balance.

In both of these drying methods the boards were immediately weighed as they were removed from the tunnel for the determination of the moisture content. They were then further processed and tested. A sample was cut from each of the boards for moisture content measurement. This was weighed, then oven dried and reweighed.

Drying of Small Samples

The drying of small samples was performed using the drying chamber. The samples were removed from the freezer and thawed in a refrigerator for 24 hours prior to the start of the experiment. The chamber was brought up to the required conditions before the sample was added. The sample was weighed and then the attachment was screwed onto it. The two were then weighed together before being placed in the chamber.

The sample could be removed periodically during drying simply by opening the chamber and detaching the sample from the load cell rod. The conditions could also be changed to hold the sample at a particular temperature and equilibrium moisture content. At the end of drying the sample was removed from the attachment and weighed, before being oven dried and reweighed for moisture content determination.

Sample Slicing

The boards were sliced using the wood slicer designed for a previous project. The sample size suitable for use in this equipment is a 20-25mm square slicing face. The samples for slicing were prepared from the large boards by first cutting a 25mm thick cross section from a clear part near the centre of the board. A 25mm square block was then cut from this section in a place where the growth rings were roughly parallel to the surface. In a 40×100mm board this produces in a 25×25×40mm block. This process is shown in Figure 21.

The block is mounted in the slicer with the top drying surface facing the blade, aligned so that the slice will be in the longitudinal grain direction. Each slice is labelled as it is cut, and for a moisture content profile weighed immediately. When all of the slices had been cut and weighed, the thickness of the slices is measured. This measurement is performed using digital callipers and the measurement is taken on the top edge of the slice where the blade first entered. This is because the other side can have varying thickness depending on the grain in the wood.

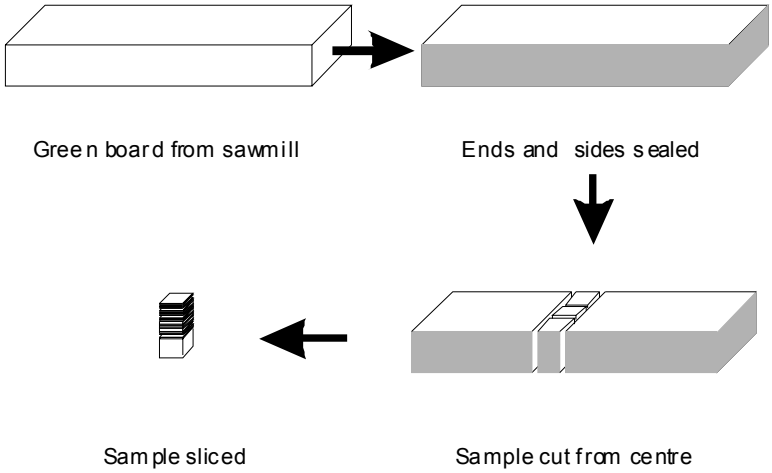

Figure 21. Method for cutting sample blocks for slicing. The upper two processes occur prior to drying and the lower two processes are performed after drying.

Measurement of Checking

The quality of dried timber is also affected by checking which occurs during drying. Two methods were developed to measure checking in this project. Initially for the full-size boards checking was determined by visual inspection. Small, within-ring checks, were counted as 0, <10 or >10 while large, across-growth-ring checks were counted individually. Visual inspection was done at both ends of each board and at 6 cuts (including the cuts for the oven-dry weight sample), roughly equi-spaced along the board lengths for end-checks and internal checks respectively. This simple visual inspection method was also used initially to measure checking in the smaller samples, however no checking was apparent so another method was developed.

Dye Penetration and Image Analysis

This method is based on the idea that the permeability to liquids of dried wood is lower than it is for green wood. This is due to the aspiration of pits, which blocks the pathways for liquid movement in the longitudinal direction of the wood. When internal checks occur in wood they create fine holes in the longitudinal direction of the wood. This should increase the permeability for liquid flow in the wood in this direction as the liquid can now flow through the check. If a pigment or dye were to penetrate into the wood then it would do so through the checks. The checks in the wood will therefore be accentuated by the dye or pigment whereas the rest of the wood will not.

Various pigments and methods of application were tested with the following method being the best tested. The end of the board being tested is dipped in Indian ink for 1 hour and then dried under a vacuum at 50°C for 24 hours. When dried the dipped face is cut off 5mm from the transverse surface using a drop-saw. Checks in the board are emphasised by the blue ink which contrast with the colour of the wood. At this point the checks can be counted visually or analysed using an image analysis technique which was also developed in this project.

For image analysis a picture is taken of the transverse section using a scanner. This produced a RGB TIFF image (Figure 22) that was reduced to a greyscale image of the red component in Corel Photo-paint. This accentuates the blue checks as black while the wood comes out white or grey. The bit plane, of the red image, was adjusted to emphasise tonal changes. There are however still spots of black on the image that do not represent checks.

There were no visible checks in the subsequent samples tested and none of the dye penetration treatments revealed any checks. This means that the samples were probably check-free. For this reason the technique was not developed further in this thesis. It does however seem to work where checking is present and a suitable test method would be to dock samples into 300mm lengths, dip one end of each sample into dye for one hour and then dry. The first 5mm of the dipped end would be removed and the checking measured based on NZS 4787:2001.

Qualitative Measurement of Colour

There are three methods used for the qualitative measurement of colour in this project. These methods are used to determine the relative colour differences within samples, rather than for comparison between samples. In all three cases the methods are only qualitative because a standardised light source is not used.

Image Analysis of Cross-section

This method was originally developed for a previous project to assess the effect of biological treatment on kiln brown stain formation (McCurdy et. al., 2001). The method involves cutting the board being test to expose the cross-sectional face. A digital image of this cross-section is then taken using either a digital camera or a scanner. The scanner offers a more consistent light source than the digital camera as long as

the scanner is run a few times before the actual images of interest are taken, so that the light source in the scanner is sufficiently warmed up to give a consistent spectrum.

The area of the image of interest is then selected using image editing software such as Corel Photo-Paint or Macromedia Fireworks. The selected area is then broken into three separate greyscale images representing the L*, a* and b* coordinates. Each of these images was then converted into a matrix of values using MatLab software. Each matrix was converted into a vector by averaging the values parallel to the drying surface. The resulting vectors were then converted into text files for further analysis in a spreadsheet.

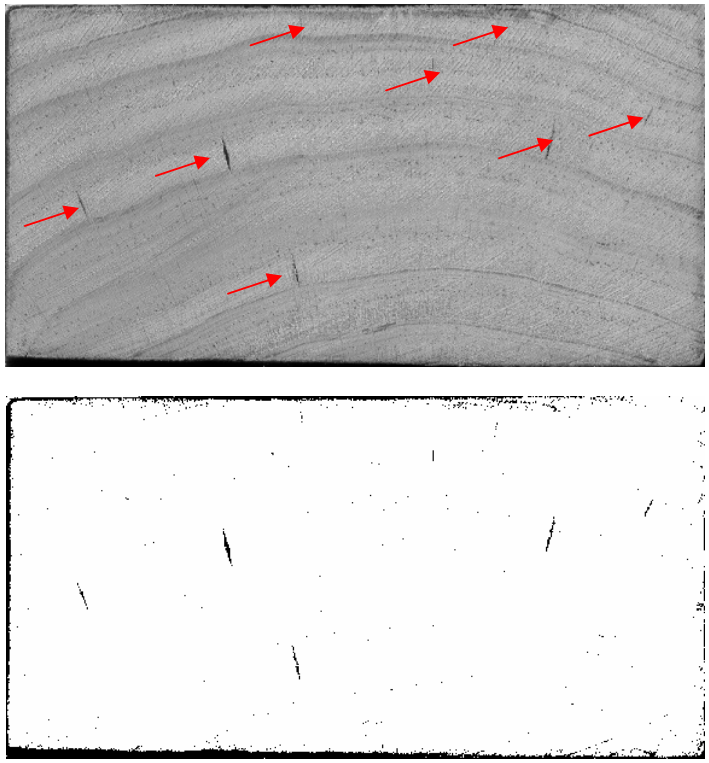

Figure 22. Images of transverse section of wood after ink penetration to show internal checks, Original RGB image (Upper) and red component adjusted to emphasise tonal changes (Lower).

Microscopic Image Analysis

This method is the further development of the image analysis method described above. In this method a sample is cut from the surface layer of the wood using a razor blade. Using this method samples can be taken on the tangential, radial and longitudinal faces. The samples are soaked in water prior to cutting to give a cleaner surface.

The samples are mounted on microscope slides using Blue-Tack so that the cut surface is parallel to the surface of the slide. The samples were observed with reflected light usually with the dark field. Once mounted on the microscope it was simply a matter of finding something of interest, focussing the camera and taking a picture.

The image analysis focussed on the longitudinal face samples. Prior to the samples being photographed a scale was photographed under the microscope so that the dimensions of the resulting pictures could be determined. The longitudinal sections were then photographed and the pictures opened in a drawing program alongside the scale. A mask of known size was created in the program and used to cut a section of the longitudinal face micrographs for image analysis. These images were analysed in the same way as the cross-sections above.

Colour Development Movies from Digital Stills

This method was developed for two main purposes. Firstly it was intended to get pictures of different levels of colour development for the purpose of surveying industry and also develop a colour severity scale. Secondly the intention was to combine the still pictures for a single sample into short movie showing the development of colour on a surface. This second use was mainly for presentation purposes.

The development of this technique encountered a problem with the consistency of the light source. The ambient light conditions were sufficiently different at the different times the images were taken that the colour changes associated with the lighting masked the colour changes caused by the drying process. A consistent light source was not readily available and this was not a major part of the project so further details of the technique will not be discussed in this thesis.

Quantitative Surface Colour Measurement

There are two methods that were developed for this project for the quantitative measurement of wood colour. In both cases the actual measurement of colour was performed using the surface reflectance spectrophotometer.

The first method was developed to measure the colour profile through the cross-section of large samples and the second method was developed to measure the surface discolouration of a sample during the drying process. The second method has been only applied to small sample in this project but could easily be applied to larger samples.

Colour Profiles through Cross-section

This colour measurement technique can be applied to green, partially dried and fully dried wood. It is based on a method developed by McCurdy (2000) to measure moisture content and density profiles in wood during high temperature drying.

In this project the wood to be measured was most often in the form of short (~800mm) lengths of 40×100mm flat-sawn Pinus radiata boards. When the wood to be measured had been suitably prepared based on the aims of the experiment a sample was cut from it. This sample had a 25×25mm surface from the top drying face of the board and extended through the thickness of the original board, resulting in a 40mm long sample.

Following cutting the sample was then sliced parallel to the drying surface using the wood slicer. This part of the operation produced a slight dilemma about the thickness to cut the slices. On one hand it is

desirable to have very thin slices to maximise the resolution of the profile, especially near the surface where the colour can change significantly over a short distance. It is possible when the slicer is kept sharp to cut slices thinner than 0.5mm. This, however, presents a problem as the thin slices are translucent and the measured colour of the slice is therefore influenced by the background colour of the surface it is measured on. On balance the slices were cut to approximately 1mm thick so that they were opaque and the profile had sufficient resolution. The actual thickness of each slice was measured using digital callipers.

The slices are immediately measured for colour if the original board was dried completely (to ~10% MC) during preparation. Where the wood is green or partially dried the slices are first dried in a low temperature vacuum oven or freeze-dried. This removes the effect of moisture content from the colour of the slices.

The actual measurement of colour simply involves placing the aperture of the spectrophotometer in the centre of the slice and activating the measurement on the computer. It was essential that the aperture is placed consistently in the centre of the slices as there is a temptation to pick areas on the slices that would yield interesting results, such as stained areas or nice bright areas. Giving in to such temptation would result in biased and useless results.

Wood Surface Colour Changes during Drying

This colour measurement technique is applied to samples while they are being dried. It is not a continuous measurement process but allows for multiple measurements of a single point, or set of points, through an entire drying schedule.

Preparation of the wood sample being tested is very important for this method. The samples are prepared green by carefully smoothing the surface with a hand plane. The key in this step is to remove the damaged layer from the surface of the wood so that there are intact tracheids near the surface. Preparing the surface while it is still saturated with water makes this process easier. Rudimentary woodworking skills are required to determine the correct grain direction to prevent gouging of the wood.

The intact tracheids at the surface alters the way in which colour develops at the surface. In normal rough-sawn timber the evaporative front recedes through the layer of damaged tracheids at the surface early in drying forming what is known as the thin dry layer. This means that most colour development occurs a few millimetres below the surface and is not always apparent on the surface. The process of removing the damaged layer means that the evaporative front stays nearer to the surface for a pronounced period of time in the early stages of drying and thus the formation of colour is more obvious and can be measured non-destructively during the drying process. When the surface is planed after drying the stain is removed from the wood showing that the stain is very near the surface.

The surface to be measured is marked with sample points before drying commences so that the parts of the surface measured are consistent throughout the process. This is done by marking each point with a circle slightly larger than the aperture of the spectrophotometer. A pencil is used for this marking as the

graphite does not dissolve or melt in the drying conditions. In this project four measurement points were used for each sample.

The measurement of the surface during drying is performed by removing the sample from the dryer, recording the time and weight. The colour of each of the measurement points is then determined using the surface reflectance spectrophotometer. In addition a photograph can also be taken of the surface at this stage for qualitative analysis of the colour development. The entire measurement process only takes a few minutes and so that cooling and drying outside of the drying apparatus was kept to a minimum.

Chemical Measurement of C and N

The amount of carbon and nitrogen in wood samples was measured by combustion analysis. The actual analysis was performed by Lincoln University and the results were supplied as a spreadsheet. The samples were prepared using the Wiley mill and mortar and pestle to produce a fine powder. This is based on the technique used by Dieste (2002).

Liquid-based Experiments

These experiments involved measuring the in vitro colour development with time of real and artificial sap solutions at various different temperatures and concentrations. This required the collection of real sap and the formulation of artificial sap solutions.

Expression of Sap

The real sap solutions were gathered by expressing sap from freshly sawn timber. The timber was obtained from the sawmill grading table as soon as it had been cut. The boards selected were short lengths of 50×100mm section and were from the sapwood of the log. Care was taken to avoid any heartwood or pith in the boards. The boards were transported from the sawmill to the laboratory as quickly as possible in an open trailer.

Upon arrival at the laboratory the boards were cut into approximately 75mm long blocks and squeezed in a hydraulic press to remove the sap. The blocks were placed between two plastic lined steel blocks, one above and one below. A tray was placed between the wooden block and the lower steel block and the entire unit put on the hydraulic press. The ram from the press pushed downwards on the top steel plate, which spread the load evenly over the wooden block. The sap expressed from the wood collected in the tray and when the ram was released the sap was poured off into a plastic carboy for storage. A total of 10L of sap was expressed in this manner and stored in a refrigerator until used in the experiments.

Concentration of Sap

To concentrate the expressed sap 6L was frozen in three stainless steel trays (2L per tray) to a temperature of -30°C. The sap was then freeze dried to remove all of the moisture. The freeze drying operation was carried out at -10°C, which is higher than normal freeze drying operations. The higher temperature was suitable as there was no structure to be maintained, the temperature only had to be low enough to prevent a reaction from occurring.

The freeze-dried sap powder was scraped from the trays and then reconstituted with 60mL of purified water to make a sap solution 100 times the concentration of normal sap. The resultant liquid was a very dark almost black colour and contained a precipitate. This made it unsuitable for colour kinetic experiments.

Artificial Sap Solutions

The artificial sap solutions were made by dissolving three sugars glucose, fructose, sucrose and an amino acid glutamic acid into purified water. The sugars were dissolved into solution separate from the amino acid to prevent a reaction from occurring before the experiment began. Each of these solutions was made up to twice the final concentration so that equal parts of each could be added together to get the desired concentration.

The amounts of each compound added to the solutions is shown below in Table 7. These values were determined from the work of McDonald et. al (2000) and the recipe is for a sap solution 200 time more concentrated than normal sap. More dilute solutions were made from this solution through a dilution series.

Heating of Sap Solutions

The heat treatment of sap solutions was performed in McCartney bottles. The bottles were placed into trays and then put into ovens at the appropriate temperature. There were 10 bottles used for each solutions being tested. At various time intervals, bottles were removed from the ovens and immediately quenched in an ice bath. The bottles were then placed in a refrigerator for storage until all of the bottles had been removed from the ovens. The bottles remained sealed until testing.

Table 7. Recipes for the artificial sap solution based on the chemistry of Pinus radiata sap.

Component	Solution 1. (1L)	Solution 2. (1L)	Full Solution (2L)
Glucose	47.74g (0.27mol.)	-	47.74g
Fructose	50.92g (0.28mol.)	-	50.92g
Sucrose	213.49g (0.62mol.)	-	213.49g
Glutamic Acid	-	162.84g (1.11mol.)	162.84g

Colour Measurement by Absorbance

The absorbance of the heated artificial sap solutions was measured using the Shimadzu spectrophotometer. A quartz cuvette was required as part of the range was in the UV spectrum.

The spectrophotometer was calibrated using a purified water blank and an un-reacted sap solution blank was used to establish a baseline. The concentration of the sap solution blank was the same as the final concentration of the samples being tested. Each concentration series for each temperature was measured separately as a unit, starting with the baseline blank, followed by the first sample removed from the oven then sequentially to the last sample removed from the oven. This sequence was used as it minimised the effect of any cross contamination on the results as only one quartz cuvette was available and had to be used for all of the samples.

Colour Measurement by Reflectance

The colour change in the in-vitro experiments was also measured using the Minolta CM-2500D surface reflectance spectrophotometer. In order to measure the reflectance of the samples, 0.5mL of each sample was soaked into a 30mm disk of filter paper. The samples were dropped directly into the middle of the papers and allowed to soak out to the edges. The filter papers used were first tested to measure the initial colour and they were all found to have a uniform colour.

After the filter papers had been soaked, they were placed on a stainless steel tray and frozen to -18°C. The papers were then freeze-dried at -10°C until completely dried. The colour of each filter paper was then measured using the spectrophotometer.

Calculations and Analysis

This section covers some of the standard calculations and analysis techniques used in the experiments described in later chapters.

Calculations

The moisture content is a fundamental property of timber both when it is green and when it is dried. The moisture content is a measure of the mass of water in a board compared to the mass of oven dry material and is calculated from Equation (3.1) below. In this equation the green weight (Wgreen) is the weight of the moist wood sample and the oven-dry weight (Woven-dry) is the weight after the sample has been vacuum dried at 104°C until there is no weight change.

$$MC = \frac{W_{green} - W_{oven-dry}}{W_{oven-dry}} \qquad 3.1$$

The maximum amount of water that is bound into the cell wall material of wood is dependant on the temperature of the wood. The higher the temperature of the wood the less water can be held in the cell wall material. The moisture content where there is only bound moisture in the cell walls and the cell walls are saturated is known as the fibre saturation point. The fibre saturation point (FSP, or MC_{fsp}) was determined for each schedule using an equation developed by Siau shown in Equation (3.2) below. T_{sap} is the temperature of the sap in the drying board. This is assumed to be either the dry-bulb temperature or the wood temperature, whichever is lower. This equation is an approximation and a more detailed equation is used in the computer model presented in Chapter 6.

$$MC_{fsp} = 0.3 - 0.001\left(T_{sap} - 293.15\right) \qquad (3.2)$$

Subtraction Spectra

This is a technique used in the analysis of data from a spectrophotometer and aids in pinpointing areas where significant changes in colour are occurring. The method is a relatively simple mathematical operation where a base spectrum is subtracted from subsequent spectra in the case of absorbance measurements. Where reflectance measurements are being analysed the subsequent spectra are subtracted

from the base spectrum. This means that an increase in absorbance or an analogous decrease in reflectance at any wavelength will appear as a positive change.

The plot in Figure 23 shows an example of the reflectance spectra obtained from the spectrophotometer for wood dried using the method for surface colour measurement. The spectrophotometer software converts the spectral data into Microsoft Excel format so that the data can be easily manipulated using a spreadsheet. It should be noted that these spectra only cover a range from 400nm to 700nm on the x-axis as the device was not able to measure in the UV range of the light spectrum. The reflectance value on the y-axis is the percentage of the incident light reflected off the surface at each wavelength. The gradient on the spectra show that more of the longer wavelength light is reflected (70-80%) than shorter wavelength light (10-40%). This means that the shorter wavelengths are being absorbed more than the longer wavelengths. In this case the reflected light includes both the diffuse and specular components. The top spectrum is the earliest measured on the plot and represents the lightest colour measured. The bottom spectrum is the last measured and is the darkest colour measured.

The subtraction spectra shown in Figure 24 are from the same data presented in Figure 23. Each of the spectra has been subtracted from the earliest spectra so that the earliest spectrum is a straight line at 0 on the y-axis and the latest spectrum is the top line in the subtraction spectra. This has essentially transformed the reflectance spectra plot into a plot of absorption spectra relative to the lightest sample. The plot of subtraction spectra makes it easier to determine how the reflectance/absorption spectrum of the wood sample has changed with drying.

The plot in Figure 25 shows the raw absorption spectra for a series of artificial sap solution samples. The chromophores are reasonably clear in this plot thought there is some minor noise towards the longer wavelengths. The chromophore in the UV region is off the scale which makes it difficult to analyse.

The plot in Figure 26 shows UV-visible absorbance subtraction spectra for the same series of artificial sap solution samples. The absorbance spectra generated by the spectrophotometer are converted into ASCII files by the software that operates the machine. These files are then opened using Microsoft Excel and converted into spreadsheets. The raw spectra have been converted into absorbance subtraction spectra and this better identifies the wavelengths where chromophores are produced. In this set of spectra a peak has formed at a wavelength of 305nm. The chromaphore in the UV region is also easier to identify in this plot at the peaks are on the scale of the y-axis.

The identification of the chromophores allows a reaction rate to be calculated based on the absorbance data. To calculate the reaction rates the absorbance at the peak wavelength is plotted against time as shown in Figure 27a. The linear portion of this plot is then used to determine the rate of reaction as shown in Figure 27b. The reaction rate is determined as the slope of the linear fit line in this case 0.0245.

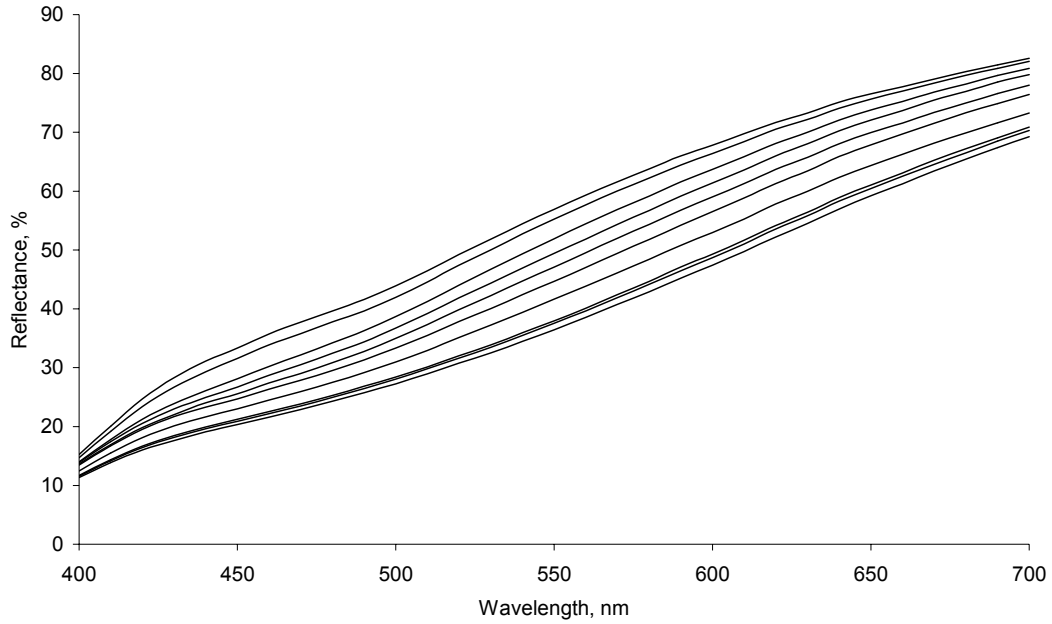

Figure 23. An example of reflectance spectra obtained using the surface reflectance spectrophotometer at different times during drying. The top line represents the earliest spectrum measured and the bottom line represents the latest.

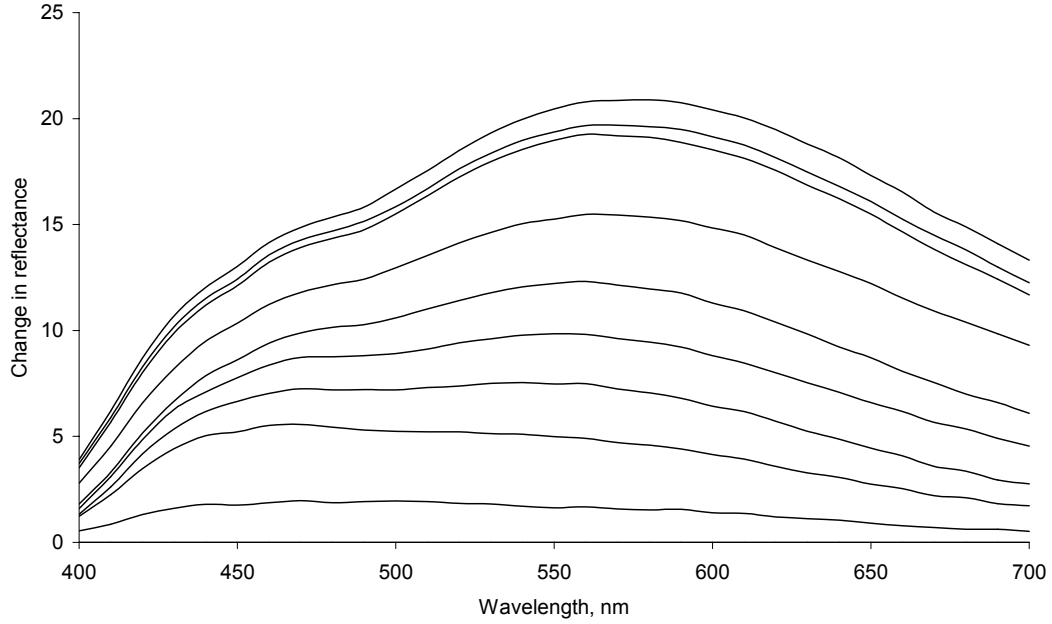

Figure 24. Subtraction spectra based on the same data displayed in Figure 23. Each of the spectra has been subtracted from the earliest spectrum to show the change in reflectance with time.

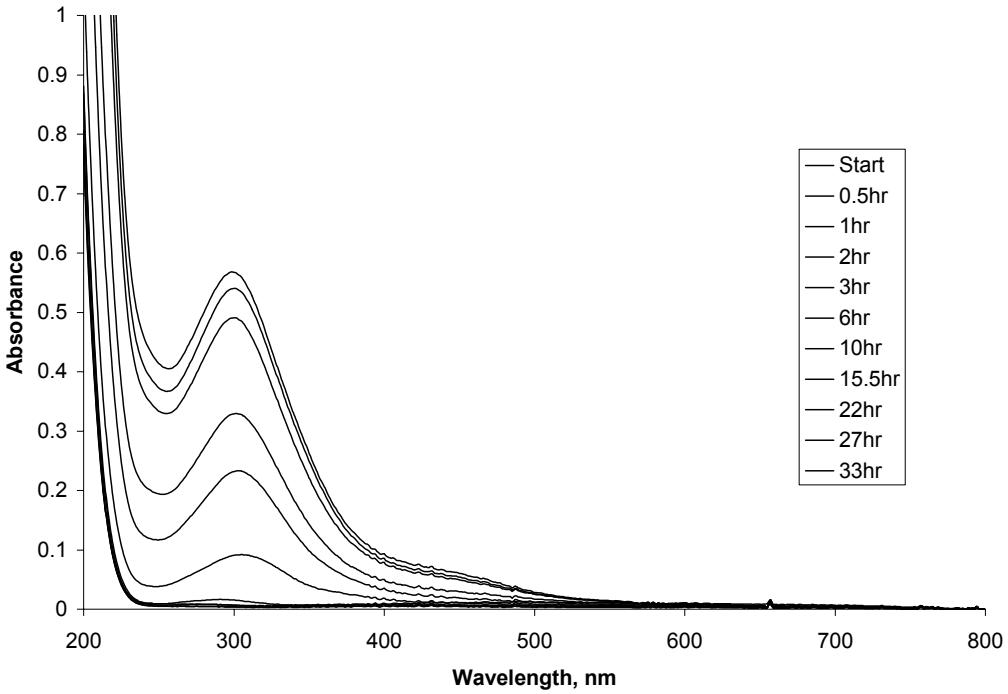

Figure 25. Absorption spectra for the 200× concentration series at 90°C. The samples were diluted to 1× normal sap concentration before the measurements were made.

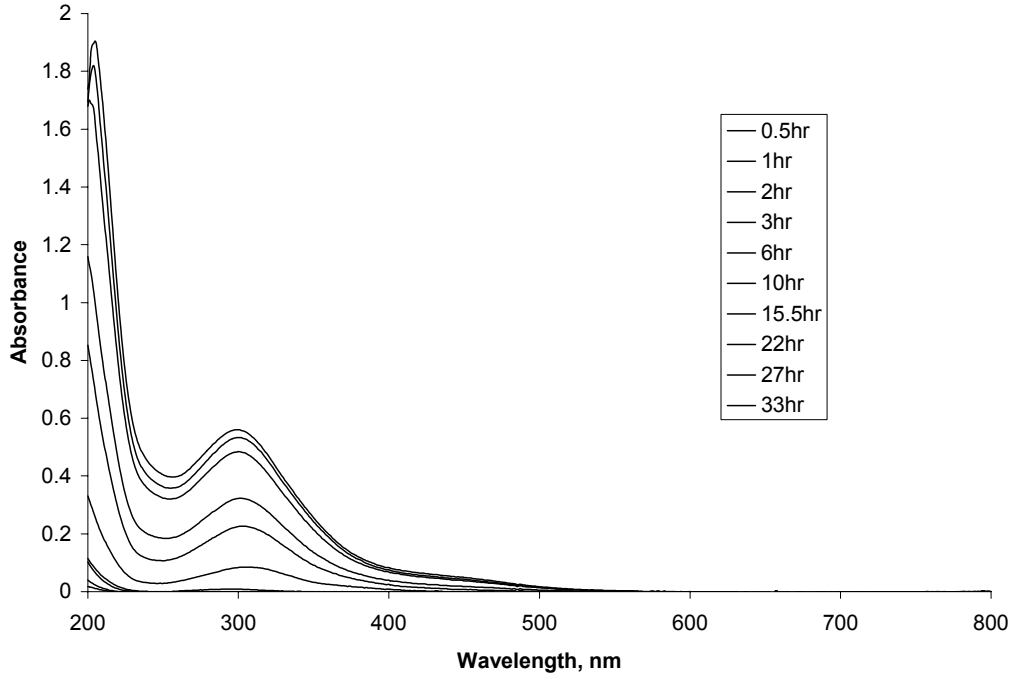

Figure 26. UV-Vis absorbance subtraction spectra (tx-t0) for 200× concentration series at 90°C.

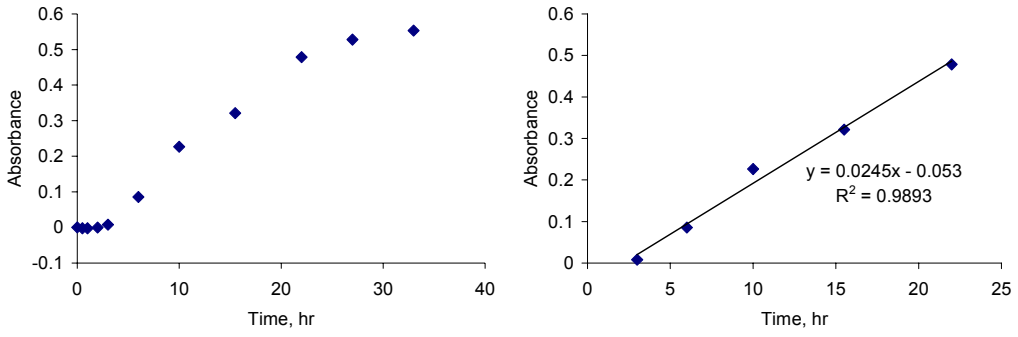

a. b.

Figure 27. Change of absorbance at peak wavelength with time for the 200× concentration series at 90°C a.) showing all points and b.) showing the points used for the slope determination. The equation for the linear fit is shown along with the R2 value for the fit.

Chapter 4

Board Drying Experiments

Summary

This chapter, consisting of four parts describes drying experiments carried out to determine the effect of drying schedules on the development of colour and checking in boards. In part one, experiments were undertaken to determine the effect of schedule selection on the development of colour and internal checking in radiata pine during drying. Eight schedules were tested ranging from LT (50/40) to HT (120/70). The variables measured were moisture content, colour expressed using the CIELab colour space, and nitrogen content. No checking was present in any of the samples tested so no conclusions could be drawn.

The experiments have shown that colour development, both as kiln brown stain and core darkening, is influenced by drying temperature and drying time. The recommendation is therefore that low-temperature low-humidity schedules be developed for controlling colour development.

A number of different ways of present colour data have been investigated. The lightness and yellow-blue coordinates both give a good indication of kiln brown stain, while the red-green coordinate is not as good an indicator. The combination of all three coordinates as ΔE provides the best representation of kiln brown stain formation. Colour planes within the CIELab colour space give a good indication of overall colour change in boards at different drying times but not the variation within a board.

In the second part of this chapter the microscopic analysis of the kiln brown stain layer formed in the large boards is described. This analysis included observations of the microstructure of the stain layer as well as computer analysis of stain layer images. These analyses have shown that the humidity of a schedule effects the position and size of the stain layer as well as the intensity.

In part three, experiments were carried out on full-size boards in a semi-scale kiln to determine the effect of four standard commercial schedules on the development of colour and internal checking. These experiments have shown that higher temperature schedules produce severer kiln brown stain and that within-ring checking also increases with temperature but the cross checks at drying temperature of 140°C are actually less than those at drying temperatures of 120°C and 90°C.

Part four covers colour measurements performed on samples obtained from a wood processing company specialising in the production of light colour radiata pine for export to remanufacturing companies in the USA. The samples provided are compared to a sample dried to a schedule developed from the

experiments presented in this chapter. The results show that this sample compares favourably with the ideal colour desired by this company.

Finally conclusions drawn from all four parts are presented at the end of the chapter.

Colour Development in Large Boards

This set of experiment investigated, in details, the effects of drying schedules on the development of wood colour changes and the colour profile across the board thickness. The development of colour in radiata pine occurs in the form of kiln brown stain near the surface of boards and overall darkening of the wood that occurs throughout the board. Both kiln brown stain and core darkening were investigated in these experiments.

`In order to understand the fundamentals for formation of kiln brown stain, the accumulation of nitrogen at the surface of the boards dried was also measured in these experiments to determine the relationship between colour development and accumulation of nitrogen compounds at the wood surface.

Experimental

Schedule Selection

Originally nine schedules were chosen for testing in this set of experiments to cover a range of temperature from low temperature drying through to high temperature drying. The details of the schedules used are shown in Table 8. The ACT and CT schedules also cover a range of different relative humidity values at the same temperature. The calculated fibre saturation points and equilibrium moisture contents are also shown for each schedule.

Table 8. Details of schedules used for determining the influence of drying schedule on colour development.

Schedule No.	Description	Dry Bulb	Wet Bulb	RH	FSP	EMC	Notes
1	HT	120°C	70°C	14.3%	0.22	0.015	
2	ACT -HRH	90°C	80°C	67%	0.23	0.079	Partial Data
3	ACT –MRH1	90°C	70°C	43%	0.23	0.048	
4	ACT –MRH2	90°C	60°C	25%	0.23	0.032	Abandoned
5	ACT -LRH	90°C	50°C	16.7%	0.23	0.020	
6	CT -HRH	70°C	60°C	62%	0.25	0.085	
7	CT -MRH	70°C	50°C	35%	0.25	0.050	
8	CT -LRH	70°C	40°C	17%	0.25	0.029	
9	LT	50°C	40°C	54%	0.27	0.085	

One of the schedules had to be abandoned due to an error that occurred during drying. Unfortunately this was the 90/60 schedule, which is a standard ACT schedule, however there are 90°C schedules with higher and lower RH that have been included. There were also some problems with Schedule 2 which resulted in some data being lost.

For each schedule an initial full run was done to dry a sample board to completion. A drying curve was recorded for each of these full runs to determine the drying times for subsequent partial drying runs. The

drying curves for the HT and ACT schedules are shown in Figure 28 and the drying curves for the CT and LT schedules are shown in Figure 29. The partial drying runs were done for 20%, 40%, 60% and 80% of the full drying time. The initial moisture contents for the sample boards dried are shown in Table 9 with the label of the boards and schedule they were dried at.

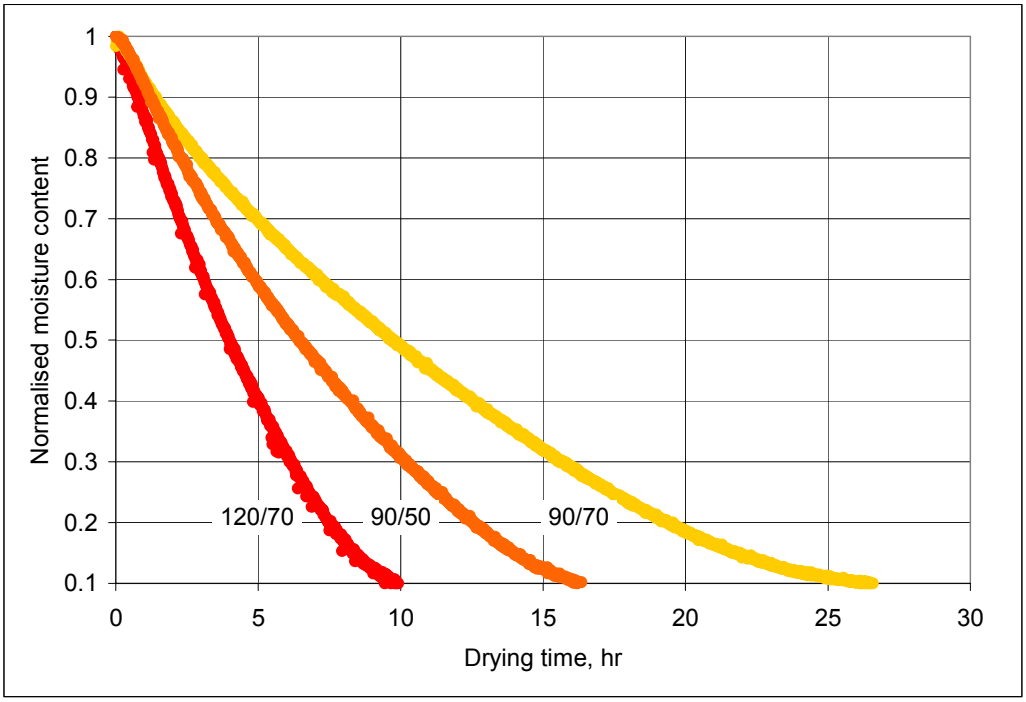

Figure 28. Normalised drying curves for the HT and ACT schedules. The 90/80 drying curve is not plotted due to difficulties with data acquisition.

Table 9. Labelling and initial moisture content for sample boards.

Schedule No.	Pair				Notes
	Fully dried sample		Partially dried samples		
	Label	Initial MC	Label	Initial MC	
1	G2F	1.30	G1A	1.34	Non-matched
2	B1D	1.41	B2D	1.42	
3	B1C	1.12	B2C	1.39	
4	C1D	1.36	C2D	1.22	
5	B1B	1.39	B2B	1.31	
6	G1E	1.23	G2E	1.22	
7	G1C	1.16	G2C	1.26	
8	G1D	1.17	G2D	1.25	
9	G1B	0.98	G2B	1.36	

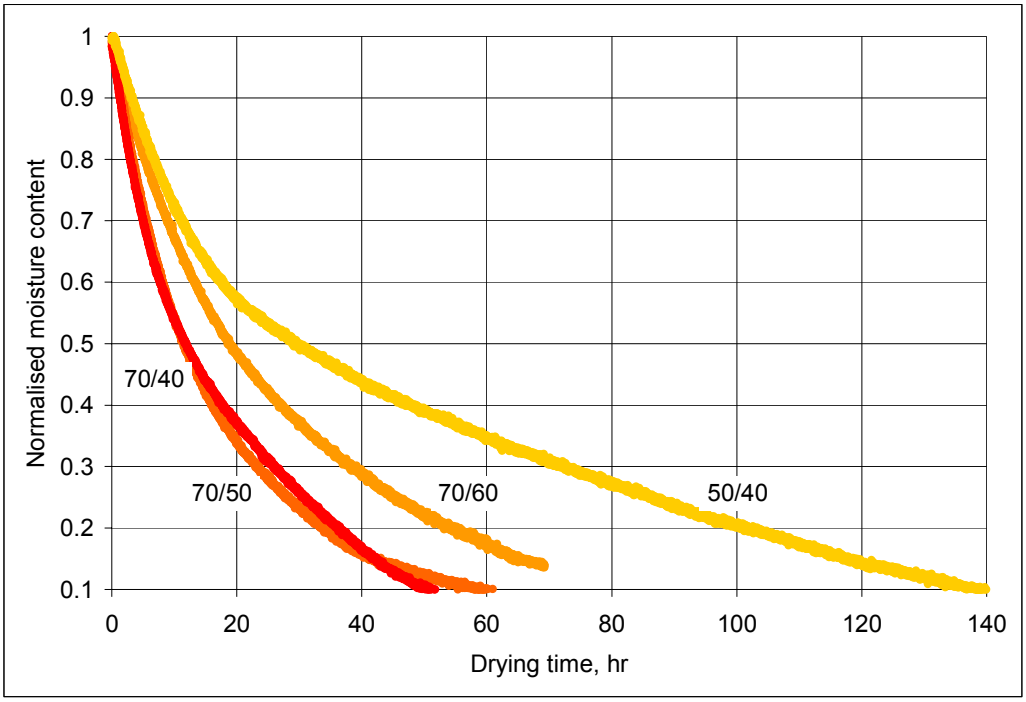

Figure 29. Normalised drying curves for the CT and LT schedules

Drying Runs

The fully dried samples were dried individually, one board in each run, while the partially dried samples were dried as a group for each of the schedules. These groups are shown in Table 10, schedule 4 has been omitted as no results were obtained from it. The drying time shown in the table is the time that the sample was dried at the particular schedule. The start time is the time when the sample boards were put into the drying tunnel and the number in brackets indicates the day. Start times mark with an asterisk (*) indicate the start time for the group schedule. The finish time is when the sample board was removed from the drying tunnel and the number in brackets is the day removed. Finish times marked with a dagger (†) indicate the finish time for the group schedule.

Boards were placed in the drying tunnel such that the outer wood part of the boards were the top drying surfaces and the inner wood part of the boards were the bottom drying surfaces.

Sampling

After each board was removed from the tunnel after drying for the preset time it was immediately weighed to determine the dried weight. The board was then marked for cutting into two 25mm wide samples in the centre of the board. These samples were cut out using a circular saw to produce two 25×40×100mm blocks. The first of these blocks was then marked and cut into a 25×25×40mm block for moisture content measurement. This block was cut at a point in the board where the growth-rings were parallel to the drying surface to provide a more defined moisture content profile.

Table 10. Drying time and scheduling for partially dried samples.

Schedule No.	Sample	Drying Time	Start Time	Finish Time
1 120/70	20%	2hr	08:00 (1)*	10:00 (1)
	40%	4hr	08:00 (1)*	12:00 (1)
	60%	6hr	08:00 (1)*	14:00 (1)
	80%	8hr	08:00 (1)*	16:00 (1)†
2 90/80	20%	9hr	24:00 (1)	09:00 (2)
	40%	18hr	22:00 (1)*	16:00 (2)†
	60%			
	80%			
3 90/70	20%	7.5hr	09:00 (2)	16:30 (2)†
	40%	14hr	20:00 (1)	10:00(2)
	60%	21hr	12:00 (1)*	09:00 (2)
	80%	28hr	12:00 (1)*	16:00 (2)
5 90/50	20%	3.5hr	09:00 (2)	12:30 (2)
	40%	7hr	09:00 (2)	16:00 (2)†
	60%	10hr	23:00 (1)*	09:00 (2)
	80%	12hr	23:00 (1)*	11:00 (2)
6 70/60	20%	16.5hr	23:30 (3)	16:00 (4)†
	40%	30hr	09:00 (3)	15:00 (4)
	60%	47hr	11:00 (2)	10:00 (4)
	80%	62hr	24:00 (1)*	14:00 (4)
7 70/50	20%	10hr	24:00 (2)	10:00 (3)
	40%	20hr	17:00 (2)	13:00 (3)
	60%	30hr	10:00 (2)	16:00 (3)†
	80%	40hr	23:00 (1)*	15:00 (3)
8 70/40	20%	9hr	24:00 (1)	09:00 (2)
	40%	18hr	21:00 (1)*	15:00 (2)
	60%	27hr	09:00 (2)	12:00 (3)†
	80%	36hr	21:00 (1)*	09:00 (3)
9 50/40	20%	26hr	09:00 (5)	11:00 (6)†
	40%	53hr	09:00 (2)	14:00 (4)
	60%	81hr	24:00 (1)*	09:00 (5)
	80%	107hr	24:00 (1)*	10:00 (6)

After cutting, the sample blocks were both weighed and the smaller block sliced into twenty slices, each approximately 1mm thick, starting at the top drying surface and finishing in the centre of the board. Each slice was weighed immediately after it was cut to determine the dry weight and then labelled. The slices were vacuum dried at 104°C for 24hr and then weighed to determine the moisture content of each slice after drying.

The second sample block, which was used for colour measurements, was vacuum dried at 40°C for 48hr before being further cut into 25×25×40mm blocks and sliced in the same manner as the moisture content samples. The lower vacuum drying temperature was used in this case to prevent any further darkening or staining of the wood. The slices from this block were then labelled and used for the measurements of colour and nitrogen content.

The thickness of each of the slices from the two sample blocks were measured using digital callipers after oven-drying. The measurement was taken across the edge where the slicing blade entered the sample as this part of the slices had the most regular profile.

Measurements of Colour and Nitrogen Contents

The colour of each of the slices was measured using a Minolta CM-2500D handheld reflectance spectrophotometer. After the colour measurements were completed on the slices the chemical measurements were performed using the same samples. The four slices at the surface were used for the surface chemical analysis and the four slices at the centre were used for the centre chemical analysis. The slices were reduced to a powder and sent away for combustion analysis

Results and Discussion

The main results of the drying experiments have been presented in eight figures, one for each of the schedules. Each of the figures contains three graphs showing the moisture content profiles, lightness profiles and the nitrogen content for the schedule. The moisture content profiles are discussed first, followed by the lightness profiles and colour changes and lastly the nitrogen analysis. After the main results, further results are presented and discussed.

Main Results

Moisture Content Profiles

The top graph presented, in each of the following eight figures, is the moisture content (MC) profiles. In all graphs the moisture content, in kg water per kg oven dry wood, is on the y-axis and the distance from the surface, in mm, is on the x-axis. Each line on the graphs is identified by drying time in the legend.

The MC profiles for the boards' dried using schedule 1 are shown in Figure 30a. The boards dried for 2hr and 4hr are still well above fibre saturation point (FSP) with a similar core moisture content of about 1 kg/kg. These two profiles differ in that in the 4hr profile the evaporative front, as indicated by a sharp change in the MC, has receded further into the board. In both of these boards there is still probably movement of liquid water, driven by capillary tension, to the evaporative front. In the 2hr sample the evaporative front is most likely located adjacent to the surface layer that was damaged during cutting. This means that there is likely to still be accumulation of sap constituents at the surface at this stage of drying under schedule 1. In the 4hr sample the evaporative front has probably receded to the first intact growth ring below the surface, a phenomenon noted in previous studies (McCurdy, 1999). This means that the flow of liquid sap to the surface has probably stopped and so the accumulation of sap constituents at the surface has also stopped at this stage in drying. There may still be accumulation of sap constituents at the evaporative front 5mm below the surface.

The 6hr and 8hr profiles have similar core moisture contents, closer to FSP. They differ in that the surface of the 8hr board has a lower MC than the 6hr board. In both boards the flow of liquid water has

probably ceased to occur and the dominant mechanism for moisture movement will be vapour diffusion. This means that there should be no movement of sap constituents during these stages of drying.

The fully dried board has a much lower MC well below FSP, due to its much longer drying time of 19hr. The board has essentially reach equilibrium moisture content (EMC) and so very little drying will be occurring. This board has been over-dried, from a commercial perspective.

The MC results for schedule 2, shown in Figure 31a, show only three profiles as two were lost to experimental failure. The profiles that are available show that after 9hr of drying the MC of the first board was still well above FSP. The profile has an irregular shape with the core MC varying from approximately 0.5 kg/kg to 1.5 kg/kg. The surface is still the driest part of the board, however, and in spite of the variations in MC there is still likely to be movement of liquid sap to the evaporative front. This means that at this stage of drying using schedule 2 sap constituents are still accumulating at the surface.

The board dried for 18hr has a more regular MC profile with a core MC closer to FSP, the surface layer to 4mm appears to be at FSP. At this stage in drying liquid movement will have ceased and vapour diffusion will be the dominant mechanism of moisture movement, so the accumulation of sap constituents at the surface will also have stopped. There is some indication that the evaporative front may have recede to about 5mm below the surface, though this is not as clear as with schedule 1. The fully dried sample is below FSP with a mean MC of approximately 0.1kg/kg, which is close to EMC, so there will be no accumulation of sap constituents at the surface.

The MC results for schedule 3 are shown in Figure 32a. The board dried for 7hr has a mean core MC of about 1kg/kg and the evaporative front is approximately 5mm from the surface of the board. This means the front has receded from the surface to the first intact growth ring and therefore the flow of liquid sap to the surface has ceased. So for schedule 3 the accumulation of sap constituents at the surface will occur within the first 7hr of drying.

The boards dried for 14hr, 21hr and 28hr have similar MC profiles with the 14hr board having a slightly higher core MC than the other two. The 21hr and 28hr boards differ slightly in that the surface of the 28hr board is slightly drier than the surface of the 21hr board. The core of both boards is at FSP so liquid sap movement would have entirely stopped, though it may still have been occurring in the core of the 14hr sample.

The fully dried board has a very flat, even MC profile with the entire board below FSP. This board has probably reached EMC and has been over-dried by commercial standards.

The MC profiles for the boards' dried using schedule 5 are shown in Figure 33a. The MC profile after 3.5hr has a core moisture content of about 1kg/kg with some variation and the evaporative front is located about 2mm from the board surface. This means the evaporative front is still located at the surface of the boards and therefore there was liquid sap movement to the surface and accumulation of sap constituents.

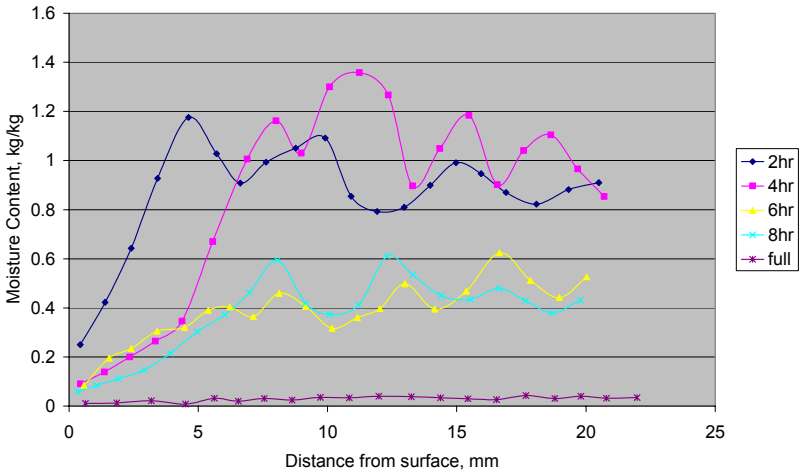

a.

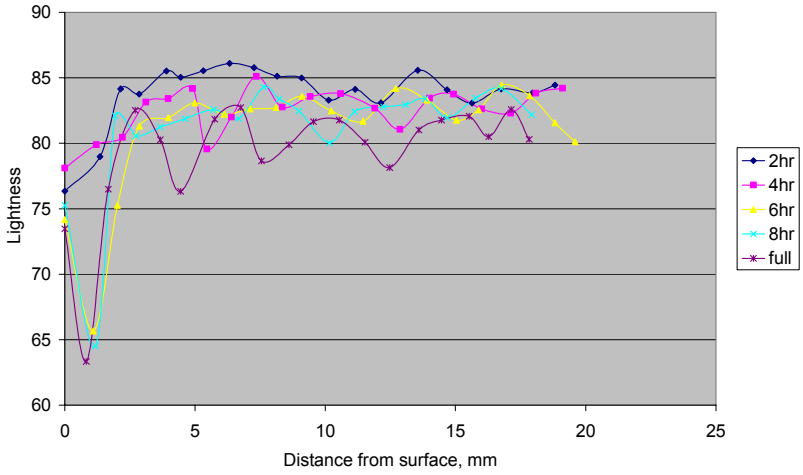

b.

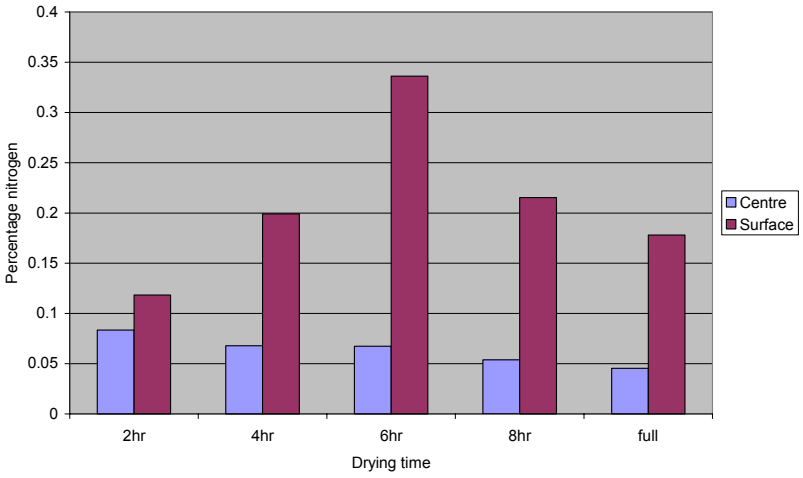

c.

Figure 30: Results for the 120/70 schedule showing a) moisture content profiles, b) lightness profiles and c) nitrogen analysis

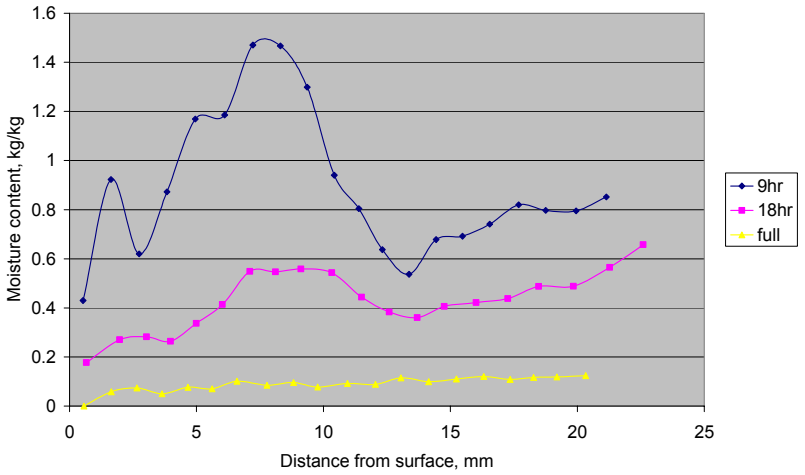

a.

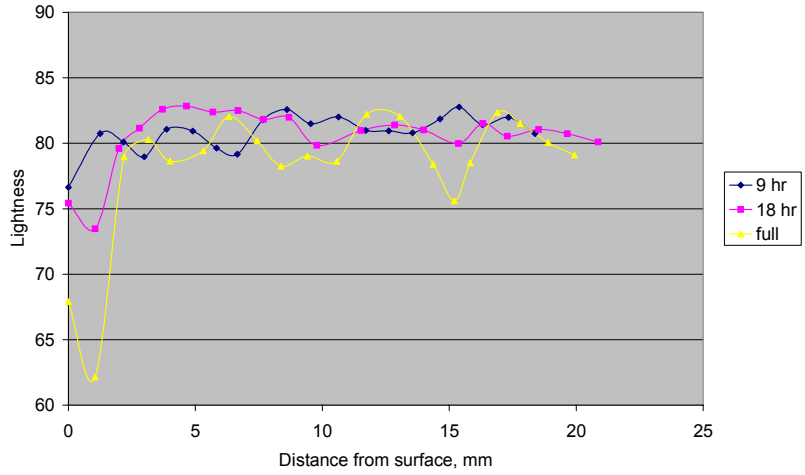

b.

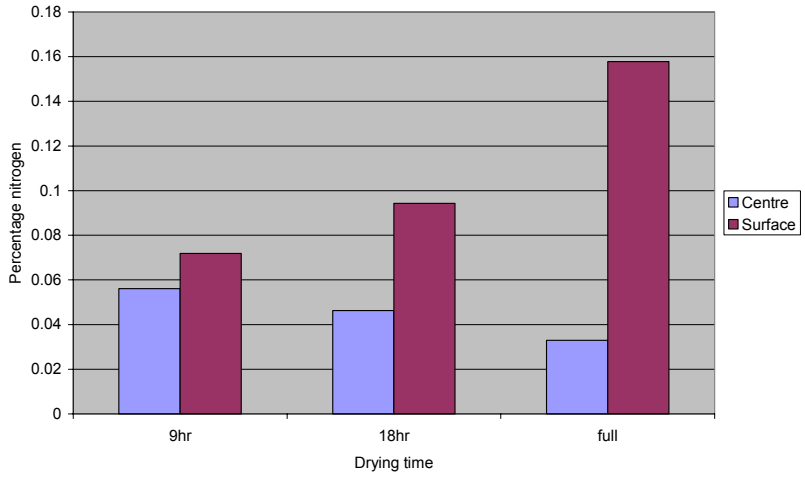

c.

Figure 31: Results for the 90/80 schedule a) moisture content profiles, b) lightness profiles and c) nitrogen analysis.

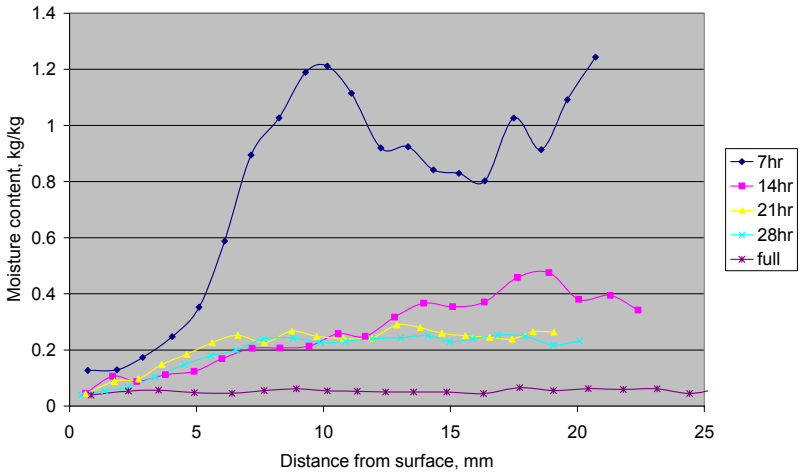

a.

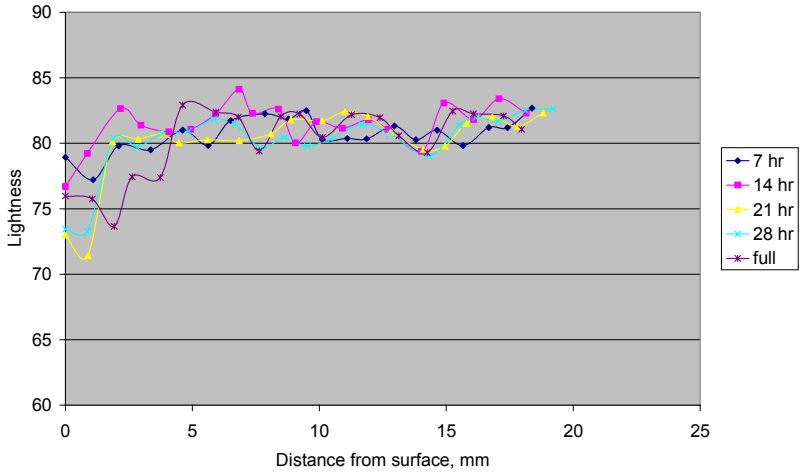

b.

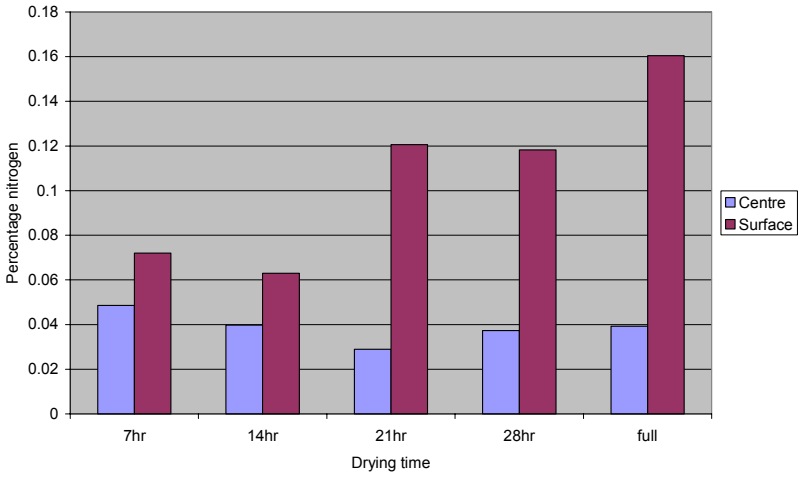

c.

Figure 32: Results for the 90/70 schedule a) moisture content profiles, b) lightness profiles and c) nitrogen analysis.

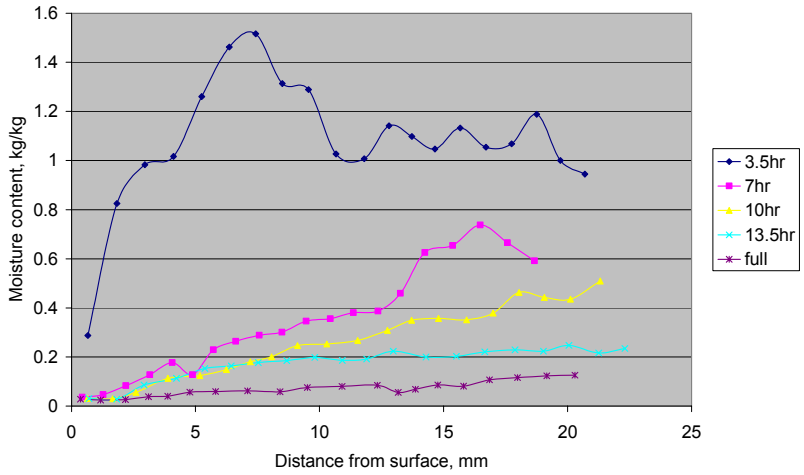

a.

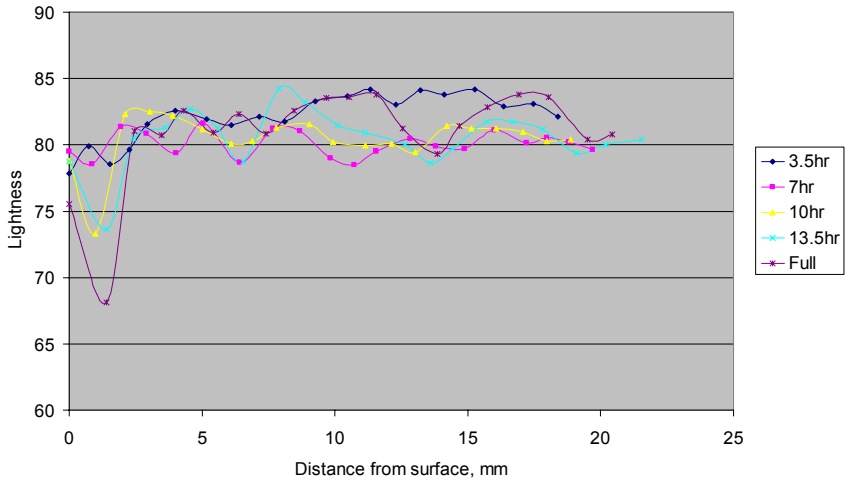

b.

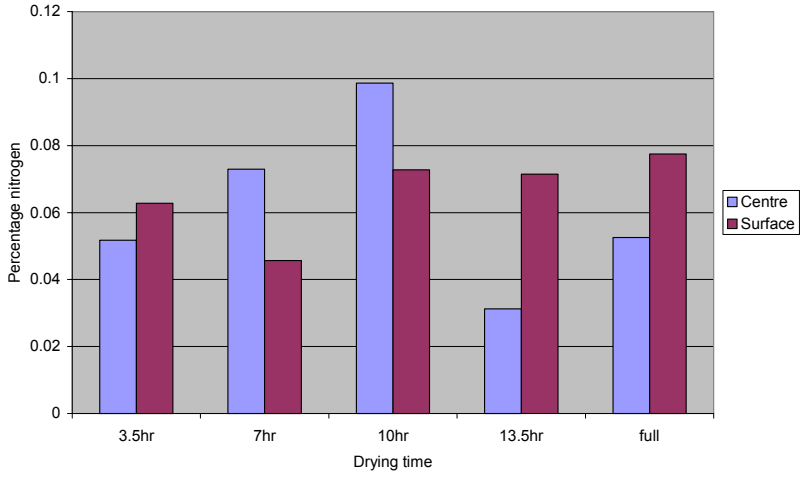

c.

Figure 33: Results for the 90/50 schedule a) moisture content profiles, b) lightness profiles and c) nitrogen analysis.

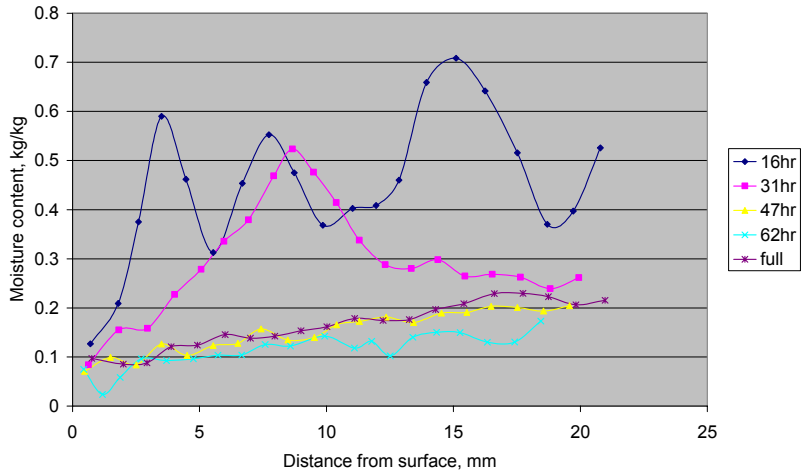

a.

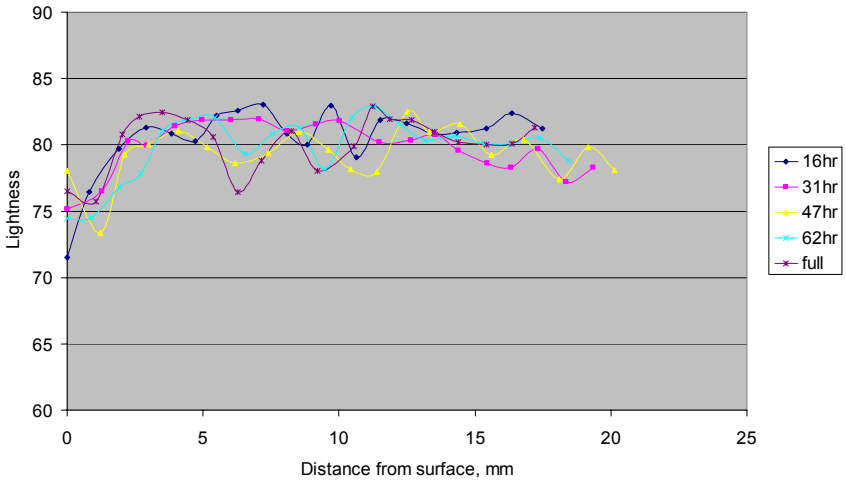

b.

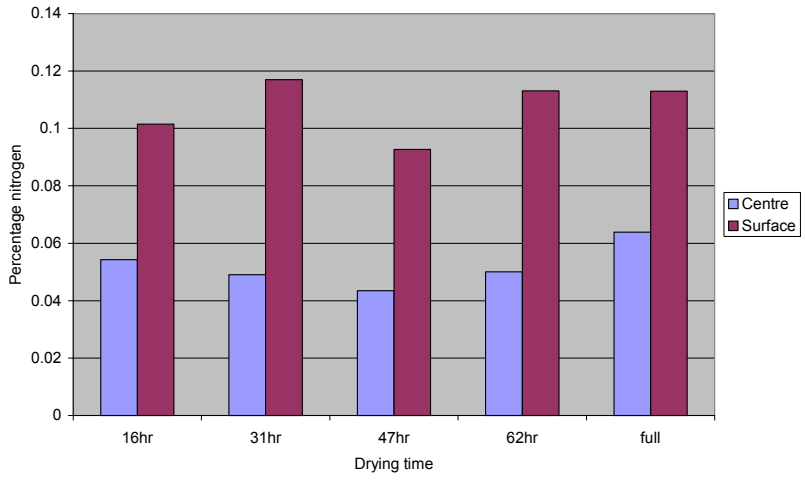

c.

Figure 34: Results for the 70/60 schedule a) moisture content profiles, b) lightness profiles and c) nitrogen analysis.

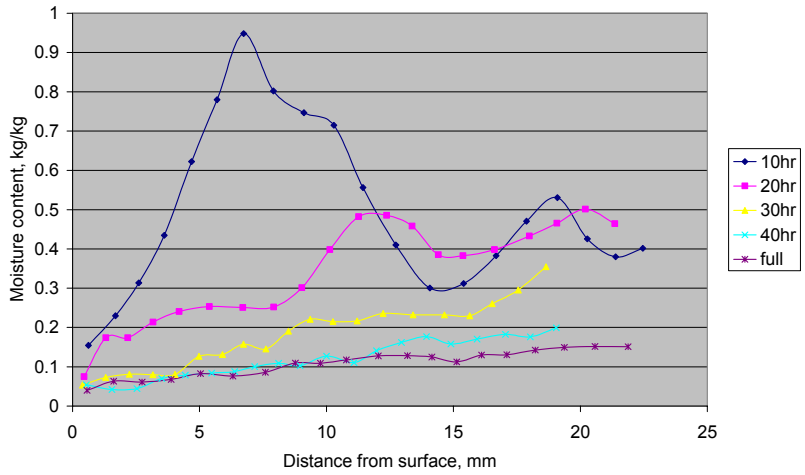

a.

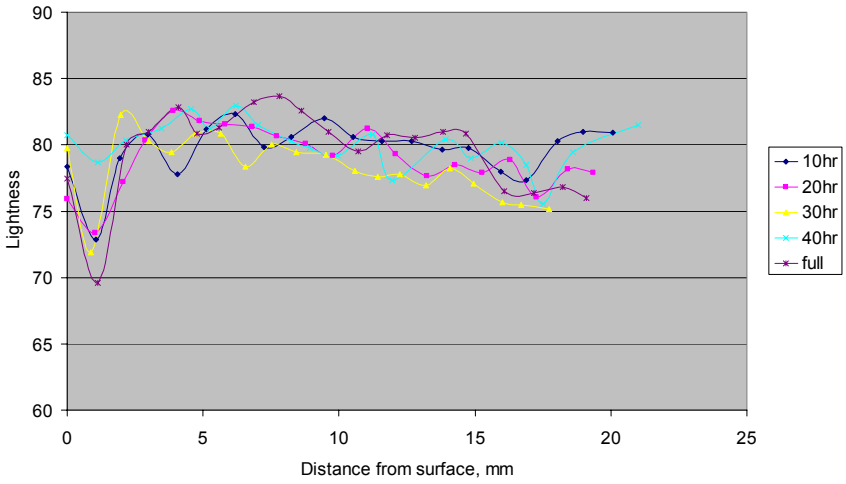

b.

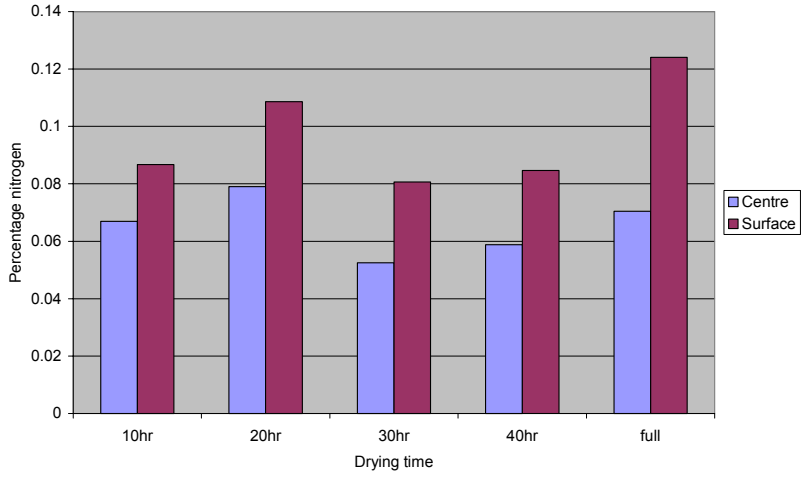

c.

Figure 35: Results for the 70/50 schedule a) moisture content profiles, b) lightness profiles and c) nitrogen analysis.

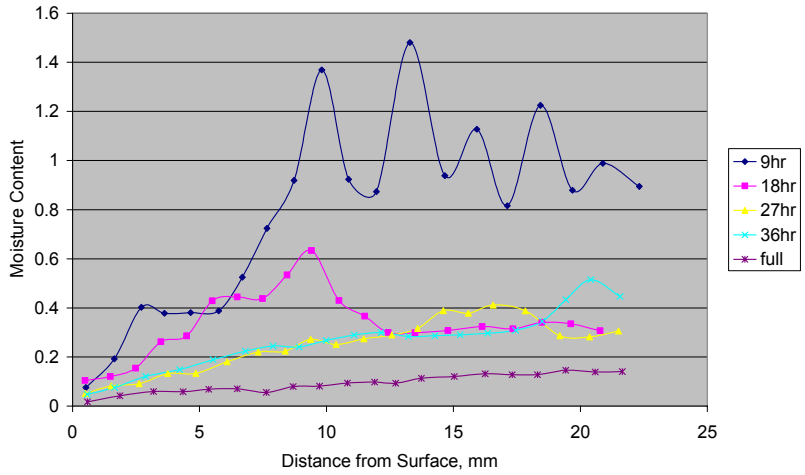

a.

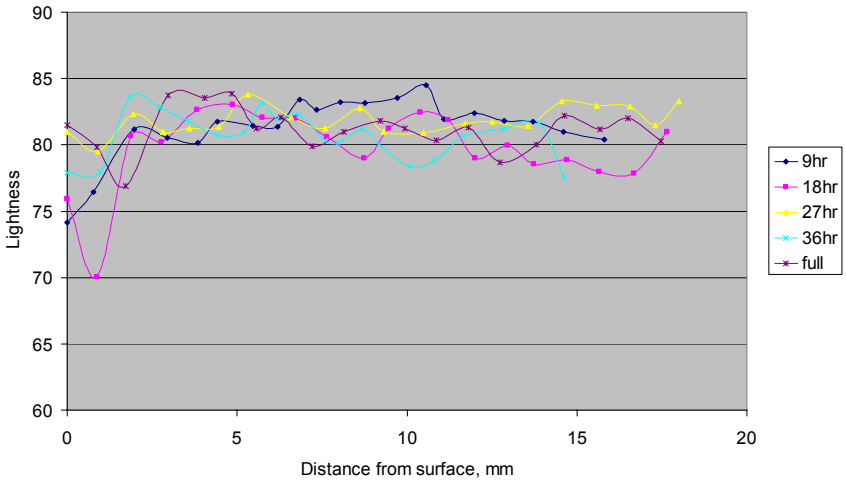

b.

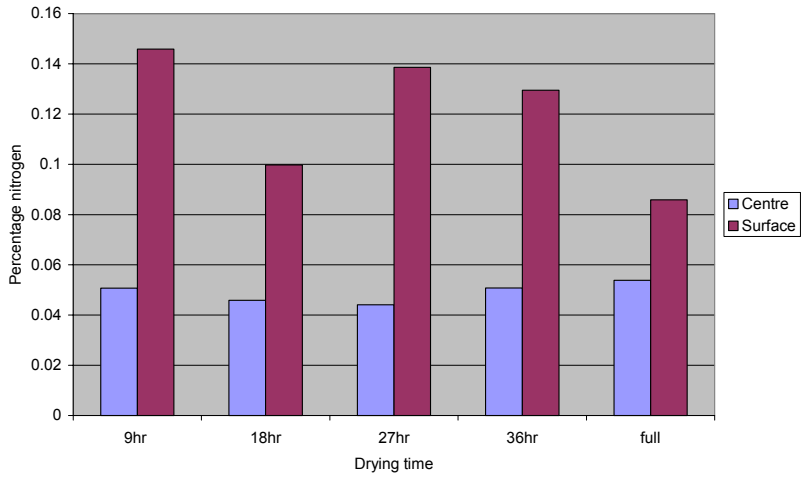

c.

Figure 36: Results for the 70/40 schedule a) moisture content profiles, b) lightness profiles and c) nitrogen analysis.

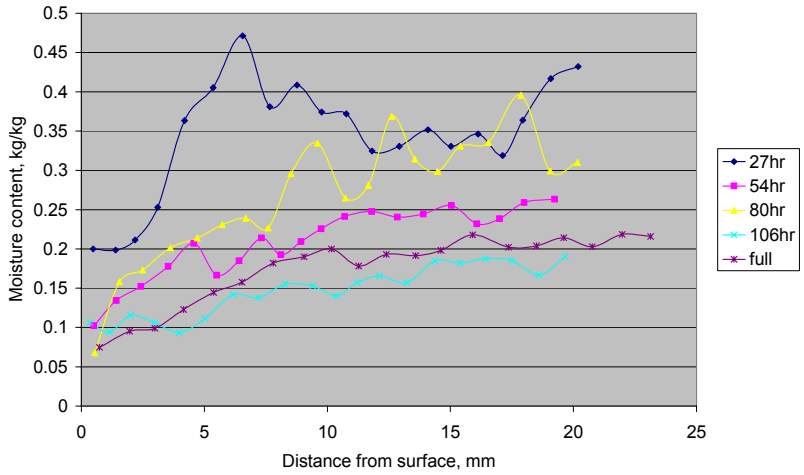

a.

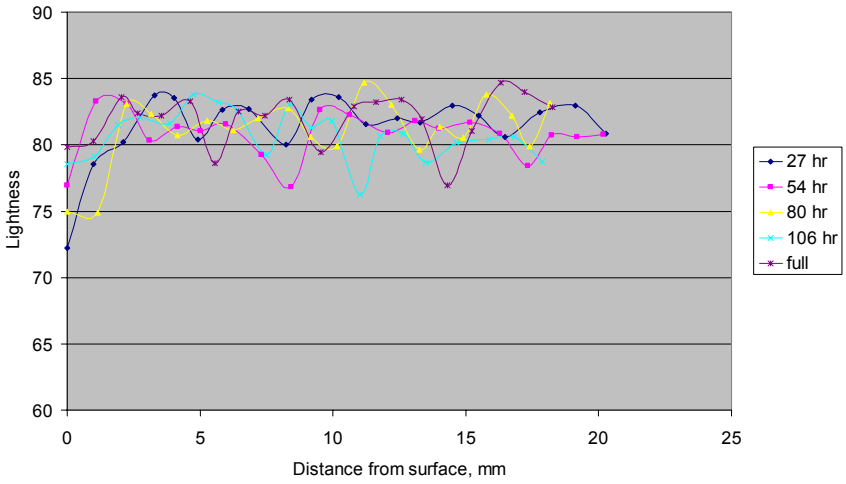

b.

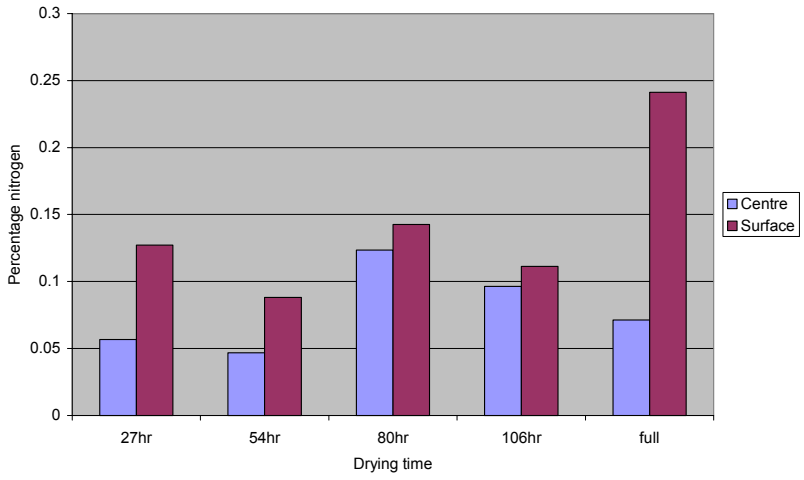

c.

Figure 37: Results for the 50/40 schedule a) moisture content profiles, b) lightness profiles and c) nitrogen analysis.

The remaining four profiles are closer to FSP and have a gradient of MC from the core to the surface. In these profiles the surface layer, of at least 5mm, is below FSP. There may still have been some liquid sap movement in the core of the 7hr sample and the step change in MC at about 14mm from the surface may indicate the position of an evaporative front. Regardless of this the accumulation of sap constituents at the board surface will have ceased in all of these samples. The 13.5hr sample and the fully dried sample are both below FSP throughout the core so the only mechanism for moisture movement in these boards would have been vapour diffusion.

The MC profiles for the boards' dried using schedule 6 are shown in Figure 34a. The 16hr and 31hr profiles are both mainly above FSP but the mean core MC is well below the green MC. Both of these profiles show some variability. The variability in the 16hr sample is due to density variations associated with the annual growth rings. The core of the 31hr sample seems to actually be at FSP, which is unusual and suggests that the board was already partially dry before drying or dried faster from the bottom surface than the top surface. There was probably still liquid sap movement in both boards but accumulation of sap constituent at the surface had probably ceased in the 31hr sample.

The remaining three profiles are similar to each other with a gradient of MC decreasing from the core to the surface. The fully dried sample has a higher MC than the 62hr sample, similar to the 47hr sample. This is due to the fact that the fully dried sample was not actually dried to completion as shown previously. As all three boards were below FSP liquid moisture movement had ceased and therefore accumulation of sap constituents at the surface had also stopped.

The MC profiles for schedule 7 are shown in Figure 35a. The 10hr and 20hr profiles are both above FSP except for at the surface. The 10hr profile shows the same variability seen in Figure 34a, with the core MC almost at FSP. The evaporative front appears to be close to the surface in this profile so there may still have been some liquid sap movement to the surface and accumulation of sap constituents occurring. The evaporative front has receded to approximately 10mm from the surface in the 20hr sample and the area between the surface and the front is at FSP. This means that liquid sap movement to the surface had stopped in this sample.

The 30hr profile is below FSP to approximately 10mm below the surface, with the remainder of the core only slightly above or at FSP. The 40hr and fully dried samples are below FSP and have similar profiles with a gradient decreasing from the core to the surface. The 40hr sample is moister in the core than the fully dried sample. In all three cases the dominant mechanism of moisture movement would have been vapour diffusion so there would have been no accumulation of sap constituents occurring at the surface.

The MC results for schedule 8 are shown in Figure 36a. The 9hr profile has a high and variable core MC with a mean of about 1kg/kg. The MC drops sharply and plateaus at 0.4kg/kg approximately 6mm from the surface and then drops below FSP about 2mm from the surface. This looks as though the evaporative front is in transition from the surface to the first intact growth ring below the surface. This would be the point at which liquid sap movement to the surface ceased and accumulation of sap constituents stopped.

In the profile after 18hr of drying some of the core is still above FSP but the surface and the core have dried out considerably compared to the 9hr profile and vapour diffusion was probably the dominant mechanism of moisture movement. The 27hr and 36hr profiles are similar, both having a gradient of MC decreasing from the core to the surface, with some slight differences in the core. The fully dried sample has a low MC throughout well below FSP.

The MC profiles for schedule 9 are shown in Figure 37a. All of the samples have been dried to below 0.5kg/kg MC. On the 27hr and 80hr profiles the core is still mostly above FSP and there is some variability in the core MC. The remaining profiles are mostly below FSP. The profiles for this schedule are difficult to interpret as they do not vary uniformly with drying time. The profiles do show, however, that the movement of liquid sap to the surface has certainly stopped after 27hr of drying.

Lightness Profiles and Colour Change

The middle graph presented, in Figure 30 to Figure 37, is the lightness profiles for the eight schedules. In all figures the lightness is on the y-axis and the distance from the surface, in mm, is on the x-axis. The scale on both axes is the same for all figures to allow for easy comparison of results.

The lightness profiles for schedule 1 are shown below in Figure 30b. The 2hr and 4hr profiles show that there was a slight darkening at the surface of these boards but that this was not much more than the lightness variation within the core of the board. A distinct change occurs at the surface in the 6hr profile where there is a significant drop in the lightness about 1mm from the surface. This drop in lightness is continued in the 8hr and the fully dried samples.

The sharp decrease in lightness indicates the presence of kiln brown stain (KBS) and the profiles show that the stain has formed between 4hr and 6hr into the schedule. At about the same point in drying the MC profiles indicate the movement of liquid sap to the surface has ceased and the evaporative front has receded into the board. This would therefore be the time when the concentration of sap constituents at the surface has reached a peak and so the rate of reaction should be greatest.

The rapid change in colour is also like to be due to the change in temperature as the evaporative front recedes from the surface. Pang (1994) showed using both drying experiments and computer modelling that the temperature of the surface layer during drying is below the dry bulb temperature of the drying schedule. The temperature of the evaporative front cannot be over 100°C without superheating the water in the wood and Pangs results show that the temperature early in drying is somewhere between the wet bulb temperature and 100°C. As the evaporative front recedes into the boards the temperature of the surface layer increases gradually approaching the dry bulb temperature. A simple way to view this phenomenon is to assume that when the surface layer is above FSP the temperature is the same as the wet bulb temperature of the drying schedule and below the FSP the temperature is the same as the dry bulb temperature of the schedule.

The lightness profiles after 8hr and 19hr (fully dried) only show a slight increase in darkness of the KBS layer. There are a number of possible explanations for this. It may show that the reaction that produces

KBS has almost completely used up the reactants after 6hr of drying and so the reaction rate is diminished later in drying. Alternatively, the surface layer is below fibre saturation point later in drying and so there will be no free water present in the surface layer. This may reduce the rate of reaction even if there are still high concentrations of reactants. Finally, the darkening may not increase linearly as the reaction proceeds, so the reaction may be continuing at a similar rate as earlier in drying but be producing less darkening.

The average lightness of the core of the samples also seems to be decreasing with increased drying time. The variation in lightness values is also greater in the fully dried sample. This is probably due to an increase in contrast between the earlywood and latewood, with the latewood being darker than the earlywood. It is also interesting that the first dip in the profile at about 5mm is darker than subsequent dips further from the surface. This first dip probably corresponds with the first intact latewood band below the surface where the evaporative front recedes to in the middle stages of drying. The darkening may be due to the accumulation and reaction of sap constituents at this second evaporative front.

The lightness profiles for schedule 2 are shown in Figure 31b. The 9hr profile only shows a slight decrease in lightness at the surface and no evidence of a KBS layer forming. This shows that the rate of stain formation is clearly slower than in schedule 1 where there was a fully form stain layer after 6hr.

After 18hr of drying a stain layer has begun to form. At this stage in drying the MC profiles indicated that the surface layer to about 4mm was at FSP and that the core was close to FSP. At this stage in drying the concentration of the sap constituents would have peaked. The final profile shows that a very dark stain layer has formed about 1mm below the surface. This KBS layer is even more severe than that formed in schedule 1. The majority of the darkening occurred when the surface was at or below FSP. It is unfortunate that the two samples between 18hr and fully dried could not be tested as they would have made it easier to determine how the stain layer formed.

The lightness profiles for the boards' dried using schedule 3 are shown in Figure 32b. The 7hr and 14hr profiles show a slight darkening at the surface. The MC profiles showed that the surface of the board was below FSP after 14hr of drying. This means that the KBS layer had not formed even though the concentration of reactants at the surface had peaked.

The 21hr, 28hr and fully dried samples all show that a stain layer has formed, but the intensity of this layer varies inconsistently with drying time. It does appear, however, that the majority of the darkening in schedule 3 is occurring below FSP.

The lightness profiles for schedule 5 are shown in Figure 33b. The 3.5hr and 7hr samples show very little darkening at the surface. The MC profiles for schedule 5 showed that after 3.5hr of drying the board was still quite wet in the core. This means the concentration of sap constituents at the board surface was probably still reasonably low, which would reduce the rate of reaction. After 7hr, however, the board is much drier and the surface layer is below FSP, so at this stage the concentration of sap constituents at the surface would be quite high. It is clear that the KBS has not formed, above FSP, when the surface layer contained free water.

The 10hr and 13.5hr profiles do show a KBS layer has formed about 1-2mm below the surface. In both cases the MC of the surface layer is well below FSP. The fully dried sample shows even greater darkening in the surface layer, so clearly the KBS reaction has continued even at very low MC.

The lightness profiles for schedule 6 are shown in Figure 34b. The profiles for this schedule are fairly inconsistent so are difficult to interpret. On all profiles there is some darkening at the surface, but only the 47hr profile shows the normal dip in lightness associated with KBS. Overall the darkening of the samples in this schedule was less than in the previous higher temperature schedules.

The lightness profiles for schedule 7 are shown in Figure 35b. A KBS layer is present in all of the profile except for the 40hr profile. In this schedule the boards seem to have started darkening when the surface layer was above FSP and only darken a small amount below FSP. The darkening seems to have developed faster than some of the higher temperature schedules but is ultimately not as severe.

The lightness profiles for schedules 8 and 9 are shown in Figure 36b and Figure 37b respectively. Neither of the schedules showed the consistent formation of a KBS layer and also neither showed very much darkening overall compared with previous schedules.

In general all of the schedules tested showed some stain formation. To further analyse the data for each of the samples the mean of the L, a* and b* values for all slices was calculated. The mean was also calculated for the three surface slices and the 17 core slices. To get an indication of the total colour change throughout drying the mean core lightness for the first sample (20% drying time) was subtracted from the mean surface lightness for the fully dried sample, for each schedule. This was repeated for the a* and b* values as well. The quantity ΔE was then calculated from these values to give a measure of the total change in colour.

The results of these calculations are shown in Table 11, with the percentage change also being noted for the ΔL, Δa^* and Δb^* values. The first thing of note in this table is that the 50/40 schedule has a very high Δb^* value and consequently a high ΔE value. This is assumed to be an anomaly and so these values will not be considered further in the analysis. The ΔE values show a clear trend in all of the other schedules. The higher temperature schedules are clearly producing the greater colour change. The ΔE values also show that the slow drying schedules are producing the greatest colour change.

The change in lightness, ΔL, also shows a clear differentiation between different dry bulb temperature schedules, but the differentiation is not so clear between different humidity schedules with the same dry bulb temperature. The 50/40 schedule produced the least significant decrease in lightness while the 120/70 schedule produced the most significant decrease in lightness.

The change in the red-green chromaticity coordinate, Δa^*, does differentiate between the HT and ACT schedules based on both dry bulb temperature and relative humidity, but is not very effective in differentiating between the lower temperature schedules. A positive increase in this coordinate indicates a reddening of the sample. These results suggest that the formation of kiln brown stain does not greatly increase the redness of the wood.

The change in yellow-blue chromaticity, Δb*, coordinate differentiates reasonably well between the different humidity schedules at 90°C and 70°C, but does not differentiate so well between the different temperature schedules. Also as noted earlier the 50/40 schedule showed an unexpectedly high change in Δb*. A positive increase in the yellow-blue chromaticity coordinate indicates that the colour contains more yellow, so clearly the formation of kiln brown stain makes the stain layer more yellow.

Table 11. Total colour change for schedules tested, expressed as ΔL, Δa*, Δb* and ΔE.

Schedule	ΔL	Δa*	Δb*	ΔE
1 (120/70)	-13 (16%)	3 (71%)	5 (23%)	14.7
2 (90/80)	-11 (14%)	2 (42%)	7 (32%)	13.6
3 (90/70)	-6 (7%)	1 (24%)	6 (29%)	8.8
5 (90/50)	-8 (9%)	1 (20%)	3 (14%)	8.5
6 (70/60)	-4 (5%)	0	4 (17%)	5.3
7 (70/50)	-4 (6%)	0	2 (9%)	4.9
8 (70/40)	-3 (3%)	0	2 (9%)	3.3
9 (50/40)	-1 (1%)	0	7 (33%)	7.0

Chemical Analysis

The bottom graph presented, in Figure 30 to Figure 37, is the chemical analysis of the surface and centre slices for each sample in each schedule. The results shown are for the nitrogen analysis and in all figures the percentage nitrogen is on the y-axis and the drying time is on the x-axis.

The results for the chemical analysis of the 120/70 schedule are shown in Figure 30c. The nitrogen levels in the core of the boards show a decrease with time. This is what is expected because moisture moving to the drying surfaces will be transporting soluble nitrogenous compounds away from the core. This observation is in agreement with the results in the literature.

The nitrogen levels at the surface increase with drying time to a peak at 6 hours and then decrease with drying time. This is an unexpected result as it is assumed that the nitrogenous compounds from the core will accumulate at the surface. It is likely that there was an error in the measurement at 6hrs as the nitrogen concentration for this sample is considerably greater than in any of the other samples. It could also be due to the original board having a higher than normal concentration of nitrogenous compounds. This is however unlikely as all of the sample were matched and from the same tree and the core sample does not have a higher concentration.

If it is assumed that the 6 hr sample is erroneous then the surface concentration would appear to increase in the early stages of drying (2-4hr) and then reach a maximum at about 6 hrs. This corresponds to the time when the moisture content at the surface has dropped below fibre saturation point, so there should no longer be any movement of liquid sap to the surface. This is also the time when the kiln brown stain layer first becomes obvious.

The results for the chemical analysis of the 90/80 schedule are shown in Figure 31c. These results show a very clear reduction in the core concentration with time and a clear increase at the surface. It should be

noted however that the two samples that could not be tested were between the 18hr sample and the fully dried sample. It is likely that these samples would have had a nitrogen concentration similar to the fully dried sample as the 18 hr sample was almost dried to the fibre saturation point. The surface concentration reaches a level similar to the 120/70 schedule if the 6 hr sample is ignored for that schedule.

The chemical analysis for the 90/70 schedule (Figure 32c) shows some variability. The greatest change in the levels of nitrogen at the surface occurs from 14hr to 21hr. This is unusual as the moisture content of the surface layer is at FSP for both samples so there should not have been movement of liquid sap to the surface. The MC of the 14hr sample near the surface is actually lower than in the 21hr sample. This suggests that the 14hr sample may have begun with a lower MC, which could also mean a lower concentration of sap components (based on the wood volume). An alternative possibility is that there was a dense latewood band, about 12mm from the surface, in the 14hr sample that created a diffusion layer. Such a layer would reduce the quantity of sap compounds reaching the surface and also cause the surface layer to dry faster and the core to dry slower. Given the destructive nature of the tests it is not possible to determine the exact cause for the variability, which could simply be experimental error. In spite of the variability, however, the nitrogen levels at the surface reach values similar to the previously discussed schedules.

The chemical analysis results for the 90/50 schedule, shown in Figure 33c, are unusual as the concentration of nitrogen in the centre is, for some of the samples, greater than at the surface. Assuming this is not the result of experimental error, these samples clearly differ from those in the previous, and indeed, subsequent schedules. The unusual results may be due to the presence of large protein molecules in the core of the boards that are not mobile in the sap. Also there is an indication, from the slope on the MC profiles, that the board may have a low permeability, which would affect the distribution of sap compounds if there were points where the moisture only moved by diffusion. Regardless of the cause of these results they will not be used in the overall analysis.

The results for the 70/60 schedule, shown in Figure 34c, are quite uniform with all the samples showing similar nitrogen levels in the core slices and in the surface slices. This is a reasonable result as the MC of all the samples were low enough to be at or below irreducible MC. This means that bulk flow of liquid moisture would have ceased in all samples so the nitrogen levels would be static. The nitrogen levels are about the same as for the previous schedules, though the core levels are slightly higher and the surface levels slightly lower.

The results for the 70/50 schedule, shown in Figure 35c, are more variable than the 70/60 schedule. The overall nitrogen levels are similar, however, being higher in the core and lower at the surface than the ACT and HT schedules.

The chemical analysis for the 70/40 schedule, shown in Figure 36c, is similar to the results obtained for the higher temperature ACT and HT schedules. There is however some variability with the fully dried sample having quite a low level of nitrogen at the surface compared to the other samples.

The results for the 50/40 schedule, shown in Figure 37c, are very variable. The results for the first two samples are similar to previous schedules, but in the third and the fourth samples the core nitrogen levels are much higher. The surface measurement for the fully dried sample is very high as well. It is difficult to find an explanation for these results, though it does appear that the surface levels are similar to the other schedules.

In general the results from the chemical analysis of the wood slices were not as clear as they needed to be to show the link between nitrogen accumulation and kiln brown stain formation. This is due in part to the design of the experiment and also the variable nature of the wood. The experiment was designed to measure the samples at five evenly space time periods within the total drying time. The low temperature schedules were therefore almost dried to FSP by the time the first sample was taken. In these cases the movement of liquid moisture would have all but ceased to occur after the first sample. Any future experiments should focus on the drying above FSP.

What can be determined from the experiments is that there is nitrogen accumulation at the surface of boards in all schedules from LT through to HT. Also the level of nitrogen at the surface is similar for all of the schedules tested, with the higher temperature schedules having only a slightly higher level at the surface and a slightly lower level at the centre. One possible explanation for this difference could be related to the speed of drying in the lower temperature schedules. The faster drying rate means that the moisture in the board is effectively moving very fast so the slow diffusion of compounds against this flow is insignificant. In the lower temperature schedules the moisture flow is lower so the diffusion processes have more of an effect on the redistribution of sap compounds. This idea is supported by the fact that the 70/40 schedule, with a drying rate similar to the 90/80 schedule, has nitrogen levels comparable to the ACT and HT schedules.

An alternative explanation for the difference could be that the higher temperatures are releasing more bound proteins in the centre to be transported to the surface. This will have the effect of reducing the nitrogen concentration at the centre and increasing the nitrogen concentration at the surface. This idea is supported by the sap displacement experiments performed by McDonald et. al. (2000), which showed that protein and free amino acid extraction increased when samples were heated before sap displacement.

Other Results

Core Darkening

So far kiln brown stain has dominated the analysis of the lightness, however it has been noted, especially with the higher temperature schedules, that there is also an overall darkening of the wood throughout the boards. In some cases, the overall darkening is also significant in wood processing as the kiln brown stain is commonly removed by planing in the remanufacturing.

To show the darkening effect more clearly the mean of the lightness values of the slices, excluding the four nearest the surface, was calculated for each board. The four slices nearest the surface were excluded as they contained the kiln brown stain layer, which would swamp the colour changes in the core.

The mean lightness values for the 120/70 schedule are plotted in Figure 38. This schedule showed the greatest decrease in core mean lightness of all the schedules tested. This graph shows that the core colour is darkening even during the early stages of drying. The decrease in lightness of approximately 4 over the entire schedule is greater than the colour change at the surface for some of the milder schedules.

In order to compare the core colour changes for different schedules the lightness values need to be normalised. The mean core lightness values for four of the schedules were normalised so that the maximum lightness value was 85. These normalised values were plotted and a linear trend line was then drawn through each set of points. The maximum lightness values for each schedule were adjusted to bring the trend line together for ease of analysis. This does not affect the results as it is the gradient of the trend line that is important rather than actual lightness values.

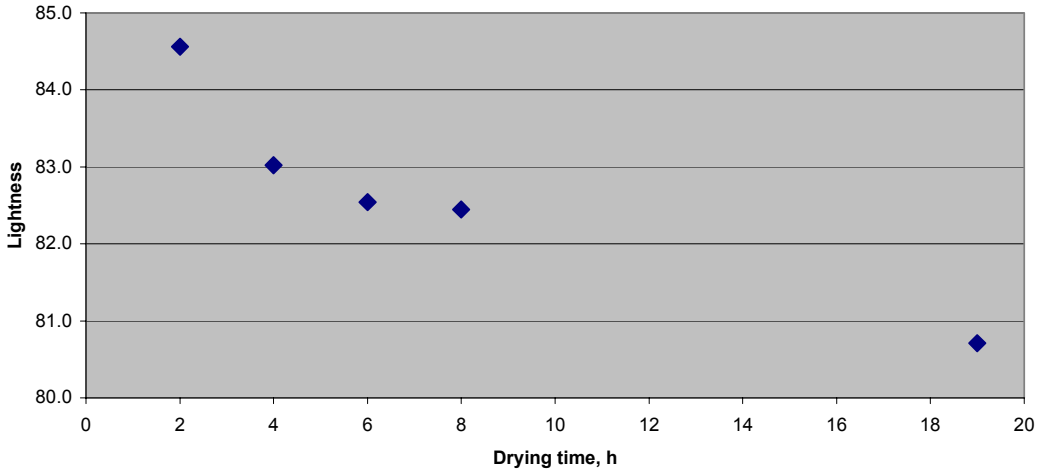

Figure 38. Change in mean core lightness with drying time for 120/70 schedule.

The normalised and adjusted lightness values for the four selected schedules are shown in Figure 39. The gradient of the trend lines represents the rate of core darkening. The fit for the 120/70 and 90/80 schedules are reasonably good at R^2=0.9032 and R^2=0.8786 respectively. The fit for the 70/60 and 50/40 schedules are not good at R^2=0.1121 and R^2~0 respectively. This difference in fit may be due to the relative influence of the schedule and the sample wood properties on the darkening effect. In the higher temperature schedules the core darkens more so the variation in initial colour is less significant than in lower temperature schedules where the rate of darkening is very low.

If the error in the trend lines is accepted then it appears that the rate of core darkening is greater at higher temperatures. The low temperature 50/40 schedule does not show a significant change in the mean lightness of the core during drying. The conventional temperature 70/60 schedule does show some change in core lightness of about 0.5 over the entire drying time. The level of core darkening in the ACT schedule is about three times greater than this and the HT schedule approximately six times greater. More research will be required to confirm the rates of core darkening.

Another way to look at core darkening is to calculate the mean yellow-blue chromaticity coordinate, b*, at each time in each schedule. As the core darkens the b* coordinate increases in the positive direction indicating an increase in the yellowness of the sample. In Figure 40 the change of b* with time has been plotted for the ACT schedules (90/80, 90/70, 90/50). The 90/80 and 90/70 schedules both show a definite increase in b* with drying time but the 90/50 schedule shows more variability. When linear fits are made to the 90/70 and 90/50 data the gradients for the three schedules are similar and the final b* value increases with drying time. The first observation reinforces the idea that the rate of discolouration is temperature dependant and the second observation shows that the discolouration is worsened with extended drying times.

The yellow-blue chromaticity coordinate may give a better indication of core darkening than the lightness coordinate. This is probably because the colour change in the core has more of a yellowing effect rather than a darkening effect.

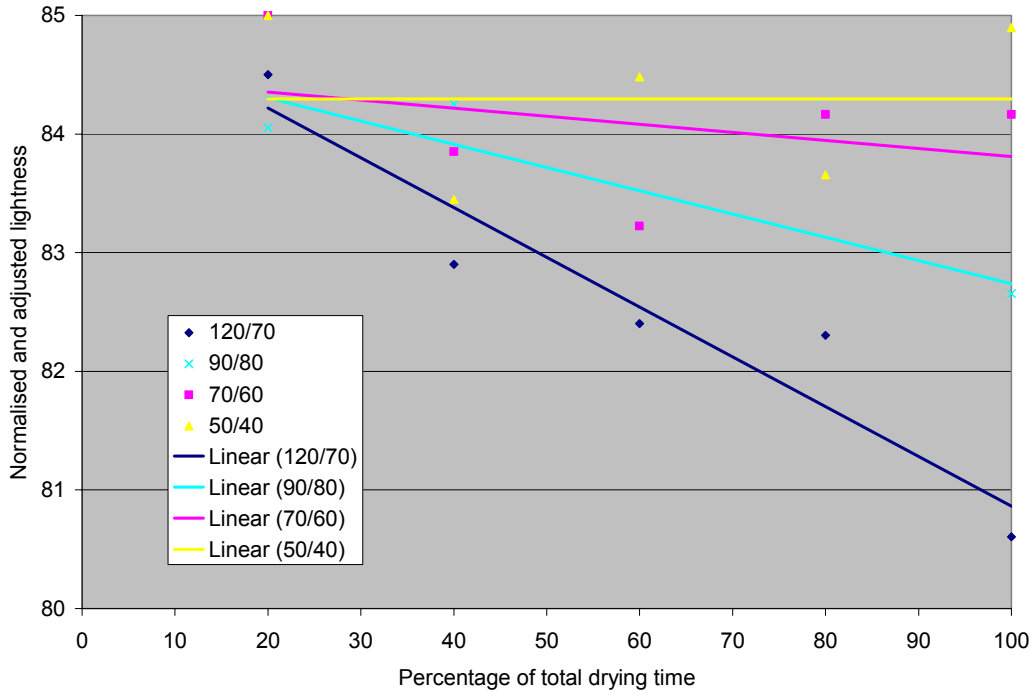

Figure 39. A comparison of core darkening for four selected schedules. The lightness values have been normalised and then adjusted along the y-axis to align the trend lines.

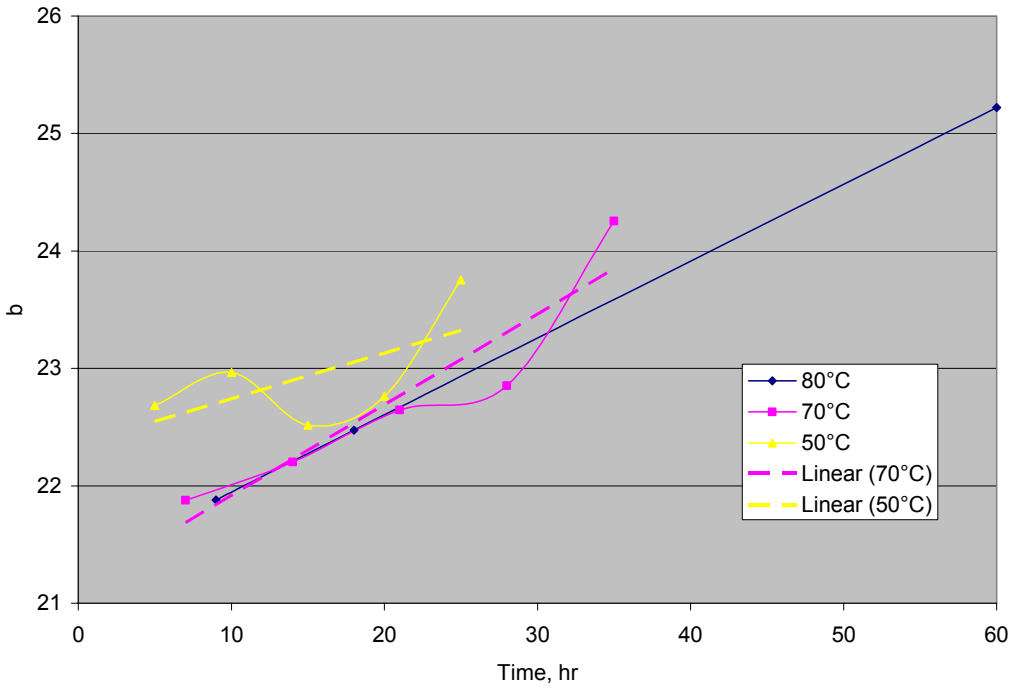

Figure 40. Increase in yellow-blue chromaticity coordinate, b*, with drying time for the ACT (90°C dry bulb temperature) schedules. The legend indicates the wet bulb temperature for each schedule.

Colour Planes

So far only a single colour coordinate has been plotted with time to give an indication of colour change. It is also possible to plot the colour data on a colour plane. This method has been used by Ledig and Seyfarth (2001) to characterise the surface colour of wood. The results for the 120/70 and 70/40 schedules are shown here as the former produced the most colour change and the latter showed the least. Graphs for the remaining schedules are provided in the appendices. In each graph all of the points for each time period have been plotted and are enclosed in a box of the same colour to give an idea of the range of values.

The results for the 120/70 schedule plotted in the L-b* plane are shown in Figure 41a. Most of the points for all five time periods are grouped in the lower right quadrant of the graph. This area of the graph represents relatively light colours with a relatively low intensity of yellow. Most of the points in this region are from the core of the boards and indeed most of the points from the core of the boards are in this region. All of the points for the 2hr sample are in this quadrant indicating a light coloured wood throughout the board. The points nearer to the top and left are from slices close to or at the surface. The points for the 4hr sample are also grouped in this quadrant except for one of the surface slices that is more yellow and therefore in the top right quadrant.

Later in drying the points on the graph shift in the direction of the top left quadrant, indicating a darkening and yellowing of the boards. There is a significant shift to the left with the 6hr sample due to

the decrease in lightness at the surface. There is also an increase in the yellowness, though the extremes of yellowness and darkness are not in the same samples. The 8hr and fully dried sample shift slightly more to the left but the change is not as dramatic as the change from 4hr to 6hr.

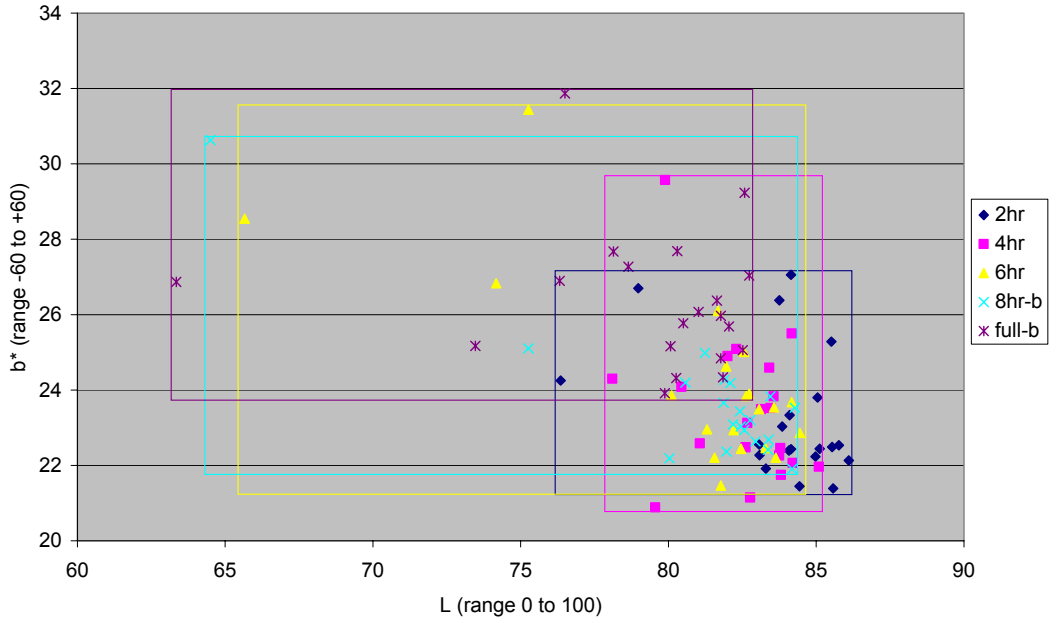

a.

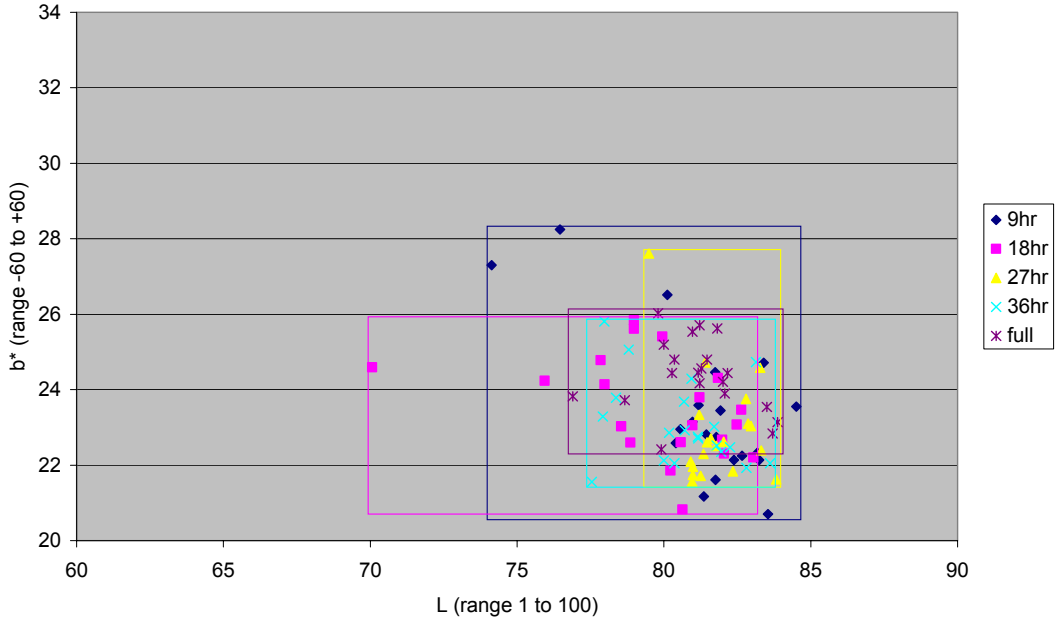

b.

Figure 41. L-b* colour planes for the a.) 120/70 and b.) 70/40 schedules

The points for the 70/40 schedule samples almost all lie in the bottom right quadrant. The change with time for this schedule is not as clear as it is for the 120/70 schedule. There does however seem to be a slight shift towards the yellow with time, but no significant increase in darkness. As with the 120/70 schedule the yellowing and the increase in darkness do not correlate very closely.

The L-a* colour planes for both schedules are shown in Figure 42. The shifts in colour in these graphs show trends similar to those in the L-b* plane. The difference is that the a* chromaticity coordinate more closely correlates to the lightness than does the b* chromaticity coordinate.

The a*-b* colour planes for both schedules are shown in Figure 43. This colour plane shows a clear distinction between the different drying times for the 120/70 schedule but no real distinction for the 70/40 schedule.

The colour planes are a useful way of representing wood colour as they provide more detailed information than a simple lightness profile. Of the three possible planes the L-b* plane is probably the best as there is the least correlation between these two values. Also it has been shown previously (Table 11) that a* is only a good indication of colour change at high temperatures.

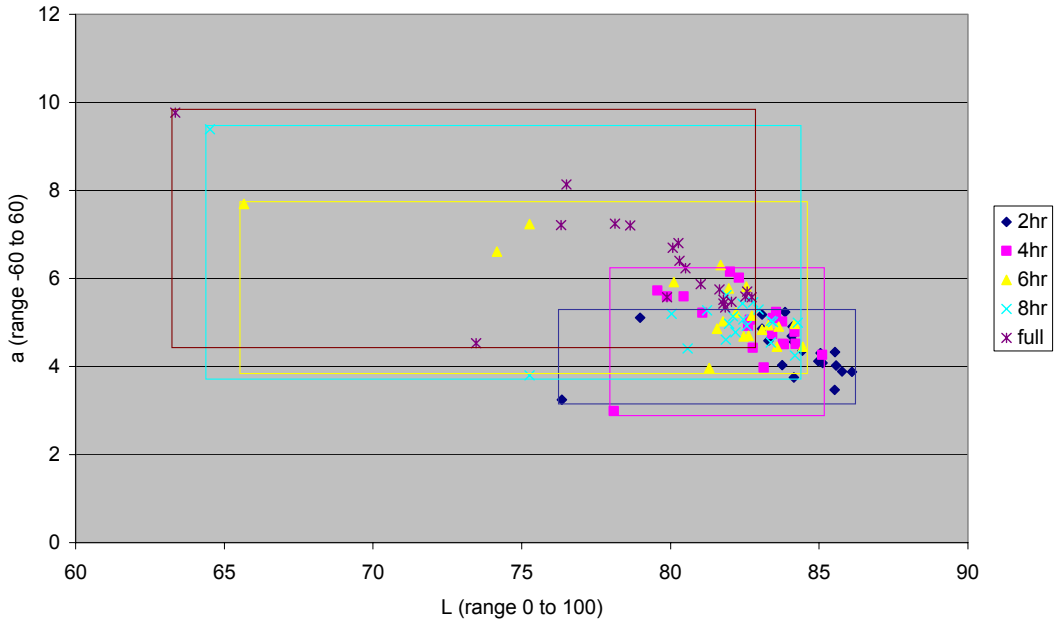

a.

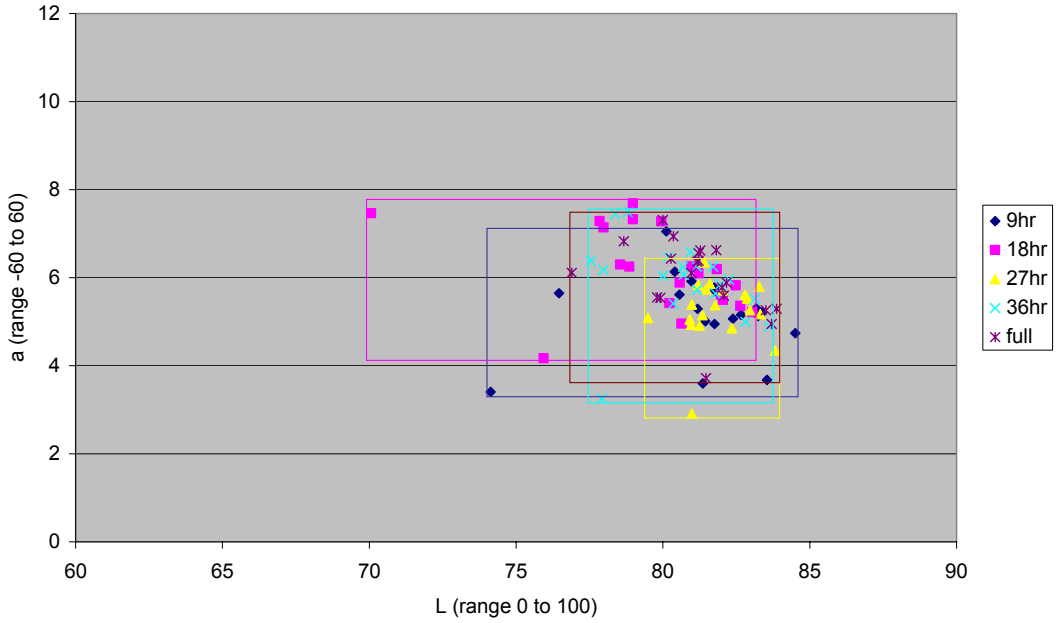

b.

Figure 42. L-a* colour plane for a.) 120/70 schedule and b.) 70/40 schedule.

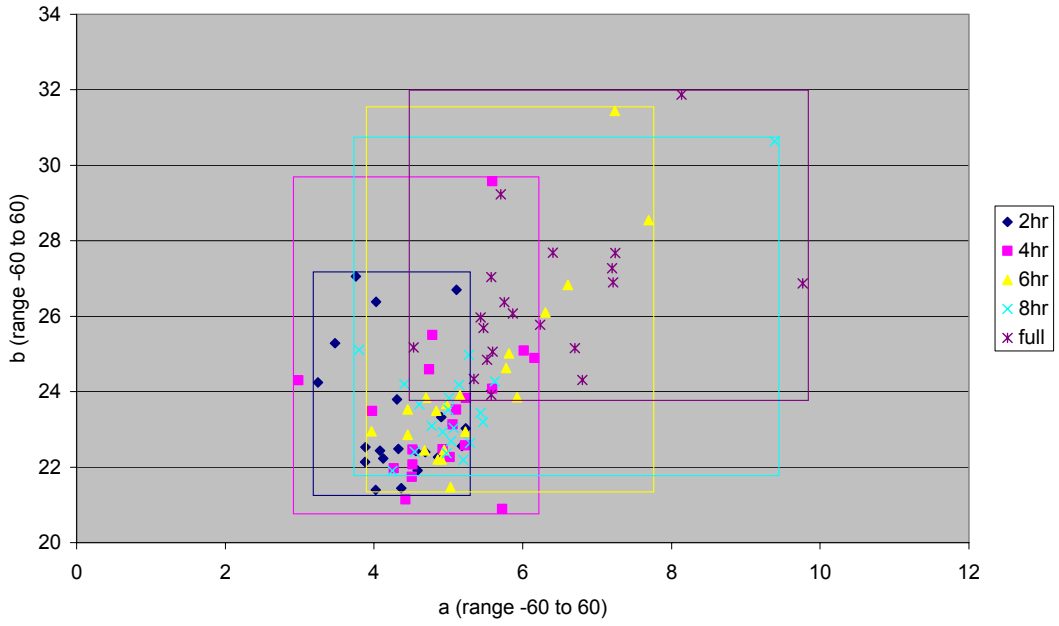

a.

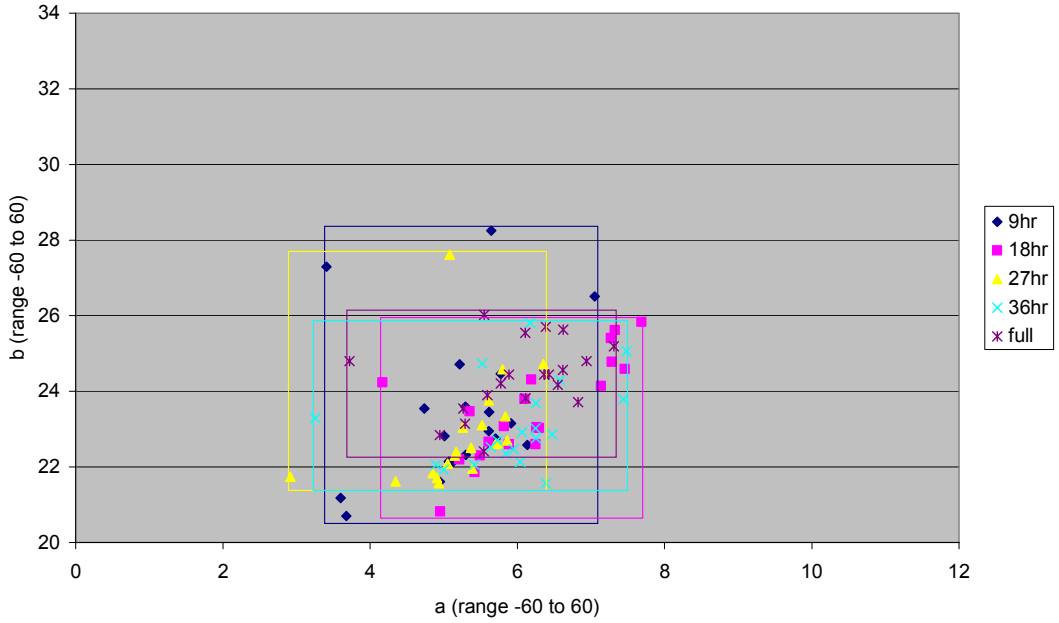

b.

Figure 43. a*-b* colour plane for a.) 120/70 schedule and b.) 70/40 schedule.

Microscopic Investigation of the Kiln Brown Stain Layer

The experiments using large boards described in part two showed that there was a difference in the colour development for different humidity drying schedules with the same dry bulb temperature. The experiments described in the following pages further explore the effect of schedule humidity on the development of kiln brown stain by using a microscope to look in detail at the stain layer.

Experimental

In this experiment the wood used came from the large boards dried in experiments described in Part two above. The samples came from the boards dried at the three schedules shown in Table 12.

Table 12. Drying schedules used to dry the boards before analysis of colour development.

Schedule	Dry Bulb Temperature, °C	Wet Bulb Temperature, °C
1	70	60
2	70	50
3	70	40

A 20mm thick section was removed from the middle of each of the fully dried boards for analysis of colour. Small samples were cut from these sections and analysed using the method described in Chapter 3 for microscopic image analysis.

Results and Discussion

The micrographs shown in Figure 44 to Figure 46 show the three faces at the surface of the board dried using a 70/60 schedule. There are two notable observations that can be made from these pictures. These observations are more noticeable when observed under the microscope than they are in the figures presented here.

The first observation of note is that the ray tissue is generally darker than the wood around it. This can be seen, and has been highlighted, in both the radial face and the tangential face. There are probably three reasons for this darkening occurring. Firstly the ray tissue contains parenchyma cells that are the living cells of the tree and therefore contain a variety of metabolites that can react in a Maillard reaction. Secondly the ray tissue may contain resin ducts that carry coloured resinous compounds so these would be responsible for some of the darkening, although most of the darkened ray tissue did not appear to contain resin ducts. The final reason is that the ray tissue is likely to be a major conduit for moisture transport to the surface as there are very few bordered pits on the radial face of the axial tracheids. This means that accumulation of sap compounds, and therefore Maillard darkening, is more likely to occur in, or adjacent to, the ray tissue.

The second observation of note is that the darkening in the ray tissue extends further than the stain in the axial tracheids, both towards the surface and away from the surface. The extension towards the surface suggests that the ray tissue is more likely to remain intact in the damaged surface layer. This is probably due to the cells in the ray tissue being shorter compared to the axial tracheids. The extension into the core

of the board is another indicator of the role of ray tissue in the transport of moisture and sap compounds to the evaporative front.

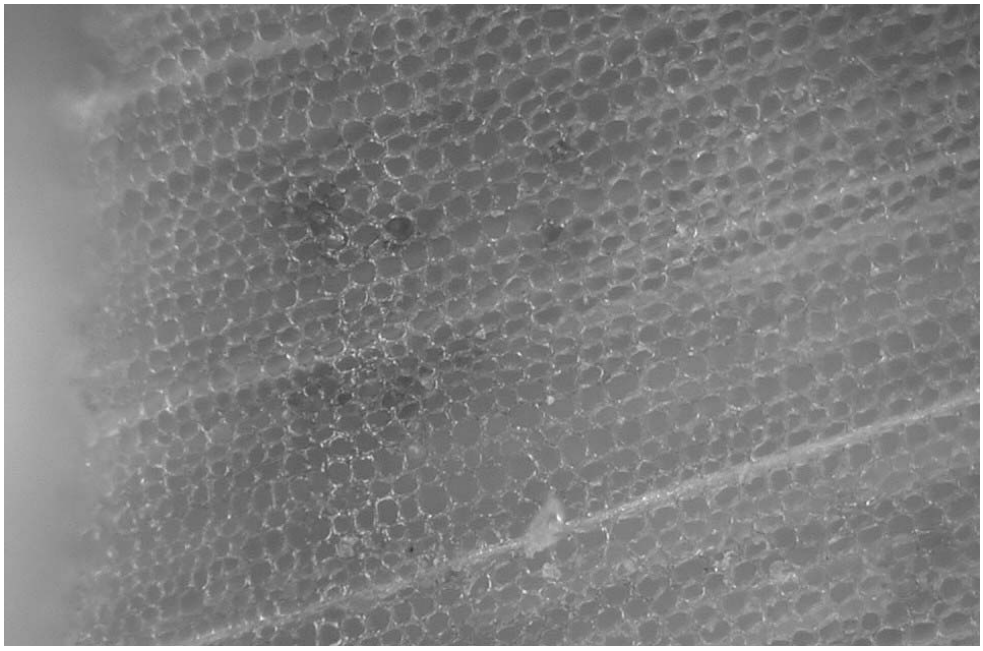

Figure 44. Light micrograph of the longitudinal face at the surface of the board dried at 70/60.

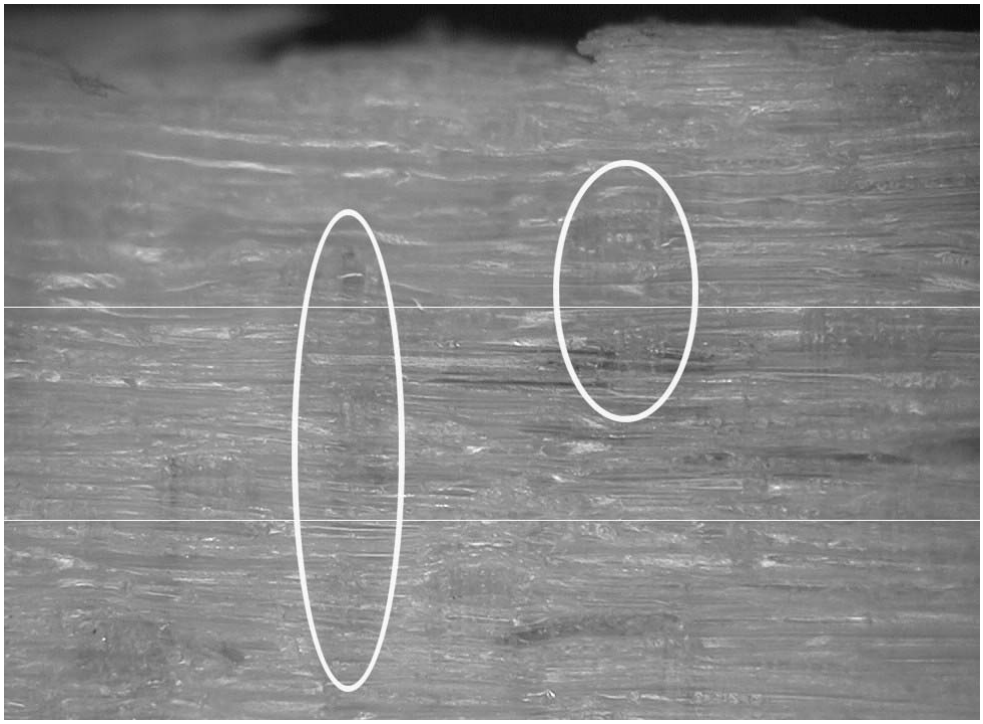

Figure 45. Light micrograph of the tangential face at the surface of the board dried at 70/60. The kiln brown stain layer is indicated approximately by the parallel white lines and the ellipses highlight darkened ray tissue.

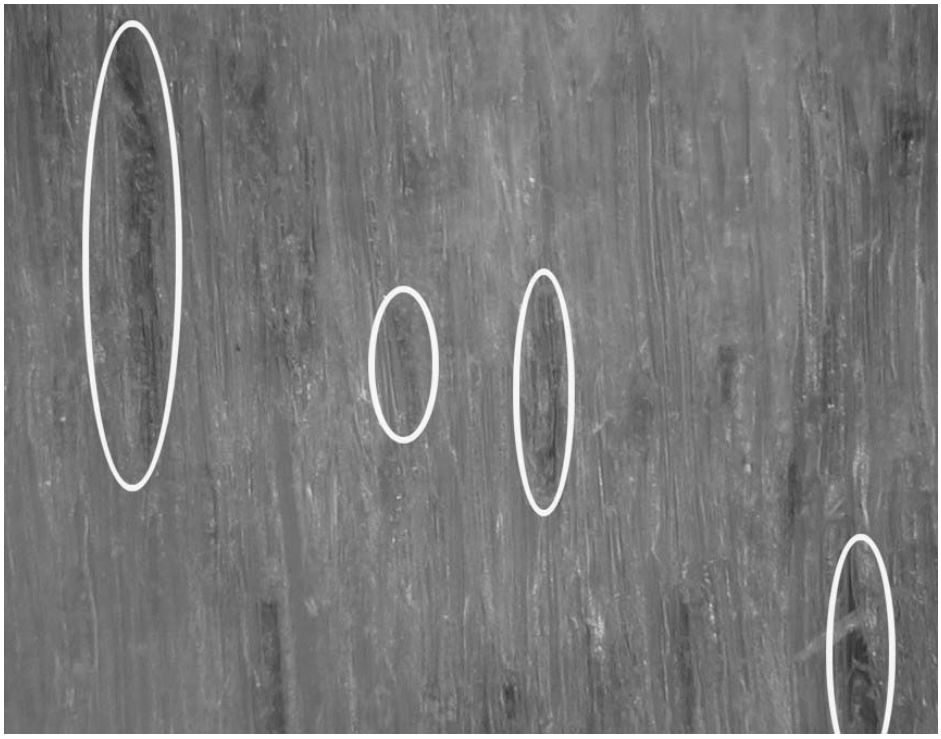

Figure 46. Light micrograph of the radial face at the surface of the board dried at 70/60. The ellipses highlight some of the darkened ray tissue.

The composite image in Figure 47 shows an image of the longitudinal face at the surface of the board dried at 70/60, which has been split into the three colour coordinates of the CIELab system. The image on the left shows the lightness coordinate in greyscale. This image shows most of the features on the face, with the outline of the cell walls quite clear and also some detail in the lumens.

The centre image is the red-green coordinate in greyscale. This image shows very little of the detail seen in the lightness image and only shows cell walls clearly in the kiln brown stain layer. Another feature that is highlighted is what appear to be a ray and a resin canal. The fact that the a* coordinate mainly picks up colour in the kiln brown stain layer suggests that it is a useful coordinate to use for observing the stain layer microscopically without interference from the structure of the wood. This differs from the findings of the drying studies where this coordinate was only useful at high temperatures. The grey colour of the image also suggests that there may be some lumen detail in the image but it is difficult to determine.

The right image is the blue-yellow coordinate in greyscale. This image picks out clearly the detail of the cell walls but does not show any detail in the lumens. The cell walls in the kiln brown stain layer are darker so this coordinate is also able to show the presence of a stain layer. The colour profiles derived from these images and similar images for the 70/50 and 70/40 schedules are shown for the individual co-ordinates in Figure 48 to Figure 50. These graphs have been plotted to show the differences between different humidity schedules at the same temperature.

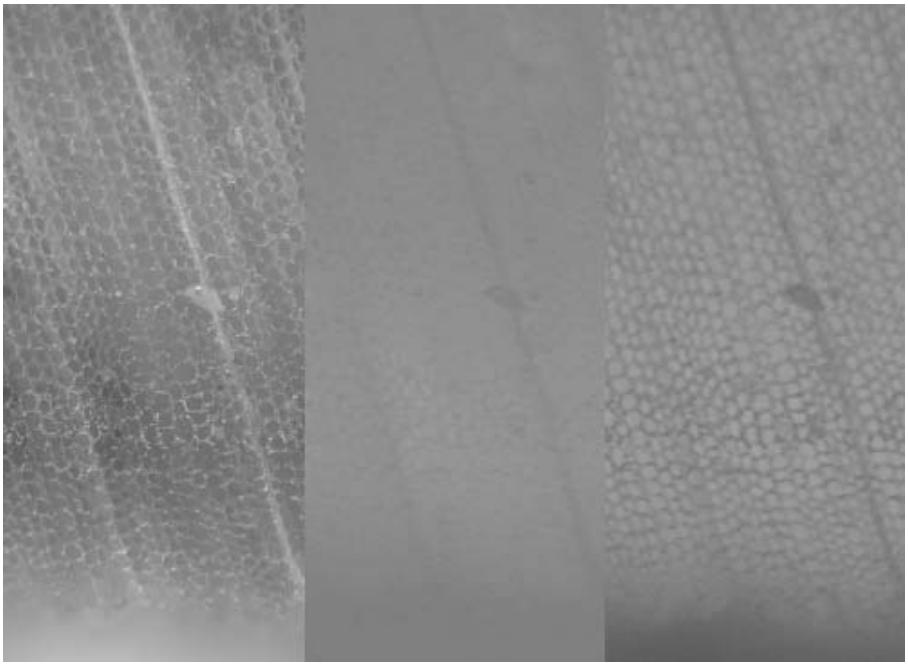

Figure 47. Composite image showing the same image of the longitudinal face at the surface of the board dried at 70/60. The left image is the greyscale image of the lightness coordinate, the centre is the greyscale image of the red-green chromaticity coordinate, and to the right is the blue-yellow coordinate.

All three sets of profiles show a distinct difference between the different relative humidity schedules. The lightness profiles in Figure 48 show that the kiln brown stain layer produced by the 70/60 schedule is not only darker but also closer to the surface and thicker than those produced by the 70/50 and 70/40 schedules. The blue-yellow coordinate profiles in Figure 50 also show that the stain layer is closer to the surface with the higher humidity schedule. This coordinate also shows that the peak intensity of the stain layer is closer to the surface with the higher relative humidity. The a* coordinate shows the clearest difference between the three schedules in Figure 49. This is probably due to the fact that this coordinate does not pick up much of the detail of the wood structure.

All of the profiles show a peaked shape, where the intensity of the stain layer increases over a distance to a peak and then decreases in a similar fashion. This is not necessarily an accurate representation of how the colour changes along a single line passing through the stain layer. It may be the result of averaging a stain layer that has a slightly variable distance from the surface.

The thickness of the stain layer, distance from the surface and point of peak intensity can be estimated from the three graphs to determine how these dimensions are influenced by the relative humidity of the drying schedule. The values for each of these dimensions estimated from the graphs are shown in Table 13. There is clearly a difference between the schedules. Firstly, the distance of the layer from the surface increases as the relative humidity decreases. This is probably due to the greater temperature profile at the board surface for the lower relative humidity schedules that increases the driving force for moisture

movement and therefore forces the evaporative front further into the wood before it can reach equilibrium. This is also an explanation for the position of the peak intensity of colour.

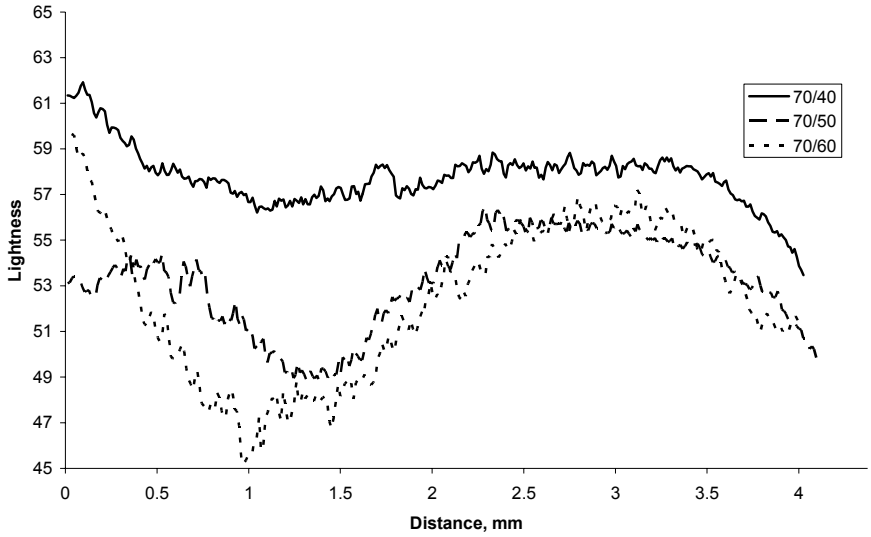

Figure 48. Colour profiles at the surface using the lightness coordinate, L*, for three different humidity schedules at 70°C.

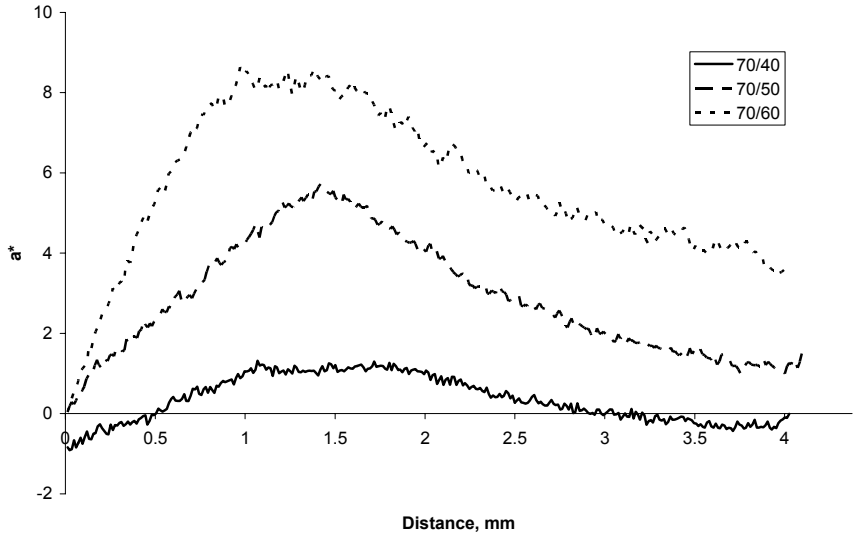

Figure 49. Colour profiles at the surface using the red-green chromaticity coordinate, a*, for three different humidity schedules at 70°C.

The thickness of the stain layer is most likely to be influenced by the drying time above irreducible moisture saturation. The higher humidity schedules have a slower drying rate and therefore the free water flow phase of drying is longer. There is more time for sap compounds, and some coloured reaction products, to diffuse back into the core of the board. The influence of humidity on the redistribution of

sugars in wood determined by Terziev et al. (1993), as shown in chapter two, shows that low humidity (fast) schedules result in a narrower concentration of sugars at the surface compared to high humidity (slow) schedules. This is in agreement with the results for stain development found in this experiment as the development of stain is a direct consequence of the accumulation of sap compounds.

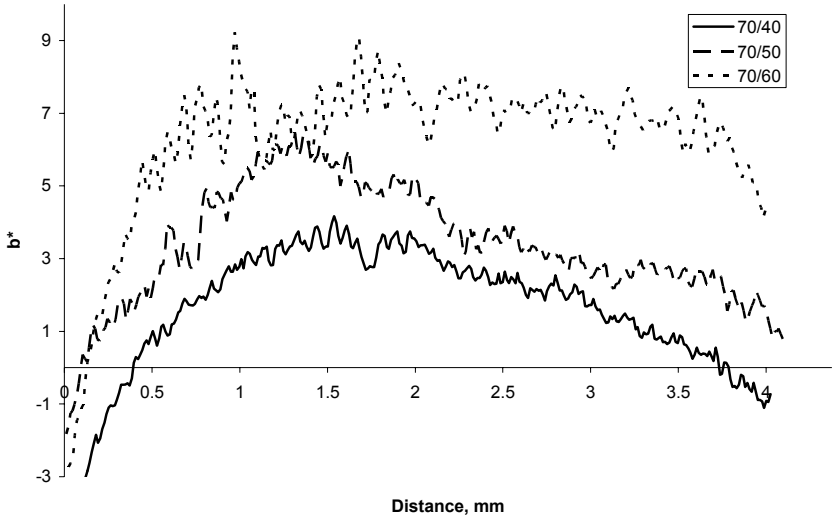

Figure 50. Colour profiles at the surface using the blue-yellow chromaticity coordinate, b*, for three different humidity schedules at 70°C.

When estimating the extent of the kiln brown stain layer for the purposes of determining a maximum concentration of sap compounds it is not sufficient just to use an average thickness based on the values in Table 13. This is due to the peaked nature of the profiles, which suggests that the concentration of sap compounds over the thickness of the stain layer is not uniform. For this reason it is probably more accurate, when calculating the maximum concentration, to say that the actual thickness of the stain layer is half that determined from the profiles. In the 70°C schedules the thickness of the stain layer ranges from 0.75mm to 1.1mm. These dimensions correspond to a 20-fold concentration of the sap at the surface for a 40mm board.

Table 13. Dimensions of the kiln brown stain layer produce by three different humidity schedules at 70°C.

Schedule	Distance from Surface	Peak Intensity	Thickness
70/40	0.6mm	1.5mm	1.5mm
70/50	0.5mm	1.4mm	1.6mm
70/60	0.3mm	1.2mm	2.2mm

The measurement of nitrogenous compound accumulation in previous experiments presented in part two showed that there was a 2-4× increase in concentration of the compounds at the surface. This measurement was taken from an approximately 4mm thick sample. When combined with the thickness of the stain layer determined above this corresponds to a concentration increase from 8-21× at the stain layer.

This concentration increase represents an average value over the entire stain layer. In a real stain layer there will be some cells that have cavitated early and therefore have a lower concentration of sap compounds. Conversely there will also be those cells that are the last to cavitate, which will have a much higher concentration of sap chemicals. It is reasonable to use the average value if the reaction rate increases linearly with concentration.

Drying of Full-size Boards

This set of experiments was originally designed to provide data for the validation of a computer model and as such the experimental design was done in consultation with the model developers. However, the results have shown some consistencies with the experiments presented earlier in this chapter.

Experimental

The boards were selected and prepared as described in Chapter 3 and dried in the semi-scale kiln using four schedules selected to be similar to commercial schedules and cover a range of temperature conditions. These schedules, which were determined by the model developers, are as follows:

a) 140/90 °C for 14 hours, followed by 2 hours of cooling (everything turned off) and finally 6 hours of steam conditioning using saturated steam (100/100 °C).

b) 120/70 °C for 20 hours, followed by 2 hours cooling and finally 4 hours steam conditioning.

c) Pre-steam using saturated steam (100/100 °C) for 4 hours, followed by 90/60 °C drying for 56 hours then 4 hours steam conditioning.

d) Pre-steam (100/100 °C) for 4 hours, followed by 70/60 °C drying for 120 hours and then 4 hours steam conditioning.

The pre-steaming steps were used but the final steam conditioning steps were not applied because the kiln was not able to maintain the required steam saturation condition and the steaming would have resulted in over-drying of the sample boards. The maximum airspeed of the kiln was used for all schedules and the airflow check shows that the within-stack airflow varied along the stack height with air velocity of 3.2 m/s in the upper part, 3.8 m/s in the middle height and 3.1 m/s in the lower part of the stack.

The normalised drying curves for the four schedules are shown in Figure 51 with both the moisture content and the drying time normalised. Each of the curves shown in this graph is averaged from the eight boards dried at each schedule. In these plots the normalised moisture content of zero is the final moisture content of the boards which was different for each schedule.

Results and Discussion

The level of checking produced for the four schedules is shown in Figure 52 where the data is split into within-ring checking and cross-ring checking. Within-ring checks are those that form in the earlywood and are contained between the two adjacent latewood bands. Cross-ring checks are those that cross one or more growth-rings including earlywood and latewood bands.

The results show a distinct difference in checking between the four schedules tested. The level of within-ring internal checking decreases with decreasing drying temperature. The results confirmed that the within-ring checking occurrence is related to the drying temperature and drying rate. However, the cross ring checking has a different mechanism but high temperature is likely a factor for the cross ring checking occurrence. The lowest temperature schedule still has the lowest level of checking both of the within-ring and cross ring, but the next best for the cross ring checking is the highest temperature schedule.

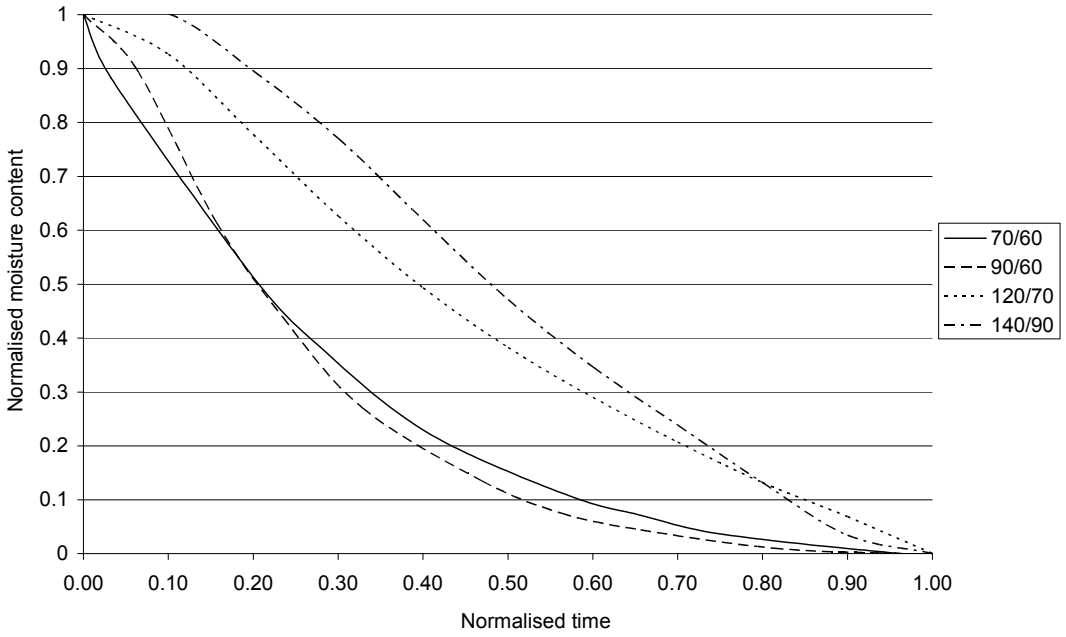

Figure 51. Normalised drying rate curves for the full-size boards dried in the semi-scale kiln at four different schedules. Each curve is an average curve for the eight boards dried at each schedule.

The relationship between drying temperature and incidence of within-ring internal checking is consistent with a mechanism based on internal water tension during the capillary phase of drying. This assumes that the water tension inside the wood is higher for high temperature schedules where the drying rate is highest. In this case the rate of drying is probably the significant factor driving the formation of checks. There may also be a softening effect at high temperature where the cell wall strength is reduced by the softening of constituents of the cell wall matrix. The 90/60 and 70/60 schedules have the same wet bulb temperature and a similar incidence of within-ring checking. The temperature of the wood during the capillary phase of drying will be above but close to the wet bulb temperature, so this is an indication of the importance of the wood temperature during this phase on the incidence of checking.

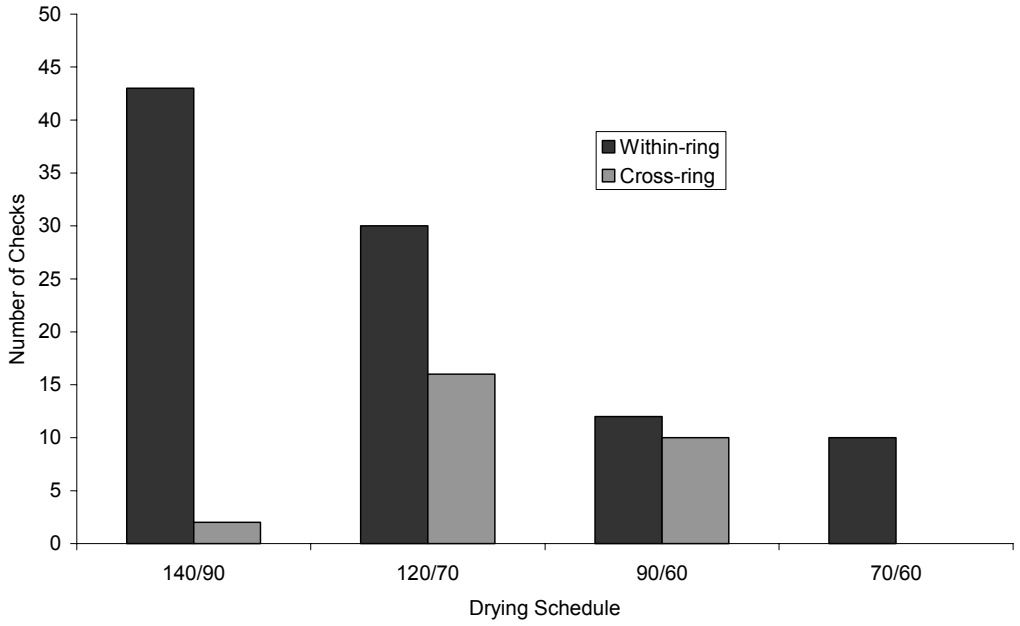

Figure 52. Results of within-ring checking and cross-ring checking from the drying of full-size boards in a semi-scale kiln showing effects of drying schedules.

The differences in the incidence of cross-ring checking can probably be explained as being a result of lignin softening at the higher temperature. This means that these checks will form during the vapour phase of drying when the temperature of the wood is closer to the dry bulb temperature of the schedule. The larger checks will most likely form due to stress in the boards caused by differential shrinkage between layers with different moisture contents as the evaporative front passes through the board. There may also be an effect from case hardening that occurred earlier in drying. At the highest temperature schedule the dry bulb temperature is above the glass transition temperature of lignin and it has been shown that this dramatically increases the creep rate of the wood when it is subject to stress (Keep, 1998). The increased creep therefore allows the stresses to be relieved by deformation before the cross-ring checking can occur. Below the glass transition temperature the incidence of checking clearly increases with increasing temperature which suggests that the severity of the drying stresses is increased by the higher rate of drying.

The formation of kiln brown stain for the four schedules is shown in Figure 53. In the figure, the severity of the stain is a relative measure based on visual inspection with zero the lightest and 5 the severest. The results presented here are an average for the eight boards dried at each schedule. There is a clear temperature dependence on stain formation with the higher temperatures causing more severe staining. This is what would be expected based on previous research as noted in Chapter 2. The experiments described in the second part of this chapter use a more detailed and repeatable method for measuring the stain so these experiments will be used for the analysis of schedule on colour development.

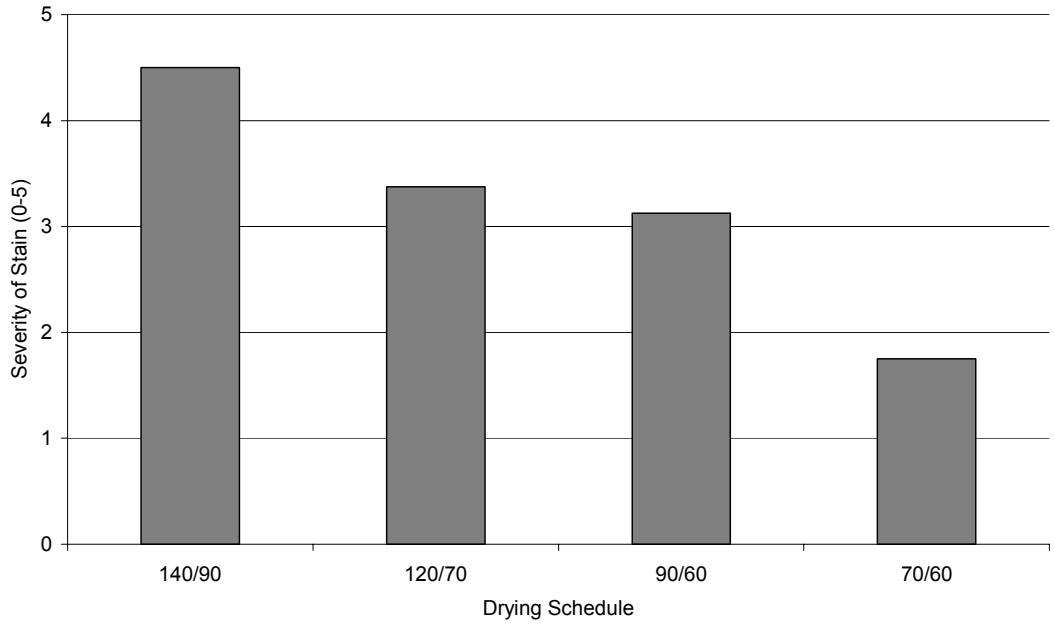

Figure 53. Severity of kiln brown stain for four different drying schedules from the drying of full-size boards in a semi-scale kiln.

Commercial Colour Measurements

The experiments described so far in this chapter provided the basis for a recommendation to a commercial wood drying company on a schedule to minimise the development of stain in timber intended for export for use in appearance products. The schedule was tested on a stack of commercial timber source from Southland forests and dried in a newly built Fogarty timber drying kiln. This was an opportunistic experiment based on an offer from John Fogarty Ltd to test a schedule in a commercial environment. The wood was destined for export so it was not possible to do detailed sampling as the wood was required in commercial lengths.

The original recommendation was to use a 70/40°C schedule but this was not within the humidity control capabilities of the kiln during the initial drying phase when evaporation from the timber was high. The wet bulb depression was therefore reduced to 20°C which the kiln was able to cope with and then increased again to 30°C later when the evaporation from the stack had decreased.

When the drying schedule was complete and the stack had reach its target moisture content a sample was removed for colour testing. Three samples of wood were also obtained from the Quality Control Manager at Brightwood Ltd. One of these samples was considered to be an ideal colour for appearance grade applications while the other two were considered OK.

The results of the measurement of surface colour of the four samples are shown in Figure 54. The measurements were made using the same technique used in the experiments described in the first part of this chapter. For each sample four measurements were taken and plotted independently on the graph.

The lightness profiles for the ideal sample are plotted in green and show that there is still surface discolouration indicating that a small amount of KBS has formed near the surface. The sample was provided as rough sawn and further processing would remove most of the darkened layer so the more important information is the colour from 2-5mm layer. For the ideal sample the lightness between 2mm and 5mm from the surface is between 80 and 85. By comparison the samples considered OK the lightness is as low as 75. It is probably reasonable to assume however that the ideal minimum lightness for appearance grade timber is 80.

The test samples easily reached the minimum lightness requirement of 80 with all of the samples being closer to a lightness of 83. This suggests that the use of low humidity schedules can minimise discolouration in commercial kilns. The wood is slightly lighter than that in the previously described experiments, which is most likely due to the different source of the timber as Southland timber is generally regarded to be lighter than timber from further north.

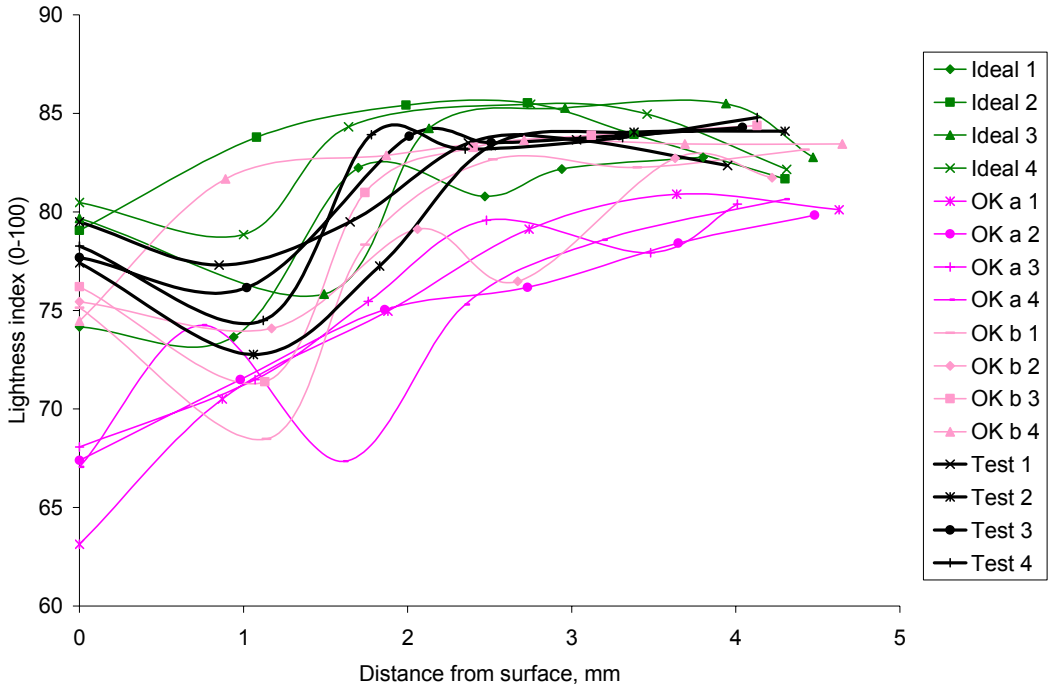

Figure 54. Surface colour development in wood sample dried using recommended schedule. Results are compared to wood samples deem ideal or OK for appearance grade timber.

Conclusions and Recommendations

The semi-scale kiln experiments described in part three successfully measured the development of colour and checking in full-sized boards at four schedules. The drying experiments described in part one have successfully measured the colour development in radiata pine boards during drying at eight schedules ranging from LT (50/40) to HT (120/70). These experiments have also measured the redistribution of sap

compounds at each of the schedules, though these results have not been as accurate as were needed. The measurement of checking was not successful in these experiments.

Both sets of experiments have shown that colour development increases with increasing drying temperature. The HT schedules showed the greatest change in colour, followed by the ACT schedules and then the CT schedule. The results from the LT schedule were inconclusive though it is thought that this schedule should have shown the lowest level of colour development. This result is not a new discovery, nor is it at all surprising, as it has been reported previously in the literature.

The experiments have also shown that the development of colour is increased with high relative humidity schedules. This result differs from some that have been reported in the literature but can be explained as follows. The higher humidity schedules take longer to dry the wood so it is subject to the elevated temperature for a longer period of time. This means the reactions that cause colour development will continue for a longer period of time and therefore there will be more colour development. The microscopic studies described in part two support this idea and show that the colour extends deeper into the wood with high relative humidity schedules due to the diffusion of stain precursors against the bulk flow of sap during the capillary flow phase of drying.

The points discussed in the previous two paragraphs show that the effect of drying schedule on the development of colour in wood is controlled by a number of variables, with drying time and temperature being the most important. Both of these variables need to be minimised, but unfortunately they are not independent of each other. Lowering the temperature will increase the drying time but this increase can be partially countered by reducing the humidity or increasing the air speed. This results in a low-temperature low-humidity schedule being recommended to minimise colour development, indeed the 70/40 schedule was the best of those tested. There are however energy efficiency and practicality issues when applying such a schedule to a commercial kiln operation. These issues are analysed in a chapter 6.

The microscopic studies have also shown the importance of the capillary flow phase in determining the nature of the kiln brown stain layer. When this phase is shortened by a low humidity schedule the kiln brown stain layer is narrower. A further advantage is that the layer is at a lower temperature as the wet bulb temperature is lower.

In measuring the colour of wood samples the use of the lightness coordinate alone gives a good indication of presence and intensity of kiln brown stain. There is however also variation in the chromaticity coordinates, most significantly in the yellow-blue coordinate. To account for this variation it is useful to calculate the total colour change, ΔE, from all of the colour space coordinates.

The results from the chemical analysis of the surface and core slices for each sample produced some quite variable results. This has meant that only a few conclusions can be drawn from the data. In general the samples show similar levels of nitrogen at the surface for all schedules and likewise for the core nitrogen levels. There did appear to be a slightly greater accumulation of nitrogen in the higher temperature schedules, with a corresponding reduction in core nitrogen levels. This could be due to the greater release

of nitrogenous compounds, or the lesser effect of diffusion against the flow of sap in the higher temperature schedules. There is evidence to support both ideas.

Information on the darkening of the wood below the board surface was also extracted from the data. More experiments are required to validate these results but there are two trends that appear in the data; firstly, the level of core-darkening increases with drying temperature; and secondly, the level of core-darkening increases with drying time. The darkening of the core is therefore related to the drying time and temperature in the same way as the development of kiln brown stain. The yellow-blue chromaticity coordinate seems to show the discolouration of the core better than the lightness coordinate.

The colour results have also been presented using the three colour planes within the CIELab colour space. This is a useful way of presenting the data as it shows variation of two coordinates simultaneously. Of the three planes the L-b* appears to be the most useful as these coordinates show independent variation. The downside of the colour planes is that it is difficult to identify the position of each point of data relative to the surface of the board.

The work presented in this chapter has answered a number of questions about the effect that the kiln schedule has on colour change in wood. There still, however, remains the question of the rate of colour change under different kiln conditions. This question will be explored further in the following chapter.

Chapter 5

Kinetics of Wood Colour Changes

This chapter describes experiments carried out to determine the kinetics of kiln brown stain formation at different temperatures and concentrations. This work was done with the aim of deriving colour change equations that can be used in conjunction with wood drying models to simulate the change of wood colour during drying.

The first part of this chapter describes in-vitro experiments using both real and artificial sap solutions that were heated and sampled periodically. Colour changes in the heated solutions were measured by absorbance in a spectrophotometer and also by reflectance on filter papers soaked in the solutions.

The experiments using real sap solutions were not successful as at high concentration the solutions darkened too much from the concentration effect alone. The artificial sap solutions, however, did produce useful results and these results were used to derive some colour equations. The results are also useful for the fundamental understanding of the process of kiln brown stain formation.

The second part of this chapter describes colour kinetics experiments performed using actual wood samples that were measured for colour periodically during drying. This is a new technique developed for this thesis and provided sufficient rate data to derive an equation for colour development. This colour equation was used in the drying simulations described in the next chapter.

In-vitro Colour Kinetics

The aim of this set of experiments was to determine the rate of reaction for kiln brown stain formation using artificial and real sap solutions. From discussion in Chapter 2, it is generally accepted that the main cause of kiln brown stain in radiata pine during drying is due to Maillard reactions between soluble sugars and proteins that accumulate at the board surface during drying. The accumulation of sap compounds has been researched extensively as noted in Chapter 2 and was also studied briefly in this project (Chapter 4).

Previous research into the rate of the kiln brown stain reaction was also described in Chapter 2. Such research included in-vitro experiments using artificial sap solutions made up from sugars and amino acids (McDonald et. al., 1997) and expressed wood sap (Sehlstedt-Persson, 2003) as well as experiments using wood samples (Dieste and Williamson, 2002). The artificial sap test and wood sample test techniques have been used in this project and will be presented as follows.

Experimental

The first set of experiments involved measuring the in-vitro colour development with time of real and artificial sap solutions at various different temperatures and concentrations. This required the collection of real sap and the formulation of artificial sap solutions. This was done using the methods described in Chapter 3. The dilution series used for the artificial sap solutions is shown in Figure 55.

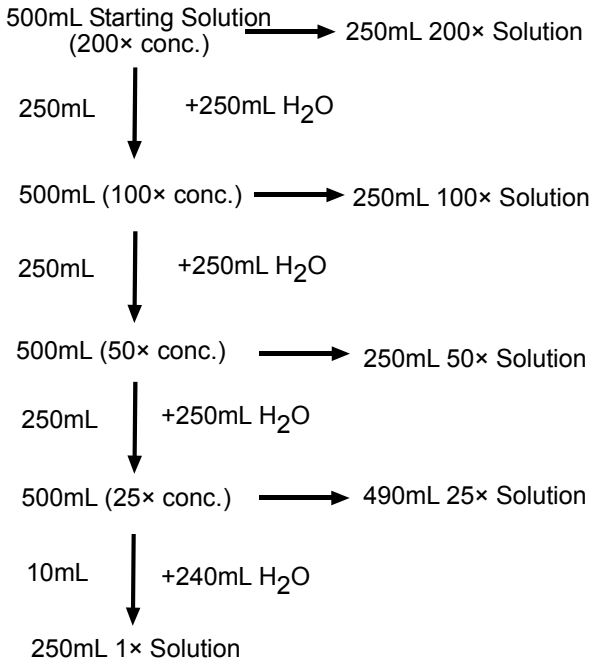

Figure 55. Dilution series used to get different concentration of artificial sap solutions for each temperature.

Temperature Selection

The temperatures selected were 90°C, 80°C, 70°C, 60°C, 50°C and 40°C which correspond to the wet bulb and dry bulb temperatures of the schedules tested in the drying experiments except that the high-temperature schedule (120/70°C) was not included. The highest temperature was omitted because there would be difficulties in maintaining a constant volume of solution and the 90°C temperature is the highest that is likely to be used for appearance grade timber. The lowest temperature was also chosen as it represents a drying temperature where kiln brown stain is unlikely to be noticeable.

The temperatures were controlled using the controllers on a laboratory oven. For the two low temperatures (40°C and 50°C), the temperature control was somewhat variable but the deviation was less than 5°C from the set point. The higher temperatures were more stable and deviated less than 2°C from the set point.

The Experiment

For each of the trials a series of McCartney bottles were filled with artificial sap solutions, sealed and labelled. There were 10 bottles for each sap concentration, so there were 50 bottles for each temperature. The bottles were placed into trays and then put into an oven at the appropriate temperature.

At various time intervals, shown in Table 14, samples of each concentration were removed from the ovens and immediately quenched in an ice bath. The bottles were then placed in a refrigerator for storage until all of the bottles had been removed from the ovens. The bottles remained sealed until further colour testing.

Table 14. Time intervals when bottles were removed for the oven for the artificial sap solutions.

Test No.	90°C Series	80°C and 70°C Series	60°C, 50°C and 40°C Series
1	0.5h	1h	2h
2	1h	2h	4h
3	2h	4h	8h
4	3h	8h	12h
5	6h	16h	24h
6	10h	24h	36h
7	15.5h	32h	48h
8	22h	40h	60h
9	27h	48h	72h
10	33h	60h	80h

Colour Measurement

The light absorbance and reflectance of the heated artificial sap solutions was measured using spectrophotometers as described in Chapter 3. The 70°C, 80°C and 90°C Series were diluted back to 1× concentration using the dilutions shown in Table 15 to eliminate the effect of the solution concentration on the absorbance result. This was also necessary, in some cases, to keep the absorbance within the measurement limits of the spectrophotometer. The high concentration solution in both series had absorbance readings well over 2.5 in the undiluted state. The 40°C, 50°C and 60°C Series were measured undiluted in order to get absorbance values that could be detected. The values for absorbance were later 'diluted' mathematically by dividing the absorbance result by the concentration. None of the samples were diluted for the reflectance measurements.

Table 15. Dilution of samples down to 1× normal sap concentration.

Concentration	Volume of sample	Volume of water added
200×	15μL	3mL
100×	30.3μL	3mL
50×	61.2μL	3mL
25×	125μL	3mL

The absorption subtraction spectra were used to determine the rate of reaction as described in Chapter 3 for the absorbance results. The CIELab coordinates were calculated from the reflectance spectra using

the computer program that operates the spectrometer and directly calculates the colour change from the measured results. Plots of the L, a*, b* and overall colour change are shown in Figure 56 for 200× concentration at 90°C. The chroma and hue coordinates are plotted for the same conditions in Figure 57.

The plots show that there is an initial lag period followed by a constant rate period for colour change until the reaction reaches a plateau. This shape of curve was common for all of the samples though some did not reach the plateau. The rates for colour change were calculated from the slope during the period when colour changes at a constant rate.

The absorbance spectra plots for all of the samples tested show a peak forming at approximately 300nm and the absorbance subtraction spectra also shows a second peak around 200nm. An example of this is shown in Figure 58. These bands are different to those found by McDonald *et.al*. (1997), which were positioned at 220nm and 280nm. The 200nm band found in these experiments is possibly caused by the presence of glutamic acid, which normally gives a peak at 210nm. However, it is uncertain why this peak increases with time when, if the peak represents a reactant, it should decrease with time. The expected 220nm peak may be overshadowed by the 200nm peak. For the 300nm peak, it is reasonable to assume that this peak in the current study is caused by the same, or similar, compound that produced the 280nm peak. The reaction rates were calculated from the 300nm peak as described in Chapter 3. When plotted these points show the same lag and plateau periods as the reflectance data, shown in Figure 56 which is to be expected given that they come from the same samples.

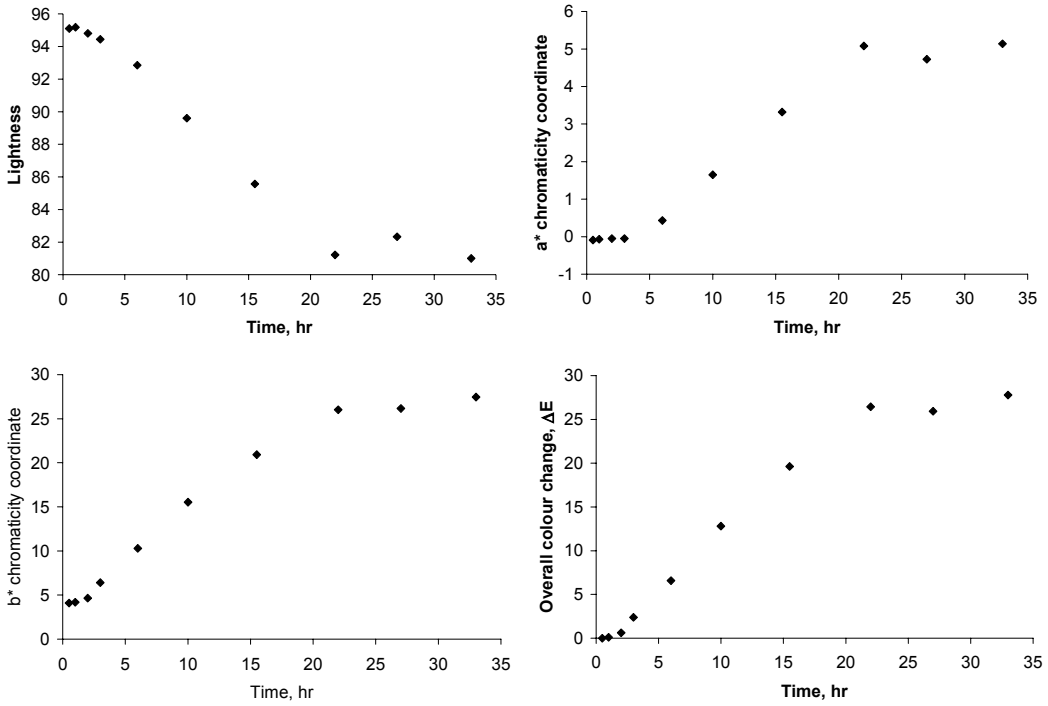

Figure 56. CIELab coordinates and colour changes as a function of elapsed time calculated from the reflectance spectra for 200× concentration at 90°C.

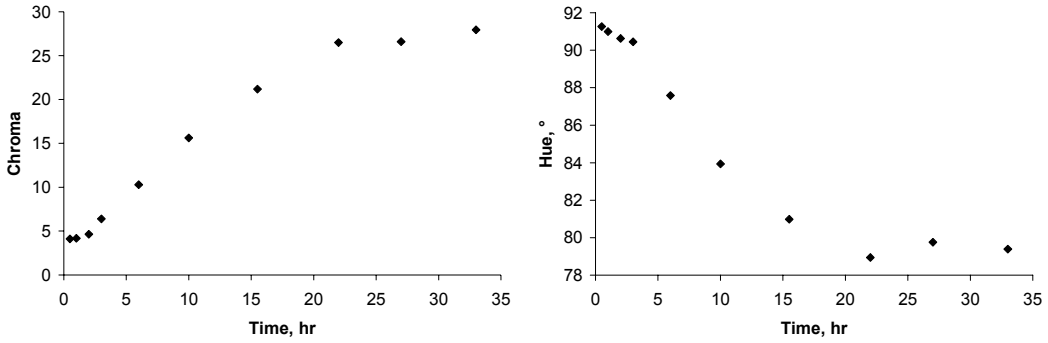

Figure 57. Chroma and hue coordinates as a function of elapsed time calculated from the reflectance spectra for 200× concentration at 90°C.

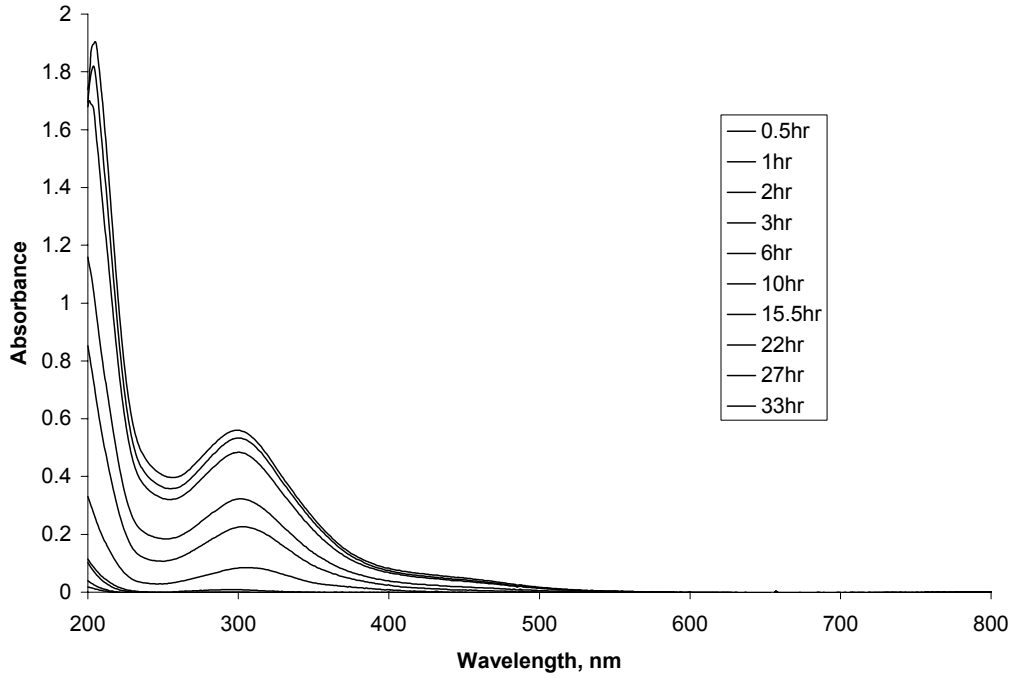

Figure 58. Absorbance subtraction spectra for 200× concentration at 90°C

Results and Discussion

The 40°C Series did not produce data that could be used to determine reaction rates as the absorbance values were so low and variable (R^2<<0.1) even at the highest concentration. This suggests that the temperature was too low for a reaction to occur, which shows that critical temperature for the reaction rate to become insignificant is between 40°C and 50°C.

The lag period noted in both the absorbance and reflectance measurements can be explained by the chemistry of the Maillard reaction. The first compounds produced by the reaction are simple molecules and do not have visible colour. This means that while the reaction has begun it takes a while for any coloured compounds to be produced. This is supported by the fact that the 200nm peak in the absorbance

increases before the 300nm peak. This lag period seems to be slightly shorter at the higher concentrations suggesting that the length of the lag period may be related to the rate of reaction.

After the lag period there is a constant rate stage when the increase in absorbance is linear with time. This indicates that there is an excess of coloured compound precursors and so the formation of colour is happening at the maximum rate. This is therefore also the maximum rate period and the period of greatest interest for determining the rate of colour formation.

After the stage of maximum colour change rate, the rate of colour change slows down which may mean that the reactants are diminishing and the rate of reaction has decreased as a result of this. Alternatively it could be due to the coloured compounds reaching such a level of complexity that further reactions are much less likely to occur.

Absorbance

The graph in Figure 59 shows the results for the 90°C series presented as the increase in absorbance at the peak wavelength with time in the oven. This graph only shows the points in the linear region of the data in order to show the linear fit. The R^2 values (0.98) for all but one show that the data had very close linear fits except for the 1× concentration where R^2 is 0.51. The equations for the linear fit lines are also shown in Equations 5.1-5.5 and the colour change rates determined from these equations are presented in Table 16. The greatest colour change rate occurs at the highest concentration and the lowest rate occurs at the lowest concentration. This is expected from most chemical reactions.

The results for the 70°C series are shown in Figure 60 presented in the same way as those for the 90°C series. Note that the values in the y-axis are smaller than those in the previous figure. This series also shows a very good linear fit for the high concentrations (R^2>0.98) but the fit to the 1× concentration is very poor due to the very low absorbance values in this series. The rates extracted from the linear fit lines are also included in Table 16.

The results for the 50°C series are shown in Figure 61 presented in the same way as the 90°C and 70°C series. Note that the values in the y-axis are significantly lower than in Figure 59 and Figure 60. In Figure 61 only the two highest concentrations have been plotted as the other results did not show any consistent trend. This is, again, most likely to be due to the very low absorbance readings being more susceptible to systematic and random error. The colour change rates extracted from the linear fit lines to the viable data are presented in Table 16. Figure 61 shows that the 200× data has a very close linear fit (R^2=0.99) while the fit to the 100× data is only a reasonable (R^2=0.58). The plots for the 60°C and 80°C data are not shown but these show the same trends as the three series shown in Figure 59 to Figure 61.

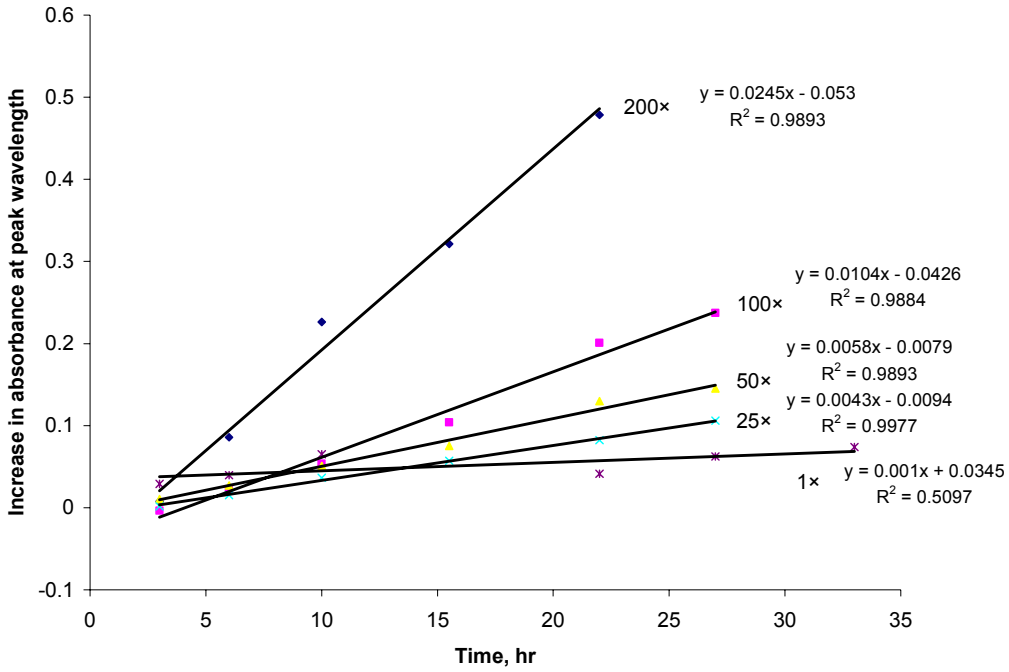

Figure 59. Linear fitting for absorbance increase with elapsed time at peak wavelength for 90°C series.

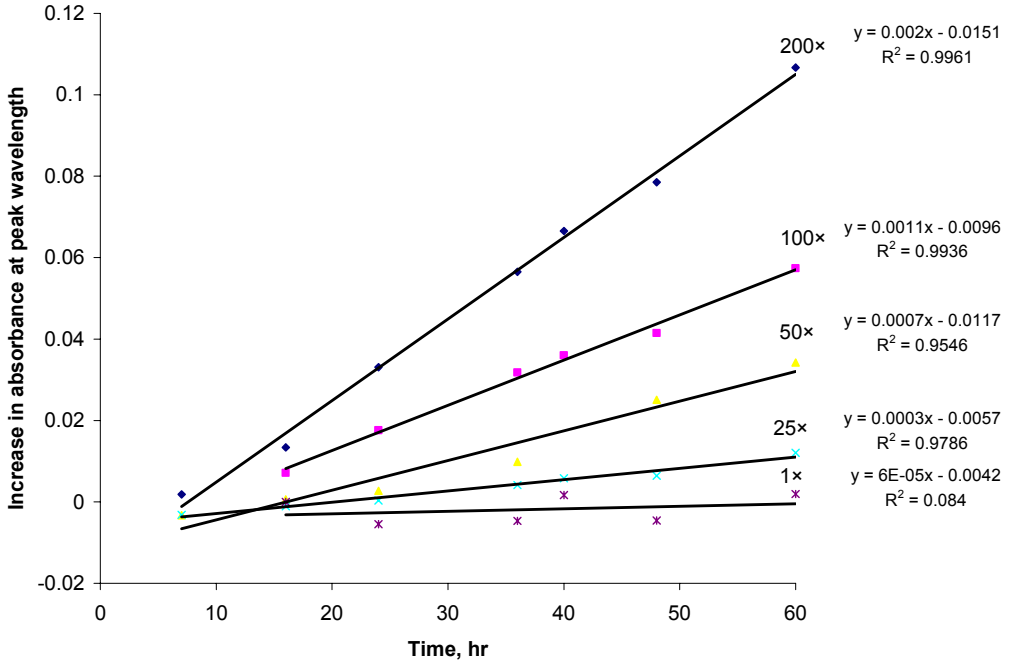

Figure 60. Linear fitting for absorbance increase with elapsed time at peak wavelength for the 70°C series.

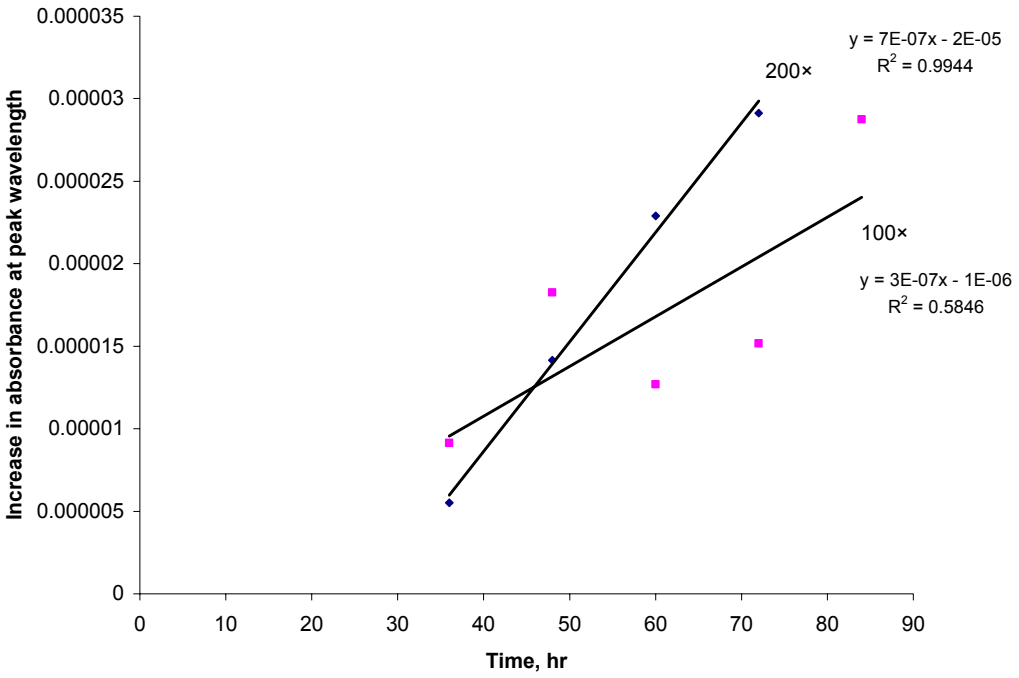

Figure 61. Linear fitting for absorbance increase with elapsed time at peak wavelength for the 50°C series. The lower concentration samples did not produce results suitable for analysis thus ignored.

The Colour Change Rate as a Function of Sap Concentration

From the values in Table 16, the colour change rates are almost doubled when the concentration is doubled suggesting a linear relationship between rate and concentration. These results have therefore been plotted in Figure 62 to determine such a relationship. The rate at 50× concentration for the 50°C series has been extrapolated based on the 70°C and 90°C results at this concentration.

Table 16. Colour development rates for artificial sap solutions (h^{-1})

Concentration	90°C Series	80°C Series	70°C Series	60°C Series	50°C Series
1×	0.001	-	0.00006	-	-
25×	0.0043	0.0004	0.0003	0.00003	-
50×	0.0058	0.0007	0.0007	0.00004	0.00000018*
100×	0.0104	0.0017	0.0011	0.00005	0.0000003
200×	0.0245	0.0033	0.002	0.00011	0.0000007

The clearly linear relationship between reaction rate and concentration is useful as it shows that the concentration does not affect the mechanism of the reaction. These results in their current form will be useful for simulating the development of colour at the temperatures tested, based on the increase in concentration during drying. The equations for the five temperatures for the colour change rates as a function of concentration factor (CF) are given as follows:

90°C $$\frac{d[abs]}{dt} = 1.19 \times 10^{-4} \cdot CF \qquad (5.1)$$

80°C $$\frac{d[abs]}{dt} = 1.64 \times 10^{-5} \cdot CF \quad (5.2)$$

70°C $$\frac{d[abs]}{dt} = 1.04 \times 10^{-5} \cdot CF \quad (5.3)$$

60°C $$\frac{d[abs]}{dt} = 5.61 \times 10^{-7} \cdot CF \quad (5.4)$$

50°C $$\frac{d[abs]}{dt} = 3.37 \times 10^{-9} \cdot CF \quad (5.5)$$

The Colour Change Rate as a Function of Temperature

By analysing the absorbance data, it was found that the relationship between temperature and colour change rate was not linear. To further illustrate this, the data has been plotted as a bar graph in Figure 63.

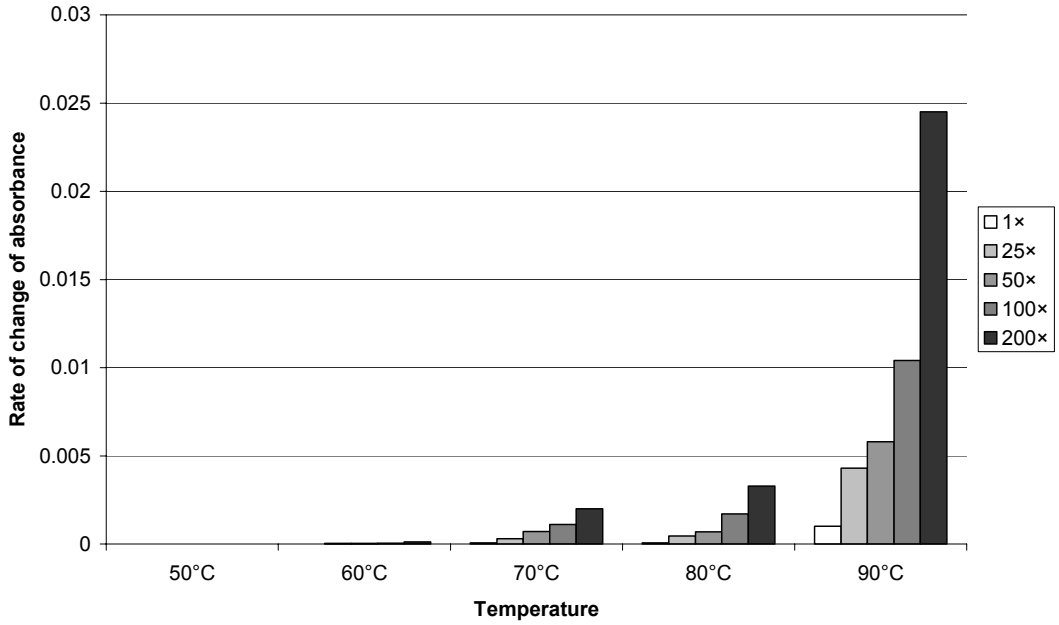

Figure 63 The data presented in this graph does not fit an exponential, power or polynomial equations. It is however possible to fit the coefficients for different temperatures in Equations (5.1) to (5.5) by using the Arhenius law as shown in Figure 64. This results in the following equation for colour change rate (h^{-1}), where T is the temperature in °C:

$$r_{abs} = CF \cdot e^{-\frac{28823}{T} + 71.051} \quad (5.6)$$

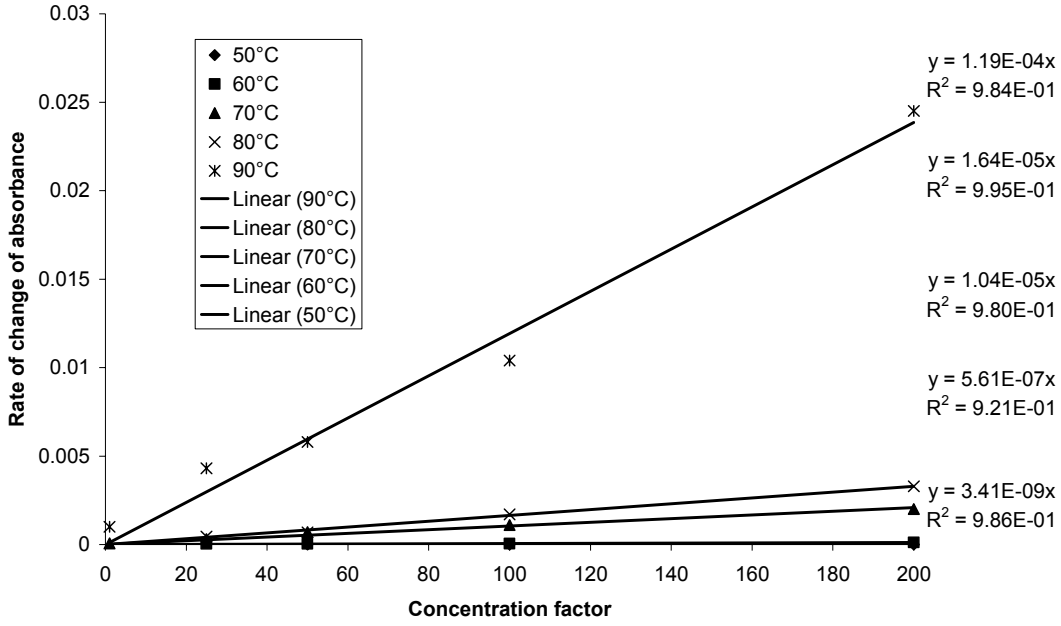

Figure 62. Plot of rate of colour formation with concentration for at three temperatures for the artificial sap solutions. The 50× concentration point at 50°C has been extrapolated based on the higher temperature data.

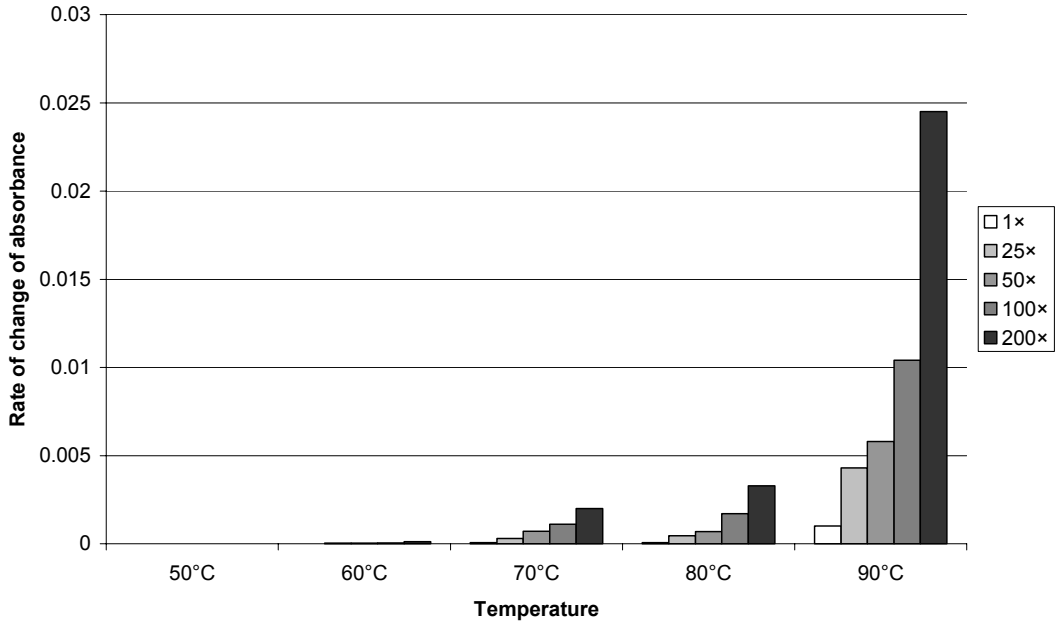

Figure 63. Relationship between rate of colour change at different concentrations for artificial sap solutions.

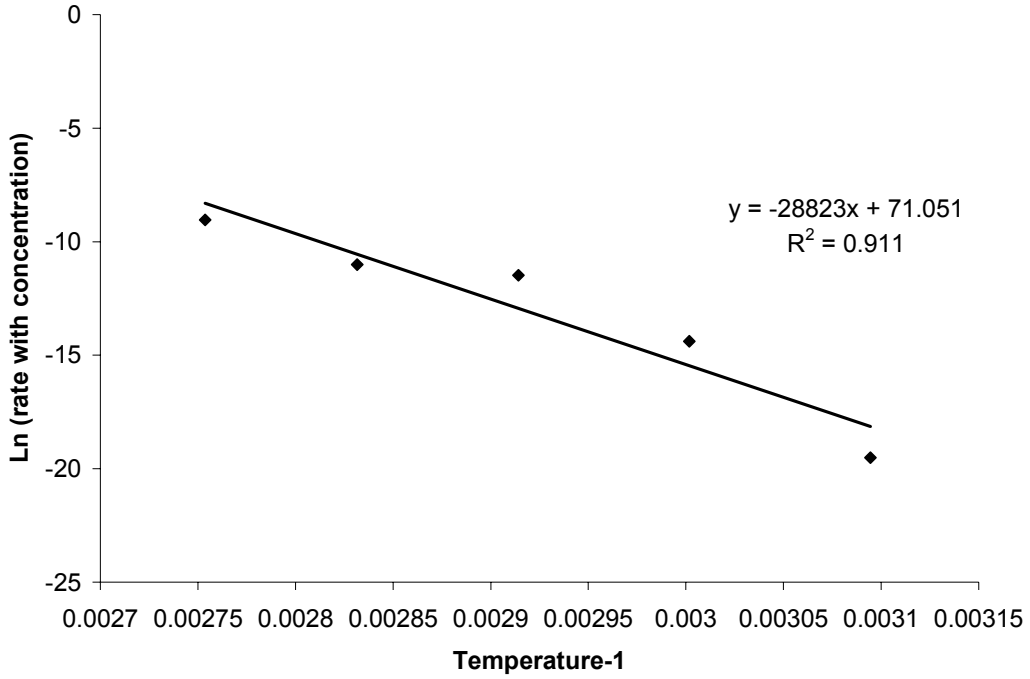

Figure 64. Arhenius plot of the reaction rate data

In order to test the Arhenius law fitting, the calculated results are compared with experimental data as shown in Figure 65. The different fits referred to in the legend are fits to the arhenius plot in Figure 64. While the Arhenius law fit to the data in Figure 64 is good, when it is used to calculate the colour change, the relationship unfortunately does not fit the data very well. When the results from the three fit equations was averaged, however, the fit looks more realistic assuming that the 80°C data is in some way anomalous. This average line can be described by the following equation, where T is in °C:

$$r_{abs} = CF \cdot e^{\frac{4118373}{T^3} - \frac{234687.4}{T^2} + \frac{3082.359}{T} - 19.93505} \qquad 5.7$$

To test how the results from these experiments compare with the similar study by McDonald et. al. (1997) the data from that study was fitted with the following equations:

Glucose: $$\frac{d[ABS]}{dt} = 7 \times 10^{-21} \cdot T^{9.7659} \qquad (5.8)$$

Sucrose: $$\frac{d[ABS]}{dt} = 2 \times 10^{-20} \cdot T^{9.8207} \qquad (5.9)$$

Fructose: $$\frac{d[ABS]}{dt} = 4 \times 10^{-18} \cdot T^{8.7103} \qquad (5.10)$$

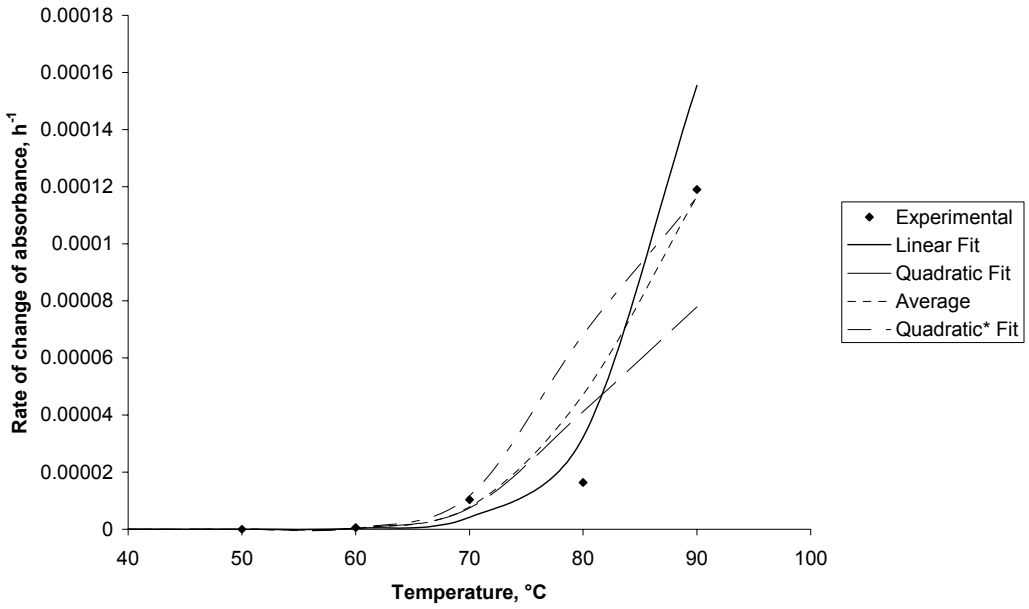

Figure 65. Comparison of various fit equations with experimental data for the rate of colour change.

The colour change rates calculated from Equations (5.8)-(5.10) for 70°C and 90°C are presented in Table 17. These predictions will be used for sensitivity analysis which will be discussed in the following paragraphs, however, the predictions cannot be directly used for colour change prediction and the solutions used by McDonald et. al. (1997) only contained a single sugar along with glutamic acid whereas the sap solution is a combination of all three sugars. In addition, as previously mentioned in Chapter 2, the sugars and glutamic acid used by McDonald et al. (1997) were not used in the same proportion as they are found in sap.

The colour change rates based on the sucrose and glutamic acid system are expected to provide the best comparison as performed in this work as sucrose was used in greatest quantity in the artificial sap solutions and is a combination of glucose and fructose. Also the proportions of sucrose to glutamic acid in the McDonald et. al. (1997) experiments are closest to that of real sap.

As mentioned above, the colour change rates given in Table 17 are different from those in Table 16 as the rates in Table 16 have been corrected for concentration but the rates in Table 17 have not. However, based on total moles of sucrose, fructose and glucose found in sap the sugar solutions used by McDonald et al. (1997) were approximately 34 times the concentration of real sap. By similar calculation the glutamic acid solutions is approximately 36 times the concentration of normal sap. It will therefore be assumed that the solutions used were 35 times the normal sap concentration.

When the rates at are calculated from Equations (5.1) and (5.2) at a concentration factor of 35 the results are 0.0042 for 90°C and 0.00036 for 70°C. The colour change rates for the sucrose system when corrected for concentration are 0.008 and 0.0007 respectively which is approximately double in both

cases. The ratio of the rates at 70°C and 90°C are however almost identical at 11.4 in both cases which shows that while the actual results are different the trends in the results are very similar.

Table 17. Rates of colour formation at 70°C and 90°C calculated from equations fitted to data from McDonald et. al. (1997). Units are abs/h.

Temperature	Glucose	Sucrose	Fructose
70°C	0.007	0.026	0.047
90°C	0.085	0.311	0.421

Reflectance

The reflectance subtraction spectra shown in Figure 66 indicate that for the majority of the samples tested the reflectance of light from the filter papers decreased with elapsed time over the entire measured spectrum. It is also shown that the reflectance decreased more at the shorter wavelengths and these wavelengths correspond to the blue and green regions of the electromagnetic spectrum. When these wavelengths are absorbed more by a material than the longer wavelengths then the reflected light appears to be a yellow-red colour. This colour change was noticeable on many of the filter papers tested.

It is also noticed from Figure 66 is that the lines on the subtraction spectra appear to be on the tail of a peak. When compared to the absorbance subtraction spectra shown in Figure 58 the section between 400nm and 700nm has a similar shape. This suggests that the change in colour noted in the artificial sap solutions may be due to a phenomenon known as dye dichroism rather than the production of complex molecules. Dye dichroism occurs with organic compounds when the light absorption of the compound occurs in both the visible and UV regions. In this case the wings of the peak can have more effect on the perceived colour than the peak itself. This effect results in a transition from yellow to orange and then to red/brown as the concentration increases with black the ultimate colour at very high concentrations.

For the artificial sap solutions the increase in concentration required for the dye dichroism effect will be due to the production of the coloured compound absorbing at 300nm. As the reaction proceeds the increase in concentration of this compound in the solution has the same effect as increasing the concentration of a dye would have.

Most of the results from the reflectance experiments were similar to those shown in Figure 56. These graphs show an initial lag period, similar to that noted in the absorbance measurements followed by a roughly constant rate period and then finally a plateau. At lower concentrations and temperatures the trends were less distinct and did not reach a plateau. The plateau may mean that the reaction has stopped or that new double bonds and other light absorbing structures are no longer being formed.

The colour change rate derived from the L*, a* and b* results for the 90°C samples are shown in Table 18. The units for the colour change rate are the change in coordinate per hour. Given that the coordinates are dimensionless this makes the units hr^{-1}, though the units could be expressed as $\Delta L^*/hr$, $\Delta a^*/hr$, etc for clarity. The same results for the 70°C and 50°C samples are shown in Table 19 and Table 20 respectively. Plots of these results can be found in the appendices.

For all of the three temperatures the b* chromaticity coordinate shows a greater change with heating time than does the a* chromaticity coordinate. This is similar to the results presented in the Chapter 4 and again it suggests that there is more yellowing than reddening in kiln brown stain formation. The reddening is likely to cause more degrade, however, as it creates a colour that differs more from the colour of the wood.

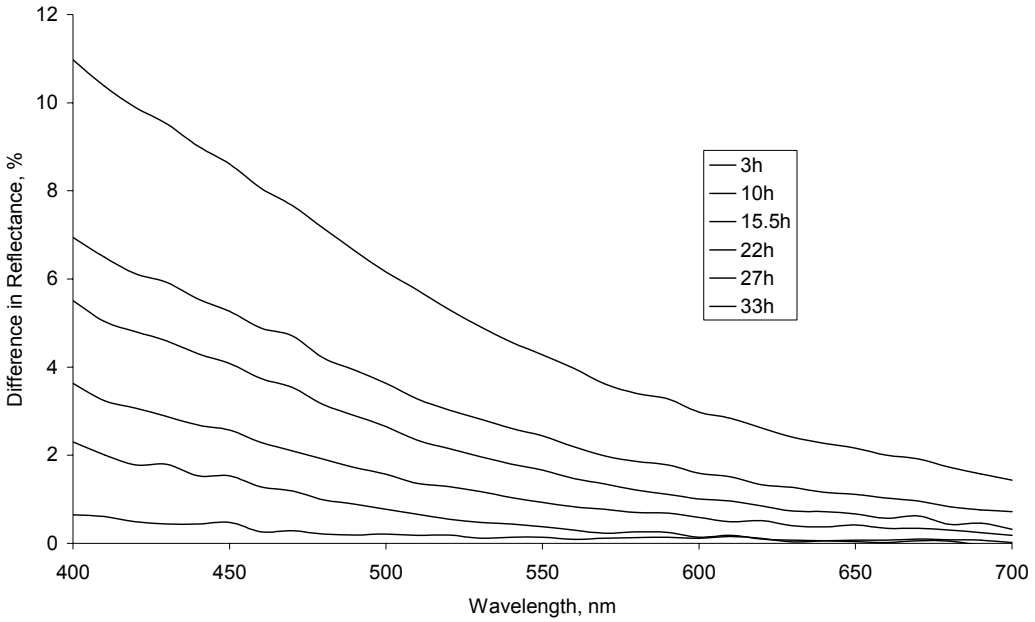

Figure 66. Reflectance subtraction spectra for the artificial sap solutions 25× normal sap concentration heated at 90°C.

Table 18. Colour change rates from the reflectance results for the artificial sap solutions at 90°C. Units are change in coordinate/hr and the R^2 value is in brackets.

Concentration	25×	50×	100×	200×
L*	-0.07 (0.93)	-0.09 (0.99)	-0.19 (0.99)	-0.71 (0.99)
a*	0.013 (0.94)	0.019 (0.99)	0.052 (0.99)	0.279 (0.99)
b*	0.09 (0.97)	0.16 (0.99)	0.36 (0.99)	1.03 (0.99)

Table 19. Colour change rates from the reflectance results for the artificial sap solutions at 70°C. Units are change in coordinate/hr and the R^2 value is in brackets.

Concentration	25×	50×	100×	200×
L*	-0.0021 (0.39)	-0.012 (0.61)	-0.036 (0.97)	-0.0952 (0.99)
a*	0.0006 (0.58)	0.0044 (0.74)	0.0097 (0.92)	0.032 (0.99)
b*	0.003 (0.72)	0.022 (0.72)	0.066 (0.99)	0.189 (0.99)

Table 20. Colour change rates from the reflectance results for the artificial sap solutions at 50°C. Units are change in coordinate/hr and the R^2 value is in brackets.

Concentration	25×	50×	100×	200×
L*	-	-	-0.0016 (0.19)	-0.0013 (0.03)
a*	-	0.0002 (0.04)	0.0002 (0.08)	0.0003 (0.22)
b*	-	0.001 (0.1)	0.003 (0.85)	0.005 (0.66)

The results for the effect of sap concentration factor on the rate of overall colour change (ΔE/hr) are plotted in Figure 67. In this graph the rates have not been divided through by the concentrations so the rate is based on both the formation of coloured compounds and the higher concentration of the solution. The plots for the chromaticity coordinates a* and b* have similar trend to this in Figure 67, but the trend for the lightness plots are inverted (opposite sign)..

The plot in Figure 68 shows the same data as Figure 67 corrected for concentration by dividing the rate values at each point by the concentration factor. The effect of concentration on colour change when presented this way seems to be more of a linear relationship which is similar to the results for the absorbance measurements.

The rate of colour change with concentration factor (Figure 67) when represented this way shows that there is not a simple linear relationship between the two variables. This means that a thicker board will be more susceptible to kiln brown stain formation as the concentration at the surface will reach higher levels due to the lower surface to volume ratio of the board. Also as the board approaches fibre saturation point (or irreducible moisture saturation) it will become more susceptible to the formation of kiln brown stain. This may mean that it is valuable to reduce the drying temperature during this stage of drying.

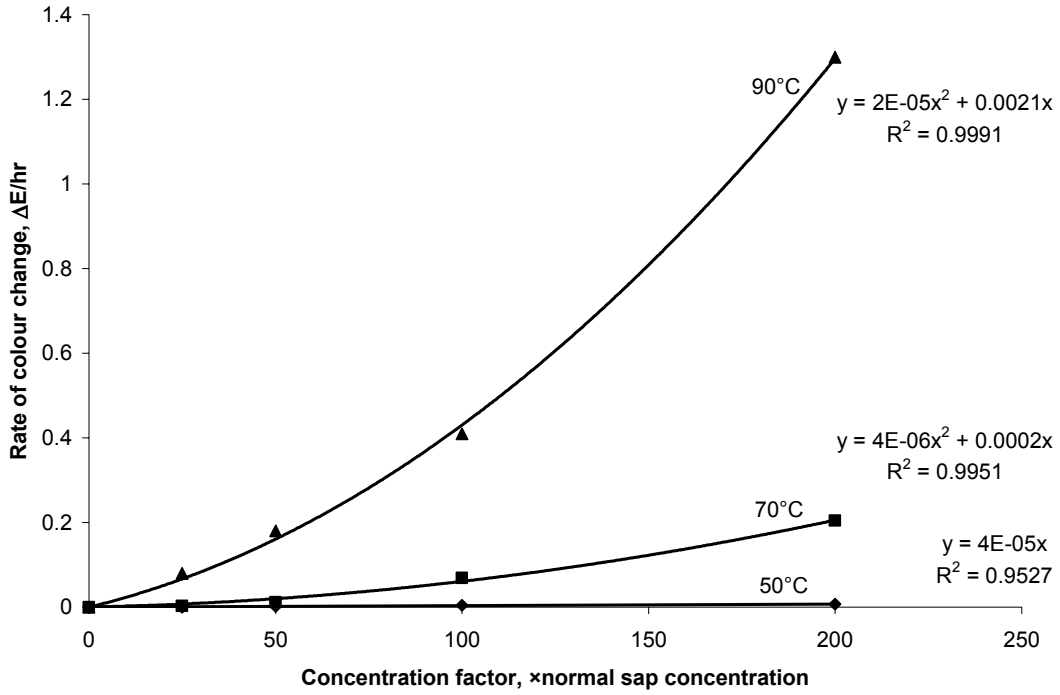

Figure 67. The effect of sap concentration factor on the rate of colour change in artificial sap solutions at three temperatures. The rates are based on reflectance measurements.

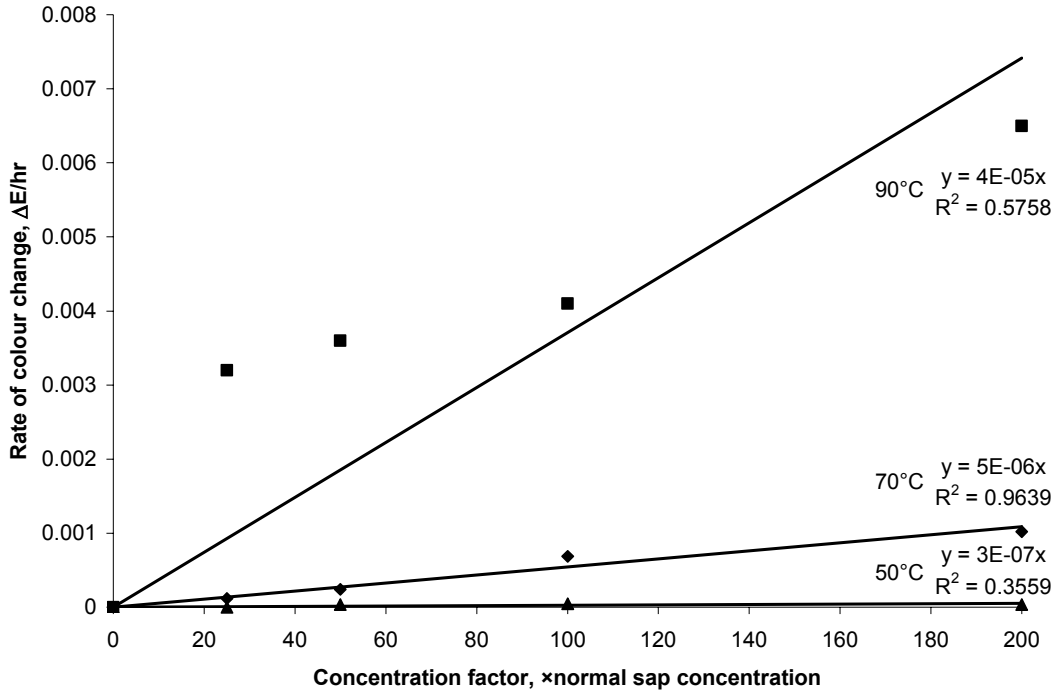

Figure 68. The effect of sap concentration on the rate of colour change per unit concentration factor, based on reflectance measurements.

Colour Kinetics for Wood Drying

This section will describe experiments carried out to measure the rate of kiln brown stain development on the surface of wood during drying at different temperatures. The primary aim of these experiments was to derive equations to describe the development of kiln brown stain in individual samples throughout the drying process. The secondary aim was also to measure the development of kiln brown stain below fibre saturation point and determine what affect moisture content has on the rate of colour development below fibre saturation point. These experiments were also intended to test the validity of using artificial sap solutions to model kiln brown stain formation, as was done in the first section of this chapter.

In the experiments described in Chapter 4, kiln brown stain was measured at various intervals in the drying schedules tested. The measurements were, however, made on different samples at the different time intervals, which introduced uncertainty due to the non-homogeneous nature of wood. The experiments presented here utilise a new technique developed to overcome this problem.

Experimental

This experiment utilised the method developed for measuring surface colour during drying described in the Chapter 3. Small matched samples obtained from the same board were used and these were dried in the drying chamber.

Initial Experiments

Initially three drying runs were done to test the method and determine its usefulness for further experiments. In these experiments the wood samples were subject to three different two stage drying schedule. The first stage of each schedule was a drying stage based on a standard drying schedule with a 10°C wet bulb depression to drive the drying process. The samples were dried using this schedule to a moisture content of approximately 20% at which point the schedule was advanced to the second stage, which was designed to maintain the moisture content of the wood at approximately 20% at a preset dry bulb temperature. The humidity was therefore set to hold the sample at an EMC of 20%. The schedules used for these three experiments are shown below in Table 21.

The first two schedules used a constant dry-bulb temperatures at 50 and 70°C, respectively. This was intended to examine the effect of dry-bulb temperature on the development of colour. The third schedule used the same drying conditions as the first schedule but in the second EMC holding stage, the third run used the same condition as the second run. The intention of this experimental design was to see if a step change in temperature would produce a step change in colour development.

Table 21: Drying conditions and EMC hold conditions for the three schedules used in the initial experiments.

Schedule	Drying Conditions	EMC Hold Conditions
10	50/40	50/48
11	70/60	70/69
12	50/40	70/69

Rate Determination Experiments

Following the initial three drying runs, a set of experiments were performed to determine the rate of colour development below fibre saturation point at five temperatures between 50°C and 70°C. The intended target moisture content in the first stage of drying was also 20%. The samples were initially dried to this moisture content using a 50/40 schedule and then held at this value (EMC) at various temperatures. The conditions used are shown in Table 22.

The samples' colour was measured firstly when they were green and then when they had been dried to 20% moisture content. After that, the samples' colour was measured periodically over a time period of two days as the sample was held at the preset holding condition. At the same time that the quantitative colour measurement was being made, a digital still was taken of the sample surface using a digital camera.

Table 22: Drying schedules used for the determination of colour development below fibre saturation point

Schedule	Drying conditions for drying samples to 20% MC	EMC holding conditions
13	50/40	50/48
14	50/40	55/54
15	50/40	60/59
16	50/40	65/64
12	50/40	70/69

Results and Discussion

Initial Experiments

The initial experiments provided very useful information for developing the subsequent experiments and at the same time provided an insight into how colour develops below the fibre saturation point. The change in colour and moisture content for the three schedules are shown in Figure 69 to Figure 71.

The results for schedule 10 show a normal drying curve with a large drop in moisture content early in drying, gradually decreasing to the target moisture content of 20% in then late stage of drying. In the holding condition stage, the EMC has not been held constant in this case though the moisture content profile is much flatter in the high humidity period. This is mainly due to the schedule being changed before the required moisture content (20%) had been reached due to difficulties in determining this accurately. This may also reflect the difficulties of maintaining humidity conditions in the experimental apparatus. The resolution of the temperature controllers on the drying chamber is 1°C so the variation in temperature is up to ±0.5°C. This variability makes it difficult to accurately maintain humidity conditions for fixing the EMC.

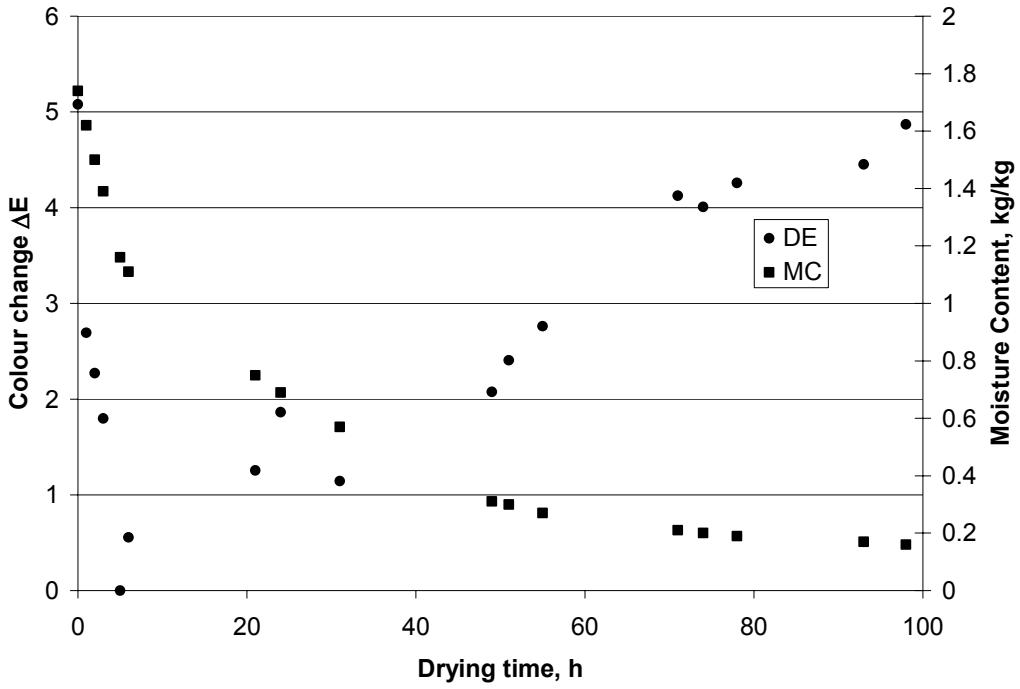

Figure 69. Results for Initial Run 1 (schedule 10) showing the change in colour and moisture content as a function of elapsed time.

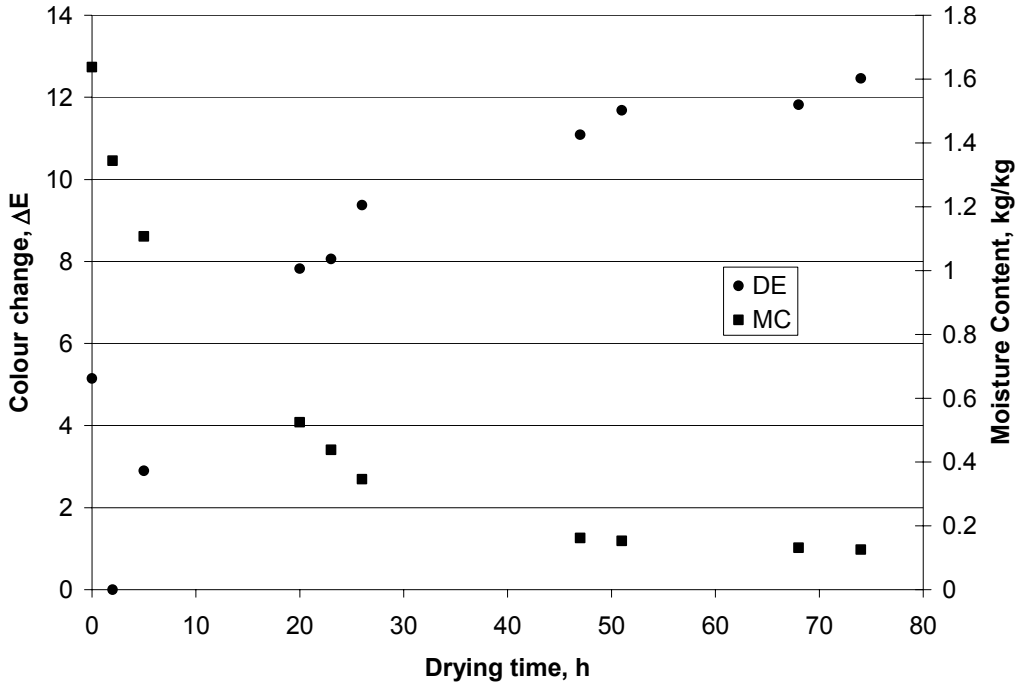

Figure 70. Results for Initial Run 2 (schedule 11) showing the change in colour and moisture content as a function of elapsed time.

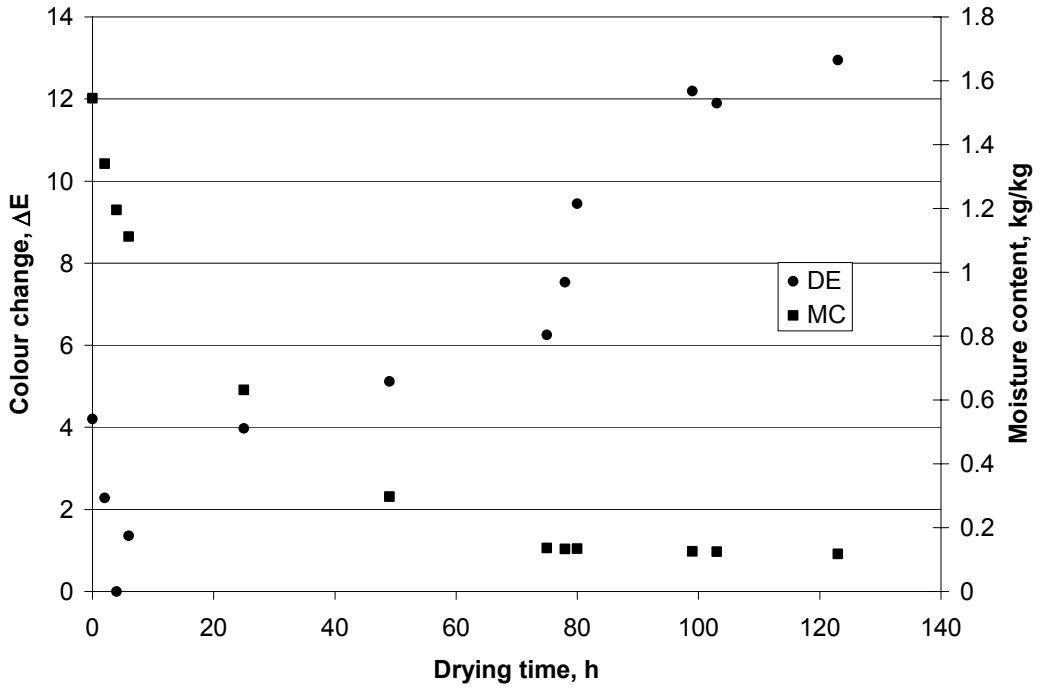

Figure 71. Results for Initial Run 3 (schedule 12) showing the change in colour and moisture content as a function of elapsed time.

The overall colour change (ΔE) was determined by taking a reference point when the wood colour is the brightest.

The time point with the greatest value for lightness was chosen as the datum with which the change in wood colour was compared. This point occurred within a few hours of drying when the surfaces of the samples had dried out but discolouration had not begun. The ΔE values calculated for each run have been plotted in Figure 69 to Figure 71, with the moisture content also plotted on these graphs.

The results for the Initial Run 1 (Figure 69) show that the colour change drops sharply at the beginning of drying, as the wood colour gets lighter due to the surface losing moisture. After reaching peak lightness at about 5h into the schedule the surface colour of the sample darkens in an approximately linear relationship with elapsed time. There appears to be a slight change in the slope at 72h when the schedule was changed to holding conditions to maintain the moisture content.

The results for the Initial Run 2 (Figure 70) show a similar increase in lightness at the beginning of drying. However, the colour change beyond this point is not in linear relationship with elapsed time as found in the first run. The colour change is approaching an asymptotic value with a much higher value. At 48h when the schedule was changed to hold the moisture content the wood colour seems keeping changing at a constant value.

The results for the Initial Run 3 (Figure 71) also show a sharp increase in lightness when the surface begins drying. This is followed by a slow increase in colour, up to the point where the schedule is changed to the holding conditions at 78 hours. At this point the colour change increases sharply and then gradually decreases when the colour change appears to tend toward an asymptotic value in a similar way to the Initial Run 2.

The subtraction spectra for the Initial Run 3 are plotted in Figure 72. These spectra were obtained by subtracting the 4h spectra from the spectra of each measurement after 4h. This means that the higher the value on the y-axis the greater the absorbance of light at that wavelength thus darker colour. The spectra show that as drying progresses there is an overall increase in light absorption across all wavelengths. As drying progresses there is also a shift in the wavelength of peak light absorption towards higher wavelengths.

The results for the rate determination experiments (Rate Runs 1 -5) are arranged to plot the colour change in the approximately linear region as a function of elapsed time as shown in Figure 73. The slopes of the lines represent the colour development rate, or colour change rate, in ΔE/h. This colour change rate data fits quite well to a linear relationship with R^2 values greater than 0.8 for all five data sets.

Most importantly, the rate of colour change clearly shows an increase with drying temperature. In order to quantify the relationship between the temperature of the drying schedule and the rate of colour changes, the colour change rates for all of the runs are plotted in Figure 74. It has been found that such relationship is non-linear and could only be fitted by a 4^{th} order polynomial. The plot shows that the

colour change rate increases remarkably between 65°C (338K) and 70°C (343K). The full coefficients for the 4th order polynomial fit to the colour rate-temperature relationship are shown in Table 23 below.

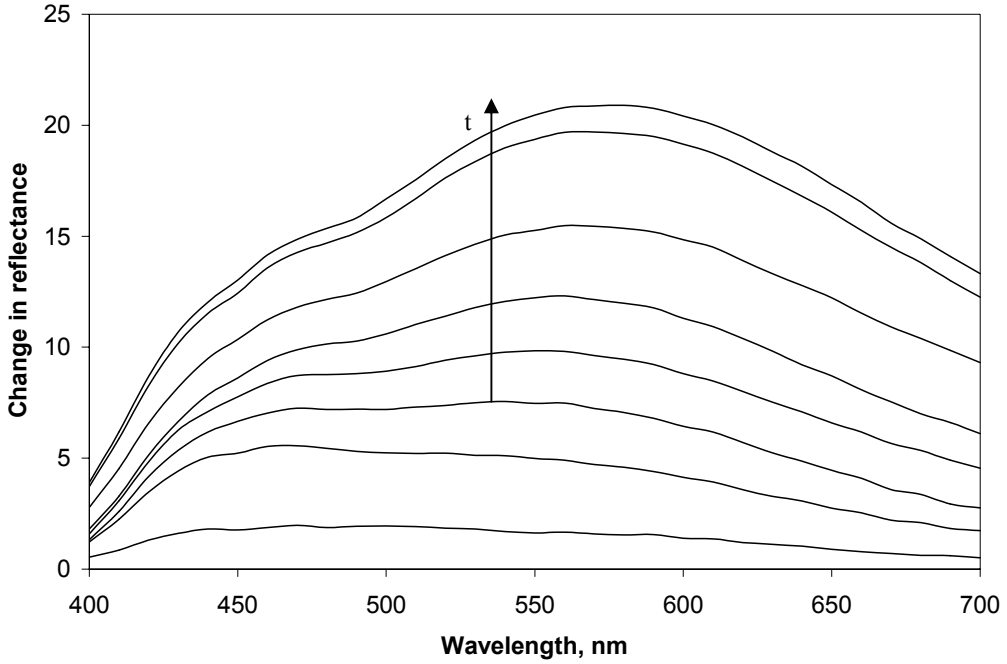

Figure 72. Subtraction spectra for Initial Run 3 with the values showing spectra of each measurements after 4 hours being subtracted by the spectrum at 4 hours.

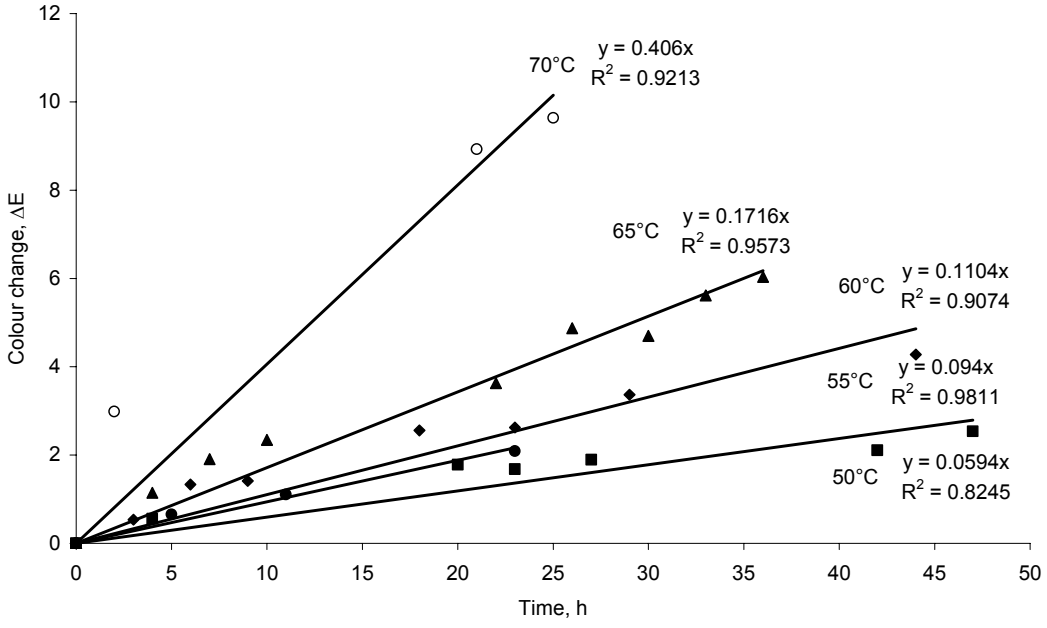

Figure 73. Colour change with time for 5 different drying temperatures. The gradients and R^2 values for the linear fits are also shown on the graph.

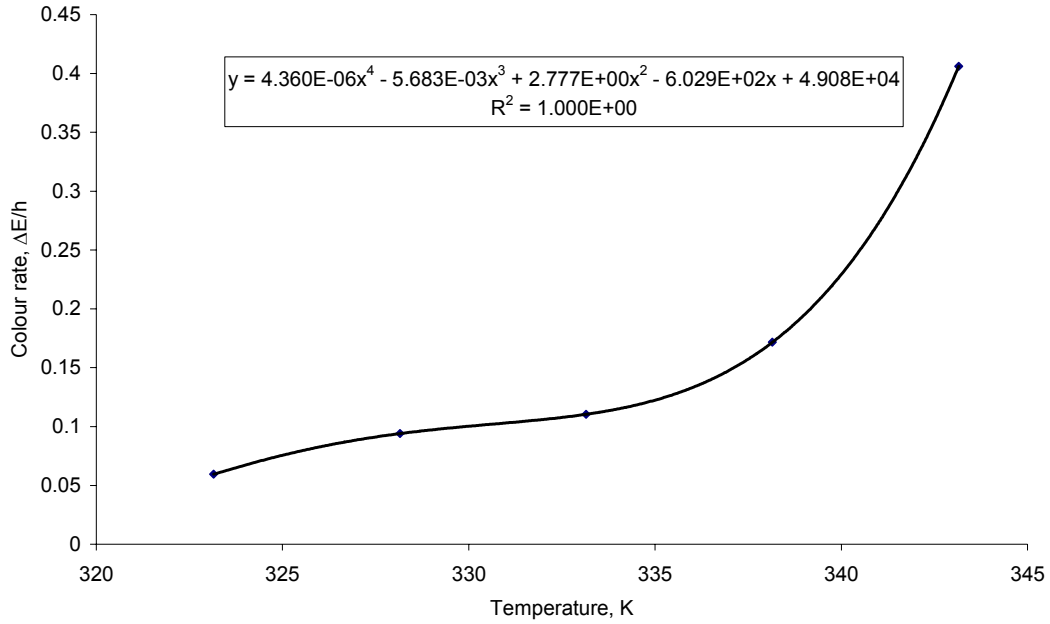

Figure 74. Plot of colour change rate with temperature for *Pinus radiata* dried at 5 different temperatures.

Table 23. Coefficients for the 4th order polynomial fit to the relationship between colour change rate and the drying temperature between 50°C and 70°C.

Coefficient	Variable	Magnitude
a_4	T^4	4.36×10^{-6}
a_3	T^3	-5.682536×10^{-3}
a_2	T^2	2.77672739
a_1	T	-6.02893983×10^{2}
C	-	4.90766422×10^{4}

From the results described above, it is observed that Initial Run 2 drying run at first seems to suggest that there is a reduction in the rate of colour development as moisture content decreases. The results from the Initial 3 run however show that the higher rate of colour development caused by the increase in temperature from the drying schedule to the holding schedule is not affected by the moisture content. This means that there must be another explanation for the change in rate of colour development.

The alternative explanation is that there is a maximum possible colour development caused by initial reaction of sap compounds based on the concentration of these compounds in the board before drying. Once these compounds have reacted, further reactions become more complex and proceed at a slower rate. The early stages of the Maillard reaction are reasonably well understood, but beyond the first (Amadori) products there are a large number of possible reactions (Fayle and Gerrard, 2002), so it is difficult to imagine the actual structure of the coloured compounds produced.

The shift towards more complex reactions is supported by the shift to higher wavelengths in the subtraction spectra. The colour exhibited by the Maillard reaction products is most likely caused by a

combination of extended polyene structures attached to electron-donor and –acceptor groups as is the case with most organic colorants (Nassau, 2001). The addition of more conjugated double bonds or donor-acceptor groups will cause the reaction products to absorb longer wavelengths. Studies of the Maillard reaction have shown that complex products containing cyclic polyenes and donor-acceptor groups are produced (Tressl *et. al*, 2002).

The development of colour below fibre saturation point at a similar rate to colour development above fibre saturation point suggests that the majority of colour development is occurring in the cell walls. This is because the only water in the wood below fibre saturation point is the bound water in the cell walls. Digital micrographs of stain layers do show that the majority of kiln brown stain is due to darkened cell walls.

The rate measurement experiments show clearly that there is a non-linear relationship between temperature and the rate of colour development. This is to be expected for any chemical reaction, though in this case it was not possible to fit the data to the arrhenius equation. This is likely to be due to there being more than one reaction involved in the formation of colour. Regardless of the reaction mechanism the rate of colour development increases greatly above 60°C.

The experiments have shown that the smoothing of the surfaces of green wood samples with a plane has caused the kiln brown stain to form closer to the surface where it has been successfully measured using a reflectance spectrophotometer.

In normal rough-sawn timber the evaporative front recedes through the layer of damaged tracheids at the surface early in drying forming what is known as the thin dry layer (McCurdy and Keey, 2002). This means that most colour development occurs at 1 to 2mm below the surface and is not always apparent on the surface. The process of removing the damaged layer means that the evaporative front stays at the surface and the formation of colour is more obvious and can be measured non-destructively during the drying process.

This technique for measuring the development of colour in wood during drying shows potential to be a useful research tool and results from initial experiments show that further research is warranted and should yield useful and interesting results. In particular the formation of kiln brown stain below fibre saturation point is significant for the design of schedules to combat the formation of such discolouration.

The results presented here have shown that surface colour formation can be measured during drying if the surface is planed in the green state. Using this method the experiments performed have measured the rate of colour formation between 50°C and 70°C and shown that the rate is greatly increased above 60°C. The experiments have also shown that colour formation occurs both above and below the fibre saturation and the moisture content has little effect on the rate of colour formation.

Conclusions

The significant differences between the reflectance subtraction spectra shown in Figure 66 and Figure 72 illustrate the difficulty associated with using simplified artificial sap solutions to simulate the formation

of kiln brown stain. These two plots show clearly that the chemical phenomena being measured in each of the experiments was different. The colour change in the artificial sap solution experiments seems to be largely due to the effect of dye dichroism as the concentration of the compound absorbing at 300nm increases in the solution. There was no indication in the absorption spectra of another peak forming or of any significant shift in the position of the peak either of which would indicate the formation of a more complex coloured compound. In contrast the reflectance subtraction spectra for the in-wood experiments which re basically absorption spectra show that there is a distinct shift in the position of peak absorbance toward the lower energy end of the visible spectrum. This indicates that there is an increase in the complexity of the compounds causing the colour rather than simply an increase in concentration. This is not to say however that the concentrations of the compounds are not changing and that this is not affecting the colour.

The difference between the in-wood and in-vitro experiments noted in the previous paragraph shows that the heating of simple solutions of sugars and amino acids does not accurately represent the formation of kiln brown stain. For this reason the equations derived from the in-vitro experiments presented here and similar experiments presented in the literature should not be used in the modelling of colour development in wood.

The reason for the differences between the in-wood and in-vitro experiments is obviously due to the greater complexity of the substances in the in-wood experiments. This complexity is something that cannot be replicated in a test tube and may also include reactions involving the polymers in the cell wall structure. While this is not a simple Maillard reaction between known amino acids and sugars this does not prevent it from being described as a Maillard reaction. Most Maillard reactions that occur in biological systems involve many reactants therefore most of the colour development that occurs in wood can still be attributed to Maillard reactions.

Chapter 6

Energy Efficiency Modelling and Colour Quantification

The objective of this part of the thesis was to develop a broad computer model for the efficiency of kiln schedules including elements of colour development and energy efficiency. This model is used to compare different kiln schedules as well as different kiln configurations.

Overview of Model Structure

The model will be developed in a number of stages with each stage being an element that can be dealt with separately. The core of any kiln simulation is the drying of the stack inside the kiln as this is the operation being performed.

A simplified structure of a one-dimensional kiln stack model is shown below in Figure 75. The inputs shown on the left are the kiln schedule parameters (dry- and wet-bulb temperatures and air velocity) as well as the initial conditions of the stack (initial moisture content and stack configuration). The outputs of the model are the changes of moisture content in the stack with time and profiles of the humidity and temperature. The total drying time is also determined at the end of the simulation. The stack model could also be expanded into a two-dimensional model to include the effect of flow mal-distribution on the outputs.

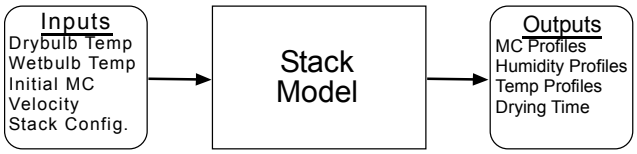

Figure 75. The simplified structure of one-dimensional stack simulation model.

There have been a number of models designed similar to the one in Figure 75, such as those of Nijdam (1998), Pang (1994) and Ashworth (1977). These will be discussed in more detail later in this chapter. The outputs from the stack model can provide useful information about quality of kiln drying, such as the moisture content variation. With the addition of a colour model, as shown in Figure 76, the colour development can also be simulated, thus providing another quality parameter.

The work on colour development during drying presented in previous chapters has shown that the formation of colour during drying is a function of the surface temperature and the drying time. There is

little evidence that the moisture content in the surface layer has a significant effect on the colour development. The variables of temperature and moisture content also interact as lower moisture content means the surface temperature will be higher than at higher moisture contents. This will be discussed further in the development of the colour model later in this chapter.

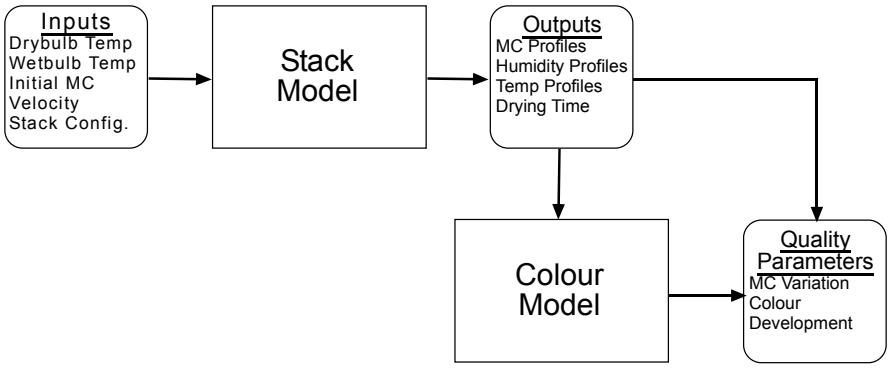

Figure 76. One-dimensional kiln drying model being incorporated with a colour model to output quality parameters.

A further improvement on the kiln drying model is to include a kiln efficiency model and an economic model, as shown in Figure 77.

The kiln efficiency model will determine the energy use and efficiency of the kiln, based on the operating conditions in the kiln, the external conditions and the kiln design. Efficiency models for wood drying kilns and other industrial driers have been developed and these will be discussed in more detail later in this chapter. The energy efficiency of the kiln is affected by the amount of venting that occurs as a result of the choice of kiln schedule. Kiln schedules with a large wet-bulb depression require a lot of venting to control the humidity. The external humidity and air temperature also have an effect on the loss due to venting.

Convective heat loss from the external surfaces of the kiln also needs to be accounted for in the energy efficiency model as do possible losses from fugitive emissions. Various kiln designs will be included in the kiln efficiency to provide a comparison of different technologies.

Finally an economic model will be established with the aim being to convert the data on energy efficiency and quality into economic terms such as capital cost, running cost and return on investment. This model will have a standard production level and determine how many kilns are required to meet the production targets. The cost of ancillary equipment such as boilers will also be included in the economic model.

Kiln Model

There are a number of different approaches to the development of kiln-wide drying models, as noted in Chapter 2. The more rigorous models based on transport phenomena in wood have been found to be computationally too slow for the analysis of commercial kilns. The lumped parameter approach based on van Meel's batch drying equations does however provide a reasonably accurate model for the behaviour

of the stack that is computationally fast. This latter approach will be adopted in this work for the modelling of the colour development and energy efficiency because of its mathematical simplicity.

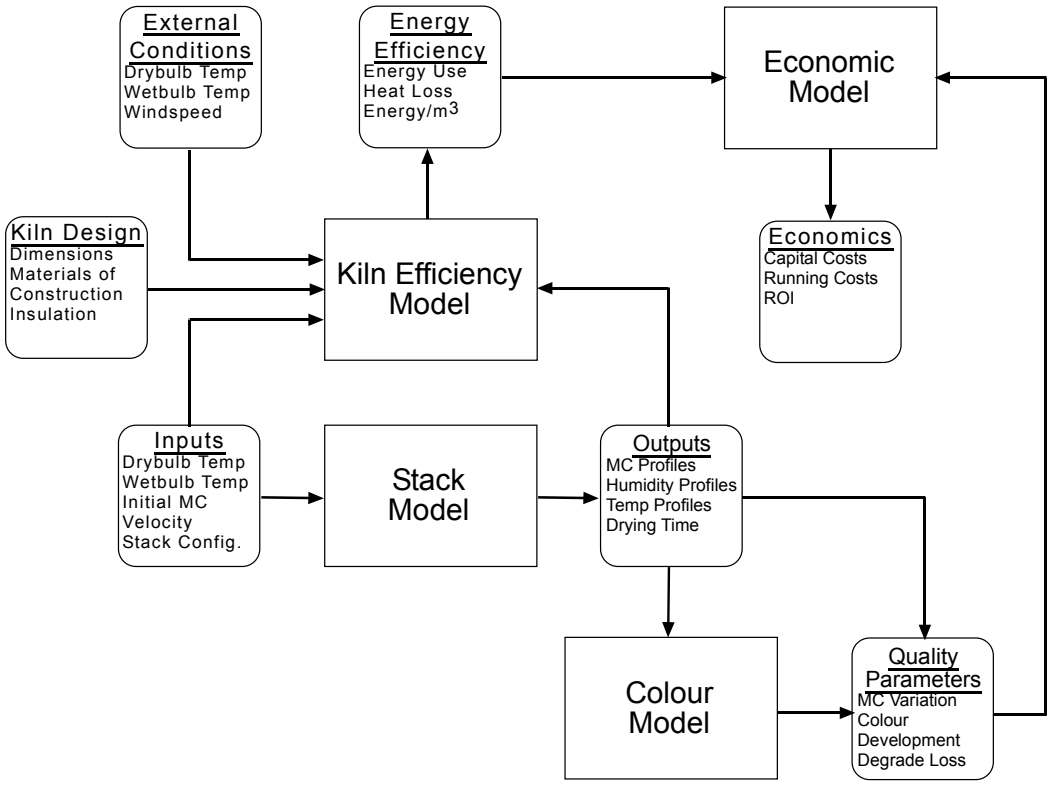

Figure 77. An integrated model system of one-dimensional kiln drying model being incorporated with a colour development model, a kiln energy efficiency model and an economic model.

van Meel's Batch Drying Equations

The model for convective batch drying developed by van Meel (1958) states, with certain assumptions, that a single characteristic drying curve can be used to describe the change in drying rate as a function of normalised moisture content for a material. It also states that this curve is unique for a given material but not affected by drying conditions. In this way, the relationship between the characteristic drying rate and normalised moisture content derived from laboratory experiments under constant conditions can be applied to a commercial scale dryer even under various drying conditions.

The original equations were derived for a tray dryer but have since been developed for the analysis of wood drying kilns with the addition of terms to describe the wood stack (Nijdam, 1998; Ashworth, 1977).

Characteristic Drying Curve

The characteristic drying curve is a function that describes the relationship between the relative drying rate, f, and the normalised moisture content, Φ, as described by the following equations:

$$f = \frac{N_v}{N_{cr}} \qquad 6.1$$

$$\Phi = \frac{X - X_e}{X_{cr} - X_e} \qquad 6.2$$

N_v is the drying rate (kg/m^2/s) of the material at a particular mean moisture content, X. X_e is the equilibrium moisture content at the drying conditions. N_{cr} is the constant drying rate at the moisture content above and at the critical moisture content, X_{cr}. This means that the characteristic drying curve only applies to the decreasing rate of drying when the moisture content is below the critical point.

A graphical representation of a characteristic drying curve is shown below in Figure 78. The relative drying rate is on the y-axis and the normalised moisture content is on the x-axis. This graph shows that the characteristic drying curve can also be described by the generalised function:

$$f = f(\Phi) \qquad 6.3$$

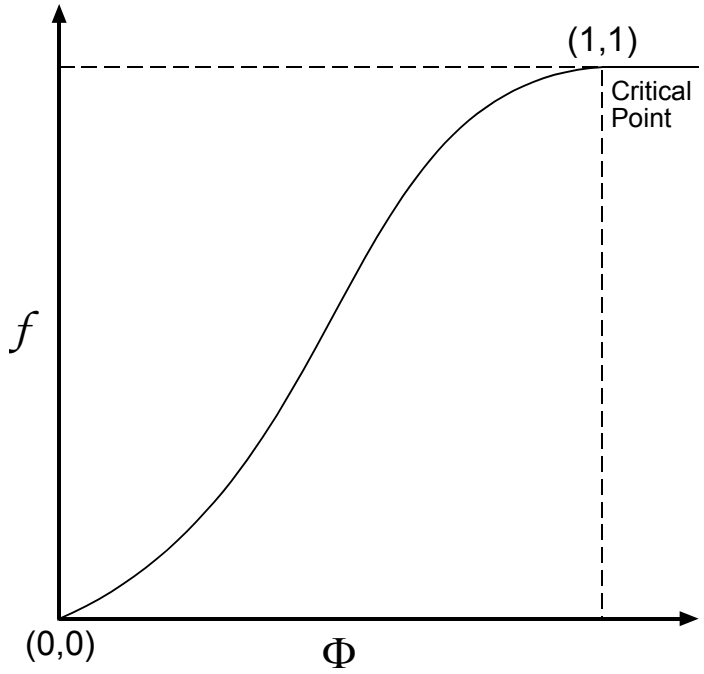

Figure 78. Characteristic drying curve (after Keey, 1992).

At and above the critical moisture content the drying rate is at a maximum (f=1) as the surface is covered in moisture so the drying rate is essentially the same as evaporation from free water. This means the rate of drying of a material can be represented by the following equation:

$$N_v = f\left[\beta\phi_m\left(Y_w - Y_G\right)\right] \qquad 6.4$$

In this lumped parameter expression the external mass transfer coefficient, β, represents the influence of the dryer design and the function, f, represents the drying characteristics of the material. The remaining variables represent the influence of the process conditions, where ϕ_m is the humidity potential, Y_W is the humidity adjacent to a fully wetted surface and Y_G is the bulk gas humidity of the drying medium.

The characteristic drying curve is a gross approximation, as noted by Keey et al. (2000) as it assumes the average moisture content of the material rather than the actual moisture content profile in the material. This is generally not the case with even the most permeable wood species. Ashworth (1977) and Nijdam (1998) have shown that the characteristic drying curve concept can be applied to the drying of wood as long as the curve is derived from tests on samples of the same thickness. Pang (1996) has examined the influence of the sample thickness and the curves can apply to different thickness with some modification.

The characteristic drying curve concept also relies on the assumption that all drying curves for a specific substance are geometrically similar. The characteristic drying curves for the samples dried in the single board drying tunnel described in chapter 6 are shown in Figure 79. These curves illustrate the variability in the characteristic drying curve for matched samples dried at different conditions. This suggests that the shape of the characteristic drying curve is not entirely independent from the drying conditions. At first glance it appears that the higher temperature schedules produce a concave-down curve, while the lower temperature schedules produce more of a concave-upward curve. The humidity seems to have a similar effect.

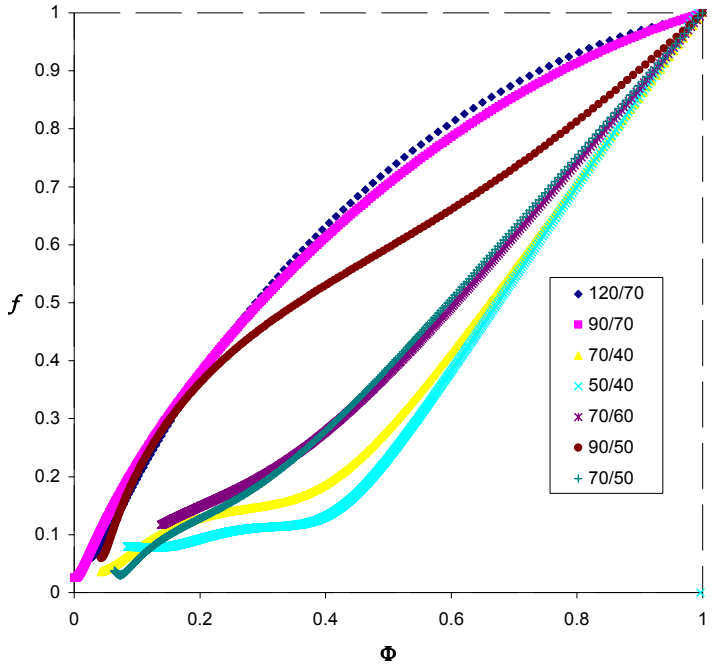

Figure 79. Characteristic drying curves for the 40mm Pinus radiata sapwood boards dried in the experiments described in chapter 6.

The assumption was made here that the drying conditions were having the greatest influence on the shape of the characteristic drying curve, though this may not be the only factor involved. Davis (2001) investigated the influence of various factors on the shape of the characteristic drying curve for 50mm Pinus radiata boards dried at 55/36. These experiments showed that there is considerable variability in the shape of the curve, including concave-up, concave-down and linear falling rate curves, even when the

drying conditions were the same. Some of the variability was linked to physical properties and storage of the wood while some could not be explained within the bounds of the experiments.

The influence of drying schedule on the characteristic drying curve seen in the experiments in this thesis clearly needs to be accounted for in a model if it is to give a reasonable prediction of drying time and the drying curve. A simple linear falling rate curve will over predict the drying time for high temperature schedules and predict shorter than normal drying times for low temperature schedules. To counter this problem a two stage linear falling rate curve was developed.

The two-stage linear falling rate curve came about from the observation that the slope of the low temperature characteristic drying curves change markedly at a normalised moisture content of about 0.4. It was therefore proposed to develop a characteristic drying curve model represented graphically in Figure 80.

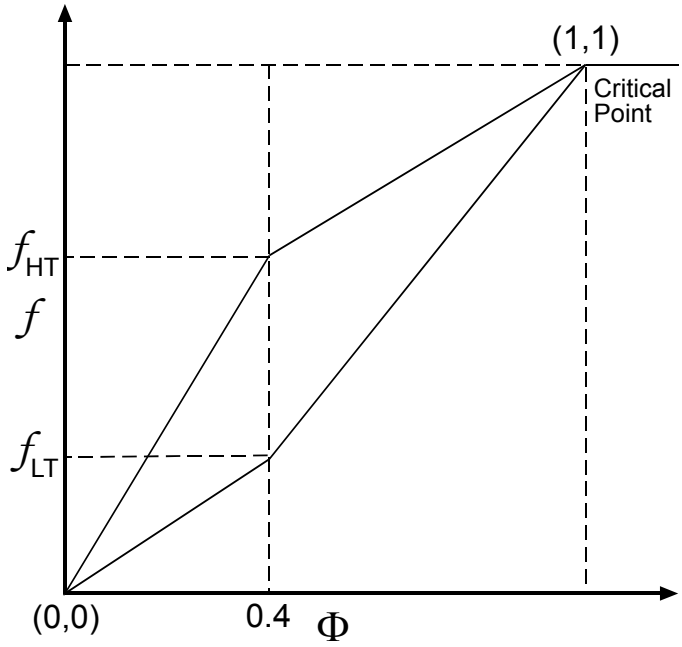

Figure 80. Two stage quasi-linear falling rate curve representation of the characteristic drying curve for wood.

In the two-stage linear falling rate curve there is a value for the relative drying rate that corresponds to a normalised moisture content of 0.4. As shown in Figure 80 for high temperature schedule the value of f_{HT} is high resulting in a concave down curve, whereas for a low temperature schedule the value of f_{LT} is low resulting in a concave upward curve. This special value for the relative drying rate at Φ=0.4 will be given the label $f_{0.4}$. The following expression for calculating a value for $f_{0.4}$ was determined from the experimental characteristic drying curves:

$$f_{0.4} = 0.0078e^{0.05T_{DB}} + 0.35(\psi - 0.54) \qquad 6.5$$

where TDB is the dry-bulb temperature in degrees Celsius and ψ is the relative humidity. The function $f(\Phi)$ therefore becomes:

$$f(\Phi) = \frac{(1 - f_{0.4})}{0.6} \cdot (\Phi - 0.4) + f_{0.4} \quad (0.4 \le \Phi \le 1)$$
$$f(\Phi) = \frac{f_{0.4}}{0.4} \cdot \Phi \qquad (\Phi < 0.4) \qquad 6.6$$

This approach to calculating a characteristic drying curve is not highly accurate but will provide a better approximation than a simple linear falling rate curve.

The characteristic drying curve concept is also reliant on the assumption that the critical moisture content does not vary with initial moisture content or external conditions. It is difficult to determine whether this assumption holds true for the drying data analysed above as there was no observed constant rate period in any of the samples. For wet samples, the initial constant drying rate can be taken as the average value in the initial period of drying, but for samples which surface is drying or initial moisture content is low (such as heartwood), the critical moisture content can be taken as the initial moisture content. The absence of a constant rate period may be due to pre-drying of the samples during storage. For the purposes of modelling it will be assumed that the critical moisture content does not vary and corresponds to an actual moisture content of 1.2kg/kg for all the sapwood.

Derivation of Batch Drying Equations

The derivation of an expression for the characteristic drying curve is only the first step in the development of the kiln drying model. This expression is used in the set of batch drying equations derived to quantify the change in moisture content and humidity through the stack. The following is a derivation of van Meel's batch drying equations for a wood drying kiln. This is based on work by Ashworth (1977), Pang(1994) and Nijdam (1998).

The derivation of the batch drying equations begins by considering the stack shown in Figure 81. The stack comprises a number of boards of thickness, b, arranged into rows with a fillet space of s. The total length of the stack is L and air flows through the fillet spaces at a velocity, u_f. The cross-sectional area free for air flow, or void space (ε), is given by the following expression:

$$\varepsilon = \frac{s}{(b + s)} \qquad 6.7$$

The specific dry gas mass flux through the fillet space is given by:

$$G = u_f \rho_G \varepsilon \qquad 6.8$$

where ρ_G is the density of the hot air (kg/m^3).

Drying of the stack is analysed by considering the moisture transfer from an infinitesimally small zone, *dz*, for a short time interval, *dt*. The transfer of moisture, or evaporation, from the boards into the air can be described by the following equation:

$$-\frac{\partial X}{\partial t}\rho_b(1-\varepsilon)=G\frac{\partial Y_G}{\partial z} \qquad 6.9$$

where ρ_b is the basic density of the wood. The term on the left represents the change in moisture content of the wood with time due to evaporation of moisture. The term on the right represents the change in the humidity of the air with distance due to the evaporation of moisture.

The evaporation of moisture from a board is also described by Equation (6.4) and combining this with Equation (6.9) gives the following expression:

$$-\frac{\partial X}{\partial t}\rho_b(1-\varepsilon)=G\frac{\partial Y_G}{\partial z}=f(\Phi)\beta\phi_m a(Y_W-Y_G) \qquad 6.10$$

where *a* is the exposed surface of the boards per unit volume of the kiln given by the following equation:

$$a=\frac{surface}{volume}=\frac{2\times l_s\times w_s}{l_s\times w_s\times(s+b)}=\frac{2}{s+b} \qquad 6.11$$

where l_s and w_s are the length and width of the stack respectively.

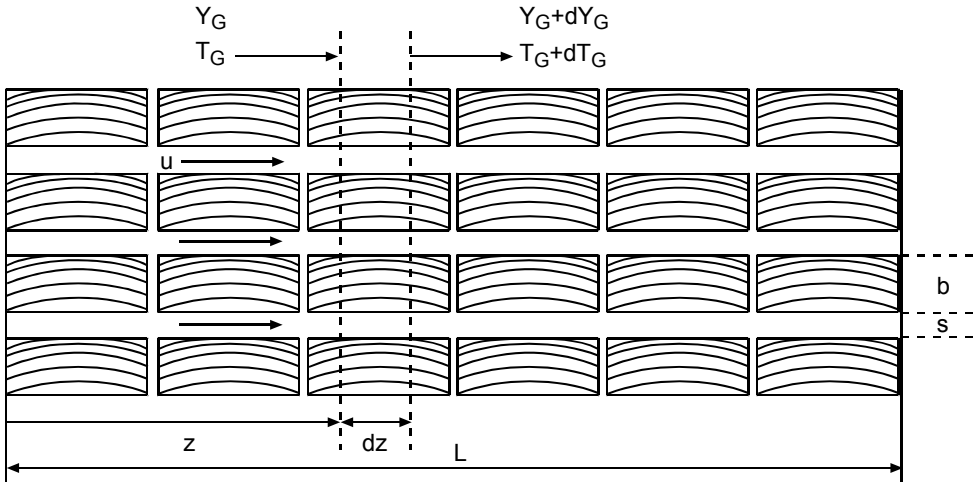

Figure 81. Model of timber stack showing the infinitesimally small zone used in the derivation of the batch drying equations (From Pang, 1994).

Equation (6.10) may be put into non-dimensional form for convenience, which results in the following expression:

$$\frac{\partial\Phi}{\partial\theta}=\frac{\partial\Pi}{\partial\zeta}=-f(\Phi)\Pi \qquad 6.12$$

In this equation, Π is the normalised humidity potential which is the fractional humidity potential normalised with respect to the inlet potential, as given by the following equation:

$$\Pi = \frac{Y_W - Y_G}{Y_W - Y_G^o} \qquad 6.13$$

where Y_W is the saturated humidity adjacent to the drying surface, or the wet bulb humidity, and Y_G is the humidity of the air. The wet bulb humidity remains constant under adiabatic drying conditions while the dry bulb humidity changes.

The normalised moisture content, Φ, is the same as given in equation (6.2). This dimensionless number represents the moisture content at any point relative to the critical moisture content.

The relative drying time, θ, is given by the following equation:

$$\theta = \frac{\beta \phi_m a \left(Y_w - Y_G^0\right)}{\left(X_{cr} - X_e\right)\rho_b\left(1-\varepsilon\right)} t \qquad 6.14$$

This dimensionless number represents the extent of drying to be undertaken based on the capacity of the kiln.

The relative distance across the kiln, ζ, is given by the following equation:

$$\zeta = \frac{\beta \phi_m a}{G} z \qquad 6.15$$

The solution of these equations gives the change in humidity through the stack and the change in moisture content of the boards with time and position in the stack.

Temperature Change in Stack

The temperature of the air passing through the stack decreases as heat is removed from the air stream to evaporate moisture from the boards. Pang (1994) has shown that a heat balance across a small distance, *dz*, in the stack yields the following equation for the temperature change:

$$\Delta T = -\frac{H_{wv}}{\left(1+\alpha_H\right)C_{PV}} \ln\left(\frac{C_{PG} + Y_G C_{PV}}{C_{PG} + Y_G^0 C_{PV}}\right) \qquad 6.16$$

where H_{wv} is the heat of vaporisation of liquid water, α_H is the ratio of radiation to heat transferred by the hot air, C_{PG} is the specific heat of air and C_{PV} is the specific heat of water vapour. This approach was used initially but later the following heat balance equation was used and solved iteratively:

$$T_i = \frac{C_{PYS} T_S}{C_{PYi}} - \frac{H_{wvi} Y_i - H_{wv}^0 Y_G^0}{C_{PYi}} \qquad 6.17$$

Calculation of Parameters

Many of the variables included in the batch drying equations in the previous section need to be calculated based on either the initial conditions or the conditions during the simulation.

Properties of Air and Water Vapour

The specific heat for air and water vapour were calculated from the following expressions fitted to data by Pang (1994):

$$C_{PV} = -247.5 + 22.20T_{GK} - 8.043\times10^{-2}T_{GK}^2 + 9.990\times10^{-5}T_{GK}^3 \quad 6.18$$

$$C_{PG} = 1038.1 - 0.2388T_{GK} + 4.599\times10^{-4}T_{GK}^2 \quad 6.19$$

The heat of vaporisation of liquid water and bound water are given by the following correlations from Pang (1994):

$$H_{wv} = 2.792\times10^{6} - 160T_{GK} - 3.43T_{GK}^2 \quad 6.20$$

$$H_{bv} = 2.792\times10^{6} - 160T_{GK} - 3.43T_{GK}^2 + 1.17\times10^{6}e^{-14X} \quad 6.21$$

The saturated vapour pressure for water in air at a given temperature T can be estimated using the following correlation:

$$p_s^v = \frac{1.0133\times10^5}{760}\times10^{f(T)} \quad 6.22$$

where the function f(T) has the following form:

$$f(T) = 16.3737 - \frac{2818}{T} - 1.6908\times\log_{10}(T) - 5.7546\times10^{-3}T + 4.007\times10^{-6}T^2 \quad 6.23$$

The wet-bulb humidity, Y_W, can be estimated from the following equation:

$$Y_W = \frac{p_s^v}{\frac{M_G}{M_v}\left(P_t - p_s^v\right)} \quad 6.24$$

where P_t is the total pressure and M_G/M_v = 1.61 for air-water vapour system. Using the wet-bulb humidity and the dry/wet-bulb temperatures (T_{GD} and T_{GW} respectively) the humidity of air can be estimated using the following equation:

$$Y_G = Y_W - \frac{1.8(T_{GD} - T_{GW})(0.24 + 0.44Y_W)}{1351.4 + 0.792T_{GD} - 1.8T_{GW}} \quad 6.25$$

The relative humidity, ψ, is calculated as the ratio of the saturated vapour pressure at the dew-point temperature and the saturated vapour pressure at the dry-bulb temperature.

Mass Transfer Coefficient

The mass transfer coefficient can normally be calculated from standard correlations using boundary layer theory. For ease of calculation, in this study a fitted correlation by Pang (2005)) is used, as shown here:

$$\beta = 0.022 - 0.0001\left(T_{GD} - 393.15\right) + \frac{0.327\left(u-3\right)}{T_{GW} - 251.52} - 7.83\times10^{-6}T_{GW}^{2} + 0.005T_{GW} - 0.79685 \qquad 6.26$$

This correlation was fitted to data from ACT and HT drying so there may be some error associated with applying it to drying at lower temperatures.

Related to the mass transfer coefficient is the humidity potential, ϕ_m. The humidity potential is a correction factor that accounts for the deviation from direct proportionality when using humidity difference as a driving force for evaporation. Under kiln conditions the humidity potential can be calculated from the following equation:

$$\phi_m \cong \frac{0.622}{0.622 + \left(Y_W + Y_G\right)/2} \qquad 6.27$$

Equilibrium Moisture Content

The equilibrium moisture content of Pinus radiata, X_e, was calculated from the relative humidity and dry-bulb temperature using the following correlation fitted by Pang (1994):

$$X_e = \frac{18}{W}\left[\frac{K_1K_2\Psi}{1+K_1K_2\Psi} + \frac{K_2\Psi}{1-K_2\Psi}\right] \qquad 6.28$$

where the coefficients W, K_1 and K_2 are given by the following:

$$K_1 = 9.864 + 0.04773T_{GD} - 5.012\times10^{-4}T_{GD}^{2} \qquad 6.29$$

$$K_2 = 0.7196 + 1.698\times10^{-3}T_{GD} - 5.553\times10^{-6}T_{GD}^{2} \qquad 6.30$$

$$W = 187.6 + 0.6942T_{GD} + 0.01853T_{GD}^{2} \qquad 6.31$$

Numerical Method for Solving the Kiln Stack Model

The batch drying equations were solved by the same method used by Nijdam (1998). This involves a simple Euler-based finite difference method where Equation (6.12) was discretised in the following way:

$$\frac{\partial\Pi}{\partial\zeta} \approx \frac{\Delta\Pi}{\Delta\zeta} \approx -f\left(\Phi\right)\Pi \qquad 6.32$$

$$\Delta\Pi = -f(\Phi)\Pi \cdot \Delta\zeta \qquad 6.33$$

$$\Pi_{i+1} = \Pi_i - f(\Phi_{i,j})\Pi_{i,j} \cdot \Delta\zeta \qquad 6.34$$

Equation (6.12) was similarly discretised to give the following formula for the change in normalised moisture content:

$$\Phi_{j+1} = \Phi_j - f(\Phi_{i,j})\Pi_{i,j} \cdot \Delta\theta \qquad 6.35$$

Equations (6.34) and (6.35) are solved on a grid as shown in Figure 82. On this grid the nodes are numbered …, i-1, i, i+1,… in the 'distance through the stack' direction and the distance between each node in this direction is $\Delta\zeta$. The nodes are numbered …, j-1, j, j+1,… in the 'drying time' direction and the distance between each node in this direction is $\Delta\theta$.

The size of the steps $\Delta\theta$ and $\Delta\zeta$ determines the accuracy of the solution. The optimum step sizes were determined by decreasing them until the difference between successive simulations was negligible. The time step size eventually used in the simulations was 5s for all schedules which corresponded to a slightly different $\Delta\theta$ in each case. There are still some slight difference in the results with this time step and smaller time steps, but the larger step was chosen to reduce the simulation time. The distance step size used was 0.01m which corresponds to 240 points across the stack. Using a step size any smaller than this did not produce differences significant enough to justify the increase in simulation time.

Boundary and Initial Conditions

The initial moisture content of all of the boards in the stack is assumed to be the same and equal to the critical moisture content. The former assumption is for convenience to reduce the complexity of the calculation and is justified by the fact that initial moisture content variation is not being studied. The latter assumption is based on evidence from the experimental drying curves. These drying curves show no discernible constant rate drying period for the conditions that the model is being used to simulate. Based on these assumptions the following initial condition is true:

$$\Phi_{i,0} = 1, \text{for all } i \qquad 6.36$$

The humidity potential at the inlet to the stack will always be 1 based on the definition of humidity potential

Program Structure

The basic structure of the stack simulation program is in the flowchart shown in Figure 83. This program was written in MatLab, with the code provided in the appendices.

The first step determines the value of the characteristic drying at each point from the conditions at the point. The *f* function is then calculated from this and used as a correction factor on the humidity potential calculations. The calculation of humidity is an iterative process over the width of the stack which results

in a humidity potential profile. The normalised moisture content profile is then determined from the humidity potential profile. This process is then iterated for the required number of time steps. The outputs were recorded at every hour of simulated time, which means the j = 720 for a time step of 5s.

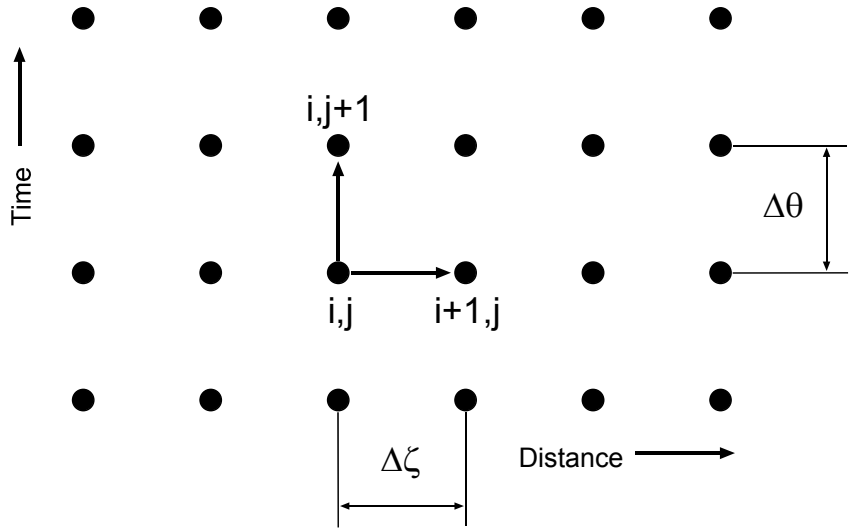

Figure 82. Grid layout for the numerical solution to the batch drying equations.

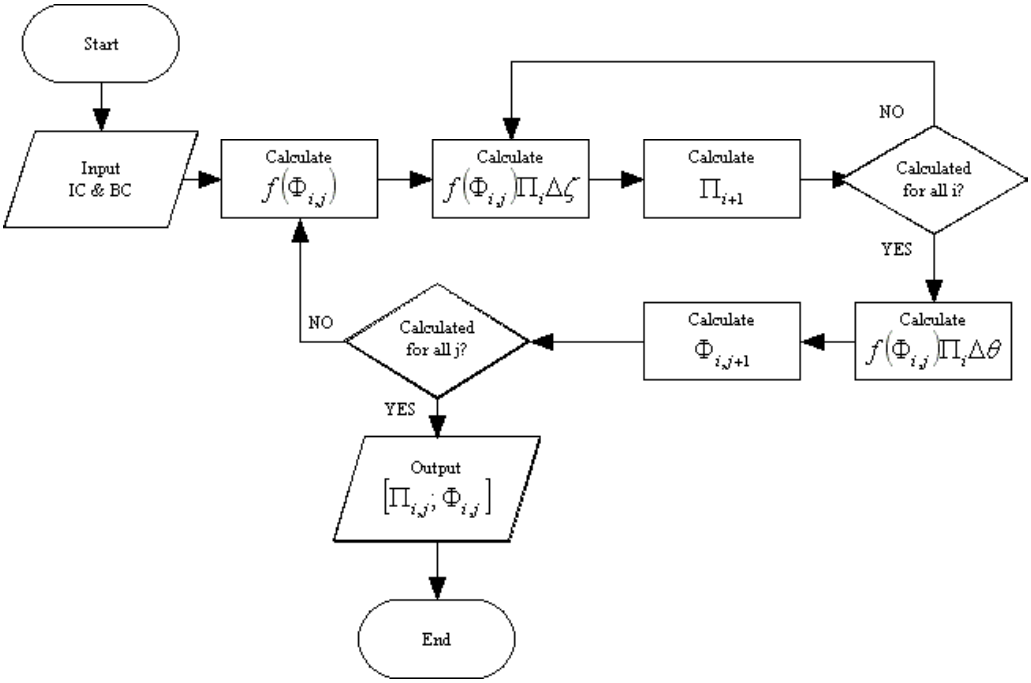

Figure 83: Flowchart for the numerical solution of the batch drying equations. The function $f_{0.4}$ was recalculated at each iteration when the characteristic drying curve was recalculated.

There are a number of other calculations performed in the program that are not included in the flowchart. The absolute humidity, relative humidity and temperature are calculated for each step as well. The latter two are required to define the characteristic drying curve based on Equation (6.5). The temperature and absolute humidity are also important for calculating many of the physical properties used in the energy use calculations described later in this chapter. The absolute humidity is required to determine the recycle ratio and venting ratio which are also required for the kiln energy use calculations. The temperature and moisture content data was required for the calculation of colour development, described later. All of these values were also included in the output.

The final program structure also incorporated a mechanism to simulate the airflow reversal that occurs in a kiln to prevent excessive moisture content gradients across the stack. This reversal was set up so that it could be varied but for the simulations present in this thesis the reversal period was set at 6 hrs. This reversal basically involved switching the iterations so that they went from …i-1, i, i+1… to …i+1, i, i-1… in direction.

The energy use and colour development calculations were incorporated into the program structure as they were developed and refined.

Validation of Kiln Stack Model

The kiln stack model used in this thesis has been previously validated by a number of different studies including Nijdam (1998), Pang (1994) and Ashworth (1977). For this reason it was not considered necessary to perform drying experiments to test the model. The experimental data presented in Chapter 4 is for single boards and therefore is not suitable for the rigorous validation of a kiln stack model.

Energy Efficiency Model

The drying of wood is an energy intensive process. This is true of any drying operation as a significant amount of heat is required to evaporate moisture from the wood. The drying of wood is particularly energy intensive as some of the moisture that needs to be removed is bound to the cell wall structure. This bound water requires more energy to evaporate as shown by the extra term in Equation (6.21). Given the large energy requirement one of the goals in designing and running wood drying processes is to minimise any extra energy used above what is required. The energy efficiency model presented here seeks to identify factors effecting energy efficiency and optimise the kiln operation to maximise the efficiency.

Energy Consumption during Wood Drying

There are six categories of energy consumption in wood drying kilns as noted by Simpson (1991), which encompass all elements of energy consumed. These are as follows:

1. Latent Heat: This is the heat required to evaporate moisture from the wood and includes heat of absorption for drying below fibre saturation point and can include heat of fusion if some of the moisture is frozen.

2. Vent Heat Loss: This is the heat lost when air is vented from the kiln and cool fresh air drawn in to remove water vapour for control of humidity. This can also include fugitive emission from leaky drying structures.

3. Sensible Heating: This is the heat required to bring the kiln charge and the kiln internal structure to the drying temperature, also referred to as heat capacity.

4. Heat Loss: This is unintentional heat loss to the environment surrounding the kiln. This includes heat loss due to conduction through the walls, floor and ceiling which is then lost to the ambient environment by convection and radiation from external surfaces. This heat loss also includes the draining of condensation from internal walls.

5. Air Movement: This is the energy required to move air through the timber stack and is most often electrical energy supplied to fans. This category also includes energy wasted through air bypassing the stack.

6. Energy Source and Delivery System: This encompasses the energy efficiency of the heat generation used by the kiln and the losses associated with delivering the heat to the kiln.

There are also a number of factors that affect how energy is consumed during the drying of wood. These are as follows:

1. Wood Properties: The density and initial moisture content are particularly important for determining the latent heat requirement and also the sensible heat requirement for heating the stack.

2. Stack Properties: The design of the stack is also important for calculating the latent and wood sensible heat requirements as it determines the total amount of wood in the kiln. The fillet spacing and board thickness also influence the energy required for air movement. Where a stack is poorly built it can also contribute to bypass of air.

3. Kiln Design: The design of the kiln impacts on the heat capacity of the kiln structure and heat loss through the structure and from fugitive emissions. The kiln design also influences the air movement and poorly designed kilns can have airflow misdistribution through the stack and bypass.

4. Kiln Schedule: The kiln schedule has a major impact on the vent heat loss from the kiln as low humidity schedules require the vents to be open for a lot more time than with high humidity schedules. The schedule will also influence the heat loss to the environment by setting the internal temperature of the kiln. It may also have some influence on the efficiency of the energy source and delivery system.

5. External Environment: The external environment directly affects the vent heat loss and the unintentional heat loss from the kiln. It also affects the sensible and in some cases latent heating required.

6. Operator Influence: This is the human element of the kiln drying operation and mainly influences the heat loss, air movement and energy source and delivery system elements of energy consumption.

Latent Heat Requirements

The latent heat requirement to evaporate the moisture contained within a stack of wood is the absolute minimum energy required in a conventional convective kiln dryer. In most cases the wood is dried to a moisture content well below fibre saturation point so the total latent heat requirement, Q_v, is made up of two components:

$$Q_v = Q_{wv} + Q_{bv} \tag{6.37}$$

Where Q_{wv} is the heat required to evaporate free water and Q_{bv} is the heat of adsorption, additional heat required to evaporate bound water. The heat of fusion is not considered here as it is unlikely that wood will be dried from a frozen state in New Zealand.

The first term, Q_{wv}, can be readily calculated from the wood properties, stack design and drying schedule using the following equation:

$$Q_{wv} = V_s(1-\varepsilon)\rho_b \times (X_0 - X_{fsp}) \times H_{wv} \tag{6.38}$$

The first term in this equation determines the total mass of wood in the stack from the stack volume, Vs, the void space (Equation 6.7), ε, and the basic density, ρ_b. The second term is the moisture content change from the initial moisture content, X_0, to fibre saturation point, X_{fsp}. The final term is the latent heat of vaporisation for free moisture, H_{wv}, calculated from Equation (6.20).

The latent heat required to evaporate bound moisture is calculated from the same basic equation but requires integration due to the presence of the moisture content term in Equation (6.21). Combining Equation (6.21) and Equation (6.37), and integrating over moisture content from fibre saturation point to actual moisture content, gives the following:

$$Q_{bv} = V_s(1-\varepsilon)\rho_b \times (X_{fsp} - X_e) \times H_{wv} + V_s(1-\varepsilon)\rho_b \times 8.35 \times 10^4 \left(e^{-14X_e} - e^{-14X_{fsp}}\right) \tag{6.39}$$

With the equations above it is possible to calculate the latent heat requirement for a stack of 40mm thick boards, of basic density 400kgm-3, with the following dimensions: 3.6m high, 2.4m wide, 7.0m long, and 20mm fillets. The volume of the stack is 60.5m3 with a void space of 0.33. Assuming a drying temperature of 70°C, then H_{wv}=2333kJkg-1 and X_{fsp}=0.25kgkg-1. With initial moisture content of 1.2kgkg-1 and a final moisture content of 0.1kgkg-1 the total energy required is calculated as follows:

$$\begin{aligned} Q_{wv} &= 60.5(1-0.33)400 \times (1.2-0.25) \times 2333 \\ &= 35.75 \times 10^6 \text{kJ} \end{aligned}$$

$$
\begin{aligned}
Q_{bv} &= 60.5(1-0.33)400\times(0.25-0.1)\times 2333 + 60.5(1-0.33)400\times 83.5\left(e^{-14(0.1)} - e^{-14(0.25)}\right) \\
&= 5645860 + 291688 \\
&= 5.94\times 10^{6}\,\text{kJ}
\end{aligned}
$$

$$
\begin{aligned}
Q_{v} &= 35.75\times 10^{6} + 5.94\times 10^{6} \\
&= 41.69\times 10^{6}\,\text{kJ}
\end{aligned}
$$

This is a considerable amount of energy, over 12MWh, to dry approximately 40m3 of wood. This is approximately 1.1kWh per lineal metre of 40×100mm board in the stack.

Ideal Heat Demand

The ideal heat demand of a kiln is the heat required to maintain the humidity and temperature conditions in the kiln without allowing for heat loss or sensible heating (Keey et. al., 2000). This is a useful first step in an investigation of the energy efficiency of a kiln as it provides a baseline energy use which other factors can be added to. The key influences that are investigated are the effect of the kiln schedule and kiln configuration on the energy use. There are a number of ways that the airflow, heating and venting of a kiln can be configured. Five configurations are explored for this project.

Kiln Configuration 1

The most basic configuration for a batch kiln is shown in Figure 84. This configuration comprises an enclosed batch kiln with a single heating coil and an overhead axial flow fan for air movement. Humidity is controlled through vents that draw in ambient air on the low pressure side of the fan and expel humid air on the high pressure side of the fan. This form of humidity control assumes that only dehumidification is required, actual kilns have some mechanism, such as water sprays or water baths, to increase the humidity when required.

The calculation of the heat supply required to maintain conditions inside the basic batch kiln considers two possible arrangements. These are the fresh air being mixed either before going through the heating coils or after going through the heating coils in the case where a heater is installed only on one side. Therefore, the heat balance changes when the direction of airflow is changed. The two flow directions are represented in Figure 84 as configuration 1(a) where the air is being pushed through the heater and configuration 1(b) where the fan is pulling air through the heater. On both configurations T_A is the ambient temperature, T_S is the controlled stack inlet temperature and T_O is the stack outlet temperature. In configuration 1(a), T_V is the venting temperature that comes from the mixing of the outlet stream and the ambient inlet stream and in configuration 1(b) T_H is the temperature of the outlet stream after it has passed through the heater but before mixing with the ambient air inlet stream.

The letter v in Figure 84 is the venting ratio. This is similar to the recycle ratio that would normally be used in this calculation for an industrial dryer (Keey, 1992). The layout of a wood drying kiln means that there is not a true, separated, recycle loop in the drying process and the vented stream is an important part

of the process. The venting ratio, which is the proportion of the stream passing though the stack that is vented, is determined in much the same way as a recycle ratio, from a mass balance on the air streams. This mass balance is independent of the heater position and therefore is the same for both of the configurations. The mass balance, per unit volume of air passing through the stack, for the air streams in both cases 1(a) and 1(b) can be described by the same equation as follows:

$$vY_{GA} + Y_{GO} = Y_{GS} + vY_{GS} \qquad 6.40$$

Where Y_{GA} is the ambient air humidity, Y_{GO} is the humidity at the outlet of the stack and Y_{GS} is the humidity of the air entering the stack. This balance can be rearranged to give the venting ratio as:

$$v = \frac{Y_{GO} - Y_{GS}}{Y_{GS} - Y_{GA}} \qquad 6.41$$

This ratio will be at a maximum when the outlet humidity is greatest, such as when the air is leaving the stack saturated with water vapour. This will occur early in the drying schedule. Later as the stack dries out the humidity at the outlet will be reduced and therefore the venting ratio will decrease.

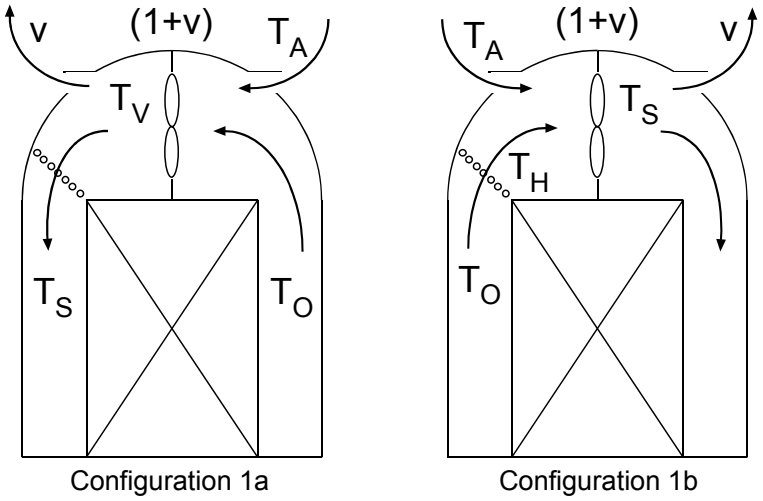

Figure 84. Schematic representation of kiln configuration 1 showing the operation with airflow in both directions: 1(a). Fresh air is mixed with circulating air before heating coils; 1(b). Fresh air is mixed with circulating air after heating coils.

The calculation of the heat balance for basic configuration requires the use of sensible heat of the humid air which is the combination of the specific heat of the dry air and the specific heat of the water vapour in the air as given by the following equation:

$$C_{PY} = C_{PG} + YC_{PV} \qquad 6.42$$

Where C_{PG} is the specific heat of the dry air that can be calculated using equation 6.17 and C_{PV} is the specific heat of moisture vapour that can be calculated using equation 6.16. Y is the humidity of the air stream which is the mass ratio of the moisture vapour to the dry air.

The calculation of the heat requirements for configuration 1a requires the venting temperature, T_V, which is not available from the stack simulation results. This temperature can be determined from a heat balance over the three streams involved and the heat balance takes the following form:

$$(1+v)C_{PYV}T_V = C_{PYO}T_O + vC_{PYA}T_A \qquad 6.43$$

In which C_{PYO} is the air humidity from stack outlet side, C_{PYA} is the air humidity in the ambient and C_{PYV} is the air humidity after mixing. The above equation can be rearranged to give the temperature, T_V, as the following:

$$T_V = \frac{C_{PYO}T_O + vC_{PYA}T_A}{(1+v)C_{PYV}} \qquad 6.44$$

With the venting temperature determined, the heat required to maintain the conditions in the kiln is simply the heat required to raise the temperature of the air from T_V to controlled dry-bulb temperature, T_S, before it re-enters the stack. The heat supply for configuration 1(a) is given by the following equation:

$$Q_S^{1a} = C_{PYS}T_S - C_{PYV}T_V \qquad 6.45$$

In this case the air humidity before the heating coil is the same as that after the heating coil. Substituting equation 6.42 for T_V in Equation (6.43) results in the following equation for the heat supply:

$$Q_S^{1a} = \frac{1}{1+v}\left[(C_{PYS}T_S - C_{PYO}T_O) + v(C_{PYS}T_S - C_{PYA}T_A)\right] \qquad 6.46$$

The heat supply for configuration 1(b) can be calculated more directly from the following heat balance:

$$Q_S^{1b} = (C_{PYS}T_S - C_{PYO}T_O) + v(C_{PYS}T_S - C_{PYA}T_A) \qquad 6.47$$

With the similarities between Equation (6.46) and Equation (6.45) it is immediately obvious that the heat supplied for configuration 1(a) will always be less than that for configuration 1(b) under the same conditions. This is because the venting ratio will always be positive for a drying operation where the air gains moisture as it passes through the stack and therefore the first term in Equation (6.47) will always be smaller than the first term in Equation (6.48).

The dimensionless ideal heat demand for an industrial dryer, Q*, is defined by Keey (1992) as the ratio of the heat used to bring the inlet airstreams to the controlled dry-bulb temperature compared to the evaporative load:

$$Q^* = \frac{Q_S}{H_{WV}(Y_O - Y_S)} \qquad 6.48$$

Assuming that the air is being adiabatically saturated while passing through the stack then the following relationship for the temperature drop due to humidification applies:

$$Y_O - Y_S = \frac{(C_{PYS}T_S - C_{PYO}T_O)}{H_{wv}} \qquad 6.49$$

Substituting Equation (6.49) and Equations (6.46) and (6.47) into Equation (6.48) yields the following equations for the ideal heat demand for configuration 1:

$$Q_{1a}* = \frac{H_{wv}}{1+v}\left[1 + v\frac{(C_{PYS}T_S - C_{PYA}T_A)}{(C_{PYS}T_S - C_{PYO}T_O)}\right] \qquad 6.50$$

$$Q_{1b}* = H_{wv}\left[1 + v\frac{(C_{PYS}T_S - C_{PYA}T_A)}{(C_{PYS}T_S - C_{PYO}T_O)}\right] \qquad 6.51$$

The heat demand for configuration 1(b) will always be greater than that for the configuration 1(a) when drying is taking place. In an extreme situation when the venting ratio is unity (v=1), the heat demand for 1(b) is twice the heat demand of configuration 1(a). This is however an unrealistically high venting ratio for a normal wood drying operation and most wood drying kilns would not have sufficient heating capacity to handle such a high level of venting.

Kiln Configuration 2

The second kiln configuration evaluated in this project is the same as configuration 1 but with heating coils installed either side of the fan. This means the heating coils can be use alternately as the airflow direction is changed so that the fan will always be blowing air towards the heater thus eliminating the losses from venting heated air in configuration 1(b). The equations are therefore the same as those for configuration 1(a) for both air flow directions.

Kiln Configuration 3

The third kiln configuration is similar to configuration 2 but incorporates a heat exchanger to recover some of the heat lost from venting and use it to heat the incoming ambient air. A schematic representation of this configuration is shown in Figure 85. The inclusion of a heat exchanger complicates the calculation of the ideal heat demand as the performance of the heat exchanger is determined by the inlet and outlet temperatures as well as the design of the exchanger. To simplify the calculations it is assumed that the sensible heat of the inlet air is halfway between that of the vented air and the ambient air. The heat balance to determine the vent temperature is therefore:

$$(1+v)C_{PYV}T_V = C_{PYO}T_O + 0.5v(C_{PYA}T_A + C_{PYV}T_V) \qquad 6.52$$

This can be rearranged to give the following equation for TV:

$$T_V = \frac{C_{PYO}T_O + 0.5vC_{PYA}T_A}{(1+0.5v)C_{PYV}} \qquad 6.53$$

This configuration has the same heat balance as configuration 1a for determining the heat supplied to the kiln. Substituting Equation (6.52) into Equation (6.46) gives the following equation for the heat supplied to configuration 3:

$$Q_S^3 = \frac{1}{1+0.5v}\left[(C_{PYS}T_S - C_{PYO}T_O) + 0.5v(C_{PYS}T_S - C_{PYA}T_A)\right] \quad 6.54$$

The ideal heat demand is therefore:

$$Q_3^* = \frac{H_{wv}}{1+0.5v}\left[1 + 0.5v\frac{(C_{PYS}T_S - C_{PYA}T_A)}{(C_{PYS}T_S - C_{PYO}T_O)}\right] \quad 6.55$$

It is not immediately obvious whether this configuration is an improvement on configuration 2, however inputting realistic numbers into Equations (6.55) and (6.50) shows that configuration 3 is an improvement, particularly where T_A is much lower than T_O.

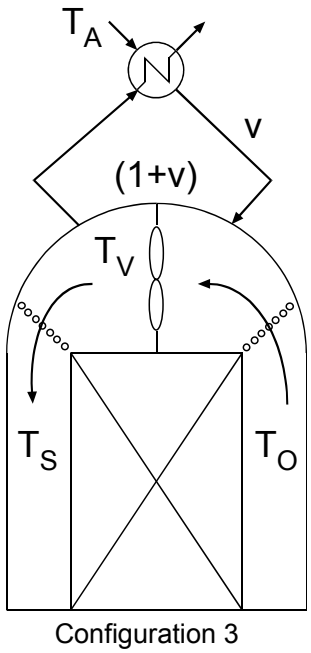

Figure 85. Schematic representation of kiln configuration 3 incorporating a roof mounted heat exchanger for the recovery of some heat from the vented air.

Kiln Configuration 4

The fourth kiln configuration, shown in Figure 86, is also an improvement on configuration 2 that eliminates venting entirely and instead incorporates a loop that air-cools a portion of the air and removes some of its moisture by condensation. As a result of these changes this configuration does contain a true recycle loop and so the calculations include a recycle ratio calculated from the following mass balance:

$$Y_{GS} = rY_{GO} + (1-r)Y_{GA} \quad 6.56$$

The above equation is rearranged to give the recycle ratio as follows:

$$r = \frac{Y_{GS} - Y_{GA}}{Y_{GO} - Y_{GA}} \qquad 6.57$$

The heat supplied to the kiln is given by the following heat balance:

$$Q_S^4 = r(C_{PYS}T_S - C_{PYO}T_O) + (1-r)(C_{PYS}T_S - C_{PYA}T_A) \qquad 6.58$$

The ideal heat demand is therefore:

$$Q_4{}^* = H_{wv}\left[r + (1-r)\frac{(C_{PYS}T_S - C_{PYA}T_A)}{(C_{PYS}T_S - C_{PYO}T_O)} \right] \qquad 6.59$$

It is difficult to compare this configuration with the previous configurations just looking at the equations due to the use of a recycle ratio rather than a venting ratio. Also to consider the heat transfer requirement in the condenser T_A is assumed to be 10°C higher than the ambient temperature for the purposes of simulation.

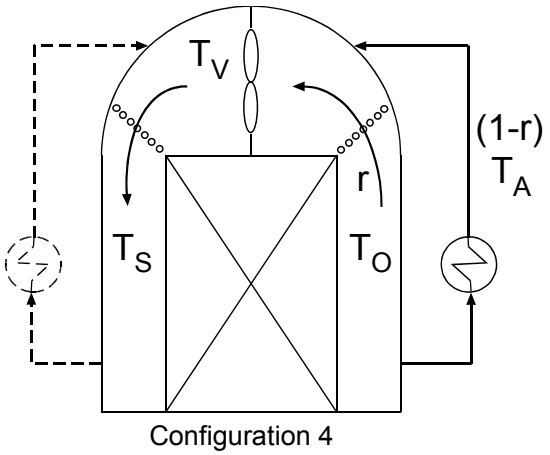

Figure 86. Schematic representation of kiln configuration 4 incorporating an air-cooled condenser to control humidity.

Kiln Configuration 5

The final kiln configuration evaluated in this project is shown in Figure 87. In this configuration the heating coils also act as cooling coils when they are up stream of the fan. This is similar to what could be achieved with a dehumidification kiln with a supplementary heat supply or in a standard kiln with the addition of cooling water.

In kiln configuration 5 there is no need for a venting ratio or recycle ratio as the entire air stream is effectively recycled and humidity is not controlled by venting. The heat supplied to the kiln is therefore given by the following heat balance:

$$Q_S^5 = C_{PYS}T_S - C_{PYW}T_W \qquad 6.60$$

The ideal heat demand is therefore:

$$Q_5^* = H_{wv}\left[\frac{(C_{PYS}T_S - C_{PYW}T_W)}{(C_{PYS}T_S - C_{PYO}T_O)}\right] \qquad 6.61$$

Unlike the previous configurations this configuration also requires cooling to operate. The cooling supplied to the kiln can be calculated using the following equation:

$$Q_C^5 = C_{PYO}T_O - C_{PYW}T_W + H_{wv}(Y_{GO} - Y_{GW}) \qquad 6.62$$

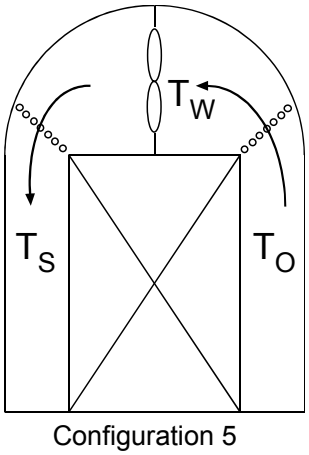

Figure 87. Schematic representation of kiln configuration 5 comprising heating and cooling elements.

Simulation results for the Ideal Heat Demand

In the kiln simulation the evaporative load and the heat supplied were calculated separately at each iterative time step. The results for all the time steps were summed at the end of the simulation to give the total heat supplied and the total evaporative load for each kiln configuration. The results for selected schedules are shown in Table 24

Table 24. Ideal heat demand for various schedules based on simulated results expressed as a ratio of the evaporative load.

Schedule	50/45	50/40	60/55	60/50	60/45	70/65	70/60	70/55
Drying Time, h	212	158	173	107	94	143	80	61
Configuration 1	1.67	1.68	1.78	1.74	1.73	2.02	1.89	1.82
Configuration 2	1.66	1.65	1.77	1.72	1.70	2.01	1.88	1.80
Configuration 3	1.43	1.40	1.57	1.49	1.45	1.82	1.68	1.58
Configuration 4	1.67	1.76	1.77	1.73	1.76	2.01	1.88	1.80
Configuration 5	3.38	4.86	3.01	3.50	4.40	2.94	2.96	3.13

Kiln configuration 5 stands out as by far the worst option, however it should be noted that the simulation of this configuration did not include any heat recovery from the cooling water. If heat recovery was

included, using for example a heat pump, the ideal heat demand would be lower. For a standard heat vent kiln this design is clearly unsuitable. It will therefore not be considered in the further analysis of energy use.

The simulation results for kiln configuration 3 show that for all schedules it requires the least amount of energy to dry the wood. This may mean that the heat transfer assumptions made when deriving the heat supply equation were a little optimistic. The clear benefits of this configuration do warrant further investigation of the potential realistic heat recovery possible.

The remaining three kiln configurations show similar ideal heat demands for the schedules tested. Kiln configuration 1 is as predicted the worse than configuration 2. In these two configurations the higher temperature schedules also seem to generally have a better ideal heat demand. Configuration 4 varies from being much worse to slightly better than configurations 1 and 2 depending on the temperature and humidity of the schedule. The assumption of air temperature being 10°C higher than ambient air temperature may have some influence on the energy efficiency and needs some further investigation.

Heat Loss

The ideal heat demand is missing one important energy cost associated with practical drying operations. This is the energy required to make up for heat lost unintentionally to the environment. This heat can be lost by radiation from the outside kiln walls to the atmosphere, conduction through the floor into the ground and free and forced convection to the surrounding environment. Heat can also be lost in the form of fugitive emissions. These pathways for heat loss are shown in Figure 88.

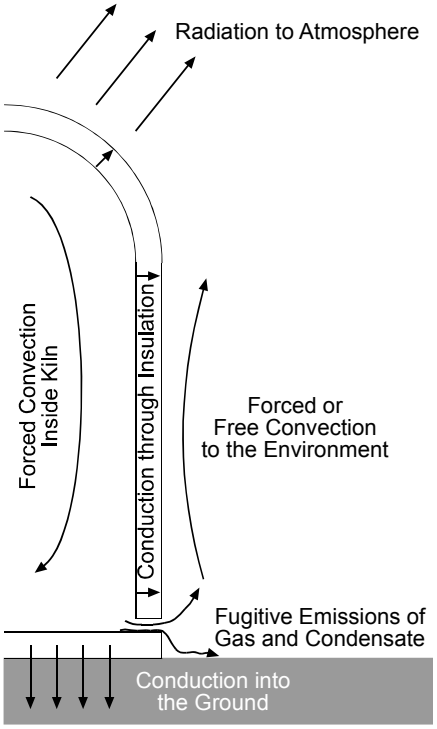

Figure 88. Pathways for heat loss from a wood kiln during drying.

Based on this diagram the equation for the heat loss from the kiln is:

$$Q_{loss} = Q_{convection} + Q_{conduction} + Q_{radiation} + Q_{fugitive} \quad 6.63$$

Where $Q_{convection}$ is the heat loss due to free and forced convection to the environment, which is through three steps: the internal forced convection, conduction through the walls and external convection heat transfer to the environment. This heat loss occurs from all of the surfaces exposed to the ambient air environment, namely the four sides and the roof. $Q_{conduction}$ is the heat loss through the bottom of the kiln into the ground that the kiln sits on and is also through three steps: internal forced convection, conduction through the slab and conduction into the ground. $Q_{radiation}$ is the heat loss through infrared radiation to the environment, which is again through three steps: internal forced convection, conduction through the walls and external radiation to the environment. $Q_{fugitive}$ is a catch-all for other heat loss not covered by the other three terms.

The external wall temperature is important for the determination of both Qconvection and Qradiation and this temperature is determined by both of these processes. This means that these two terms are not independent and must therefore be determined simultaneously.

Kilns are designed to minimise heat loss with insulated walls to reduce conductive heat transfer through the kiln walls and external finishes with low emissivity to reduce radiant heat loss. There are also rubber seals on the doors and hatches to prevent leakage of gas to the environment.

A number of assumptions have been made in the calculation of kiln heat loss to simplify the analysis. These are as follows:

1. It is assumed that the kiln is perfectly sealed so that there is no direct contact between the air inside the kiln and the environment, except through the vents. The venting heat loss has already been accounted for in the calculation of ideal heat demand. This assumption means that the last term in Equation (6.63) can be ignored.
2. The external forced convection due to climatic conditions such as wind and rain has been ignored. The external conditions are assumed to be an air temperature of 20°C with a wet bulb temperature of 10°C. This assumption reduces the number of simulations required and means the simulations are focussed on the effect of manipulating the kiln design and schedule rather than the external conditions.
3. The wall insulation is continuous so that there are no cold spots inside the kiln for condensation and no conduits for conduction to the outside. Similar to the first assumption this also removes the need for the last term in Equation (6.63) and also simplifies the determination of the wall conduction.
4. The internal conditions are uniform so that everywhere the temperature is at the dry bulb temperature of the schedule and the airflow the same at all points on the internal walls. This

simplifies the calculation of the internal convective heat transfer and will over-estimate rather than under-estimate this component.

5. The radiation heat loss is to the immediate surroundings at the same ambient temperature used for the external convection calculations. This assumption means that the radiation heat transfer can be estimated with a radiation heat transfer coefficient analogous to the convective heat transfer coefficient. This greatly simplifies the calculation of the external wall temperature and has been done for reasons of convenience.

6. The floor is well insulated and the kiln is baffled so that the air flow across the floor is effectively zero. This assumption means that the conduction of heat through the floor of the kiln will be negligible compared to the heat loss through the walls and the roof and so the second term in Equation (6.63) can be ignored.

Kiln Dimensions

The kiln dimensions used in the calculation of heat loss are based on the dimensions of the John Fogarty Ltd test kiln in Invercargill, New Zealand. This kiln is 7m long by 4m wide with the half circle roof 7m high at the centre and 5m high at the sides. This gives a footprint of 28m^2 and a roof area of 44m^2. The two sides are 35m^2 and the ends 26 m^2. This gives a total external surface area exposed to the ambient air of 166m^2. The roof, sides and ends form three distinct surfaces for external heat transfer to the ambient air and therefore the heat transfer from each of these surfaces is calculated separately.

Solving for the Heat Loss

The heat losses for different conditions (T_S, u) were solved iteratively by first guessing the internal wall temperature, T_{Wi} as T_S-5 and the external wall temperature T_{We} as T_A+10. The following equations were then repeated until the difference between the heat losses returned was negligible:

$$Q_{loss} = \frac{T_S - T_A}{1/h_i A_e + \Delta x_w / k_w A_e + 1/(h_e + h_r) A_e} \qquad 6.64$$

$$T_{Wi} = T_S - \frac{Q_{loss}}{h_i A_e} \qquad 6.65$$

$$T_{We} = T_{Wi} - \frac{\Delta x_w Q_{loss}}{k_w A_e} \qquad 6.66$$

The heat transfer coefficients h_e and h_r were recalculated on every iteration due to their dependence on the external wall temperature. Details of how the heat transfer coefficients were derived are given in the appendices.

The results from the heat loss calculations are plotted in Figure 89 for a temperature range from 1m/s to 10m/s and a temperature range from 45°C to 75°C. The plot shows that the heat loss is greatest when the

temperature is high and the airspeed is high. This is to be expected as the high speed means the internal heat transfer coefficient will be higher and the high temperature means there is a greater temperature difference driving the heat transfer.

Simulation results for the same schedules as Table 24 but with the calculated heat loss included are shown in Table 25. The results are similar but the addition of heat loss has a slightly greater impact on the efficiency of the low temperature schedules, due to the longer drying times. Overall however the impact of heat loss is small compared to the impact of the kiln configuration and the kiln schedule.

Table 25. Kiln efficiency for various schedules based on ideal heat demand with heat losses included.

Schedule	50/45	50/40	60/55	60/50	60/45	70/65	70/60	70/55
Drying Time, h	212	158	173	107	94	143	80	61
Configuration 1	1.71	1.71	1.83	1.77	1.76	2.07	1.92	1.84
Configuration 2	1.70	1.68	1.82	1.75	1.73	2.06	1.91	1.82
Configuration 3	1.47	1.43	1.61	1.52	1.48	1.87	1.70	1.60
Configuration 4	1.71	1.79	1.82	1.76	1.79	2.06	1.90	1.82

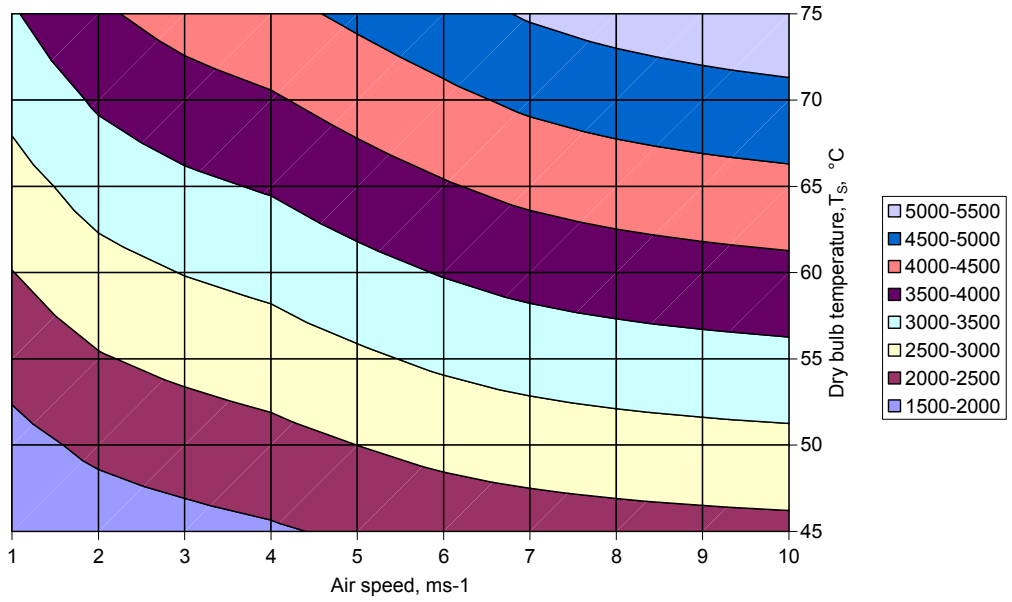

Figure 89. Surface plot showing the calculated heat loss from a kiln in W for velocity range from 1-10 ms-1 and a temperature range from 45-75°C. This graph applies to a kiln of the specific dimensions mentioned in the text.

Heat Recovery and the Vent-less Kiln

The clear advantages of kiln configurations 3 and 4 suggest that a configuration combining features of both may achieve the best energy efficiency overall. Such a configuration is shown below in Figure 90. In this case the recycle ratio will be the same as Equation (6.57).

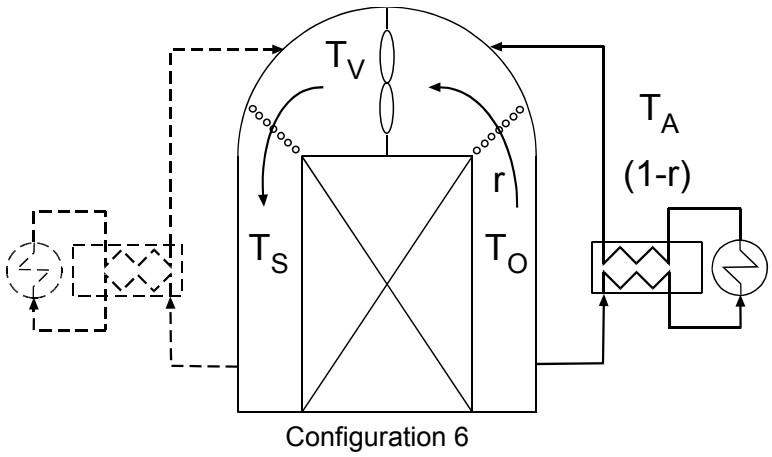

Figure 90: Configuration 6, a combination of configuration 3 and 4.

The heat balance is given by the following equation:

$$Q_s = \tfrac{1}{2}\left[\left(C_{PYS}T_S - C_{PYO}T_O\right) + \left(C_{PYS}T_S - C_{PYA}T_A\right) - r\left(C_{PYO}T_O - C_{PYA}T_A\right)\right] \qquad 6.67$$

This configuration is compared to configurations 3 and 4 in Table 26. It is an improvement on configuration 4 and at high temperatures is slightly more efficient than configuration 3. It does however retain the advantage of being vent-less, which gives it an advantage over configuration 3.

Table 26. Simulation results for configuration 6 compared to configurations 3 and 4.

Schedule	50/45	50/40	60/55	60/50	60/45	70/65	70/60	70/55
Drying Time, h	212	158	173	107	94	143	80	61
Configuration 3	1.47	1.43	1.61	1.52	1.48	1.87	1.70	1.60
Configuration 4	1.71	1.79	1.82	1.76	1.79	2.06	1.90	1.82
Configuration 6	1.48	1.48	1.61	1.53	1.50	1.86	1.70	1.59

Fan Energy

The final energy cost that will be investigated in this project is the fan energy used during kiln operation. This is the energy used to circulate air through the kiln and in particular through the stack of timber being dried. The energy used by the fan is usually more expensive than the energy used to provide heating as it must be electrical energy.

The pressure drop across the stack can be calculated using Bernoulli's equation:

$$\Delta p_s = \left(K_c + \frac{4fw_s}{D_H} + K_e\right)\rho_G \frac{u_f^2}{2} \qquad 6.68$$

Where K_c and K_e are the head loss due to contraction into the fillet space and expansion out of the fillet space, f is the friction factor and D_H is the hydraulic diameter of the fillet space. Nijdam (1998) used K_c=0.4 and K_e=1 for calculating the head losses associated with expansion and contraction. The friction factor is taken as 0.02 based on the work of Langrish et.al. (1996).

There is also a pressure drop associated with the head space and plenum space of the kiln itself. This is calculated as two components with the first component accounting for frictional duct losses and losses from contractions, expansions and bends. The second component accounts for the pressure loss from the air passing through the heat exchanger. The pressure drop in the plenum spaces was calculated using the following equation:

$$\Delta p_p = \left(2K_b + \frac{4fl_p}{D_{Hp}} \right) \rho_G \frac{u_p^2}{2} \qquad 6.69$$

Where K_b is the head loss due to the bend in the plenum and has a value of 1.5, f is the friction factor which was 0.005 in this case, l_p is the swept length of the plenum spaces, D_{Hp} is the hydraulic diameter of the plenum space and u_p is the velocity in the plenum space. The pressure drop in the head space was similarly calculated from the following equation:

$$\Delta p_h = \left(2K_b + K_{fc} + K_{fe} + \frac{4fl_r}{D_{Hr}} \right) \rho_G \frac{u_r^2}{2} \qquad 6.70$$

Where K_{fc} and K_{fe} are the head losses due to contraction and expansion through the fan which are 0.4 and 0.7 respectively. The pressure drop in the heat exchanger was determined by first sizing the exchanger based on the heat transfer requirements of the schedules (taken as double the average heat demand). This was done using basic heat exchanger design equations (Coulson et al., 1989) using a heat transfer coefficient of 400 W/m^{2}K and hot water at 130°C for heating. The result is a heat exchanger with nineteen 19mm tubes perpendicular to the flow and 6-7 rows in the direction of flow. The pressure drops in the tube banks were determined using the following approximation from Perry et al. (1984):

$$\Delta p_t = 0.32 N_r \rho_G \frac{u_t^2}{2} \qquad 6.71$$

Where N_r is the number of rows of tubes in the direction of flow and u_t is the fastest velocity of the air passing through the tube bank.

The energy used by the fan to generate the required pressure drop at the required flow is given by the shaft power equation:

$$P_{shaft} = \frac{(\Delta p_s + \Delta p_p + \Delta p_h + \Delta p_t) Q}{\eta_{fan}} \qquad 6.72$$

Where η_{fan} is the fan efficiency, which is assumed to be 0.5 for the purposes of modelling. For a real fan the efficiency varies with the pressure differential across the fan and the volumetric flow through the fan (Q). The volumetric flow through the fan is given by either:

$$Q = h_s l_s u_f \varepsilon (1 + v) \qquad 6.73$$

where the configuration of the kiln uses venting to adjust humidity, or:

$$Q = h_s l_s u_f \varepsilon \qquad 6.74$$

where the humidity is controlled without venting. Clearly from these equations the kiln configurations that use venting for humidity adjustment will require more fan energy than those not to produce the same velocity in the fillet space.

The simulation of the kiln energy requirements show that the configuration of the kiln, in particular the method by which the humidity in the kiln is controlled has the greatest affect on how much energy the kiln uses to dry the wood. The heat loss from the kiln, based on the simple heat transfer equations used here, is small in comparison to the ideal heat demand or the fan energy requirements.

Colour Model

The colour model is based on the colour change rate equation developed in Chapter 5. The first assumption made in using this equation is that the concentration of sap constituents at the surface has an insignificant effect on the overall development of colour. The second assumption is that the temperature at the surface is the same as the wet-bulb temperature while there is capillary flow in the wood and is the same as the dry bulb temperature when capillary flow has ceased. On incorporation of the colour change model into the kiln stack drying model, the third assumption is that the transition between capillary flow and vapour flow occurs at Φ=0.4. This final assumption is made as this is the point where there is a transition in the drying properties of the wood that is most likely associated with a change in the dominant moisture transport mechanism.

Based on the assumptions outlined in the previous paragraph the colour model takes the following form:

$$\begin{aligned} \Phi \geq 0.4 &: \Delta E = f_{\Delta E}\left(T_{GW}\right) \cdot \Delta t \\ \Phi \leq 0.4 &: \Delta E = f_{\Delta E}\left(T_{GD}\right) \cdot \Delta t \end{aligned} \qquad 6.75$$

Where:

$$f_{\Delta E}\left(T\right) = a_4 T^4 + a_3 T^3 + a_2 T^2 + a_1 T + C \qquad 6.76$$

The coefficients for this equation are the same as those derived in Chapter 5. In this form the model gives the colour change for a time interval Δt. The overall colour change for the schedule simulated is the sum of colour changes for all of the time intervals. Colour development during the reconditioning stage was not included as this was not included in the drying simulation. There is however likely to be some colour change that occurs during this stage.

The colour development simulated in this way is higher than the colour measured in the drying studies of Chapter 4. This is probably due to the experimental method used to measure the in-wood colour development in Chapter 5 accentuated the level of colour development. This may be due to the smoother surface resulting in a more uniform and concentrated kiln brown stain layer. Regardless of the cause the

relative magnitude of colour development is in good agreement and it will be assumed that ΔE of 15 or less is an acceptable level of colour development.

Economic Model

The economic model developed for these simulations was relatively simple and applied to the simulation data after the simulation had been run rather than being calculated during the simulation. The first assumption made in these calculations is that the capital cost of the kiln is the same regardless of the schedule used. Given the limited temperature range that the simulation is run over this is a reasonable assumption as none of the instrumentation or other components would need to be upgraded to withstand the temperature. The base capital cost was assumed to be $350,000 with the cost adjust slightly for airspeed by adding a fan cost of $102/kW based on the fan energy requirements. This fan cost was determined from the IChemE guide to capital cost estimation corrected for currency and inflation (George, 1988).

The total cost of capital was calculated based on an interest rate of 10% and even payments for the life of the kiln. This resulted in a total cost of capital between $700,000 and $750,000. The capital cost component of each run was determined from the cost of capital component, *coc*, the drying time (including 1hr loading and 4hr reconditioning), t_{dry}, and the operational time, t_{Op}, using the following equation:

$$Cost_{Capital} = \frac{t_{Op}}{t_{dry}} coc \qquad 6.77$$

The data used for the economic model is shown in Table 27. The process heat and electrical energy costs were obtained from the Ministry for Economic Development website.

The running costs components for the schedules were calculated using the following equation:

$$Cost_{Running} = P_{Shaft} t_{dry} EE_{\$} + (Q_S + Q_{Loss}) PH_{\$} \qquad 6.78$$

In which $EE_{\$}$ is the cost of electrical energy in $/GJ and $PH_{\$}$ is the cost of process heat in $/GJ.

The sum of the capital cost component and running costs component gives the total drying costs for the schedule kiln configuration combination. This can be divided by the volume of wood in each run (40m3) to get the cost per m^3 of wood dried.

Table 27. Data used for the economic analysis of simulated schedules.

Capital Cost	$350,000 + fan cost
Residual Value	5%
Lifetime	20 years
Electrical Energy Cost ($EE_{\$}$)	$22/GJ
Process Heat Cost ($PH_{\$}$)	$5/GJ
Operational Time (t_{Op})	8400 h/year

The economic model is useful to quantify the costs for various drying schedules in order to produce different quality of timber. However, if the model is used to quantify the return on investment for the kiln, more data us needed such as labour costs for example. In determining the cost effectiveness of compression rolling for reducing kiln brown stain Horgan *et al.* (1997) stated that clear wood is worth \$50/m^3 more when dried than it is when green as long as it is not degraded by kiln brown stain. An industry source did suggest that light coloured wood attracted a premium of \$20-50 per m^3 (Brightwood, 2003) in addition to the premium for just being dried and Horgan (1999) estimated the downgrade from sapstain to be \$20 to \$100 per m^3, so values of \$50, \$70 and \$100 per m^3 were chosen as the total premium for drying the wood. These values correspond to a colour premium of \$0, \$20 and \$50 respectively. The total drying costs were subtracted from these premiums and the result multiplied by the number of runs per year to get an idea of the total monetary gain from the schedule.

A variable premium was also determined based on the idea that a lighter coloured wood will attract a higher premium. The equation used is as follows:

$$premium = \frac{50}{15}(15 - \Delta E) + 50 \qquad 6.79$$

In this equation the slope determines the colour premium and the intercept is the fixed drying premium of \$50. The range of the variable premium is therefore \$50 to \$100.

Simulation Results and Discussion

The simulation data from the integrated model has shown the difference between a number of schedules and six kiln configurations. This discussion will first address the differences between the schedules based on kiln configuration 2 which is the standard configuration for a modern kiln in New Zealand. The differences between the configurations, which have been touched on in the previous section, will then be analysed in more detail.

Drying Schedules

The results from the simulations were analysed based on a number of criteria to determine which schedules produced the best results. The first criterion of interest was the colour development because this is considered the most important quality parameter for appearance grade timber. Under this criterion any schedule producing a maximum final colour change greater than 15 was rejected. The graph in Figure 91 shows the colour development results for some of the schedules simulated with a dry bulb temperature of 70°C. The schedules that meet the first criterion are marked with black bars while those that failed to meet the criterion are marked with white bars.

The schedules that meet the first criterion are clearly the faster low humidity schedules with short drying times. Low temperature schedules also performed well under this criterion. This fits with the conclusions from the drying studies in Chapter 4.

The second criterion used to eliminate schedules was the variation in final moisture content within the stack. For this criterion a variation of 20% of the final moisture content (0.1kg/kg) was considered acceptable calculated using the following equation:

$$Var_{MC} = \frac{MC_{\max} - MC_{\min}}{MC_{mean}} \qquad 6.80$$

It is possible to reduce the variation of moisture content in the stack through the use of a high humidity conditioning step at the end of drying. This is however undesirable as it will generally be at a high temperature, such as steam conditioning, and this will increase the development of colour in the wood.

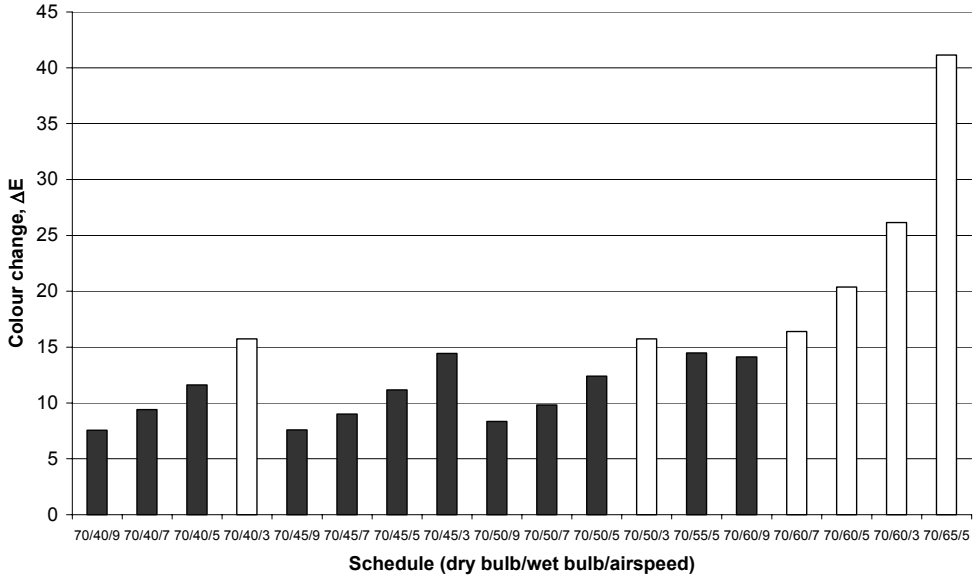

Figure 91. Colour change for various simulated schedules with a dry bulb temperature of 70°C. The black bars represent schedules passing the colour development criteria and white bars failed. The numbers of each schedule mean: dry-bulb/wet-bulb/air velocity (m/s).

The second criterion eliminated all but two of the remaining 70°C schedules as the low humidity and rapid drying in these schedules resulted in a large range of final moisture contents. There were however a number of lower temperature schedule that passed under both criteria. A wider range of schedules that passed both of the criteria are listed in Table 28 and also plotted in Figure 92. The table shows that for the two 70°C schedules that passed both criteria the high airspeed seems to be a significant factor. For Schedule A the high speed probably helps reduce moisture content variation by minimising the reduction in drying potential as the air passed through the stack. For Schedule B the higher air speed would have reduced the drying time and therefore reduced the level of colour development.

The schedules that met the two criteria for quality show that there are a number of requirements for a schedule if it is to produce quality wood. Firstly and most obviously the temperature of the schedule must be fairly low as by far the majority of the schedules that passed were below 70°C. This will be due to the large increase in the colour development rate between 65°C and 70°C. Secondly the lower humidity

schedules are more effective for reducing colour development but if the relative humidity is too low the final moisture content variation will be unacceptable. For similar reasons the higher airspeeds are more effective as well.

The usefulness of the schedules simulated can also be measured in terms of their energy efficiency which has been expressed as a total schedule cost based on the energy required to dry a standard load of timber. This cost is plotted in Figure 93 for the 17 schedules passing the quality criteria. Schedule C clearly performs the best in this test with schedules I, J, and A also performing well. These are all low relative humidity schedules and, with the exception of schedule A, lower speed as well. The lower temperature schedules generally have the highest cost associated with them.

Table 28. Simulated schedules that passed criterion one (colour development) and criterion two (final moisture content variation)

	Dry Bulb Temperature, °C	Wet Bulb Temperature, °C	Air Speed, m/s	Drying Time, h
Schedule A	70	50	9	35
Schedule B	70	60	9	54
Schedule C	65	50	5	74
Schedule D	65	55	5	92
Schedule E	60	50	9	71
Schedule F	60	50	7	85
Schedule G	60	50	5	107
Schedule H	60	50	3	145
Schedule I	60	45	3	129
Schedule J	60	45	5	95
Schedule K	60	45	7	75
Schedule L	60	45	9	62
Schedule M	50	45	5	212
Schedule N	50	40	7	125
Schedule O	50	40	9	104
Schedule P	50	40	5	159
Schedule Q	50	40	3	218

The reason that schedules with lower air speeds cost less to run is due to the fact that the increased air speed requires more energy to the fan to move the greater volume of air. A quick look at Equations (6.68) and (6.69) shows that the shaft power increases with the cube of the fillet velocity so small increases in air speed will result in much greater increases in fan energy requirements. This increase is off set by the shorter drying time resulting from the increased airspeed but the effect on energy cost is still noticeable as can be seen in Figure 94. In this figure the drying time and fan energy costs have been plotted with airspeed for the four 60/45 schedules simulated. The fan energy costs clearly increase more than linearly with increased speed but not to the cube of the airspeed.

Another way of analysing the costs of the schedules is to break the total schedule cost down into its components; the process heat cost, the fan energy cost and the cost of depreciation. This breakdown is shown for four of the simulated schedules in Figure 95. The process heat costs are the most stable

contribution to the total costs and are similar for the four schedules. The process heat cost appears to decrease with decreasing temperature and humidity. The capital cost and electricity cost contributions are more variable with higher contributions relating to longer drying times.

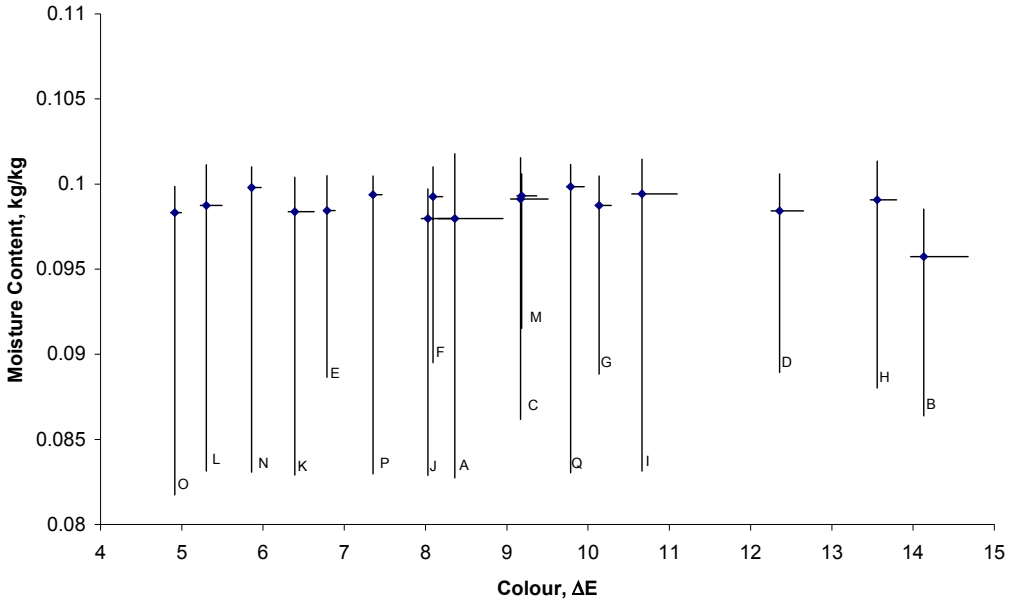

Figure 92. Moisture content and colour changes for the simulated schedules that passed the two selection criteria. The points are the mean values and the bars show the range.

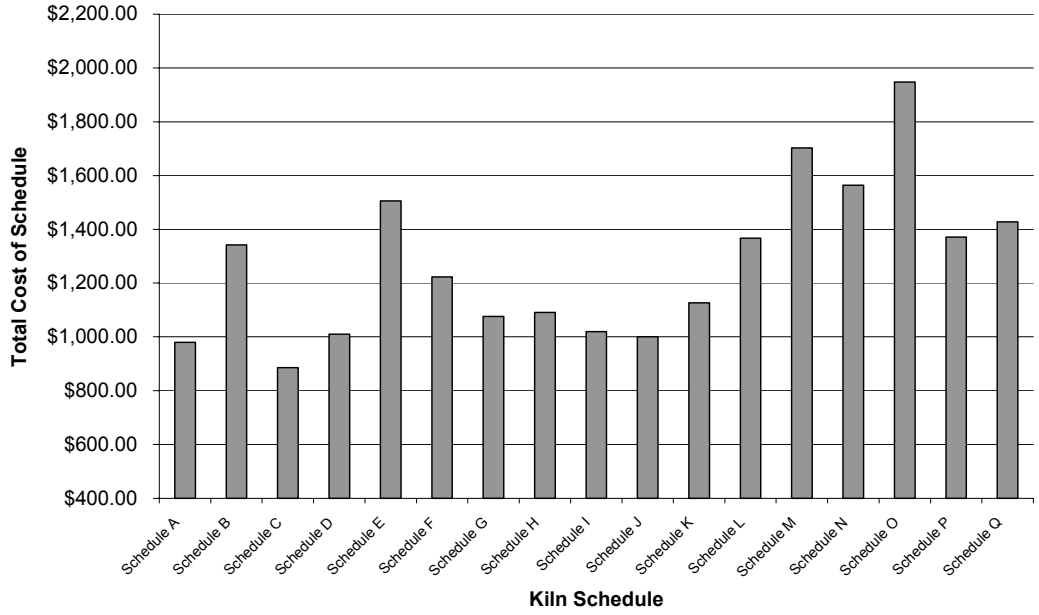

Figure 93. Total cost of simulated schedules run on kiln configuration 2 made up from running costs and cost of capital. The total cost of schedule is for a single drying run with a 40m^3 stack.

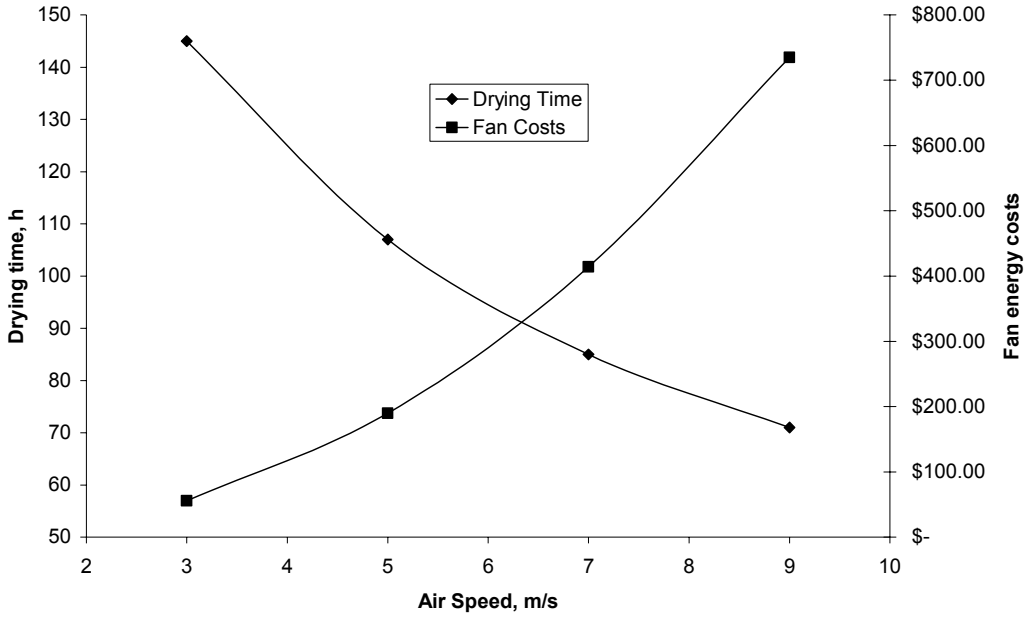

Figure 94. Comparison of drying times and total fan energy costs for the four 60/45 schedules simulated (I-L).

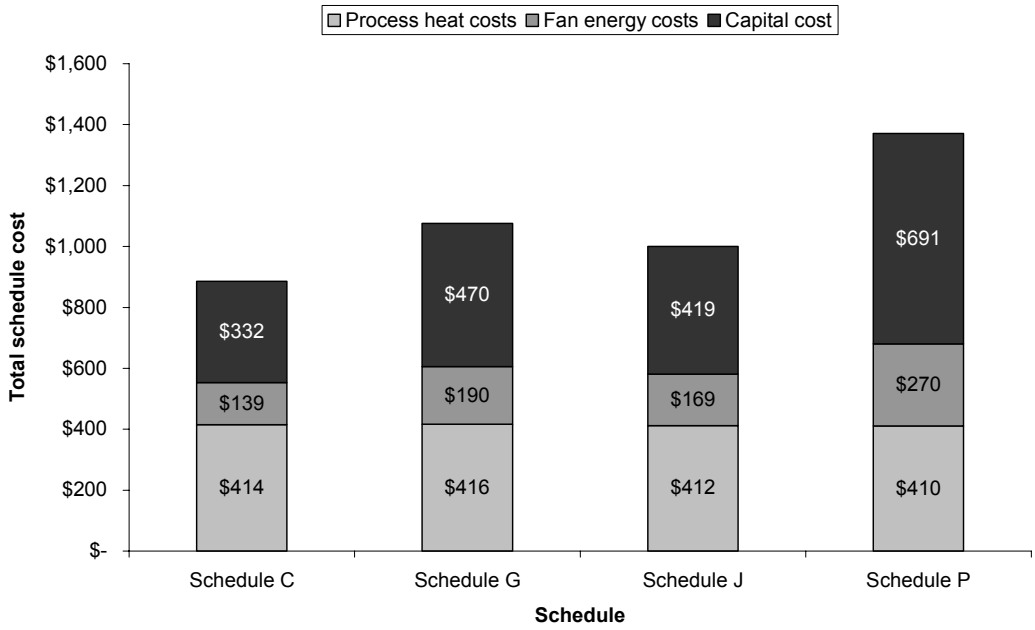

Figure 95. Contribution of different costs to the total schedule cost, per kiln charge (40m^3) for four schedules with an airspeed of 5m/s. The schedules presented are respectively: 65/50 (C), 60/50 (G), 60/45 (J), 50/40 (P). These costs are based on kiln configuration 2.

The capital costs are higher for the lower temperature and higher humidity schedules. This is because the capital cost is directly related to the drying time which is longer for these types of schedules. Longer

drying times mean that fewer loads of timber can be dried over the lifetime of the kiln so the capital cost per load is higher.

The differences in the costs associated with the fan energy requirements are also directly related to the drying time for the four schedules shown as the airspeed is the same in all cases. This is because the fan runs for a longer time in the low temperature schedules and therefore uses more energy. For all four schedules the cost of depreciation is more significant than the cost of electricity for the fan.

The contribution of cost to the total schedule cost can also be plotted for the same temperature conditions but different airspeeds, as shown in Figure 96. The schedules plotted here are the same as those in Figure 94. This analysis shows that the total schedule cost is increased by the increased in air speed. This is due to the costs from process heat and electricity increasing as the fan speed increases. The cost of capital decreases with increasing air speed due to the shorter drying times. This means the total schedule cost at 5m/s is actually less than at 3m/s but this decrease is not large enough to counter the increase in the other two contributors at higher airspeeds.

It has already been explained why the cost of electricity increases with fan speed but it is less obvious why the process heat costs increase. This increase is caused by the higher volumetric flow of air in the kiln meaning that a greater volume of air is vented per unit time and so the losses associated with venting are increased. There is a slight reduction in the process heat required to recover heat losses through the kiln walls due to the shorter drying times but this is less than the increase from venting losses.

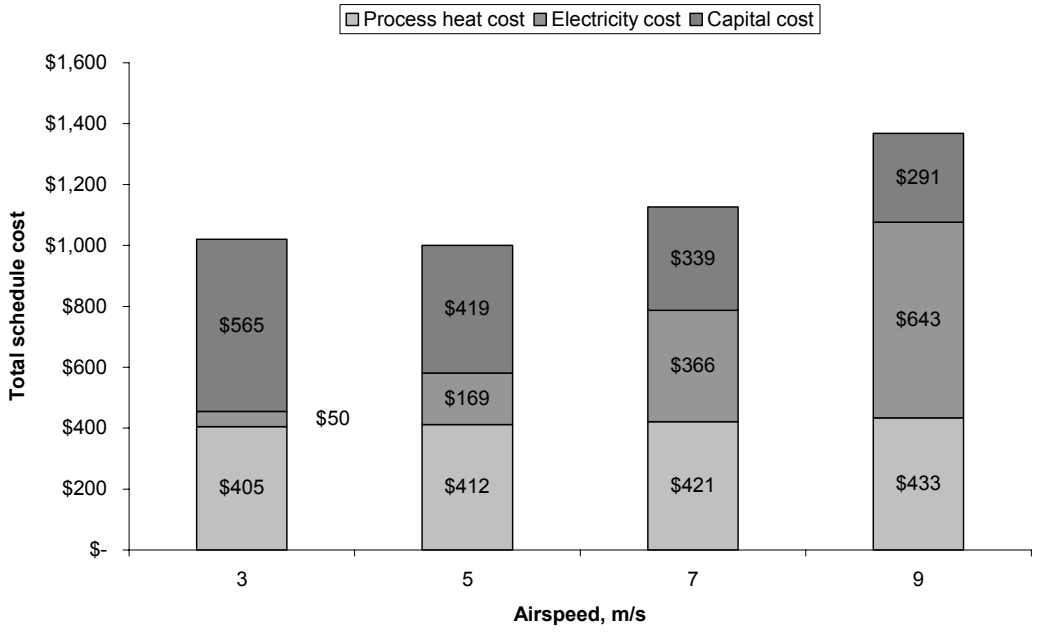

Figure 96. Contributions of different costs to the total schedule cost for the four 60/45 schedules. These costs are based on kiln configuration 2.

The graph in Figure 97 shows the profitability for each schedule based on colour premiums of \$0/m^3, \$20/m^3, \$50/m^3 and a variable premium being paid for the better quality dried wood. The total cost of

each schedule has been subtracted from the premium to account for the variable costs of the schedules. All of the schedules are profitable though some are barely profitable when there is no premium for colour. At higher premiums the drying process becomes more profitable to varying degrees depending on the schedule. When the variable premium is used it has a significant effect on the profitability of the schedules, with lower temperature schedules being favoured due to the lower colour development.

The increase in annual profit from the drying operation for one kiln using a variable premium is shown in Figure 98. The two main factors influencing the profit are the drying time as this determines how much wood can be dried in a year and the colour change which determines the premium. The former favours the higher temperature, low relative humidity schedules while the latter tends to favour the lower temperature schedules.

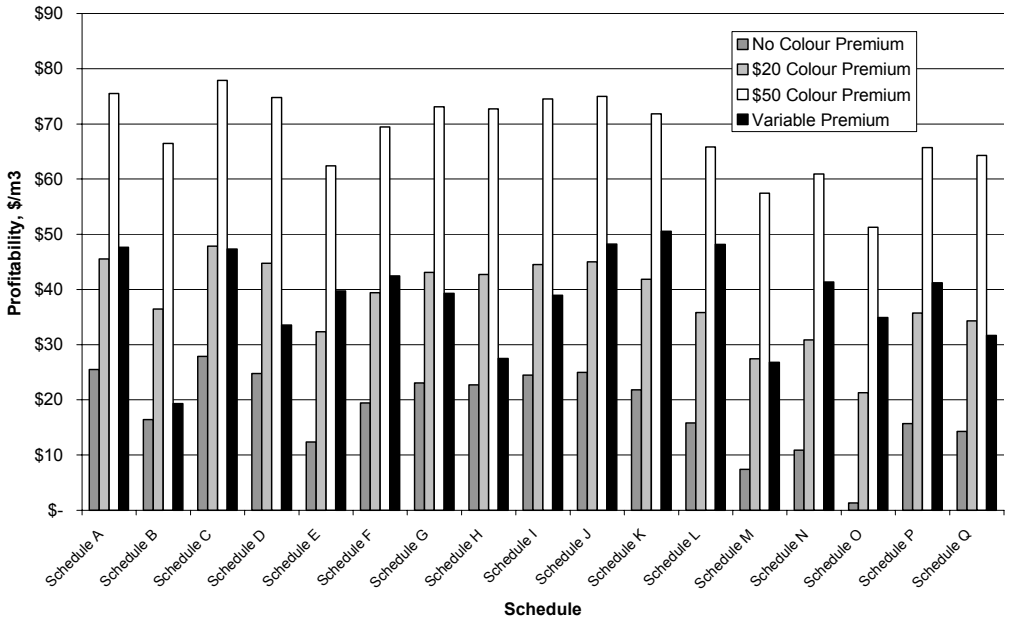

Figure 97. Profitability of colour limiting schedules, based on various premiums being paid for light coloured wood.

The increased profit figures also assume that there is sufficient supply of timber to run the kiln continuously. If the supply of wood for drying is in fact limited so that there is not sufficient supply to run schedule A continuously then other schedules such as schedule L would be more profitable due to the higher premium.

The schedules tested all performed differently depending on the criteria being used to evaluate them. Overall the best colour quality came from the lower temperature schedules (50-60°C dry bulb temperature). Specifically schedules O (50/40, 9m/s), L (60/45, 9m/s), N (50/40, 7m/s), K (60/45, 7m/s) and E (60/50, 9m/s) produce a very light colour with only a small variation in colour through the stack. As well as having a low temperature these schedule also have a high airspeed which shortens the drying time so that there is less time for the colour reaction to occur.

The narrowest moisture content ranges were from the schedules with a moderate to high humidity across the range of temperatures, specifically; schedules E, F, M, G, D and B. The airspeed in these schedules varies but there is a slight trend towards the higher speeds. The variation in final moisture content distribution is caused by the boards at the edges of the stack drying more quickly than the boards in the middle of the stack. This occurs because the drying potential of the air passing through the stack decreases as it picks up moisture from the drying boards. This means that the drying rate will be greatest at the stack inlet and lowest at the outlet. The reversal of the airflow direction means that on average the drying rate is lowest near the centre of the stack. This effect is made worse by low humidity schedules as the drying rate at the edges of the stack is much higher and the drying rate remains relatively high even when these edge boards are at low moisture contents. The lower airspeeds also make the problem worse due to the lower volume of air flowing through the stack meaning the drying potential of the air reduces more rapidly with distance from the inlet side of the stack.

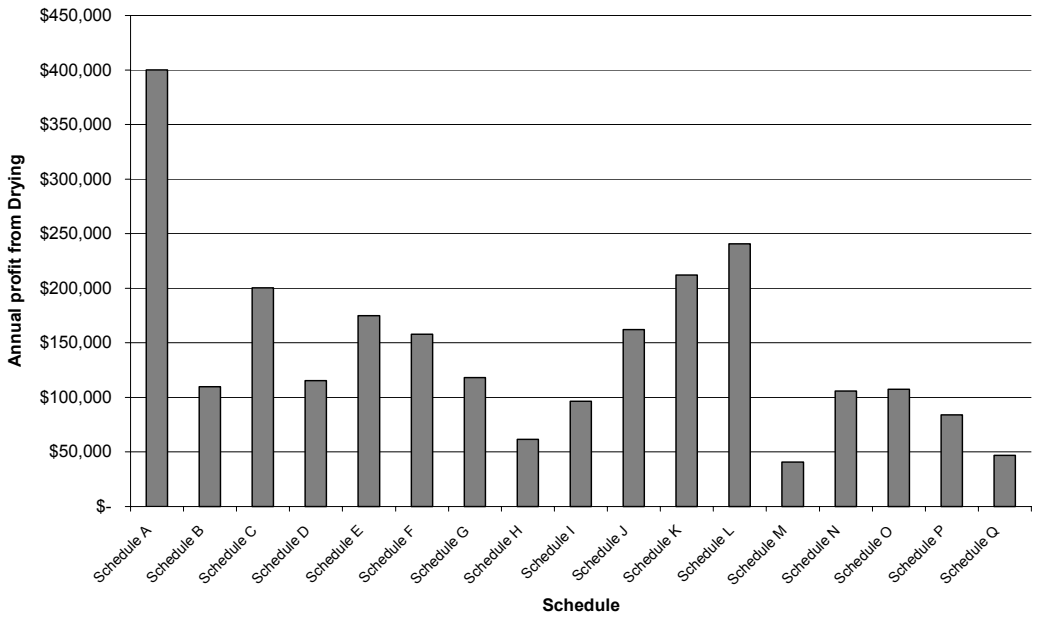

Figure 98. Annual profit increase for various schedules based on a variable premium and kiln configuration 2.

The schedules with the lowest total schedule cost were either at the higher temperature and low humidity (schedules A, C and D) or moderate temperatures with slow air speeds and low humidity (schedules G, H, I and J). With the lower humidity and higher temperatures influence the total schedule cost by reducing the drying time which reduces the electricity and depreciation costs. With the lower temperature schedules the low fan speed reduces the contribution of electricity costs to the total schedule cost.

The measure of increased profitability clearly favours the faster schedules; A, C, K and L. This is simply because more wood can be processed using these schedules

With the schedules performing so differently over the range of analyses it is difficult to select one as being the ideal schedule. The low temperature schedules, with dry-bulb temperatures below 60°C, can be eliminated as they do not produce significantly better quality to justify the greater expense of the schedules and lower overall profitability. If the colour development criteria is tightened to a maximum of $\Delta E=10$ then a few more of the schedules are eliminated. If it is also determined that the annual profit from drying must be greater than $200,000 then only four schedules are left. These schedules are shown in Table 29 in order of profitability.

Schedule A appears to be the best choice of schedule for the production of high quality timber with schedule K being the second best due to the better colour. Schedule C was the only 65/50°C schedule originally tested and further simulations have shown that increasing the airspeed to 7 m/s gives better colour (7.43) and a better moisture content range (8.7-9.9) with profit of $255,902.

Table 29. The best of the schedules simulated.

Schedule	DBT, °C	WBT, °C	Airspeed, m/s	Profit per annum	ΔE	MC Range, kg/kg
A	70	50	9	$400,267	8.36	8.3-10.1
L	60	45	9	$240,683	5.30	8.3-10.1
K	60	45	7	$212,265	6.39	8.3-10.0
C	65	50	5	$200,536	9.17	8.6-10.2

Kiln Configuration

There were six kiln configurations tested in the simulation studies covering standard heat-vent kiln configurations as well as new configurations incorporating heat recovery and humidity control by condensation. The details of the configurations have been described previously in this chapter.

Configuration 1 and 2 Comparison

The first comparison will focus on the first two configurations as these are representative of the status quo in the New Zealand timber industry. Configuration 1 reflects the older style kilns while more modern kilns usually have two heating coils as in configuration 2. The schedules are compared by subtracting the profitability of configuration 2 from configuration 1 as the latter is always higher. The change in this difference with respect to dry-bulb temperature, wet-bulb depression and airspeed is shown in Figure 99.

The comparison of the configurations shows that the difference in total schedule cost increases as the wet bulb depression increases. This means that the efficiency advantage of configuration 2 is greater for low humidity schedules. This is due to the fact that at the lower humidity, more heated air is vented and thus more heat is lost from vents than at high humidity in configuration 1 kilns.

The difference in profitability also increases as the airspeed is reduced, so configuration 2 performs much better at slow airspeeds while fast airspeeds reduce the difference between the two configurations. This is due to two effects, the first being that the higher speed reduces drying time which means the extra losses from configuration 1 are over a shorter time and so the cumulative loss is less. The second effect is that the greater flow through the stack means the increase in humidity is lower so less venting is required.

The graph also shows that there is an increase in the cost difference as the dry-bulb temperature of the schedule is reduced, which will be partially affected by the reduction in humidity with decreasing temperature at the fixed wet-bulb depression. This effect due to the lower moisture carrying capacity of the lower temperature air meaning that more venting is required to maintain low temperature schedules.

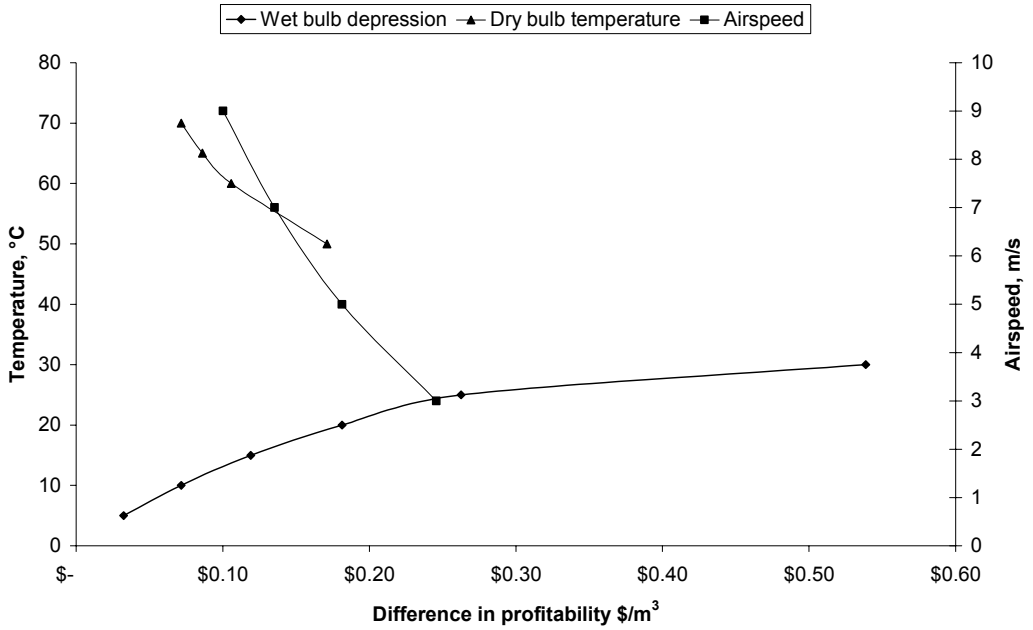

Figure 99. The effects of dry-bulb temperature (with a web-bulb depression of 10°C), wet-bulb depression (for drying-bulb temperature of 70°C and 5m/s) and airspeed (for 70/50°C schedule) on the difference between the total schedule cost of kiln configurations 1 and 2.

Configuration 2 and 3 Comparison

Kiln configuration 3 is compared with kiln configuration 2 in Figure 100 to highlight the benefits of including heat recovery in the venting system. In this case to calculate the difference in profitability the total cost of kiln configuration 3 was subtracted from the total cost for kiln configuration 2, which is higher for all of the schedules. It is obvious that there is a much more significant difference between the profitabilities for these two configurations than there was between configurations 1 and 2.

The difference between the two configurations increases with decreasing humidity (increasing wet-bulb depression) and also with decreasing dry-bulb temperature. There is a slight change associated with airspeed. The effects of temperature and humidity are due to the increased venting requirements noted in the previous comparison of configuration 1 and 2. The heat recovery occurs on the vented air streams so with schedules where venting is more significant then the heat recovery will also be more significant. Regardless of schedule the third configuration has considerable cost savings (7-16%) compared to the first two configurations.

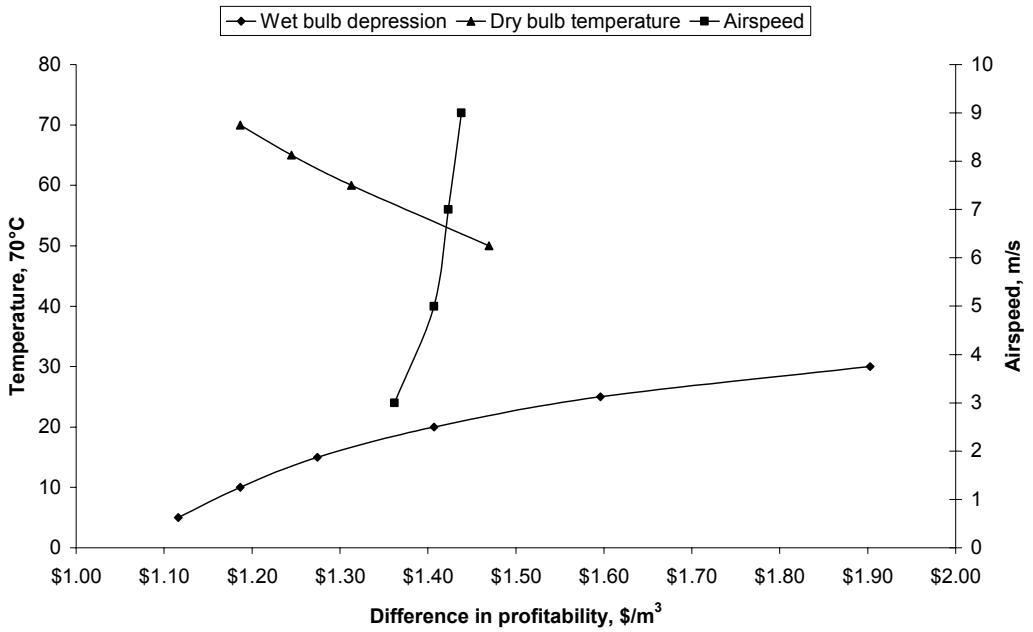

Figure 100. The effects of dry-bulb temperature (with a web-bulb depression of 10°C), wet-bulb depression (for drying-bulb temperature of 70°C and 5m/s) and airspeed (for 70/50°C schedule) on the difference between the total schedule cost of kiln configurations 2 and 3

Configuration 2 and 4 Comparison

Kiln configuration 4 is compared with configuration 2 in Figure 101 to contrast the two different humidity control methods. In this comparison the profitability of configuration 4 was subtracted from that for configuration 2, so where the difference is negative the profitability of configuration 4 was greater than configuration 2.

Kiln configuration 4 clearly performs poorly at low temperatures and low humidity (high wet-bulb depression) when compared to configuration 2 but performs slightly better at higher temperatures and higher humidity (low wet-bulb depression). This is due to the higher sensible heat loss from configuration 4 when the humidity is low. This comes about because the temperature in the condenser is above ambient and the air is saturated so more air has to be bypassed than is vented in configuration 2.

Further comparison of the venting and bypass is shown for two schedules in Figure 102 where the bypass ratio is defined as 1-r. Clearly this diagram shows that the venting and bypass ratios are much higher for the lower humidity schedule over the course of drying. The difference between the two ratios is also much greater for the lower humidity schedule. In both of the schedules the bypass ratio is always greater than the venting ratio because in configuration 4, the air humidity is always high than the ambient air thus higher proportion of humid air needs to go through the bypass condenser. However, at the higher humidity schedule (lower wet-bulb depression) the difference in the ratios between the two configurations is insignificant and the sensible heat loss from venting in configuration 2 is more significant.

From the above findings, it is concluded that configuration 4 is not an improvement over configuration 2 over the low and conventional temperature schedules to justify making the required changes to kiln

design. The benefits of changing to configuration 4 become noticeable at high temperature and high humidity (low wet-bulb depression) schedules and are apparent in controlling the kiln emissions. This does not however justify the reduced versatility of schedules that can be run over the temperature range tested but may be justified for higher temperature drying.

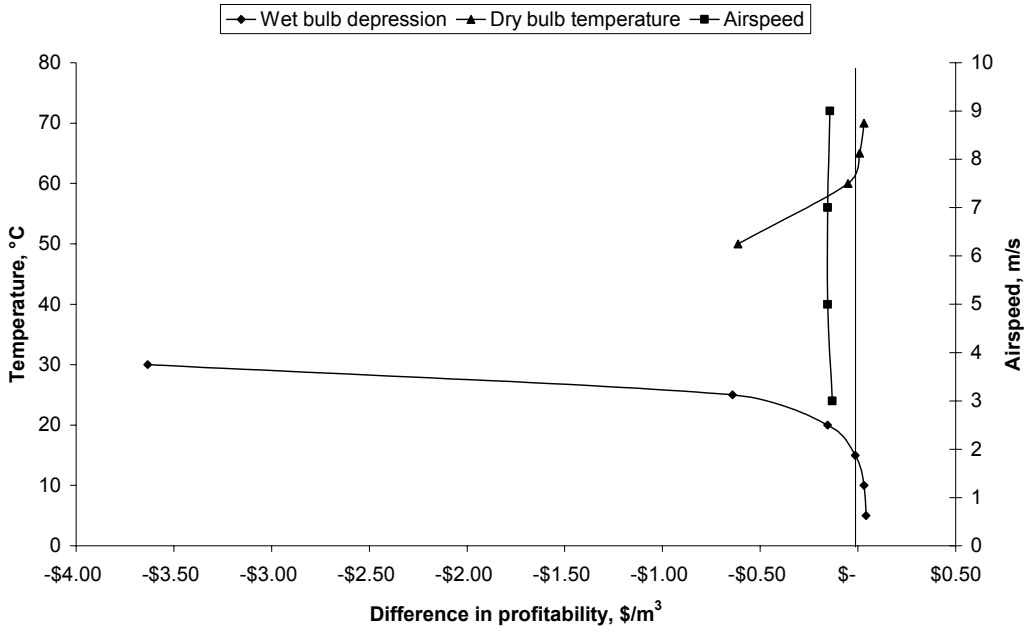

Figure 101. The effects of dry-bulb temperature (with a web-bulb depression of 10°C), wet-bulb depression (for drying-bulb temperature of 70°C and 5m/s) and airspeed (for 70/50°C schedule) on the difference between the total schedule cost of kiln configurations 2 and 4. Negative values indicate the total cost of schedule 4 was greater than that of schedule 2.

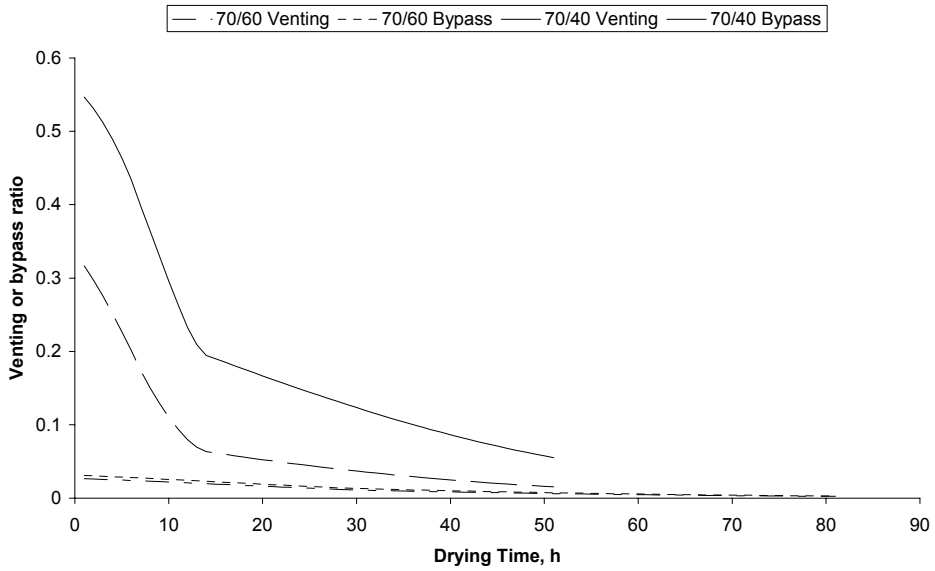

Figure 102. Comparison of venting and bypass ratios for high relative humidity (70/60°C) and low relative humidity (70/40°C) schedules.

Configuration 2 and 6 Comparison

Kiln configuration 6 was designed to incorporate the advantages of configuration 3 and configuration 4. This configuration has the energy efficiency benefits of heat recovery and the zero emissions advantage of condensation humidity control and is compared with configuration 2 in Figure 103. In this case the difference in total schedule cost is the total cost of configuration 6 subtracted from the total cost for configuration 2, which is higher for all schedules. The differences are generally smaller than those for schedule 3 but much greater than those for schedule 4.

The comparison of these two configurations shows that difference in total schedule cost actually reaches maxima with respect to wet-bulb depression and dry-bulb temperature within the ranges tested. This is due to the combination of the effects of configuration 3 and 4 which are opposite with respect to the wet-bulb depression and dry-bulb temperature.

Configuration 3 and 6 Comparison

Kiln configuration 3 and kiln configuration 6 have both performed better than the standard heat-vent kilns of configuration 2. Therefore configurations 3 and 6 are compared to determine which one is the best overall. This comparison is shown in Figure 104 where the difference in total schedule cost is the total schedule cost for schedule 6 subtracted from that of schedule 3. Negative values therefore indicate that schedule 6 is more expensive while positive values show that schedule 3 is more expensive.

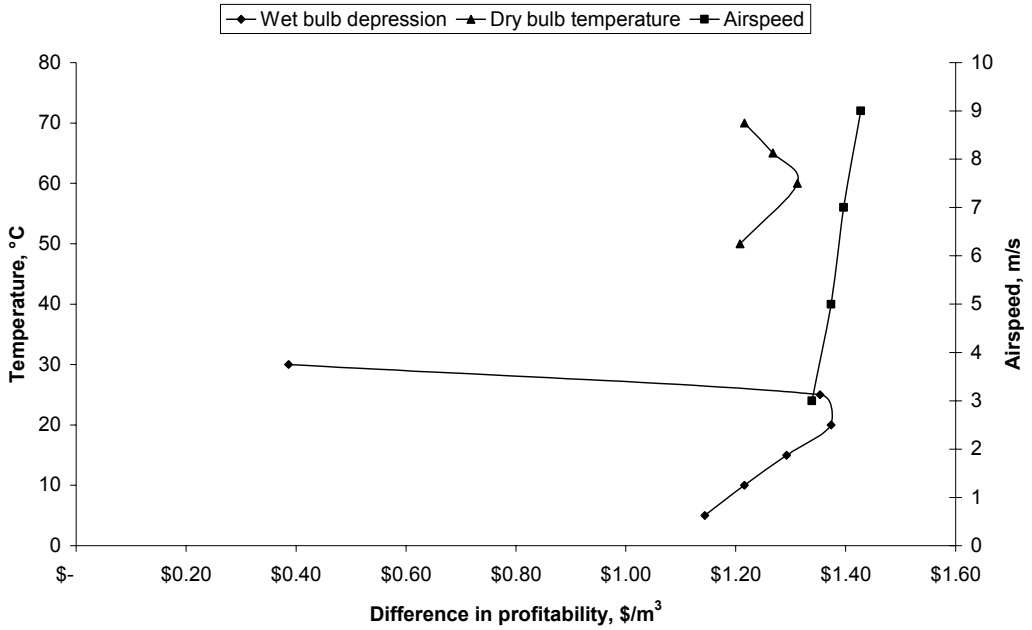

Figure 103. The effects of dry-bulb temperature (with a web-bulb depression of 10°C), wet-bulb depression (for drying-bulb temperature of 70°C and 5m/s) and airspeed (for 70/50°C schedule) on the difference between the total schedule cost of kiln configurations 2 and 6.

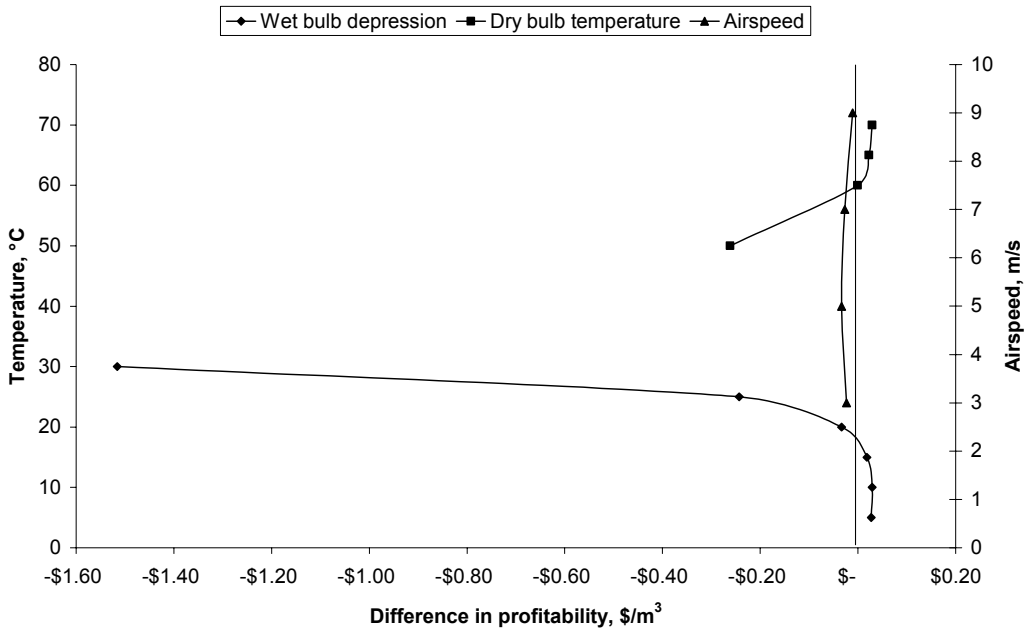

Figure 104. The effects of dry-bulb temperature (with a web-bulb depression of 10°C), wet-bulb depression (for drying-bulb temperature of 70°C and 5m/s) and airspeed (for 70/50°C schedule) on the difference between the total schedule cost of kiln configurations 3 and 6. Negative values indicate that the cost of schedule 6 was greater than that of schedule 3.

It is clear from the graph (Figure 104) that neither of the configurations is predominantly better. Configuration 3 performs significantly better at low temperature and low humidity while configuration 6 performs slightly better at higher temperature and high humidity. This means that for overall versatility configuration 3 is probably the best but for normal kiln schedules configuration 6 has a slight advantage. This configuration also has the advantage of having zero-emissions. A vent-less kiln design is being operated by John Fogarty Ltd and initial results from this kiln suggest that there is a reduction in colour change in this kiln (Fogarty, 2005). There is however insufficient evidence at present to determine the reason for the reduction.

Comparison of Configurations Running the Best Schedules

A comparison of the performance of the different kiln configurations running the best schedules for producing quality wood is shown in Table 30. The comparison is made with reference to configuration 2 and benefits are expressed by subtracting the profitability of each configuration from the profitability of configuration 2. A negative number therefore means that the configuration performed better than configuration 2.

The results show that for the best schedules configurations 1 and 4 perform worse than configuration 2 in all cases. However configurations 3 and 6 perform much better than configuration 2. The difference between the two best configurations varies depending on the schedule, though configuration 3 performs slightly better over all four schedules. The difference between the two configurations is smaller for the higher temperature schedules. Again the potential benefit of zero-emissions from configuration 6, if it

reduces regulatory compliance costs, may counter these small differences and make this the best kiln configuration. Without knowing these costs, however, configuration 3 is considered to be the best.

Table 30. A comparison of kiln configurations running the best schedules for producing high quality wood. The profitability has been subtracted from the total schedule cost for kiln configuration 2.

	Schedule A	Schedule L	Schedule K	Schedule C
Kiln Configuration 1	$0.10	$0.12	$0.15	$0.14
Kiln Configuration 3	-$2.06	-$2.63	-$2.13	-$1.59
Kiln Configuration 4	$0.19	$0.38	$0.37	$0.12
Kiln Configuration 6	-$2.01	-$1.34	-$1.33	-$1.56

Conclusions

A kiln stack drying model was developed with new characteristic drying curves being able to cover low and conventional temperature schedules. This kiln stack drying model is incorporated with a wood colour development model to simulate both the drying process and the colour changes of wood. Furthermore, an energy efficiency model and economic analysis were added to the integrated model thus the models can be employed to quantify the gains in drying quality, energy efficiency and economic benefits that can be made by altering the design of both kiln schedules and the configuration of the kilns running the schedules.

The improvement in quality comes from using schedules that minimise the development of colour and limit moisture content variation. The simulations show that schedules with a dry bulb temperature of 60-70°C and a wet bulb depression of 15-20°C are most efficient at achieving this. The temperature recommended is lower than that normally used to dry appearance grade timber in New Zealand and the wet bulb depression is also greater than is normally used with these dry bulb temperatures.

The improvement in energy efficiency comes from both the schedules and the kiln configuration. In particular the simulations show that there are significant gains to be made in energy efficiency if a heat recovery system is incorporated into the humidity control mechanism.

Chapter 7

Kiln Micro-sensors

Introduction

This chapter presents work on the development of kiln micro-sensors designed to measure the temperature and humidity conditions inside a stack of timber during drying in a commercial scale kiln. This work was undertaken to fulfil the third objective of the project: Develop micro-sensor technique for evaluating and improving kiln design, performance and control.

The Problem and Causes

The drying conditions in a stack of timber in a kiln vary with position in the stack. During drying, the hot air provides heat for evaporation of moisture in wood and carries away the moisture vapour, and thus the air temperature decreases and humidity increases along the airflow direction across the kiln stack. As a result, boards will dry at different rates throughout the stack. This causes a number of quality problems such as final moisture content variation, over-drying and discolouration. A better understanding of the causes and nature of the variation in conditions will aid in finding solutions to the drying quality issues. A better understanding of how conditions in the stack vary could also lead to energy savings if the fan speed can be reduced in the later stages of drying.

There are a number of factors that cause the drying conditions to vary within a stack of timber. The first cause is the drying process itself, which is briefly described in the above paragraph. This is an unavoidable consequence of the drying process and is well understood theoretically.

The rate of humidification of the air with distance into the stack is dependant on the rate of evaporation and the airflow. Variation in airflow through different parts of the stack will therefore result in variable drying conditions. Airflow variations can be caused by the design of the kiln, the construction of the stack or by operator error. Nijdam and Keey (2002) have shown that the dimensions of the plenum space and transition into the plenum space influence the distribution of airflow through the stack.

Variation of conditions can also be caused by hot, cold and wet spots in the kiln that result from faulty or poorly designed equipment. This sort of problem is often associated with heating coil arrangement and humidification equipment such as water baths, sprays or steam inlets.

Application of the Micro-sensors: Research or Control

There are a number of potential applications for a micro-sensor system that measures in detail the drying conditions in a stack of timber. Each of these applications will have a different set of requirements for the final design of the system. At one end of the spectrum the system could be used solely as a research tool in which case the focus would be on the accurate measurement of many points within the stack. The information may not need to be available in real time as it could be recorded and then analysed after the drying run was completed. There would also be less emphasis on integrating the system into the wood drying process as it would not be part of regular day to day operation of a kiln.

At the other end of the spectrum of applications is a sensor system designed to be used for kiln control. Such a system needs to be robust enough to handle the rigours of continuous use in an industrial environment. The system also needs to be quick and simple to install and provide continuous real time data.

Between research and control systems there are opportunities for kiln testing and auditing tools that have requirements in common with both. In this project the main focus has been on the development of research tools with some consideration for kiln testing.

Measured Variables

There are three variables that could be measured in the air space of the stack: temperature, humidity and air flow. All three determine how fast the wood will dry but the temperature and humidity indicate what the actual drying rate is. More advanced systems could include measurement of board moisture content. For this project the temperature and humidity were chosen as the variables to be measured.

Design

In this project two attempts were made to develop a kiln micro-sensor system for research purposes. In the first case the electronic design was performed by an electronics technician and in the second case by a final year electrical engineering student. This section will cover the design process for both of the prototypes developed.

Specification

The original specification for the first prototype designed was for a sensor system that could be used in a high temperature kiln operating at up to 120°C. This put very severe limitations on the types of components that could be used and increased the cost of the design. For the second prototype the operating temperature was reduced to 90°C because the focus was on drying appearance grade timber where the temperatures are normally lower than 100°C and quality is more important.

Configuration

The basic design for the kiln micro-sensor system proposed comprises three parts. The first part is the sensor array that fits inside the timber stack and measures the conditions of interest. The second part is the transducer that takes the signal from the array and converts it into an electronic signal that can be

recorded and displayed. The third part of the system is the computer interface or user interface where the conditions can be measured and recorded.

There are three main configurations for how the main parts can be put together depending on the requirements of the sensor. The first configuration is where all of the parts are connected by cables so that the system is essentially a single unit and can operate in real time providing continuous data. This type of design is the simplest electronically but does have a number of issues regarding the ease of use in a commercial kiln environment and finding suitable components to withstand kiln conditions. In particular the connection of cables between the parts of the system inside the kiln and the external parts creates a problem as there are few connectors available that are small enough and can handle the conditions.

The second configuration overcomes the problems of the first configuration by having a wireless connection between the sensor array and the external parts. There are kiln sensor systems commercially available that use wireless technology though there are some limitations. Firstly the receiver must be located inside the kiln to avoid shielding from the kiln structure. There are also temperature limitations on the components that are required for a wireless system and so they are usually only available for low temperature kilns. The maximum temperature rating for such systems is usually 70°C though in some cases the maximum operating temperature is as low as 50°C. The design of this sort of system is more complicated than a cable system but still allows for continuous real time data with easier installation and operation.

The third configuration uses a recording system built into the sensor array that stores data to be downloaded after the drying run is completed. This has temperature limitations similar to the second configuration but of the three probably offers the greatest ease of use.

Sensors

Obtaining suitable sensors that can operate under kiln conditions, while accurately measuring the conditions was the greatest challenge in this project. A high temperature wood drying kiln has conditions that stress even electronic components of the most demanding specification as in military applications. Therefore, one of the most important tasks in the project was keeping up with the latest fast developing technology. The sensors that were used in the second prototype were so new that they were not available at the time of the first prototype being made.

Temperature Sensors

Temperature sensors that could handle the conditions were not difficult to find as the temperature is a relatively simple quantity to measure and most temperature sensing technology is quite mature. There was a variety of different temperature sensors each with different precision, range, features and cost.

The two most common ways to measure temperature electronically are the thermocouple and the platinum resistance thermometer, with the latter generally being more accurate. Both of these sensors

require transducers to produce a signal that can be interfaced with a computer. There are also linear and digital integrated circuit devices that act as sensors and transducers.

Humidity Sensors

There are a number of methods that can be used to measure the air humidity with two standard methods being dew point temperature measurement and dry-bulb/wet-bulb psychrometers. Both of these are very accurate instruments but are not very well suited to this application. Psychrometers are the standard sensors used for measuring and controlling humidity in wood drying kilns but they are too large to fit into the fillet spaces in a stack, and require frequent maintenance and continuous water feed to operate. Dew point sensors can be miniaturised enough to fit into a stack but they are expensive and not well suited to kiln conditions, due to issues of corrosion and fouling of the miniature components.

There are newer techniques for measuring humidity based on capacitance changes in thin-film sensors. These sensors are very small and directly measure relative humidity but need to be calibrated for temperature. The capacitance of the sensor is also very small thus the signal may be lost over a short distance through a cable from being swamped by the capacitance of the cable. The latest humidity sensors include temperature correction and convert the capacitance signal into a digital signal that can travel through long cables or be transmitted through a wireless connection.

Other Sensors

There are other sensors that could also be included in a kiln micro-sensor array. As noted earlier air flow is of interest as it can often explain temperature and humidity variations within a stack. Nijdam et al. (2002) measured the flow variation at different heights in a stack using pitot tubes placed inside the fillet spaces. This is an accurate method for measuring airflow but the small tubes are too easily damaged and the technique requires the measurement of a very small pressure difference. There are small pressure transducers available but these are generally not capable of operating at kiln conditions.

Airflow can be measured using ultrasonic transducers and there are integrated circuits available that can analyse the signals to produce a calibrated data stream. This method of measurement is also limited by the kiln conditions, but assuming high temperature ultrasonic transducers are available they could be considered for future development of kiln sensors.

First Prototype

The first prototype, shown in Figure 105, was designed to use analogue sensors to measure temperature and humidity. The humidity sensors available at the time contained capacitance elements that could handle high temperature kiln conditions but the signal produced was too weak to measure over the distances required. For this reason the humidity sensors were not included on the first prototype, which in fact became a temperature sensor array.

The mechanical structure of the first prototype was made entirely from aluminium. The sensors were housed in six aluminium tubes attached to an aluminium channel with a thread. The mechanical design of the array has caused some difficulties with the construction. Although this was expected with any new

device, significant efforts were spent on the mechanical design to make the devices more easily built and repaired if necessary. In particular the connection of the tubes to the channel was difficult as the joint was difficult to secure in such a way that it could be easily dismantled.

The 6-sensor array using AD590 temperature sensors, with a maximum rated operational temperature of 150ºC, was constructed along with the necessary electronics to provide a readout of the individual sensor temperatures. This was based on the sensors' application notes describing the best way to use these devices for optimum linearity and accuracy over the temperature range of interest ie 100ºC -130ºC.

The circuit is an array of 6 precision current to voltage converters based on OP27 Op-Amps (operational amplifiers), and a very stable reference power supply to supply bias current to the AD590s. This produces an output of 100mV/ºC, which is connected to a voltage divider, and then to a digital panel meter (DPM) which gives a direct readout in degrees Celsius. The Op-Amps are powered from a separate fully regulated power supply and the DPM readout also has its own separate floating 5V power supply.

Some work was done on developing a second prototype with more attention to the mechanical design. This new sensor array was to be made from the PRT sensor elements, connected to data acquisition modules that read the sensors and feed the information directly into a computer. The system was to be able to read 32 sensors and be expandable to 2000 sensors. This work stalled however due to lack of electronics support in the Department and was discarded in favour of a new design of the electronic components of the sensor system, which will be described in the following section as the 'Second Prototype'.

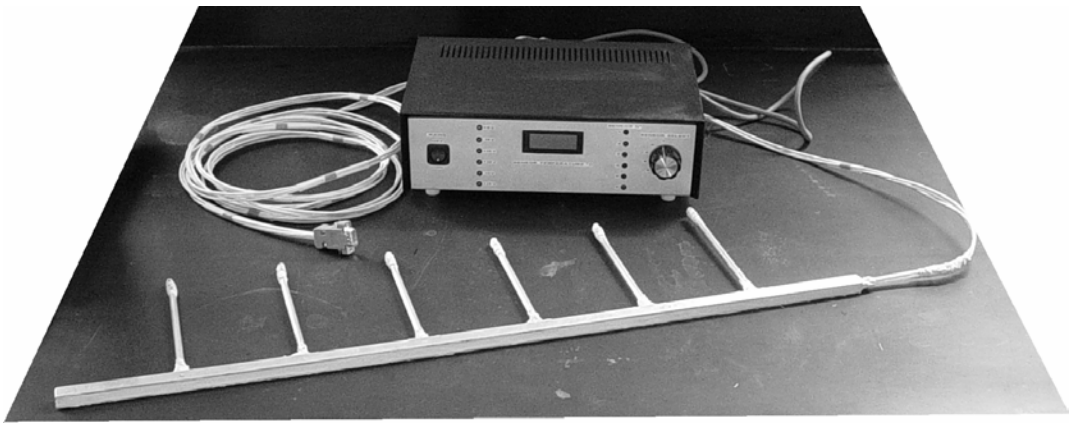

Figure 105. The first prototype microsensor with six analogue temperature sensors.

Second Prototype

The second prototype was a more ambitious design developed in cooperation with a final year electronic engineering student. The student did the work as his final year design project and details of the design can be found in Marshall (2004).

The introduction of high temperature digital humidity sensors to the market solved the problems that had been encountered with the capacitance sensors in the first prototype. The temperature conditions for this

prototype were also reduced to 90°C which allowed many more options which were not available for the first prototype. However, the main intention of the second prototype was also to produce a diagnostic tool rather than a kiln control system.

The temperature and humidity sensors used in this prototype where digital devices that contained the sensors and transducers in one small package. Both types of sensors produced a digital signal when connected to a power supply and suitable electronics to decipher the signal.

The mechanical design of the second prototype differed from the first prototype in two ways. Firstly the electronics for recording data was included in the sensor so that no external cables were required. The second difference in the mechanical design is that the sensors were flush with the body of the array rather than being held away from the array on tubes. This made the design far more robust as the sensors were better protected.

The electronics for recording data from the sensors was housed in a sealed IP56 aluminium box attached to one end of the square aluminium tube holding the sensors. A picture of this box and part of the tube are shown in Figure 106. One of the humidity sensors can also be seen to the left and the power switch and indicator LED can be seen on the box. The view inside the box can be seen in Figure 107. The USB port shown in this picture allows the sensors to be connected to a computer for calibration and so that stored data can be downloaded. More details of the electronic and mechanical design are available in Marshall's (2004) report.

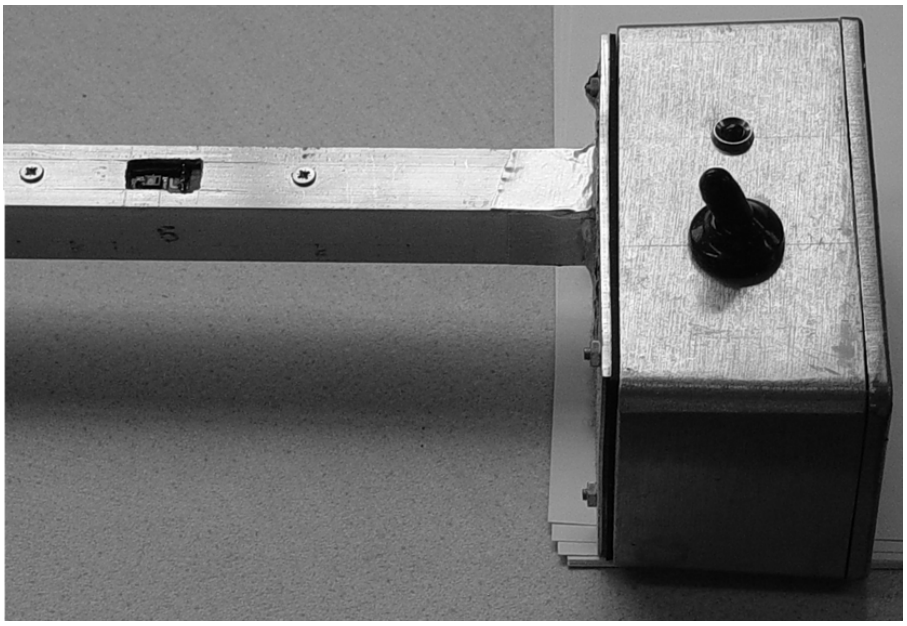

Figure 106. One end of the second micro-sensor prototype showing one of the humidity sensors and the box housing the electronics.

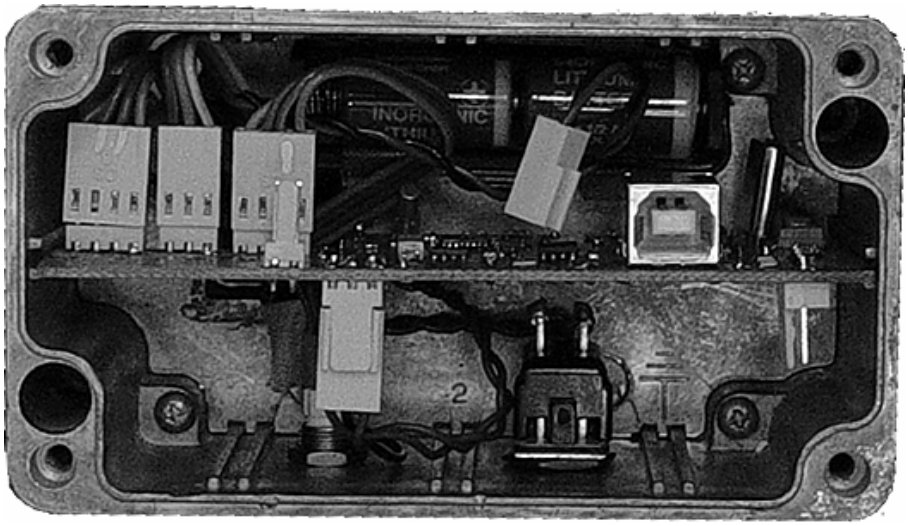

Figure 107. View inside the box housing the electronics for the second micro-sensor prototype. The batteries are shown at the top with the PCB in the middle of the picture. The connectors on the top left are for the sensors and the USB port can be seen to the right. The power switch is to the bottom right.

Test Results and Discussion

Both of the prototypes were tested in the small scale kiln using a dry stack and altering the temperature and humidity over the range of operating conditions. During these tests the first prototype had problems with holding calibration. For this reason no further tests were conducted using this design and the AD590 sensors were deemed unsuitable for this application. However, the first prototype showed a variation in temperature across the stack as the stack was heated up. For this reason it was determined that this prototype proved the concept of measuring drying conditions in a stack and highlighted the importance of good mechanical design.

The results for the second prototype test run, from Marshall (2004) are shown in Table 31. In this table Temp 1 is the temperature at the same point as Hum 1 and Temp 5 is the temperature at the same point as Hum 2. The temperature sensors are built into the humidity sensor and are different from the three temperature sensors, Temp 2-4.

The first thing that is clear in the test run for the second prototype is that one of the temperature sensors (Temp 4) is not working properly, as the temperature reading is too high and stays at a maximum for most of the run. This is, however, not a major concern as the sensor can be replaced without having to make an entirely new array and each sensor is independently calibrated.

It is also clear that more detailed calibration of the temperature sensors attached to the humidity sensors as they are not producing the same temperature as the temperature sensors. The two temperature sensors that are functioning are showing similar results, which confirms that the second prototype can operate in practical drying conditions.

The data from the two humidity sensors with integrated temperature sensors is displayed in Figure 108. These results show that the sensors are picking up the temperature and humidity lag created by the stack as the set points in the kiln were changed. The sensors have also picked up the difference as the air flow direction was change at the beginning and end of the run.

Table 31. Test results for the second prototype micro sensor (from Marshall, 2004).

Hum1 (%)	Temp1 (°C)	Temp2 (°C)	Temp3 (°C)	Temp4 (°C)	Temp5 (°C)	Hum2 (%)
51.79	49.50	50.5	50.5	121.5	50.68	50.73
51.65	49.48	50.5	50.5	121.5	50.49	50.70
52.56	49.38	50.5	50.5	121	50.30	51.61
48.99	50.43	51	51	122	50.93	51.31
50.61	50.34	51.5	51	122	51.02	55.87
50.76	50.14	51	51	121.5	50.83	57.97
48.63	50.89	51.5	51.5	122	51.26	53.73
43.12	52.80	53.5	53.5	124.5	52.84	47.62
36.86	55.13	56	56	127	55.11	42.56
32.95	56.92	58	58	127.5	56.92	41.10
30.07	58.23	59.5	59	127.5	58.25	33.90
29.36	59.11	60.5	60	127.5	59.08	33.36
28.70	59.61	61	60.5	127.5	59.59	31.41
27.87	59.91	61	61	127.5	59.88	31.89
27.14	60.14	61.5	61	127.5	60.12	31.14
25.64	60.55	61.5	61.5	127.5	60.29	29.14
43.34	63.67	64.5	64	127.5	62.45	57.03
42.34	65.97	67	66.5	127.5	65.10	51.53
45.34	68.30	69.5	69	127.5	67.39	55.64
51.61	70.26	71.5	71	127.5	69.43	57.51
54.41	71.80	73	72.5	127.5	71.15	60.63
53.54	72.13	73.5	73	127.5	71.69	59.79
53.92	71.93	73	73	127.5	71.62	59.54
55.18	71.60	72.5	72.5	127.5	71.21	58.06
56.90	71.04	72	72	127.5	70.74	59.91
59.38	70.19	71	71	127.5	70.24	62.70
59.34	69.91	71	71	127.5	69.75	65.83
60.08	69.66	70.5	70.5	127.5	69.54	63.57
55.32	71.58	72	72	127.5	70.54	63.34
41.95	77.04	78	77.5	127.5	75.02	51.81
25.99	81.81	83	82.5	127.5	79.58	31.21
28.83	86.11	88	87	127.5	83.61	34.18
26.36	87.67	89.5	89	127.5	85.40	31.73
27.36	86.42	89.5	89	127.5	87.72	28.03
27.54	86.60	89.5	89.5	127.5	89.32	25.97
26.58	87.07	90.5	90.5	127.5	90.22	25.02
26.57	87.56	91	91	127.5	90.65	24.75
26.21	87.86	91	91	127.5	90.91	24.81
25.72	88.10	91	91.5	127.5	90.90	24.38
25.56	88.20	91	91.5	127.5	90.77	24.38
25.85	88.16	91	91	127.5	90.61	24.54

Conclusions and Recommendations

The work presented in this chapter provides valuable information on development of a micro-sensor system which can be potentially very useful to monitor the conditions in a timber stack during drying. Within the time of the project the electronic technology available improved considerably particularly in the area of humidity measurement above ambient temperature. Future developments in sensor technology are likely to provide more opportunities to develop kiln sensors.

The prototypes developed in the work presented here were tested under simulated kiln conditions and produced sufficient results to be considered proof of concept. Further work is still required to develop a

tool for kiln control or kiln diagnostics. The second prototype has strong potential to achieve the goal of a diagnostic tool but further calibration and testing are required to prove this.

It is recommended that this project be continued if the electronic support is available with the possible addition of other sensors to measure airflow, board moisture content and board colour. It is also recommended that wireless sensors be investigated for real-time measurements.

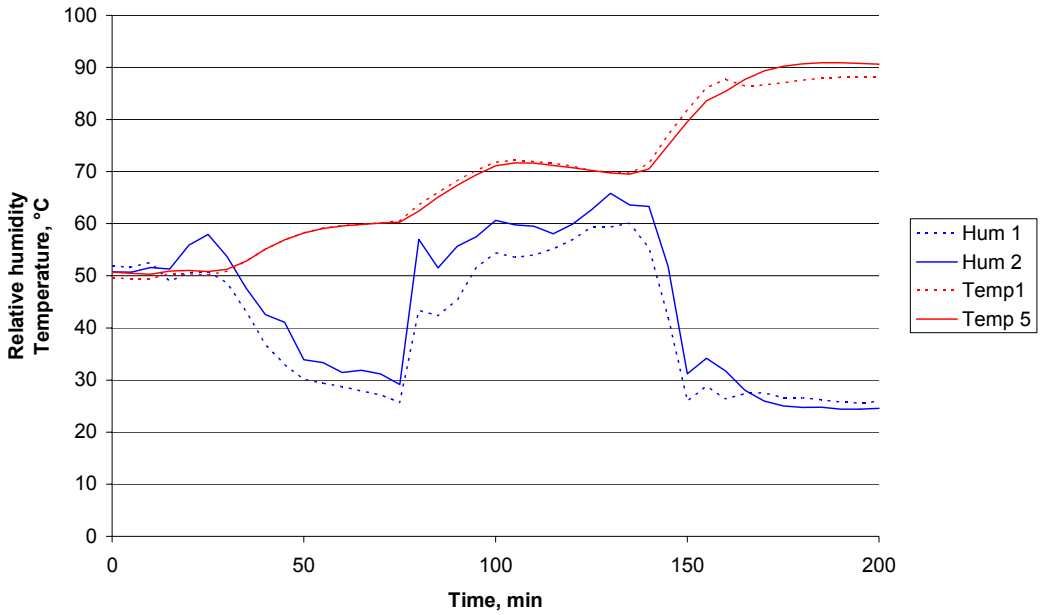

Figure 108. Initial results from the second kiln micro-sensor prototype. The data displayed is from the two humidity sensors with integrated temperature sensors.

Chapter 8

Discussion, Conclusions and Recommendations

The aim of this thesis was to explore the efficient drying of quality softwood timber with three specific objectives. The first objective was to study and quantify factors that affect kiln energy efficiency. The second objective was to develop and validate optimised conditions for kiln drying of high quality timber with a focus on bright colour of dried wood. The third objective was to develop micro-sensor technique for evaluating and improving kiln design, performance and control. This chapter will draw together the information and results presented in the previous chapters and analyse them in the context of the aim and objectives.

The original intention at the beginning of this project was to measure both colour development and the development of checking as quality parameters of specific importance for appearance grade timber. Although a limited amount of information was gained on the occurrence of checking in early drying experiments, more rigorous, experiments later did not measure any check development. From literature and this project, it was found that the checking was strongly related to the wood. A few conclusions could be made regarding the effect of kiln schedules on the development of checking based on the full-sized board drying experiments but the absence of data on the effect of relative humidity prevented this from being used in the model development. Based on this finding it was decided to focus subsequent work on understanding colour change and this became the main quality parameter measured and optimised.

Fundamental Understanding of Colour Development in Wood

There are two aspects to the development of colour in *Pinus radiata*, these are generalised colour change and localised colour variation. The work in this thesis has primarily focussed on the development of localised colour variation in the form of kiln brown stain. This is because localised variation of colour has the greatest effect on the value of the wood for appearance grade purposes due to the disruption of the natural appearance of the wood grain. In contrast the generalised colour development simple makes the wood uniformly darker. In most cases this increase in darkness is only slight and does not impact on the potential applications of the wood.

This study investigated and measured the stain formation on wood during drying. Some insight understanding was gained into how the stain formed. This information is included in this discussion as it

can contribute to the knowledge of the mechanism of kiln brown stain formation by supporting and adding to the information already available.

Migration of Stain Precursors

The chemical measurements performed in the board drying studies presented in the second part of Chapter 4 produced results with considerable variability. In general the results did show that there was an accumulation of nitrogen at the board surface during drying, which is in agreement with other experiments presented in the literature. However, the results obtained in this project only confirmed the previous findings in understanding the effects of stain precursors on wood colour changes.

The microscopic image analysis of kiln brown stain layers in boards dried at different relative humidity schedules, presented in part three of Chapter 4, provided some new insight into the movement of stain precursors during drying. These measurements showed that the relative humidity of a drying schedule affects the position and the thickness of the stain layer. The stain layer begins deeper from the surface of the boards with the faster drying low relative humidity schedules and with these schedules the stain layer is also thinner. These results also showed clearly that the level of colour changes is more severe with the higher relative humidity schedules.

Although the results from the microscopic image analysis can only be explained in general terms, they show similarities to the results published by Terziev *et al*. (1993) reviewed in Chapter 2. These experiments showed that a low relative humidity schedule produced a narrower peak of concentrated stain precursors at the surface compared to a high relative humidity schedule which produced a wider peak with a lower maximum concentration. Therefore, the results from the current project and those of Terziev *et al.* (1993) can be used to draw a picture showing how stain precursors accumulate at the surface and how the conditions of the schedule affect this accumulation. There is a difference in the nature of the schedules used however, that needs to be noted. The studies by Terziev *et al*. (1993) used a common wet bulb temperature while the schedules in this thesis used a common dry bulb temperature.

However, the kiln brown stain formation is affected by a combination of temperature, time and humidity. This can be illustrated by the observation that the studies of Terziev *et al.* (1993) shows that low relative humidity schedules cause a higher concentration of stain precursors at the surface while the current study shows that these schedules produce less colour development. This is due to the difference between these two studies in wood temperature in the stain layer. During the capillary phase of drying, which is the phase when stain precursors are migrating to the surface, the surface temperature must clearly be lower than the dry bulb temperature of the schedule. The temperature difference between the drying medium and the wood surface is the driving force for heat transfer during drying. When the moisture content is high (above the fibre saturation point), it is reasonable to assume that the surface temperature is closer to the wet bulb temperature of the schedule, which is supported by some experimental evidence available on this subject. However, when the surface moisture content is close to the equilibrium moisture content, the drying is in vapour flow phase and the surface temperature can be very close to the dry bulb temperature.

In this project, for the understanding of the colour changes, is was assumed that the wood surface temperature was at the dry-bulb temperature.

The drying time for the low humidity schedules is also shorter, thus there is less time for the colour to develop in the wood. This is probably the main reason why the higher concentration of stain precursors produced at the surface by low relative humidity schedules do not result in higher levels of stain formation. Compared with the drying time, the dry-bulb temperature will have less effect as for a significant period of time in the early stage of drying; the wood surface temperature is close to the wet-bulb temperature.

The different surface and internal temperatures during the capillary drying phase at different relative humidity schedules, where the dry bulb temperature is the common temperature, have implications for the movement of stain precursors and the characteristics of the stain layer that develops. The higher internal board temperature associated with the high relative humidity schedules is likely to aid in the release of stain precursors from cells inside the board and will also increase the mobility of these compounds. The higher temperature will also increase the likelihood and rate of reaction of these stain precursors with other stain precursors or other compounds in the wood structure.

The increased release and mobility of stain precursors with high relative humidity schedules will result in a greater quantity of stain precursors migrating during drying. A cursory examination of the data of Terziev *et al*. (1993) presented in (Figure 13) shows that there is, in fact, overall a higher concentration of stain precursors in the board dried with a high humidity schedule. In the high humidity schedule of Terziev *et al.* (1993), the overall concentration is approximately 50% higher. Because in both cases, the wet bulb temperature was the same, the effect is due to a longer time in the capillary flow phase of the drying. For the experiments presented in Chapter 4 there would probably be an even greater effect due to the higher temperature and longer time.

The data in Figure 13 also shows a clear difference in the sugar concentration profile through the board which can also be attributed to the extended drying time of the high relative humidity schedule. The movement of sap to the surface is dictated by the drying rate which is lower in a high relative humidity schedule. This is confirmed by the experimental results in Chapter 4 where the drying rate is slower using the higher relative humidity schedule although the internal temperature is higher.

The increased concentration of the stain precursors at the surface also brings into play another mechanism for the movement of stain precursors: diffusion. The direction of diffusion will be determined by the concentration gradient of component concerned. For the stain precursors, which have been brought to the surface with sap movement, their diffusion will be away from the surface and into the core of the board. The rate of diffusion of substances increases with temperature so the higher internal temperature means the rate of diffusion will be higher for the high relative humidity schedule compared to the low relative humidity schedule, with the same dry bulb temperature. Diffusion is also a slow process so is very dependant on the time available and the distance that the diffusing species need to travel. Whenever the wet bulb temperature is constant, the effect of diffusion will be greater in the high relative humidity

schedule due to the longer time in the capillary drying phase and the slower drying rate meaning the effective path length for diffusion is shorter.

From the above discussion, the concentration profile of stain precursor develops due to the balance of mass flow to the surface and diffusion away from the surface as shown in Figure 109. This diagram applies to the situation where the dry bulb temperature is the same between the schedules. In the case of a common wet bulb temperature it is probably more accurate to think in terms of significance of the diffusion process as the diffusion rate will be roughly the same for both schedules, only the mass flow rate differs. There may also be an increase in movement of moisture by osmosis up the concentration gradient, which would have an effect similar to the diffusion as the stain precursor would be effectively left behind.

The increased rate of reaction at the higher temperature may also have an impact on the distribution of stain precursors if they become immobile from the reaction. The colour kinetic experiments in the first part of Chapter 5 show that the Maillard reaction between simple sugars and glutamic acid increases exponentially with temperature. The change in reaction rate between 40°C and 60°C was however only minor so this is likely to have little significance in the experiments in Chapter 4. Whenever the common wet bulb temperature schedules are compared this effect will not be significant at all.

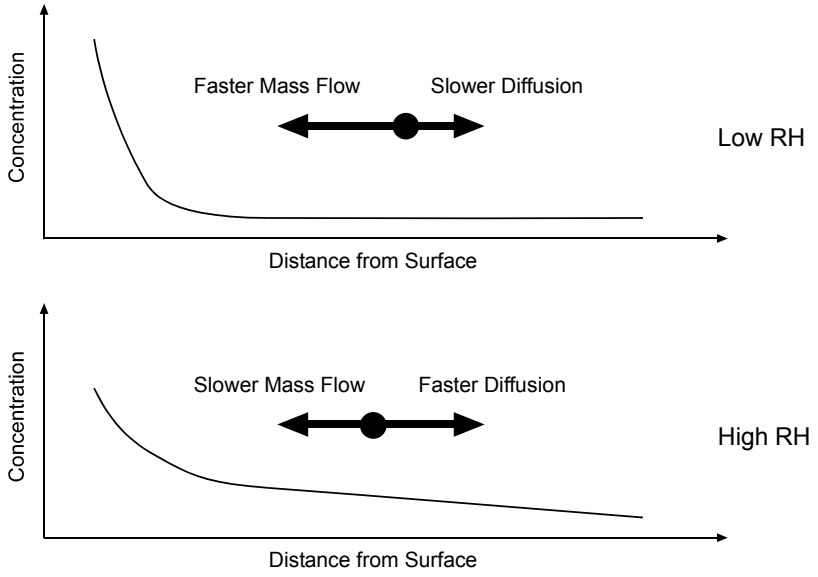

Figure 109. Diagrammatic representation of the balance of effects on the distribution of stain precursors in wood during drying at different relative humidity schedules with constant dry-bulb temperature.

In summary, the mechanisms of chemical reaction and wood colour change during drying can be attributed to two opposing transport processes; diffusion and mass flow. Where the drying rate is fast and the internal wood temperature is low, the mass flow dominates and the sugar (or nitrogen) concentration profile has a narrow high value peak at the surface with minimal gradient in the core of the board. Where the drying rate is slower and the internal board temperature is higher the diffusion processes have more of

an affect, resulting in a broader, lower value concentration peak at the surface and more of a gradient in the core of the board.

The above concept was drawn from experiments and literature; however, this was not included in the original objectives. In order to confirm this concept, more specific experiments coupled with computer modelling of the processes involved are needed in future studies.

The Colour Reaction

The chemistry of the colour development was not explored in detail in this project and no effort was made to identify any of the reactive compounds involved or the coloured compounds produced. There is plenty of information in the literature on the reactive compounds in wood that may be involved in the development of colour so repeating such work was considered unnecessary. Information available on the reaction mechanism, assumed to be a Maillard reaction, makes it clear that even for the simplest of precursor compounds the products of the reaction are varied and complex. This meant that any work in this area was likely to be complicated, time consuming and of little value to the commercial focus of this project. However, in the process of discerning the kinetics of the colour reaction, as described in Chapter 5, information was gathered that is helpful in the understanding of this part of the process of kiln brown stain formation. In particular the difference in the kinetics and absorption spectra of the experiments with simple artificial sap solutions and the experiments using wood samples gives an insight into the complexity of the colour development and hints at some processes that may be involved.

The data from the in-vitro experiments were able to be fitted using the Arrhenius Law while it was not possible to fit the data from the in-wood experiments in this way. This difference shows that the reaction kinetics of the development of kiln brown stain are highly complex and cannot be accurately simulated using simple solutions of sugars and amino acids.

The difference between the two types of experiments was also shown clearly in the contrast between the absorption spectra of the reaction products. The in-wood samples were absorbing almost entirely in the visible region and there was a very clear red-shift in the absorption spectra indicating an increase in the complexity of the products causing colour. In contrast to this the in-vitro samples were absorbing mainly in the UV range of the spectrum and the increase in colour was clearly due to an increase in the concentration of a simple compound rather than the production of increasingly complex compounds. This again demonstrates that the in-vitro experiments do not accurately simulate what occurs during the formation of kiln brown stain.

The microscopic image analysis also shows that the darkening in the kiln brown stain layer occurs both in the cell lumens and the cell walls when magnified. Some of the colour seen is due to a brown substance with an amorphous appearance that is in the lumens of some of the cells in the surface layer, but the majority of the colour seems to be associated with the cell walls.

The brown substance in the lumens could be Melanoidins, the catch-all term used to describe the complex polymeric products of the Maillard reaction, or it could be the accumulation of non-volatile extractives

and resins. The resin and extractives compounds are coloured so their accumulation at the board surface would increase colour and these compounds are also potentially reactive in the Maillard reaction. There are only a few cells that are significantly affected by these substances so this occurrence is probably the less significant contributor to the colour seen in the kiln brown stain layer.

The darkening of cell walls was observed in most of the cells in the kiln brown stain layer and is more likely to be the most significant contributor to the colour that is seen. It is unclear what is causing the darkening of the cells walls but the darkening is in most cases through the entirety of the cell wall material. There appears to be a contribution from coloured compounds adhering to the cell wall surfaces as well. The darkening is throughout the cell wall material indicates that the colour reaction involves non-mobile compounds in the cell wall structure, such as lignin and hemicelluloses. There could also be reactions with the terminal glucose monomers of the cellulose chains but generally cellulose is not considered to be very reactive.

The in-wood colour measurements show that colour development is the same above fibre saturation and below fibre saturation. This also indirectly supports the idea that the colour reaction is occurring within the cell wall structure as below fibre saturation point the moisture exist only within the cell wall material and there would be no moisture in the lumens to dissolve the reacting compounds. In this way, the moisture bound in the cell wall would provide a good environment for the reaction to proceed as well as plenty of reactive surfaces.

The evidence from the microscopic studies and the colour kinetics both point to the cell walls as being the most important site for the development of kiln brown. This aspect of the stain formation mechanism is not addressed in the literature and represents an interesting area that could be explored in more detail in future studies. It could be that the surfaces inside the cell wall structure actually catalyse the kiln brown stain reactions. Though this is merely speculation at this point further research on these ideas could lead to new options for combating kiln brown stain formation.

The data for colour change rate from the in-wood experiments represent a significant progress in the characterisation of kiln brown stain formation in radiata pine. Previous studies have suggested that the development of kiln brown stain is more severe at temperatures above 60°C but the graph in Figure 74 clearly illustrates the increase in the rate of colour development above this temperature.

Overall Mechanism of Kiln Brown Stain Formation

Over the course of this project an understanding of the mechanism of kiln brown stain formation has been developed and refined, based on the experiments performed and published studies in the literature. This is illustrated in Figure 110 which shows what occurs during the capillary flow phase of drying. This is however only a snapshot of what is happening during the capillary flow phase of drying and it is also necessary to describe the mechanism chronologically.

While the wood is still part of a living tree, transpiration from the leaves draws moisture from the roots through the xylem, bringing nitrates and other nutrients required for growth. At the same time moisture

laden with the products of photosynthesis in the leaves is distributed throughout the tree through the network of parenchyma cells that make up the phloem.

When the tree is felled and the logs are cut, the kiln brown stain precursors will be distributed throughout the wood as the ray parenchyma connect through the entire structure of the trunk. This also means that when the logs are cut into boards there is a reasonably even distribution of stain precursors throughout them, at least on the macroscopic level.

After sawing the boards are graded and then stacked for kiln drying. In an operation focussed on quality the time spent on these steps should be minimised to avoid uncontrolled air-drying, microbial effects and other consequences of exposure of the green timber to environmental factors.

At the start of drying, as the wood heats up, evaporation causes moisture to be lost from the surface layer resulting in the formation of a thin dry layer. During this stage of drying there will be a slight concentration of stain precursors in at the evaporative front as soluble compounds present in the surface layer are picked up and moved into the board with the evaporative front. Most of the cells in this damaged surface layer will be ruptured, particularly the thin-wall ray parenchyma, so the stain precursors will be mobile and uniformly distributed.

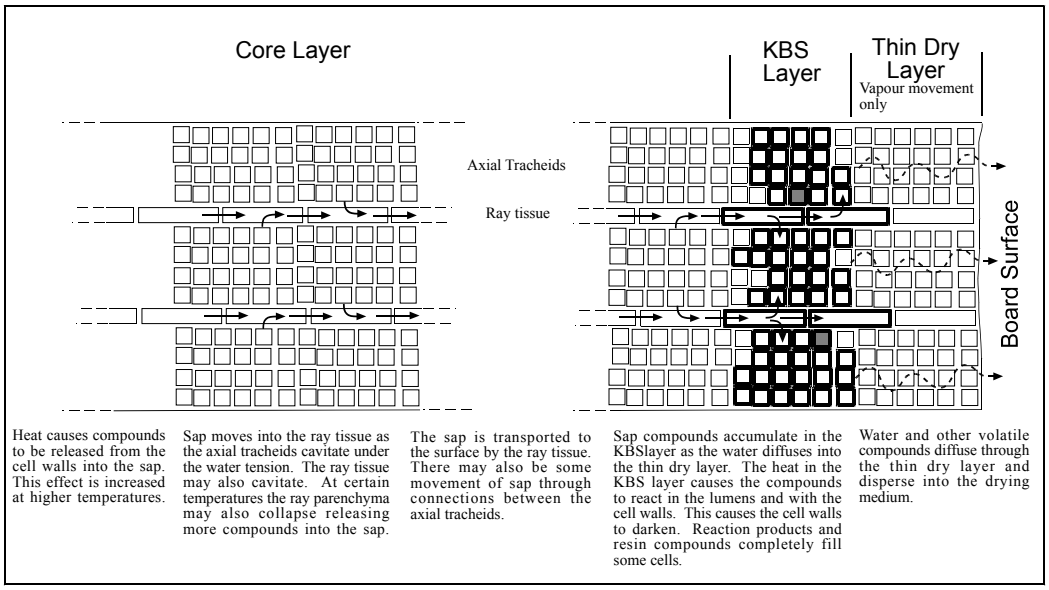

Figure 110. Illustration of mechanisms of kiln brown stain formation based on information from this study and other published studies.

When the evaporative front has receded through the damaged surface layer the capillary flow phase of drying begins and the mechanism illustrated in Figure 110 begins to take effect. Heat transfer from the surface into the core heats the wood and compounds are released into the sap from the cell walls. The effect of this process increases as the temperature of the wood increases, which means more compounds are released in wood dried at high temperature. Higher temperatures also result in the more rapid release of soluble compound from the ray parenchyma cells which, due to their storage function, are likely to contain many of the compounds that cause kiln brown stain.

The diagram shows that the majority of the transport of moisture, and stain precursors, to the surface is through the ray tissue. This will be the case when the wood is cut flat-sawn as the radial tissue is in the direction of moisture movement. Where the wood is cut quarter-sawn the moisture movement will be mainly through the bordered pits connecting the axial tracheids and movement through the radial tissue will be much less significant. Resin compounds will also be present in the ray tissue and quantities of these will migrate to the surface layer.

Moisture evaporates from the, now stationary, evaporative front drawing sap from the core of the wood. The evaporation of the water induces water flow towards the evaporative front thus the concentration of compounds in the sap increases near the front. The temperature at the evaporative front causes these compounds to react with each other producing coloured products that form the stain layer. This reaction occurs in the lumens of the sap fill cells in the stain layer and inside and on the surface of the cell walls.

Eventually the continuity of the capillary network transporting sap to the surface for evaporation breaks down. This signals the end of the capillary flow phase and the start of the vapour flow phase. During the vapour flow phase of drying although the movement of liquid sap ceases, the colour forming reactions continue inside the cell walls and the rate of these reactions is not diminished by the change from capillary to vapour flow. The rate is actually likely to be higher as the temperature at the surface increases towards the dry bulb temperature.

Experimental Techniques

This project has seen the development of a number of experimental techniques for measuring the change of wood colour during the drying process. The results from the second part of Chapter 5 show the advantage of using a spectrophotometer rather than a colorimeter when measuring colour for research purposes. The reflectance spectra that can be obtained from a spectrophotometer give more information about what is causing the colour change than could be determined from a colorimetric measurement.

The experimental technique developed for the in-wood experiments is a significant step forward in the study of colour development in wood during drying. This technique has allowed, for the first time, the measurement of colour development of the same board during drying without the need for destructive testing. This removes the variability associated with multiple samples where the differences in properties between samples can influence the way that colour develops. The technique could be developed further using a jig, in a similar way to that reported by Riley and Sargent (2005) and also shows the potential for the development of a continuous in-kiln colour measurement technique.

In this project, photographic techniques were also further developed for the qualitative evaluation of the kiln brown stain layer. The analysis of microscopic images of the surface layers of dried boards yielded some useful information about the formation of the stain layer and influence of drying conditions. This work was however an aside to the main objectives of the project and will need to be explored in more detail in future studies to provide firm conclusions. The technique also shows promise as a tool for examining the formation of the stain layer.

Schedule Selection

The three main variables that are manipulated to control the drying of timber are temperature, humidity and airspeed. However an important factor is the drying time which is a combination of these three operational factors. The experiments presented in this thesis extensively investigated the effects of the first two variables (temperature and humidity) on the development of wood colour. The single board drying experiments showed that there is an increase in colour development when the dry bulb temperature is increased. Increasing the relative humidity, or reducing wet bulb depression, at the same dry bulb temperature also has the same effect.

The effect of increased dry bulb temperature is explained simply as the result of an increased rate of reaction. On the basis of the earlier discussion on fundamental mechanism the dry bulb temperature will have the greatest effect during the vapour flow phase of drying, which is the period of drying when the surface temperature is closest to the dry bulb temperature. This means that the reaction rate can be more truly correlated with the dry bulb temperature.

In early stage of drying when the moisture content is high, the surface temperature is influenced more by the wet bulb temperature of the schedule. This is one way that the relative humidity of the schedule influences the development of colour. Schedules with a small wet bulb depression will have a higher surface temperature than schedules with a large wet bulb depression. Therefore, the rate of colour development at the surface will be greater for high relative humidity schedules compared to low relative humidity schedules. The higher surface temperature also means that the overall temperature through the board will be higher and therefore more stain forming compounds may be released into the sap from the cell walls. This is however still a hypothesis as no conclusive experimental evidence has been found in literature for this occurring, though the work of MacDonald et. al. (2000) shows that a hot water sap displacement is required to remove all stain precursors.

The colour development in high relative humidity schedules is also increased because of the longer drying time. At high relative humidity, the drying rate is slow so there is more time for the reactants to interact and therefore more coloured compounds are produced. The flipside of this is that the low relative humidity schedules have a faster drying rate and a shorter time for the reaction to occur.

The effect of air speed on the development of colour can be analysed based on its effect on the drying rate. Higher air speed increases the drying rate and will result in less colour development. Therefore, from the standpoint of reducing colour change, schedules with high air speed and low relative humidity are recommended. The costs for using various schedules have been considered in next section.

In this work, the effects of board thickness was not examined but it is believed that trend of the schedule influences would hold for both thinner and thicker boards, and the schedule recommendation will be applicable.

Modelling of Energy Efficiency of Schedules

The energy efficiency and running cost of schedule have been analysed in this thesis by employing an extended kiln stack model. In a competitive commercial environment it is necessary to minimise the cost of processing wood. This has been particularly important for NZ companies in recent years as high log prices and a strong currency has reduced the margin that can be gained from processing wood.

The most obvious finding from the simulations of energy use is that extreme relative humidity schedules, either very high or very low, do not use energy efficiently. In the case of low relative humidity schedules this is due to the large amount of heat lost with the exhaust air in order to maintain the low wet bulb temperature in the kiln chamber. For the high relative humidity schedules, the drying rate is slow and the drying time is long which causes excessive energy use.

The effect of schedule humidity on energy use for a standard kiln design is illustrated in Figure 111 at a given dry-bulb temperature of 70°C. In this graph the energy use has been simulated for wet-bulb temperatures ranging from 40°C to 65°C and the accumulated energy consumption is expressed as a function of elapsed time. For all of the schedules the greatest amount of energy is used during the early stages of drying as indicated by the steepest slope for each set of data. This is because there is a greater evaporative load at the start of drying when the drying rate is at a maximum. The slope of the data, or the energy use per unit time, becomes greater as the relative humidity of the schedule decreases due to two factors: higher drying rate and more energy loss.

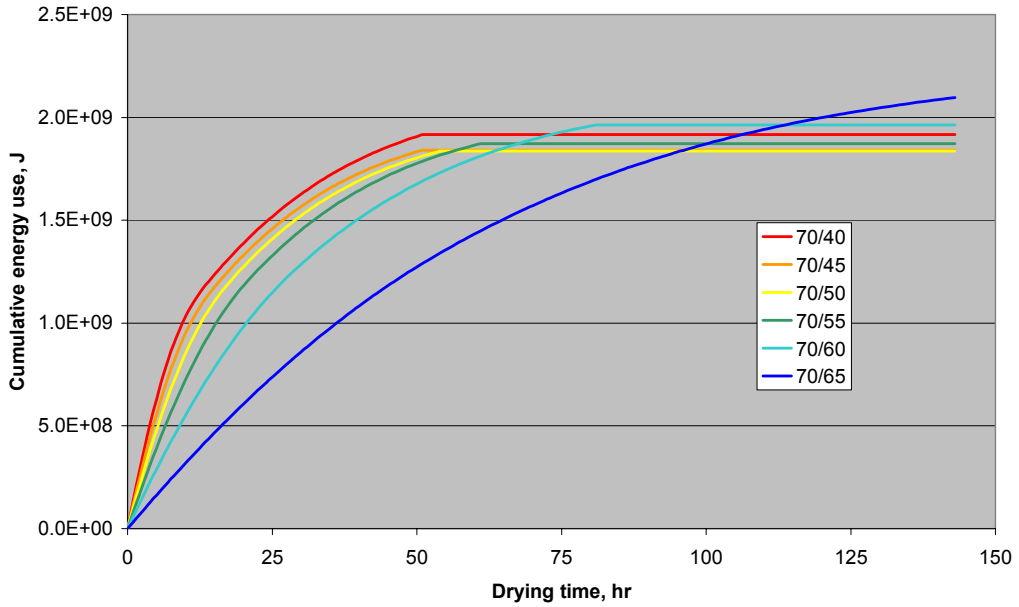

Figure 111. Cumulative energy use in timber drying for kiln configuration 2 showing the effects of wet-bulb depression.

The simulation results suggest that the most efficient drying schedules are those with a wet bulb depression of around 20°C. Usually with a dry bulb temperature of 70°C a 10°C wet bulb depression is

used so the simulated result suggests an increase in the wet bulb depression will increase the efficiency of the drying operation. Based on the results from drying tests and simulations there is a reduction in colour development when there is a move to lower relative humidity schedules, so there are gains to be made in both the efficiency and quality of drying by using schedule of 70/50°C.

One area where efficiency and quality diverge is with airspeed. An increase in the airspeed in the kiln will reduce the drying time and therefore decrease the level of colour development in the wood. There is however a significant increase in the electrical energy required when running the fans at higher speed. Electricity is a more expensive form of energy compared to process heat so ideally the use of energy should be minimised in the drying process unless its use results in significant gains in dry timber quality.

Kiln Design

By integrating the wood colour model and economic analysis into the extended kiln stack drying model, costs and benefits for different kiln configurations have been simulated. Different kiln configurations use different methods for controlling the humidity at the inlet side of the stack in the kiln chamber. The results of the simulations have shown that the humidity control method using the pressure difference across the overhead fans to exchange air through vents (Configuration 1 and 2?) is not as efficient as other modified configurations. However Configurations 1 and 2 are used in most heat-vent kilns manufactured in New Zealand due to their simplicity.

There are two reasons that the above mentioned standard kiln configuration for humidity control is inefficient. Firstly the intake air enters the kiln upstream of the outlet vent which means that there is more air passing through the fan than there is through the stack. The second reason for inefficiency is that no attempt is made to recover any of the heat in the outlet air stream.

Heat recovery is potentially an energy savings measure to incorporate into kiln design. A heat recovery system such as the one simulated with configuration 3 does not require any extra energy input and simply heats up incoming air by transferring heat from the vented air. The simulations showed that this configuration had the greatest efficiency of all the configurations, though the energy savings were based on some assumptions that may be over optimistic. Further calculations and experimental work is required to determine how much energy can be saved using a heat recovery system such as this.

The combination of heat recovery and humidity control by condensation was also an energy efficient configuration and had the greatest benefits of all the configurations. This has energy efficiency gains similar to configuration 3 but also has added environmental benefits from reducing gaseous emissions to atmosphere.

A possible design for an integrated heat recovery and condensation humidity control system utilising heat pipes is shown in Figure 112. In this system a movable baffle located in the plenum space is used to direct airflow entering the plenum from the stack into the cooling and condensation section. In this section the air is initially cooled by contacting the lower end of the heat pipe and then by heat transfer with the outside environment. During this cooling process water vapour in the air will condense and drop

down for collection. After cooling and condensation the air is heat by contact with the top end of the heat pipe, thus recovering some of the heat lost during cooling. This system would not add any extra moving parts to the kiln as the baffle would replace the roof vents.

This is obviously only one possible design for this type of system and further research and development is required to determine the best configuration based on the proposed concept.

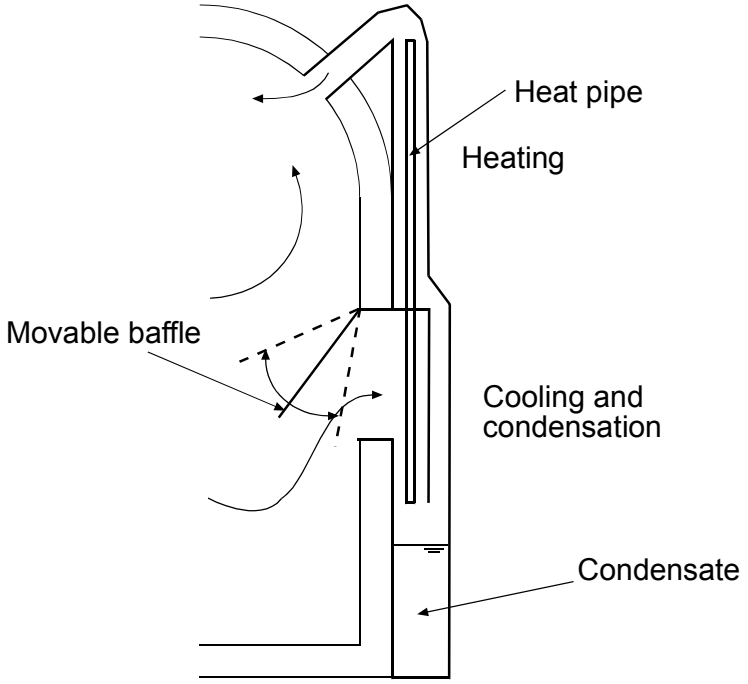

Figure 112. An option for integrated condensation humidity control and heat recovery on a wood drying kiln using a heat pipe.

Conclusions

The experiments performed in this PhD study have shown the following points:

1. The rate of colour change for kiln brown stain formation in Pinus radiata wood during drying is dependent on temperature, humidity and drying time. The relationship between temperature and wood colour change is non-linear and the rate of colour change increases rapidly above 60°C.
2. Wood colour change occurs above and below fibre saturation point and the rate of wood surface colour development change can occur at a high rate with moisture content below the fibre saturation point.
3. Low relative humidity schedules reduce the formation of colour compared to high relative humidity schedules with the same dry bulb temperature. This is due to the shorter drying time and the lower board temperature during the capillary drying phase.

The simulations of wood colour, kiln stack drying and energy efficiency, based on theoretical and empirical calculations, have shown the following:

1. Low relative humidity schedules reduce the level of colour developed during drying, which is in agreement with point 3 above.
2. The energy efficiency of the wood drying process generally increases with decreasing dry bulb temperature. The effect of relative humidity is more complex with extremes of relative humidity being less efficient than those in the middle.
3. Increasing the temperature of a schedule generally increases profitability due to an increase in the rate of drying and consequently a greater kiln throughput.

Based on this work the following recommendations can be made:

1. Kiln operators who wish to achieve light coloured kiln dried wood suitable for high value products should consider using lower relative humidity schedules and decreasing the dry bulb temperature. Specifically it is recommended that the dry bulb temperature of the drying schedule does not exceed 70°C with 60-65°C being the ideal range. The wet bulb depression should be 15-20°C with the higher value for the higher dry bulb temperature.
2. Kiln operators can achieve faster drying times and higher drying temperatures by increasing the air speed in the kiln. If this option is pursued then careful attention needs to be given to the increased electrical energy requirements of the schedule and whether these are justified by the benefits.
3. Kiln designers need to develop kilns that can operate efficiently particularly at lower relative humidity schedules. Specifically it is recommended that heat recovery is incorporated into the humidity control mechanisms in the kiln and that this be configured to minimise the electrical energy requirements of the fans.

Recommendations for Further Work

There are a number of new ideas and directions for research that have been generated from the research presented. Some of this comes from a need to further investigate areas of research that have been touched on in this project and some of it comes from the commercialisation of other aspects.

Further Experimental Investigations

There are a number of experiments that could be performed to test some of the ideas presented in this thesis. Based on the in-vitro experiments in Chapter 5 it has been suggested that thicker boards will be more susceptible to kiln brown stain due to the higher concentration of stain precursors at the surface. This could be tested by drying matched boards of different thicknesses and measuring the colour and possibly the surface nitrogen content.

There is also some suggestion that schedules with a high initial relative humidity during the capillary flow phase followed by a low relative humidity during the vapour flow phase of drying can reduce the level of wood colour change. The experiments performed in this thesis were not designed to test this idea so further experiments would be useful.

The colour change rate measurements performed in Chapter 5 could be extended to include higher temperatures as the temperatures used in this thesis were limited by the equipment available. Higher temperature measurements would provide more data points and therefore provide a better colour rate equation.

The short experiment presented in this thesis showed that the relative humidity of the kiln schedule had an effect on the position and thickness of the kiln brown stain layer. The experiments were however limited to one sample for each set of drying conditions. Further experiments would help to determine whether this is a repeatable result or just a coincidence.

Colour Change Simulations

The kiln stack model used for the simulations in this thesis was a simple one and there were also a number of simplifying assumptions made about the surface temperature for the colour change. There are more detailed models available for individual board drying and kiln drying that could probably incorporate the colour change equation relatively easily.

The model used in this thesis has treated the formation of kiln brown stain as a lumped parameter process, it is clear from the mechanisms also presented this is not a truly accurate approach to use. The colour model developed from the experimental measurements did however lump all of the colour change processes into a single equation based on temperature. For this reason it is justified to use a lumped parameter drying model to provide input into the colour model. Ideally future colour change models will include the influence of transport and diffusion processes.

In-kiln Colour Measurement

The results from the in-wood measurement of colour change show that there is an opportunity to develop in-kiln colour measurement systems. This could be achieved by mounting a colour measurement device either on a sample board in the stack or on a planed section of a standard board in the stack. It is easy to find electronic components that operate at the temperature recommended in this thesis for drying appearance grade timber (70°C). There are also a number of cheap colour measuring components available as well.

Continued Development of Kiln Micro-sensors

The development of the kiln micro-sensors should be continued and at this stage this development needs to be done by a person with knowledge of electronics.

Kiln Design

The recommendations for kiln design need to be tested using lab scale equipment to determine what level of heat recovery can be realistically expected from such a system. These tests would also show whether the vent-less design reduces colour change in wood.

References

1. **Ashworth, J.C. 1977**. The mathematical simulation of batch drying of softwood timber. PhD Thesis, University of Canterbury, New Zealand.
2. **Australian/New Zealand Standard: Timber** – Assessment of drying quality. Standards Australia/ Standards New Zealand, AS/NZS 4787:2001.
3. **Bamber, R.K. and Burley, J. 1983**. The wood properties of radiata pine. Commonwealth Agricultural Bureaux.
4. **Bechmann, R. 1990**. Trees and Man. Paragon House, New York.
5. **Beckwith, J.R. 1979**. Theory and practice of hardwood color measurement. Wood Science 11(3).
6. **Bollard, A., Rose, J. 1998**. Responding to the Asian crisis – a New Zealand perspective. Address to Strategic Management Society, Wellington Branch, http://www.treasury.govt.nz/speeches/asiacrisis/sp-sms98.pdf
7. **Booker, R.E. 1996**. New theories for liquid flow in wood. Proceedings of the 5th IUFRO Wood Drying Conference, Quebec City, Canada.
8. **Boutelje, J.B. 1990**. Increase in the content of nitrogen compounds at lumber surfaces during drying and possible biological effects. Wood Science and Technology 24: 191-200.
9. **Brightwood Quality Control. 2003**. *Private communication*.
10. **Butterfield, B.G., Meylan, B.A., 1980**. Three-dimensional structure of wood: an ultrastructural approach. Chapman and Hall, London.
11. **Butterfield, B.G., Meylan, B.A., 1972**. Three-dimensional structure of wood: a scanning electron microscope study. Reed Education, Hong Kong.
12. **Byrne, A and Hilbert, D. R. (eds). 1997**. Readings on colour Volume 1: the philosophy of color. MIT Press, Cambridge, Massachusetts.
13. **Carrington et al 2003 Workshop 2003**, Wood Technology Research Centre, University of Canterbury, Christchurch, New Zealand.

14. **Carrington, G.C., Sun, Z., Bannister, P., Chen, G. 1998**. Dehumidifier driers – what to expect and pitfalls to avoid. Workshop 1998, Wood Technology Research Centre, University of Canterbury, Christchurch, New Zealand.

15. **Choong, E.T. 1963**. Movement of moisture through a softwood in the hygroscopic range. Forest Products Journal, Nov 1963.

16. **Côté, W.A. 1967**. Wood ultrastructure: an atlas of electron micrographs. University of Washington Press, Seattle.

17. **Coulson, J.M., Richardson, J.F. and Sinnot, R.K. 1989.** Chemical Engineering: An introduction to Chemical Engineering Design. Pergamon Press Ltd, Oxford.

18. **Cown, D.J. 1975**. Variation in tracheid dimensions in the stem of a 26-year-old radiata pine tree. Áppita, 28(4).

19. **Cranswick, A.M., Rook, D.A., Zabkiewicz. 1987**. Seasonal changes in carbohydrate concentration and composition of different tissues of Pinus radiata trees. New Zealand Journal of Forestry Science 17(2/3)

20. **Dakin, M.C. 1996**. Design of a timber drying apparatus. BE Project Report, Chemical and Process Engineering Department, University of Canterbury, Christchurch, New Zealand.

21. **Dawson, B., Torr, K., Uprichard, J.M., Gallagher, S., Franich, R. 1993**. Colour stabilised wood products. FRI Internal Report 3815.

22. **Deev, A., Keey, R.B. 2001**. Observation of the "washboard effect" on the surface of quarter-sawn Pinus radiata under kiln-drying conditions. New Zealand Journal of Forestry 46(2), pp. 26-33.

23. **Dieste, A. 2002**. Colour development in Pinus radiata D.Don under kiln drying conditions. ME Thesis, University of Canterbury, New Zealand

24. **Dieste, A., Williamson, C. 2002**. Colour development in Pinus radiata D.Don under kiln drying conditions. Proceedings of the 8th APCChE Conference, Christchurch, New Zealand.

25. **FAO. 2000**. Global forest resources assessment 2000. Food and Agriculture Organisation of the United Nations, Rome, 2001.

26. **FAO. 2002**. FAO forest products yearbook 2002. Food and Agriculture Organisation of the United Nations, Rome, 2004.

27. **FAO. 2005a**. State of the worlds forests Part 1: Situation and developments in the forest sector. Food and Agriculture Organisation of the United Nations, Rome, 2005.

28. **FAO. 2005b**. State of the worlds forests Part 2: Selected current issues in the forest sector: Enhancing economic benefits from forests: changing opportunities and challenges. Food and Agriculture Organisation of the United Nations, Rome, 2005.

29. **Fayle, S.E., Gerrard, J.A. 2002**. The Maillard Reaction. Royal Society of Chemistry.

30. **Fogarty Timber Drying Kilns. 2003**. *Private communication*.

31. **Fogarty Timber Drying Kilns. 2005**. *Private communication*.

32. **Fulton, J.T. 2005**. Processes in biological vision. http://www.4colorvision.com/document.htm.

33. **Furuyama, Y., Kanagawa, Y. and Hayashi, K. 1994**. Mechanism of free water movement in wood drying. Proceedings of the 4th IUFRO International Wood Drying Conference, Rotorua, New Zealand.

34. **Gao, F. 2005**. Wood colour of radiata pine. ME Thesis, University of Canterbury, Christchurch, New Zealand.

35. **Hart , C.A. and Thomas, R.J. 1967**. Mechanism of bordered pit aspiration as caused by capillarity. Forest Products Journal, 17(11)

36. **Haslett, A.N. 1998**. Effects of kiln temperature on wood properties, lumber quality and reprocessing properties. FRI Bulletin No.206.

37. **Horgan, G. 1999**. Cost-benefits of antisapstain treatments of New Zealand radiata pine for present and future markets. Proceeding of the 2nd New Zealand Sapstain Symposium.

38. **Horgan, G., Kreber, B., Haslett, A. and Roper J. 1997.** Cost effectiveness of compression-rolling to reduce kiln brown stain. New Zealand Forest Research Institute, Wood Processing Division, Project Report No.4302 (1997).

39. **Hunter, A.J. 1995**. Equilibrium moisture content and the movement of water through wood above fibre saturation. Wood Science and Technology, 29.

40. **Janin, G., Goncalez, J., Ananias, R.A., Charrier, B., Fernandes da Silva, G., Dilem, A. 2001**. Aesthetics appreciation of wood colour and patterns by colorimetry. Part 1: Colorimetry theory by the CIE Lab system. Maderas: Ciencia Y Technologia, 3(1-2).

41. **Kapp, S., Scheepers, G.C., Rypstra, T. 2002**. Factors influencing the development of yellow stain and kiln brown stain in South African grown Pinus spp. Journal of the Institute of Wood Science 16(2) issue 92.

42. **Keep, L. 1998**. The determination of time-dependent strains in Pinus radiata under kiln-drying conditions. ME Thesis, University of Canterbury, Christchurch, New Zealand

43. **Keey, R.B., Langrish, T.A.G., Walker, J.C.F. 2000**. Kiln-drying of lumber. Springer Series in Wood Science, Springer Verlag, New York.

44. **Keey, R.B. 1992**. Drying of loose and particulate materials. Hemisphere Publishing Corp, New York.

45. **Kerr, C. 1996**. NZ Radiata Pine Users Manual. Neilson Scott Ltd.

46. **King, B., Oxley, T.A., Long, K.D. 1974**. Soluble nitrogen in wood and its redistribution on drying. Material und Organismen 9(4).

47. **Kininmonth, J.A. and Whitehouse, L.J. 1991**. Properties and uses of NZ radiata pine: Volume 1 wood properties. Ministry of Forestry and FRI.

48. **Kho, P. C. S. 1993**. Mass transfer from in-line slabs. PhD Thesis, University of Canterbury, New Zealand.

49. **Kreber, B., Stahl, M.R., Haslett, A.N. 2001**. Application of a novel de-watering process to control kiln brown stain in radiata pine. Holz als Roh- und Werkstoff 59.

50. **Kreber, B., Haslett, A.N., McDonald, A.G. 1999a**. Kiln brown stain in radiata pine: a short review on cause and methods for prevention. Forest Products Journal, 49(4): 66-70.

51. **Kreber, B., Haslett, A.N., McDonald, A.G. 1999b**. Use of sodium dithionate for controlling kiln brown stain development in radiata pine sapwood. Forest Products Journal, 49(1): 66-70.

52. **Kreber, B.; Haslett, A. N. 1998**. The current story on kiln brown stain. FRI Bulletin Issue No.23.

53. **Kreber, B., Fernandez, M., McDonald, A.G. 1998a**. Migration of kiln brown stain precursors during the drying of radiata pine sapwood. Holzforschung, 52(4).

54. **Kreber, B., Haslett, A.N., Norris, N.G.C. 1998b**. High air velocity and relative humidity reduce development of kiln brown stain. New Zealand Journal of Forestry Science 28(3).

55. **Kreber, B., McDonald, A. 1997**. An evaluation of chemical pre-treatments for controlling kiln brown stain in radiata pine. International Research Group on Wood Preservation, Stockholm, Sweden.

56. **Kreber, B.; Haslett, A. N. 1997a**. A study of some factors promoting kiln brown stain formation in radiata pine. Holz als Roh und Werkstoff 55 (4): 215-220.

57. **Kreber, B.; Haslett, A. N. 1997b**. Compression rolling reduces kiln brown stain in radiata pine sapwood. Forest Products Journal, 47(7/8).

58. **Langrish, T.A.G. 1996**. The effects of air bypassing in timber kilns on fan power consumption. 24th CHEMECA Conference, Sydney.

59. **Ledig, S. F.; Seyfarth, R. 2001**: Characterization of surface color during wood processing. Proceedings of the 7th International IUFRO Wood Drying Conference, Tsukuba, Japan: 288-293.

60. **Long, K.D. 1978**. Redistribution of simple sugars during drying of wood. Wood Science 11.

61. **Macfarlane, K., Nayagam, S.D., Button, D. 1983**. Carbohydrate redistribution during drying of wood. Biochemical Society Transactions 11.

62. **MAF. 2005a**. Exports of forestry products for the year ended 31 December 2004 (Provisional). Statistical Release, Ministry of Agriculture and Forestry, New Zealand

63. **MAF. 2005b**. Production and stocks of sawn timber December 2004 quarter (Provisional). Statistical Release, Ministry of Agriculture and Forestry, New Zealand

64. **MAF. 2004**. A national exotic forest description as at 1 April 2003, Ministry of Agriculture and Forestry, New Zealand.

65. **MAF. 2000**. National exotic forest description: National and regional supply forecasts. Ministry of Agriculture and Forestry, New Zealand.

66. **Marshall, C. 2004**. Kiln monitoring system. ENEL 427 Final Report, Department of Electrical and Electronic Engineering, University of Canterbury, Christchurch, New Zealand.

67. **McCurdy M.C., Keey, R.B. 2002**. The effect of growth-ring orientation on moisture movement in the high temperature drying of softwood boards. Holz als Roh- und Werkstoff 60.

68. **McCurdy, M.C., Nijdam, J.J., Keey, R.B. 2002**. Biological control of kiln brown stain in radiata pine. Maderas: Ciencia y Technologia 4(2).

69. **McCurdy, M.C. 1999**. Moisture movement and strain development in Pinus Radiata boards during high-temperature drying. M.E. Thesis, University of Canterbury.

70. **McDonald, A.G., Fernandez, M., Kreber, B., Laytner, F. 2000**. The chemical nature of kiln brown stain in radiata pine. Holzforschung, 54(1): 12-22.

71. **McDonald, A.G., Fernandez, M., Kreber, B. 1997.** Chemical and UV-Vis spectroscopic study on kiln brown stain formation in radiata pine

72. **Moslemi, A.A. 1969**. Quantitative color characterization for loblolly pine veneer. Wood Science 2(1).

73. **Nassau, K. 2001**. The physics and chemistry of color: the fifteen causes of color (2nd Edition). John Wiley & Sons, Inc. New York.

74. **New Zealand Forest Research Institute Limited. 1999**. Comparative Study of NZ Pine & Selected SE Asian Species. Wood NEW Zealand Limited, 1999. http://www.evergreen.co.nz/reports/comparativestudy.pdf

75. **Nicholls, J.W.P., Dadswell, H.E. 1962**. Tracheid length in Pinus radiata D.Don. Div-For-Prod-technol-Pap-For-Prod-Aust. 24.

76. **Nijdam, J.J., Keey, R.B. 2002**. An experimental study of airflow in lumber kilns. Wood Science and Technology, 36(1)

77. **Nijdam, J.J. 1998**. Reducing moisture-content variations in kiln-dried timber. PhD Thesis, University of Canterbury, Christchurch, New Zealand.

78. **NZFOA. 2005**. New Zealand Forestry Industry Facts & Figures. New Zealand Forest Owners Association, www.nzfoa.org.nz.

79. **Ortitz, G. 2004**. Benchmarking the competitiveness of the New Zealand wood processing industry. Report prepared by FR for MAF, June 2004.

80. **Pang, S. 2006**. Drying of Pinus radiata sapwood using methanol and ethanol vapours for production of bright colour wood. To be presented at 15th International Drying Symposium, Budapest, Hungary.

81. **Pang, S., Li, J. 2005**. Drying of Pinus radiata sapwood in oxygen-free medium for bright colour wood. Proceedings of the 9th IUFRO Wood Drying Conference, Nanjing, China.

82. **Pang, S. 2005**. *Private communication*.

83. **Pang, S. 1996**. Development and validation of a kiln-wide model for drying of softwood timber. Proceedings of the 5th IUFRO Wood Drying Conference, Quebec, Canada.

84. **Pang, S. 1994**. High-temperature drying of Pinus radiata boards in a batch kiln. PhD Thesis, University of Canterbury, Christchurch, New Zealand

85. **Pang, S., Langrish, T.A.G and Keey, R.B. 1994**. Moisture movement in softwood timber at elevated temperatures. *Drying Technology* 12(8): 1897-1914.

86. **Patel R.N. 1971**. Anatomy of stem and root wood of P. radiata D. Don. NZ Journal of Forestry Science, 1(1)

87. **Paterson, A.J. 1975**. The water soluble carbohydrates of Pinus radiata: identification and quantitation. M.Sc Thesis, University of Canterbury.

88. **Park, J. 2005**. Pruned log descriptors. NZ Journal of Forestry, Feb 2005, pp34-35.

89. **Perré, P., Moser, M. and Martin, M. 1993**. Advances in transport phenomena during convective drying with superheated steam and moist air. Journal of Heat and Mass Transfer.

90. **Perry R.H., Green, D.W. and Maloney, J.O. (Editors). 1984.** Perry's Chemical Engineers Handbook Sixth Edition. McGraw-Hill Book Co., Singapore.

91. **Phillips E.W.J. 1968**. Identification of softwoods by their microscopic structure. Forest Products Research Bulletin 22, London

92. **Powell, M.A., Webber, J.F., Eaton, R.A. 2000**. Changes in moisture, soluble carbohydrate, and bacterial numbers during water storage of pine. Forest Products Journal 50(5).

93. **Pratt, G. H. 1974**. Timber drying manual. H.M.S.O., London.

94. **Riley, S., Sargent. 2005**. Proposed quantitative method for assessing kiln brown stain in Radiata pine. Proceedings of the 9th IUFRO Wood Drying Conference, Nanjing, China.

95. **Robinson, M and Davidson, G (Eds.). 1999**. Chambers 21st Century Dictionary. Chambers Harrap Publishers Ltd.

96. **Roche, M. 1990**. History of Forestry. New Zealand Forestry Corporation.

97. **Schmidt, E.L., Kreber, B. 1998**. Effect of two fumigants and a fungicide formulation on the development of kiln brown stain in radiata pine. Holz als Roh- und Werkstoff 56.

98. **Sehlstedt-Persson . 2003**. Colour responses to heat-treatment of extractives and sap from pine and spruce. Proceedings of the 8th IUFRO Wood Drying Conference, Brasov, Rumania.

99. **Siau, J.F. 1984**. Transport processes in wood. Springer series in Wood Science. Springer-Verlag, Berlin.

100. **Siau, J.F. 1971**. Flow in wood. Syracuse University Press, Syracuse, USA.

101. **Simpson, W.T. 1991**. Dry kiln operators manual. U.S. Department of Agriculture, Madison.

102. **Skaar, C. 1972**. Water in wood. Syracuse University Press, Syracuse, USA

103. **Spolek, G.A., Plumb, O.A. 1981**. Capillary pressure in softwood. Wood Science and Technology 15.

104. **Stanish, M.A. 1986**. The roles of bound water chemical potential and gas phase diffusion in moisture transport through wood. Wood Science and Technology, 19.

105. **Stenudd, S. 2004**. Colour response in silver birch during kiln-drying. Forest Products Journal 54(6).

106. **Sullivan, J.D. 1967**. Colour characterization of wood: Color parameters of individual species. Forest Products Journal 17(8).

107. **Sundqvist, B. 2002**. Wood colour control during kiln-drying. Forest Products Journal 52(2).

108. **Sutherland, J. 2004**. *Private communication*. Sutherland and Co. Ltd.

109. **Tarvainen, V.; Saranpää, P.; Repola, J. 2001**. Discoloration of Norway spruce and scots pine timber during drying. Proceedings of the 7th International IUFRO Wood Drying Conference, Tsukuba, Japan.

110. **Terziev, N. 1995**. Migration of low-molecular sugars and nitrogenous compounds in Pinus sylvestris L. during kiln and air drying. Holzforschung 49: 565 – 574.

111. **Terziev, N.; Boutelje, J.; and Soderstrom, O. 1993**. The influence of drying schedules on redistribution of low molecular sugars in Pinus syvestris L. Holzforschung 47: 3-8.

112. **Theander, O., Bjurman, J., Boutelje, J.B. 1993**. Increase in the content of low-molecular carbohydrates at lumber surfaces during drying and correlations with nitrogen content, yellowing and mould growth. Wood Science and Technology

113. **Time, B. 1997**. Moisture in Spruce. Working Report 11, Wood Technology Research Centre

114. **Tressl, R., Wondrak, G.T., Garbe, L.A., Kruger, R.P., Rewicki, D. 1998**. Pentoses and hexoses as sources of new melanoidin-like maillard polymers. Journal of Agriculture and Food Chemistry.

115. **van Meel, D.A. 1958**. Adiabatic convection batch drying with recirculation of air. Chemical Engineering Science 9.

116. **Walker, J.C.F. 1993**. Primary Wood Processing: Principles and practice. Chapman & Hall, London, 1993, pp 197-246.

117. **Wastney, S., Bates, R., Kreber, B., Haslett, A. 1997**. The potential of vacuum drying to control kiln brown stain in radiata pine. Holzforschung und Holzverwertung 49(3).

118. **Wiberg P. 1996**. CT-scanning during drying. Moisture distribution in Pinus silvestris. Proceedings of the 5th International IUFRO Wood Drying Conference, Quebec City, Canada.

119. **Wiley A.T. and Choong, E.T. 1975**. An analysis of free-water flow during drying in softwoods. Wood Science, 7(4).

120. **Williamson, C., Dawson, B. 2003**. Review of wood colour. Report No. APP6, WQI Ltd, New Zealand.

121. **Zhang, Z. 2000**. Identification and evaluation of improved drying methods of New Zealand beeches by means of an energy-efficient kiln process. PhD Thesis, University of Canterbury, Christchurch, New Zealand

Appendix 1

Calculation of Heat Transfer Coefficients

The following calculation of the heat transfer coefficients used in Chapter 6 were not include in the main text as they are based on standard heat transfer principles. They have been included in this appendix for clarity.

Heat Loss through Kiln Walls

The heat transfer through the walls is determined by four heat transfer processes, detailed in Figure 113. Starting at the internal dry bulb temperature T_S, the temperature drops slightly as heat is transferred to the internal wall surface by the process of forced convection raising it to the temperature T_{Wi}. The heat is then transferred through the wall insulation by conduction where the temperature decreases to the external wall temperature T_{We}. The heat is then transferred by the processes of radiation and natural convection to the surrounding environment at the ambient temperature, T_A, some distance from the wall.

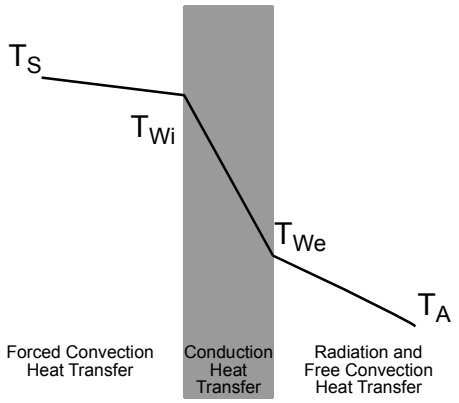

Figure 113. Heat transfer processes for the loss of heat through the kiln walls showing the four temperatures required for the heat loss calculations.

The external heat transfer coefficient is based on both radiation heat transfer and heat transfer by natural convection. Both of these processes are dependent on the external wall temperature and therefore dependent on the internal forced convection heat transfer and the wall conduction. This means that the heat transfer through the walls and roof of the kiln has to be solved iteratively using the following heat balance:

$$Q_{loss} = q_i = q_w = q_e \qquad 10.1$$

Where q_i is the heat transfer from the inside of the kiln to the internal wall surface, q_w is the heat transfer through the wall and q_e is the heat transfer from the external wall to the environment.

Internal Heat Transfer Coefficient

The heat transferred from the internal kiln environment to the internal surface of the wall is given by the following equation:

$$q_i = \overline{h}_i A_i \left(T_S - T_{Wi}\right) \tag{10.2}$$

Where $\overline{h}_i$ is the average forced convection heat transfer coefficient and A_i is the area for heat transfer. The value of h_i can be calculated from the Nusselt number. To determine the flow regime the speed of the air flow in the plenum space is required. This can be determined from the following equation:

$$u_p = \frac{w_p}{h_s \varepsilon} u_f \tag{10.3}$$

Using this equation for a plenum width, w_p=0.8m, a stack height, h_s=3.6m and a void space of ε=0.33, a fillet air speed of u_f=5m/s gives a plenum air speed of 3.33m/s. This speed is the airspeed at the top of the plenum space. The speed of the air in the plenum space will decrease down the height of the stack as air bypasses through the stack. This means that the speed at the bottom of the plenum space is effectively zero. The average speed, $\bar{u}_p$, in the plenum space will therefore be half that calculated using equation 10.3, i.e. 1.66m/s.

The flow regime in the kiln can be determined by calculating the Reynolds number, Re_L, over the swept length of the wall, L, using the following equation:

$$\mathrm{Re}_L = \frac{\overline{u}_p L}{\nu} \tag{10.4}$$

where ν is the kinematic viscosity of the air. Where $Re_L < 5\times105$ the flow regime is laminar and the average Nusselt number can be calculated using the following correlation:

$$\overline{N}u_L = 0.664\,\mathrm{Re}_L^{\frac{1}{2}}\,\mathrm{Pr}^{\frac{1}{3}} \tag{10.5}$$

where Pr is the Prandtl number given by the following equation:

$$\mathrm{Pr} = \frac{C_{PG}\mu}{k} \tag{10.6}$$

where C_p is the heat capacity of the air, μ is the dynamic viscosity of the air and k is the thermal conductivity of the air. Where $5\times105 > Re_L > 107$ the flow regime is turbulent and the average Nusselt number can be calculated from the following correlation:

$$\overline{N}u_L = \Pr^{\frac{1}{3}}\left(0.037\,\mathrm{Re}_L^{0.8} - 871\right) \tag{10.7}$$

The average heat transfer coefficient can be derived from the Nusselt number using the following equation:

$$\overline{h}_i = \overline{N}u_L \frac{k}{L} \tag{10.8}$$

Wall Heat Transfer

The heat transferred through the wall insulation is given by the following equation:

$$q_w = \frac{k_w A_w}{\Delta x_w}\left(T_{Wi} - T_{We}\right) \tag{10.9}$$

where k_w is the thermal conductivity of the insulation, A_w is the area of the wall and Δx_w is the thickness of the wall insulation.

External Heat Transfer Coefficient

As mentioned previously the external heat transfer is a combination of radiation and natural convection. The heat transferred from the external surface is therefore:

$$q_e = \overline{h}_e A_e (T_{We} - T_A) + \varepsilon_{We}\sigma A_e (T_{We}^4 - T_A'^4) \tag{10.10}$$

where the first term is the convection heat transfer and the second term is the radiation heat transfer. In the second term ε_{We} is the emissivity of the external surface of the kiln, σ is the Stefan-Boltzmann constant and T_A' is the effective ambient temperature of the surroundings for the calculation of radiation heat transfer, which is related to the ambient temperature by the following equation:

$$T_A' = T_A \varepsilon_A^{0.25} \tag{10.11}$$

where the ambient emissivity, ε_A, is given by the following equation for a clear sky where T_{Awb} is the ambient wet bulb temperature:

$$\varepsilon_A = 0.711 + 0.56(T_{Awb}/100) + 0.73(T_{Awb}/100)^2 \tag{10.12}$$

For the ambient conditions used in this project the effective ambient temperature is 18.76°C. This is not much different from the ambient temperature so to simplify the calculations the following will be assumed:

$$T_A' = T_A \tag{10.13}$$

This means that the second term in equation 10.10 can be simplified to:

$$q_r = h_r A_e (T_{We} - T_A) \qquad 10.14$$

Where:

$$h_r = \varepsilon_{We} \sigma (T_{We}^2 + T_A^2)(T_{We} + T_A) \qquad 10.15$$

So equation 10.10 becomes:

$$q_e = \left(\overline{h}_e + h_r\right) A_e \left(T_{We} - T_A\right) \qquad 10.16$$

Under the normal conditions of the kiln operation the natural convection from the external surfaces is turbulent and so the following simplified equations can be used to determine the heat transfer coefficient for the vertical surfaces:

$$\overline{h}_e = 1.31 \left(T_{We} - T_A\right)^{\frac{1}{3}} \qquad 10.17$$

and the roof:

$$\overline{h}_e = 1.52 \left(T_{We} - T_A\right)^{\frac{1}{3}} \qquad 10.18$$

Appendix 2

Configuration 6 Heat Balance Derivation

The following equations show the full derivation of the heat balance equations for kiln configuration 6 to help resolve any potential confusion regarding any of the terms. The basic balance across the heating coils is given by:

$$Q_S = C_{PYS}T_S - C_{PYV}T_V \tag{11.1}$$

The second term on the right is defined as:

$$C_{PYV}T_V = rC_{PYO}T_O + (1-r)C_{PYH}T_H \tag{11.2}$$

The second term on the right of this equation is the enthalpy of the air exiting the heat recovery exchanger and is determine by the following heat balance over this exchanger:

$$C_{PYH}T_H = \frac{C_{PYO}T_O + C_{PYA}T_A}{2} \tag{11.3}$$

This is based on the same assumptions as the heat exchanger in configuration 3 and the temperature T_A is assumed to be 10°C higher than the ambient temperature as for configuration 4. Combining the above three equations gives the following:

$$\begin{aligned} Q_S &= C_{PYS}T_s - \left(rC_{PYO}T_O + \frac{(1-r)}{2}\left(C_{PYO}T_O + C_{PYA}T_A\right)\right) \\ &= C_{PYS}T_s - rC_{PYO}T_O - \frac{C_{PYO}T_O}{2} + \frac{rC_{PYO}T_O}{2} - \frac{C_{PYA}T_A}{2} + \frac{rC_{PYA}T_A}{2} \\ 2Q_s &= 2C_{PYS}T_s - rC_{PYO}T_O - C_{PYO}T_O - C_{PYA}T_A + rC_{PYA}T_A \\ &= \left(C_{PYS}T_s - C_{PYO}T_O\right) + \left(C_{PYS}T_S - C_{PYA}T_A\right) - r\left(C_{PYO}T_O - C_{PYA}T_A\right) \end{aligned}$$

$$Q_S = \tfrac{1}{2}\left[\left(C_{PYS}T_s - C_{PYO}T_O\right) + \left(C_{PYS}T_S - C_{PYA}T_A\right) - r\left(C_{PYO}T_O - C_{PYA}T_A\right)\right] \tag{11.4}$$

Appendix 3

Nomenclature

Symbol	Definition	Equations
a	Exposed surface area of boards per unit volume (m^2)	6.10, 6.11, 6.14, 6.15
a^*	Red-green chromaticity coordinate	2.8, 2.13, 2.14, 2.15, 2.16
[abs], [ABS]	Absorbance	5.1, 5.2, 5.3, 5.4, 5.5, 5.8, 5.9, 5.10
A_e	External kiln surface area (m^2)	6.64, 6.65, 6.66, 10.10, 10.14, 10.16
A_i	Internal kiln surface area (m^2)	10.2
A_w	Area of the kiln wall	10.9
b	Board thickness (m)	6.7, 6.11
b^*	Blue-yellow chromaticity coordinate	2.9, 2.13, 2.14, 2.15, 2.16
C	Colour variable from Dieste and Williamson (2002)	2.17
C^*	Chroma	2.14, 2.16
CF	Concentration factor	5.1, 5.2, 5.3, 5.4, 5.5, 5.6, 5.7
$Cost_{Running}$	Running cost contribution per kiln load ($)	6.74
$Cost_{Capital}$	Capital cost contribution per kiln load ($)	6.75
C_{PG}	Specific heat of air (kJ/kgK)	6.16, 6.19, 6.42
C_{PV}	Specific heat of water vapour (kJ/kgK)	6.16, 6.18, 6.42
C_{PY}	Humid heat (kJ/kgK)	6.42
C_{PYA}	Humid heat of ambient air (kJ/kgK)	6.43, 6.44, 6.45, 6.46, 6.47, 6.50, 6.51, 6.52, 6.53, 6.54, 6.55, 6.58, 6.59, 6.67, 11.3, 11.4
C_{PYH}	Humid heat of heat exchanger return air (kJ/kgK)	11.2, 11.3
C_{PYi}	Humid heat at point i in stack (kJ/kgK)	6.17
C_{PYO}	Humid heat at stack outlet (kJ/kgK)	6.43, 6.44, 6.46, 6.47, 6.49, 6.50, 6.51, 6.52, 6.53, 6.54, 6.55, 6.58, 6.59, 6.61, 6.62, 6.67, 11.2, 11.3, 11.4
C_{PYS}	Humid heat at stack inlet (kJ/kgK)	6.17, 6.45, 6.46, 6.47, 6.49, 6.50, 6.51, 6.54, 6.55, 6.58, 6.59, 6.60, 6.61, 6.67, 11.1, 11.4
C_{PYV}	Humid heat at vent (kJ/kgK)	6.43, 6.44, 6.45, 6.52, 6.53, 11.1, 11.2

dep	Depreciation component ($/year)	6.75
D_H	Hydraulic diameter (m)	6.68
ΔE_{ab}, ΔE	Colour difference	2.13. 2.16, 2.18
$EE_{\$}$	Cost of electrical energy ($/GJ)	6.74
f	Relative drying rate	6.1
f	Friction factor	6.68
$f_{0.4}$	Relative drying rate at Φ=0.4	6.5, 6.6
G	Specific dry gas mass flux (kg/m^2/s)	6.8, 6.9, 6.10, 6.15
h_{ab}	Metric hue-angle	2.15
h_e	External convective heat transfer coefficient (W/m^{2}K)	6.64, 10.10, 10.16, **10.17, 10.18**
h_i	Internal convective heat transfer coefficient (W/m^{2}K)	6.64
$\overline{h}_i$	Average forced convection heat transfer coefficient (W/m^{2}K)	10.2, 10.8
h_r	External radiation heat transfer coefficient (W/m^{2}K)	6.64, 10.14, 10.16
h_s	Stack height (m)	6.70, 6.71, 10.3
ΔH^*	Metric hue-angle difference	2.16
H_{bv}	Heat of vaporisation of bound water (kJ/kg)	
H_{wv}	Heat of vaporisation of liquid water (kJ/kg)	6.16, 6.20, 6.38, 6.39, 6.48, 6.49, 6.50, 6.51, 6.55, 6.59, 6.61,
H_{wvi}	Heat of vaporisation of water at point *i* in stack (kJ/kg)	6.17
H_{wv}^0	Heat of vaporisation of water at stack inlet (kJ/kg)	6.17
k	Rate constant from Dieste and Williamson (2002)	2.17
k	Thermal conductivity of air (W/mK)	10.8
k_w	Thermal conductivity of kiln wall (W/mK)	6.64, 6.66, 10.9
K	Coefficient in tristimulus equations	2.1, 2.2, 2.3, 2.4
K_1	EMC equation coefficient	6.28, **6.29**
K_2	EMC equation coefficient	6.28, **6.30**
K_c	Head loss due to contraction (Pa)	6.68
K_e	Head loss due to expansion (Pa)	6.68
l_s	Stack length (m)	6.11, 6.70, 6.71
L	Swept length of kiln wall	10.4, 10.8,
L^*	Lightness	2.7, 2.13, 2.16
m	Reaction order from Dieste and Williamson (2002)	2.17
MC	Moisture content (kg/kg)	3.1
MC_{fsp}	Moisture content at fibre saturation point (kg/kg)	3.2

MC_{max}	Maximum final moisture content (kg/kg)	6.76
MC_{mean}	Average final moisture content (kg/kg)	6.76
MC_{min}	Minimum final moisture content (kg/kg)	6.76
M_G	Molecular weight of air (kg/mol)	6.24
M_v	Molecular weight of water (kg/mol)	6.24
[N]	Nitrogen concentration	2.17
Nu_L	Nusselt number	**10.5**, **10.7**, 10.8
N_v	Drying rate (kg/m^2/s)	6.1
N_{cr}	Constant drying rate above critical moisture content (kg/m^2/s)	6.1
p_O	Air pressure at outlet of stack (Pa)	6.68, 6.69
p_S	Air pressure at inlet of stack (Pa)	6.68, 6.69
p_s^v	Saturated vapour pressure for water in air (Pa)	6.22
$PH_\$$	Price of process heat ($/GJ)	6.74
Pr	Prandtl number	10.5, **10.6,** 10.7,
P_{Shaft}	Shaft power (kW)	6.69, 6.74
P_t	Total pressure (Pa)	6.24
q_e	Heat transferred from external kiln surface to atmosphere (W)	10.1, 10.10
q_i	Heat transferred from kiln atmosphere to internal kiln surface (W)	10.1, **10.2**
q_r	Heat transferred from external kiln surface to atmosphere by radiation (W)	**10.15**
q_w	Heat transfer through kiln wall (W)	10.1, **10.9**
Q	Volumetric flow through the fan (m^3)	6.69, 6.70, 6.71
Q_{bv}	Extra heat required to evaporate bound water (kJ)	6.37, 6.39
Q_C	Cooling supplied to kiln (kJ)	6.62
$Q_{conduction}$	Heat loss due to conduction (kJ)	6.63
$Q_{convection}$	Heat loss due to convection (kJ)	6.63
$Q_{fugitive}$	Other heat loss (kJ)	6.63
Q_{loss}	Heat loss from kiln (kJ)	6.63, 6.64, 6.65, 6.66
$Q_{radiation}$	Heat loss due to radiation (kJ)	6.63
Q_S	Heat supply to kiln, a superscript denotes the kiln configuration (kJ)	6.45, 6.46, 6.47,6.50, 6.51, 6.54, 6.58, 6.60, 6.67
Q_v	Latent heat requirement to evaporate moisture from wood (kJ)	6.37
Q_{wv}	Heat required to evaporate free water (kJ)	6.37, 6.38
Q^*	Ideal heat demand (kJ)	6.48, 6.50, 6.51, 6.55, 6.59, 6.61
r	Recycle ratio	6.56, 6.57, 6.58, 6.59, 6.67, 11.2, 11.4

r_{abs}	Colour change rate based on absorbance (h^{-1})	5.6, 5.7
$R(\lambda)$	Spectral reflectance of object	2.1, 2.2, 2.3, 2.4
Re_L	Reynolds number	**10.4**, 10.5,10.7,
s	Fillet space (m)	6.7, 6.11
$S(\lambda)$	Relative spectral power distribution of illuminant	2.1, 2.2, 2.3, 2.4
t	Time (s)	6.9, 6.10, 6.14
t	Time (h)	2.17
t	Time (days)	2.18
t_{dry}	Drying time (h)	6.74, 6.75
t_{Op}	Operational time (h/year)	6.75
T	Temperature (°C)	2.18, 6.16, 6.23
T_A	Ambient temperature (°C)	6.43, 6.44, 6.45, 6.46, 6.47, 6.50, 6.51, 6.52, 6.53, 6.54, 6.55, 6.58, 6.59, 6.64, 6.67, 10.10, 10.11, 10.13, 10.14, 10.15, 10.16, 10.17, 10.18, 11.3, 11.4
T_A'	Effective ambient temperature of kiln surroundings (°C)	10.10, **10.11**, 10.12, **10.13**
T_{Awb}	Ambient wet bulb temperature (°C)	10.12
T_{GD}	Dry-bulb temperature (°C)	6.25, 6.26, 6.29, 6.30, 6.31, 6.72
T_{GK}	Gas temperature (K)	6.18, 6.19
T_{GW}	Wet-bulb temperature (°C)	6.25, 6.26, 6.72
T_H	Temperature of heat exchanger return air (°C)	11.2, 11.3
T_i	Temperature at point *i* in stack (°C)	6.17
T_O	Stack outlet temperature (°C)	6.43, 6.44, 6.46, 6.47, 6.49, 6.50, 6.51, 6.52, 6.53, 6.54, 6.55, 6.58, 6.59, 6.61, 6.62, 6.67, 11.2, 11.3, 11.4
T_S	Stack inlet temperature (°C)	6.17, 6.45, 6.46, 6.47, 6.49, 6.50, 6.51, 6.54, 6.55, 6.58, 6.59, 6.60, 6.61, 6.64, 6.67, 10.2, 11.1, 11.4
T_{sap}	Sap temperature (°C)	3.2
T_V	Venting temperature (°C)	6.43, 6.44, 6.45, 6.52, 6.53, 11.1, 11.2
T_W	Temperature of cooled air in kiln (at the wet-bulb temperature) (°C)	6.60, 6.61, 6.62
T_{We}	Kiln wall external temperature (°C)	6.66, 10.9, 10.10, 10.14, 10.15, 10.16, 10.17, 10.18
T_{Wi}	Kiln wall internal temperature (°C)	6.65, 6.66, 10.2, 10.9
u_f	Velocity in the fillet space (m/s)	6.8, 10.3
u_p	Velocity in plenum space (m/s)	**10.3,** 10.4

Var_{MC}	Moisture content variation	6.76
v	Venting ratio	6.40, 6.41, 6.43, 6.44, 6.46, 6.47, 6.50, 6.51, 6.52, 6.53, 6.54, 6.55, 6.70
V_s	Volume of stack (m^3)	6.38, 6.39
W	EMC equation coefficient	6.28, **6.31**
w_p	Width of plenum space (m)	10.3
w_s	Stack width (m)	6.11, 6.68
W_{green}	Green weight (kg)	3.1
$W_{oven\text{-}dry}$	Oven-dry weight (kg)	3.1
x	Chromaticity coordinate	2.5
Δx_w	Kiln wall thickness (m)	6.64, 6.66, 10.9
X	Tristimulus value	2.1, 2.5, 2.6, 2.8, 2.10
X	Moisture content (kg/kg)	6.2, 6.9, 6.10
X_0	Initial moisture content (kg/kg)	6.38
X_{cr}	Critical moisture content (kg/kg)	6.2
X_e	Equilibrium moisture content (kg/kg)	6.2, **6.28**, 6.39
X_{fsp}	Fibre saturation point (kg/kg)	6.38, 6.39
X_n	Tristimulus value for perfect diffuse reflector	2.8, 2.10
$\bar{x}(\lambda)$	Colour matching function	2.1
y	Chromaticity coordinate	2.6
Y	Tristimulus value	2.2, 2.5, 2.6, 2.7, 2.8, 2.9, 2.11
Y	Humidity	6.42
Y_G	Bulk gas humidity	6.4, 6.9, 6.10, 6.13, 6.25, 6.27
Y_G^0	Bulk gas humidity at stack inlet	6.13, 6.14
Y_{GA}	Ambient air humidity	6.40, 6.41
Y_{GO}	Stack outlet air humidity	6.40, 6.41, 6.62
Y_{GS}	Stack inlet air humidity	6.40, 6.41, 6.62
Y_i	Gas humidity at point *i* in stack (kg/kg)	6.17
Y_n	Tristimulus value for perfect diffuse reflector	2.7, 2.8, 2.9, 2.11
Y_O	Humidity at stack outlet	6.48, 6.49
Y_S	Humidity at stack inlet	6.48, 6.49
Y_w	Humidity adjacent to fully wetted surface	6.4, 6.10, 6.13, 6.14, 6.24, 6.25, 6.27
$\bar{y}(\lambda)$	Colour matching function	2.2
z	Distance through stack (m)	6.9, 6.10, 6.15
Z	Tristimulus value	2.3, 2.5, 2.6, 2.8, 2.12
Z_n	Tristimulus value for perfect diffuse reflector	2.9, 2.12

$\bar{z}(\lambda)$	Colour matching function	2.3
α_H	Ratio of radiation to heat transferred by hot air	6.16
β	External mass transfer coefficient	6.4, 6.10, 6.14, 6.15, **6.26**
ε	Void space	6.7, 6.9, 6.10, 6.14, 6.38, 6.39, 6.70, 6.71, 10.3
ε_A	Ambient emissivity	10.11, 10.12
ε_{We}	Emissivity of the external kiln surface	10.10, 10.15,
λ	Wavelength	2.1, 2.2, 2.3, 2.4
θ	Relative drying time	6.12, 6.14, 6.35
ϕ_m	Humidity potential	6.4, 6.10, 6.14, 6.15, **6.27**,
Φ	Normalised moisture content	6.2, 6.3, 6.6, 6.10, 6.12, 6.32, 6.33, 6.34, 6.35, 6.36, 6.72
η_{fan}	Fan efficiency	6.69
ν	Kinematic viscosity (m^2/s)	10.4
Π	Normalised humidity potential	6.12, 6.32, 6.33, 6.34, 6.35
ρ_b	Basic density of wood (kg/m^3)	6.9, 6.10, 6.38, 6.39
ρ_G	Air density (kg/m^3)	6.8, 6.68
σ	Stefan-Boltzmann constant	10.10, 10.15
ψ	Relative humidity	6.5, 6.28
ζ	Relative distance across kiln	6.12, 6.15, 6.32, 6.33, 6.34

Appendix 4

Contents of CD-Rom

The compact disk supplied with this thesis contains relevant information too bulky to be included in the printed thesis. The contents are as follows:

1. Documents including this thesis and a copy of Craig Marshall's kiln micro-sensors report.
2. Experimental results.
3. Simulation program files and results from the simulations.